
UNIVERSITY OF BIRMINGHAM

# DRILLING OF CARBON FIBRE REINFORCED PLASTIC COMPOSITES

**by**

**ISLAM SAAD ELSAYED MOHAMED SHYHA**

*M.Sc., B.Sc. (Hons)*

A thesis submitted to
The University of Birmingham
for the degree of
**DOCTOR OF PHILOSOPHY**

School of Mechanical Engineering
The University of Birmingham
August 2010

# SYNOPSIS

Following an extensive literature survey focusing on the machinability of carbon fibre reinforced plastics (CFRP), three main phases of experimental work were undertaken to evaluate the drilling of CFRP and associated stack materials. Phase 1 and 2 involved small diameter holes (1.5 mm) in thin CFRP laminates (3 mm thick) while Phase 3 addressed the feasibility of one-shot drilling (6.35 mm diameter holes) in multilayer workpiece stacks comprising titanium, CFRP and aluminium. Machinability was assessed in terms of tool life/wear, force/torque, hole size and geometrical accuracy, workpiece surface integrity and chip morphology. Initial trials (Phase 1A) were performed to investigate the effect of peel ply layers (~100 μm thick nylon sheet attached on both sides of the laminate to assist the bleeding of volatiles and air during curing as well as preventing surface contamination) on hole entry and exit quality, as current industrial practice involves removal of the protective sheet prior to drilling. The results indicated that the presence of the peel ply significantly improved hole quality, particularly in respect of entry and exit delamination with considerable reduction in defects such as fuzzing and edge chipping. The lack of information prompted tests to determine the influence of tool geometry and operating conditions in Phase 1B. In Phase 2 experiments, the effect of composite material orientation/properties and the performance of several diamond based coatings were evaluated with respect to tool life and workpiece quality. The data indicated that a maximum operating feed rate of 0.2 mm/rev was advisable for the stepped drill configuration to avoid tool fracture, while conventional twist drill geometry was viable up to 0.3 mm/rev. Uncoated and diamond like carbon (DLC) coated tools outperformed chemical vapour deposition (CVD) diamond coated drills in terms of tool life (~ 2500 holes versus 1300 holes), as well as producing superior hole quality. In general, machining of woven laminates resulted in lower delamination levels compared to equivalent unidirectional (UD) composites, despite similar results in tool life.

Phase 3 of the research assessed the impact of stack arrangement/sequence and the performance of PCD tools together with various coated WC drills and operating parameters. Here, drilling involved 6.35 mm diameter holes in 30 mm thick Ti/CFRP/Al stacks under high pressure through spindle coolant and spray mist environments. While results showed that drilling of stacks in a single shot operation was feasible, drill material and geometry played a critical role. Stack order also significantly affected process performance as drilling into

Ti/CFRP/Al produced lower forces and higher productivity than when the sequence was Al/CFRP/Ti. A tool life of approximately 300 holes was achieved using either uncoated or C7 hardmetal coated drills in contrast to ~ 200 holes with CVD diamond coated tools. Titanium chips adhered to the machined hole surface and in production would necessitate an additional finishing process. Relatively low surface roughness values of up to 1 and 0.3 μm Ra were obtained for Ti and Al surfaces respectively whereas up to 9 μm Ra was recorded for CFRP. It was concluded that further design improvements to PCD tools are required in order to accommodate the cutting of stack material due to the catastrophic failure experienced when machining the Ti section.

# ACKNOWLEDGMENTS

The author would like to thank Dr. Sein Leung Soo (Lecturer) and Mr. David Aspinwall (Reader in Advanced Manufacturing Technology and Head of the Machining Research Group) both in the School of Mechanical Engineering, University of Birmingham for their academic supervision and guidance over the course of the research. Thanks also go to Mrs. Elaine Aspinwall for her generous time and help relating to experimental design and statistical analysis techniques.

I am indebted to Mr. Richard Fasham, Mr. Andy Loat and Mr. Alan Saywell, Technical Engineers within the School of Mechanical Engineering for their invaluable assistance with the experimental work and preparation of workpiece material. Useful discussions and the support from members of the Machining Research Group, School of Mechanical Engineering over the duration of the project is gratefully acknowledged.

My sincerest gratitude and appreciation are due to Mr. Sam Bradley and Mr. Richard Perry (GKN Aerospace), Mr. Neels Pretorius and Dr. Peter Harden (Element Six Ltd) and Mr. Stuart Dawson (Unimerco Ltd) for sharing their experience and knowledge as well as providing workpiece materials, tooling and funding for the work.

Special thanks go to Universities UK (for an Overseas Research Students Awards Scheme Scholarship), University of Birmingham, GKN Aerospace (UK), Element Six Limited (Ireland), Unimerco Limited (UK) and the Egyptian Ministry for Higher Education and Scientific Research for financial support.

Last but certainly not least, I wish to express my love and deepest gratitude to my beloved parents, wife and kids for their understanding, endless encouragement, support, patience and love throughout this work.

# TABLE OF CONTENTS

# LIST OF FIGURES

# LIST OF TABLES

# NOMENCLATURE

| | | |
|---|---|---|
| 5HS | : | Five harness satin woven carbon fibre |
| A | : | Aramid |
| ACF | : | Activated carbon fibres |
| ACGIH | : | American Conference of Governmental Industrial Hygienists |
| $A_d$ | : | Damaged area around the hole ($mm^2$) |
| AFRP | : | Aramid fibre reinforced plastic |
| Al | : | Aluminium |
| $Al_2O_3$ | : | Aluminium oxide |
| $A_{max}$ | : | Maximum damage area based on $D_{max}$ ($mm^2$) |
| ANOVA | : | Analysis of variance |
| $A_o$ | : | Drilled hole area ($mm^2$) |
| AWJ | : | Abrasive waterjet |
| C | : | Carbon |
| CFRP | : | Carbon fibre reinforced plastic |
| CMC | : | Ceramic matrix composite |
| Co | : | Cobalt |
| COF | : | Coefficient of friction |
| $C_p$ | : | Specific heat (kJ/kg $^oC$) |
| CrCN | : | Chromium carbon nitride |
| CTE | : | Coefficient of thermal expansion ($10^{-6}$ $^oC$) |
| CVD | : | Chemical vapour deposition |
| DF | : | Degree of freedom |
| DLC | : | Diamond like carbon |
| $D_{max}$ | : | Maximum damage zone diameter (mm) |
| $D_o$ | : | Drilled hole diameter (mm) |
| E | : | Modulus of elasticity (GPa) |
| Exp SS | : | Expected sum of squares |
| F | : | f-test value |
| $F_A$ | : | Critical thrust forces at which push-out occurs (N) |
| $F_c$ | : | Critical thrust forces at which peel-up occurs (N) |
| $F_d$ | : | Conventional delamination factor |
| $F_{da}$ | : | Adjusted delamination factor |

| | | |
|---|---|---|
| FE | : | Finite element |
| FRP | : | Fibre reinforced plastic |
| G | : | Glass |
| $G_{1c}$ | : | Critical energy release rate for delamination |
| GFRP | : | Glass fibre reinforced plastic |
| GP | : | General purpose |
| *h* | : | Depth of material remaining to be cut under the tool (mm) |
| *H* | : | Composite laminate thickness (mm) |
| H | : | Helix angle ($^o$) |
| HAZ | : | Heat affected zone |
| HM | : | High modulus carbon fibre |
| HP | : | High performance |
| HS | : | High strength carbon fibre |
| HSS | : | High speed steel |
| HT | : | High tenacity carbon fibre |
| IADS | : | International Alloy Designation System |
| IM | : | Intermediate modulus carbon fibre |
| K | : | Thermal conductivity (W/m $^o$C) |
| *k* | : | Peeling factor which is a function of the coefficient of friction between drill and workpiece and the drill helix angle |
| LM | : | Low modulus carbon fibre |
| MD | : | Multidirectional |
| MMC | : | Metal matrix composite |
| MQL | : | Minimum quantity lubrication |
| MRR | : | Material removal rate ($mm^3$) |
| NIOSH | : | The National Institute for Occupational Safety and Health |
| OA | : | Orthogonal array |
| *P* | : | Point angle ($^o$) |
| P | : | Probability |
| PAN | : | polyacrylonitrile based carbon |
| PCD | : | Polycrystalline diamond |
| PCR | : | Percentage contribution ratio |
| PMC | : | Polymer matrix composite |
| PVD | : | Physical vapour deposition |
| Ra | : | Average surface roughness (μm) |

| | | |
|---|---|---|
| $R_{max}$ | : | Maximum surface roughness (μm) |
| RTM | : | Resin transfer moulding |
| Sa | : | Average surface roughness for 3D (μm) |
| $Si_3N_4$ | : | Silicon nitride |
| SiC | : | Silicon carbide |
| SM | : | Standard modulus carbon fibre |
| SS | : | Sum of squares |
| taC | : | Tetrahedral amorphous carbon |
| $T_g$ | : | Glass transition temperature ($^oC$) |
| Ti | : | Titanium |
| TiAlN | : | Titanium aluminium nitride |
| TiC | : | Titanium carbide |
| TiCN | : | Titanium carbon nitride |
| TiN | : | Titanium nitride |
| $T_m$ | : | Melting temperature ($^oC$) |
| TWA | : | Time weighted average |
| UD | : | Unidirectional |
| UHM | : | Ultrahigh modulus carbon fibre |
| USM | : | Ultrasonic machining |
| $\nu$ | : | Poisson's ratio |
| $VB_{Bmax}$ | : | Maximum flank wear (mm) |
| $V_f$ | : | Fibre volume fraction |
| $V_m$ | : | Matrix volume fraction |
| $w$ | : | Weight (kg) |
| WC | : | Tungsten carbide |
| WEDM | : | Wire electrical discharge machining |
| $\alpha$ | : | Traditional delamination factor weight |
| $\beta$ | : | Ratio between the damaged area |
| $\varepsilon_u$ | : | Strain to failure (%) |
| $\gamma$ | : | Edge position angle between the cutting direction and the fibre direction ($^o$) |
| $\theta$ | : | Fibre orientation ($^o$) |
| $\rho$ | : | Density ($g/cm^3$) |
| $\sigma_T$ | : | Tensile strength (MPa) |
| $\sigma_u$ | : | Ultimate tensile strength (MPa) |

# 1. INTRODUCTION

## 1.1 Background to the project

Composites use in the aerospace industry is expanding, with carbon fibre reinforced plastics (CFRP) arguably at the forefront for replacing more conventional workpiece materials such as aluminium and steel in aircraft structural components. The nature of CFRP products still often necessitates the use of various machining processes in order to fulfil performance and design requirements. Of these, hole drilling is one of the most widely used operations as a means to facilitate mechanical joining of composite parts with other elements. Despite considerable developments in tooling and machine tool technology as well as improved process capability over the past decade, innovations are constantly being pursued by industry to obtain greater productivity and improved surface quality/integrity.

While there is a significant body of research on the drilling of CFRP, the vast majority of publications deal (understandably) with fixing holes in the region of 5 – 6 mm diameter, however there is also a need for data relating to the machinability of smaller diameter holes (< 3 mm), for example in relation to acoustic panels, where sections can incorporate up to 100,000 of such holes. More recently, multilayer metallic/composite stack materials consisting of CFRP, titanium and/or aluminium have also seen a surge in demand/use, particularly for aerospace structures subjected to high mechanical loads during service. Challenges faced when drilling such structures include not only the marked anisotropy/in-homogeneity, lack of plastic deformation and abrasive characteristics for the CFRP composites but also the dissimilar mechanical/physical properties for the stack materials. These aspects impact on selection of appropriate operating parameters, fluid supply, swarf evacuation etc. with consequent adverse effects on tool life and workpiece quality.

The research presented in this thesis was undertaken as part of a Doctor of Philosophy (PhD) degree programme based within the Machining Research Group in the School of Mechanical Engineering at the University of Birmingham. The project was carried out in collaboration with a consortium of industrial organisations including GKN Aerospace, Element Six Ltd and Unimerco Ltd who provided both financial and in-kind contributions (workpiece materials, tool materials, tooling.), see Appendix A for list of contacts. An

Overseas Research Student Awards Scheme (ORSAS) scholarship from Universities UK together with additional funding from the School provided further support.

## 1.2 Aims and objectives

The aim of the work was to extend the fundamental knowledge when machining CFRP through the (a) assessment of small hole twist drilling of carbon fibre reinforced plastic (CFRP) to improve productivity and workpiece quality and (b) investigation into the feasibility of single shot drilling of multilayer metallic/composite stacks. The specific objectives of the work were to:

- Perform a comprehensive literature survey of previous research and published machinability data for drilling CFRP and metallic/composite stacks.
- Establish the influence of operating parameters (cutting speed and feed rate), tool geometries/coatings (helix, point angles and CVD diamond based coatings) and workpiece material properties (ply configuration, prepreg form etc.) on key output measures including tool life, geometrical accuracy, cutting forces/torque and workpiece integrity criteria (surface roughness, fibre pullout/delamination etc.) when drilling 1.5 mm diameter holes in CFRP panels.
- Evaluate the performance of various tool materials (WC, PCD) and coatings, tool designs as well as the effect of operating parameters, when drilling composite/metallic stacks of Ti/CFRP/Al in a one shot operation.
- Determine the preferred operating parameters and conditions for twist drilling of 6.35 mm diameter holes in Ti/CFRP/Al stacks in order to achieve acceptable productivity levels.

# 2. LITERATURE REVIEW

## 2.1 Composite materials

### 2.1.1 Overview

Composites are materials which comprise two or more constituent parts resulting in a product with superior properties compared to its individual elements [1, 2]. One is generally a hard, stiff and strong dispersed phase known as reinforcement, which is embedded within a softer bulk phase called the matrix [3]. The former can be in the form of particles, fibres (continuous and discontinuous), wires, whiskers, etc., and are commonly made from glass, carbon, Kevlar (aramid), ceramic or metallic compounds while the latter is either a polymer, metal or ceramic [3, 4]. While such elements retain their individual characteristics when joined to form the composite, they also influence the resulting properties of the material. More recently, the term 'advanced composites' has been used to describe materials fabricated from sheets of pre-impregnated fibres in a suitable resin matrix [3, 5]. These sheets, which are also known as prepregs or plies, are typically 100-150 μm thick. The main advantages provided by advanced composites are high strength/stiffness to weight ratios resulting in significant weight reduction, superior rigidity and damping, tailorable characteristics to satisfy loading requirements and near-net-shape formability. They are particularly attractive for components in the aerospace, automotive, oil and gas, sports equipment and medical device sectors [6-10]. For example, the use of composites is expanding in the civilian aircraft industry where approximately 50% of the total weight for the new Boeing 787 Dreamliner is made from composites compared to less than 5% in the Boeing 757/767 produced in the 1980s [11, 12]. Similarly, CFRP accounts for 22-25% (35 tons) of the structural weight of the new Airbus A380 [12-14], which is estimated to provide a 12% reduction in fuel consumption [13]. A comparison between properties of various materials including conventional metals and composites is presented in Figure 2.1 [5].

### 2.1.2 Classification of composite materials

Composites are generally classified according to the matrix system used and are broadly divided into; metal matrix composites (MMCs), ceramic matrix composites (CMCs) or polymer matrix composites (PMCs). Alternatively, they can also be categorised based on their reinforcement format/arrangement which typically involves particles, whiskers, fibres

(continuous, discontinuous, aligned and random) and structural arrangements, see Figure 2.2 [4].

(a) Density (kg/m$^3$)

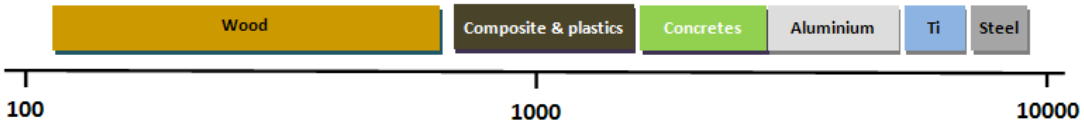


(b) Tensile modulus (GPa)

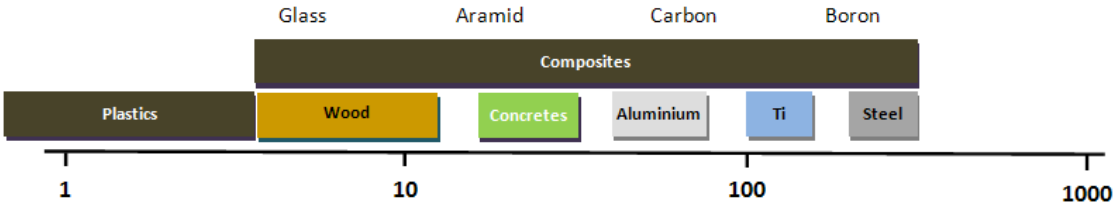


(c) Tensile strength (MPa)

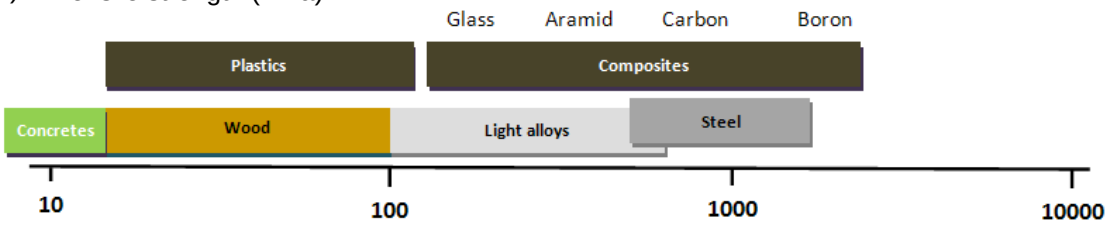


Figure 2.1: Properties of various metals and composites [5]

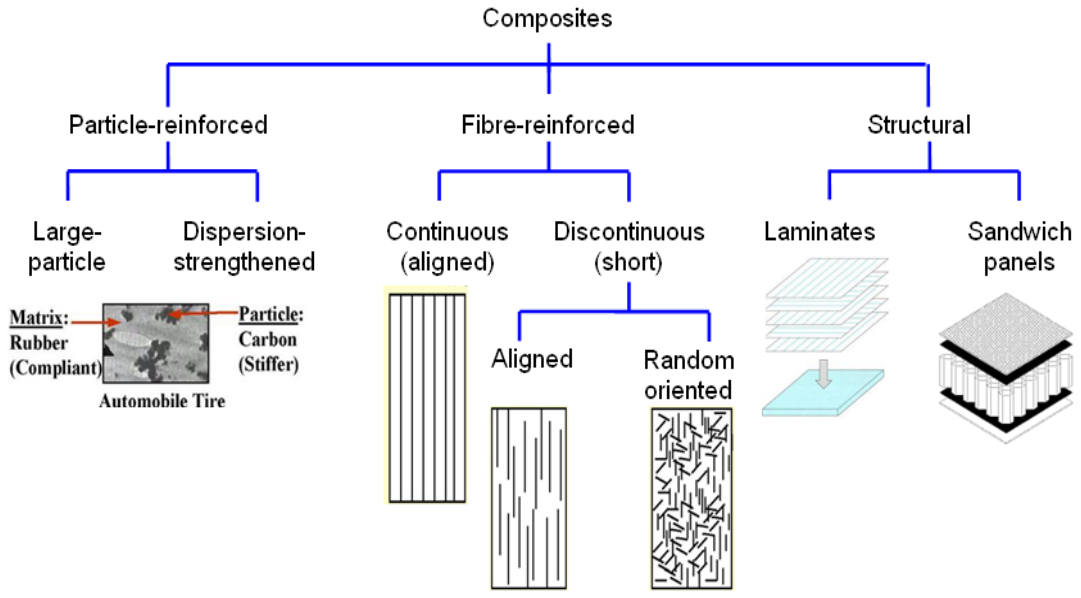


Figure 2.2: Classification for various composites according to reinforcement format [4]

Metal matrix composites are typically used for moderate operating temperature applications and examples in this group include Al-6061-T6 (51% B, continuous fibres) and Al 2124-T6 (20% SiC, particle reinforcement) [2]. The benefits of MMCs include non-flammability and high resistance to degradation by organic fluids, however, they are usually heavier than FRP's (density of Al matrix reinforced with 30% SiC MMC is 2.9 $g/cm^3$ compared to 1.6 $g/cm^3$ for CFRP) and can suffer from interfacial degradation at the fibre/matrix interface as well as being prone to corrosion [1]. Ceramic matrix composites have higher specific modulus and mechanical properties than metals at elevated temperatures which allow their use up to 2000$^oC$, although applications are limited because of inherent brittleness [1]. Reinforcement with SiC or C can significantly improve the fracture toughness of CMCs. Examples of matrix systems for CMCs include $Si_3N_4$ and $Al_2O_3$ [15]. The third group involving PMCs will be discussed further in Section 2.1.3.

Dispersion strengthened composites comprise small particles (approximately $10^{-5}$ mm to $10^{-4}$ mm in diameter) which are added to the matrix material. These particles help the matrix to resist deformation and results in a harder and stronger material. With large-particle reinforced composites, the particle diameter is typically in the order of several micrometres and carries a major fraction of the load [4]. The automobile tyre is an example of this configuration, which has relatively large carbon particles embedded within a poly-isobutylene elastomeric polymer matrix. Whiskers are anisotropic single crystals typically fabricated by chemical vapour deposition (CVD), and have length/diameter ratios of 10 – 100, where the diameter is typically between 0.1 – 1 μm. Particles and whiskers are mainly used with MMC's and CMC's because they distribute randomly to retain composites' isotropic nature.

Fibre reinforced composites were first produced around 4000 B.C. in ancient Egypt for writing paper made from the Papyrus plant [1]. Fibres currently used for 'engineering' applications have comparatively long axis and are often circular in shape (up to several tens of micrometres in diameter) and have greater mechanical properties along the length axis. Fibre reinforced composites will be described in greater detail in the following section. Structural composites are typically fabricated by stacking multiple layers of fibre reinforced plastic sheets/plies to produce a homogeneous material known as laminates. The laminate properties depend on the individual layers as well as the geometrical design of the structure (i.e. fibre orientation of the different layers) [4]. Laminates are occasionally used to create sandwich panels containing a honeycomb structure.

### 2.1.3 Fibre reinforced plastic (FRP) composites

Polymer matrix composites are often referred to as FRPs (fibre reinforced plastics) when strong/brittle fibres are incorporated within a ductile/soft polymer matrix [2]. Continuous filaments/fibres in the form of unidirectional (UD) or woven fabrics are the principal fibrous patterns in FRP composites. The term unidirectional refers to the material (prior to laying up) having fibres arranged in a single direction while woven structures involve perpendicularly intersecting fibres. Woven fabrics include plain weaves (each fibre yarn passing over and under every other perpendicular fibre yarn), twill weaves and satin weaves (e.g. five-harness satin refers to each yarn passing under every fifth perpendicular fibre yarn) [1], see Figure 2.3. Both UD and woven plies can be laid up to produce multidirectional composite laminates as shown in Figure 2.4. Carbon, glass and aramid are the most common types of fibres used in PMC, where the letters C, G or A are placed before the acronym FRP to specify the nature of the reinforcing fibres [2]. For instance, CFRP is the abbreviation for Carbon Fibre Reinforced Plastic while GFRP and AFRP are abbreviations for Glass and Aramid Fibre Reinforced Plastic, respectively. Boron and polyethylene fibres are also used for FRP composites albeit to a lesser extent. General mechanical properties and relative cost information for the various individual fibres are shown in Figure 2.5 [5].

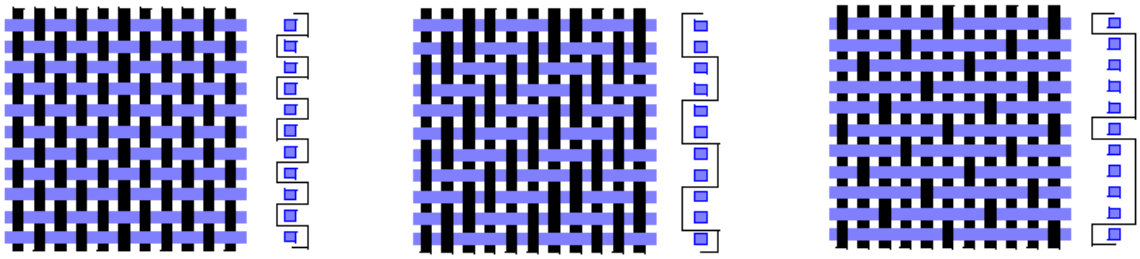


Figure 2.3: The most commonly used fabric types [5]

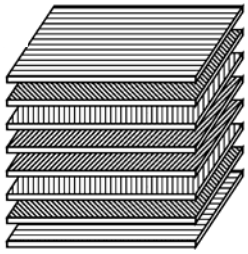

Figure 2.4: Example of stacking sequence in multidirectional layup

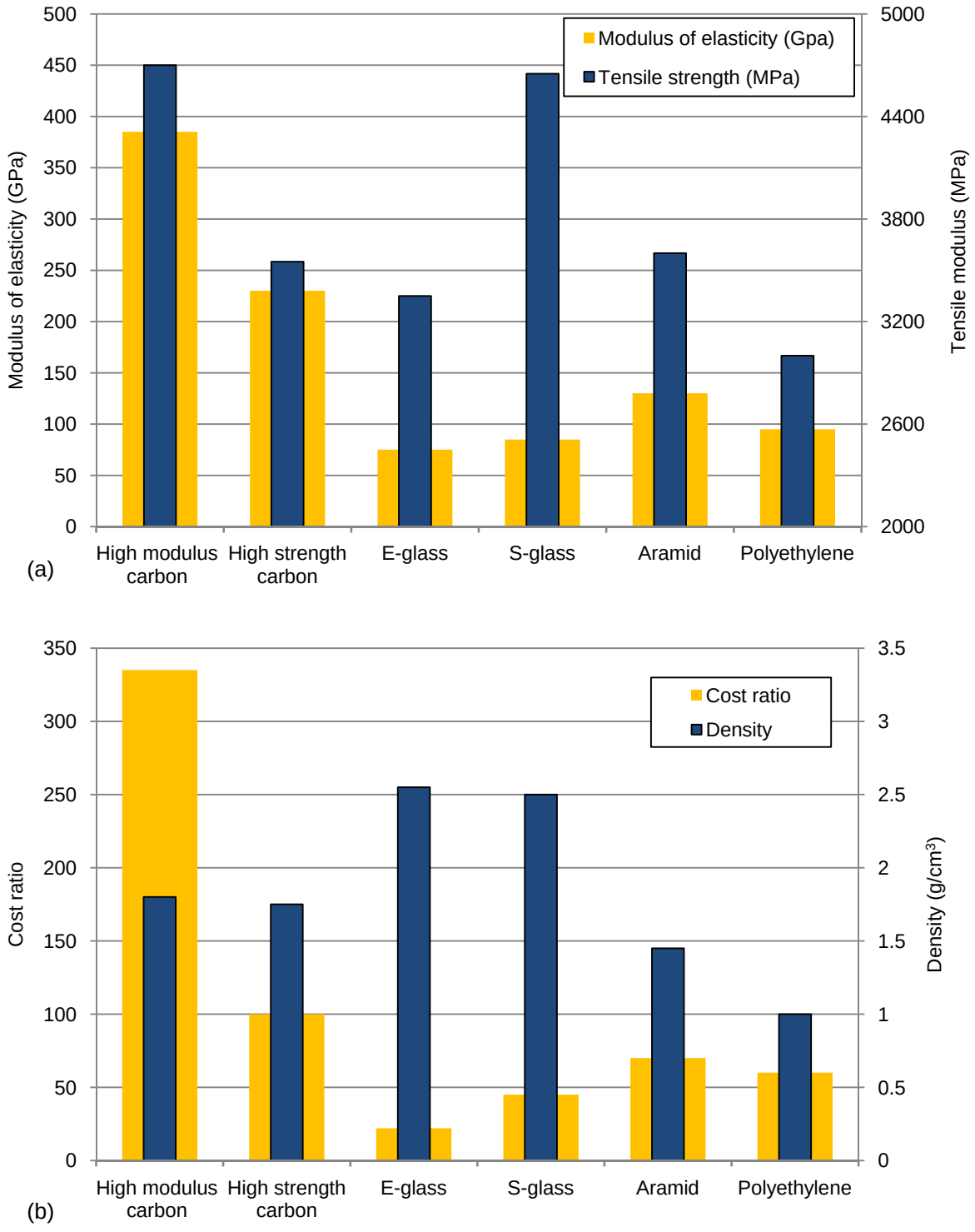


Figure 2.5: Relative properties for various individual fibres [5]

*2.1.3.1 Properties of different fibres*

Fibres are typically produced by drawing liquid material or pulling a precursor (initial/raw state of fibre material) through an orifice. They are subsequently supplied in the form of tows consisting of individual continuous fibre filaments, which generally contain in the region of between 3,000 to 30,000 filaments [1]. The three main fibre types used in industry are discussed below and include glass, Kevlar/aramid and carbon fibres.

a. Glass is the most frequently used fibre to reinforce polymer matrices because of its high tensile strength (up to 4600 MPa), low density (~2.5 g/cm$^3$), excellent chemical, fire and heat resistance as well as low cost compared to other fibres. Electrical glass (E-glass) is the type most commonly used in industry, which has superior electrical properties and durability ($\sigma_u$ = 3450 MPa and E = 73 GPa [16]). High strength and stiffness glass fibre (S-glass) is comparatively more expensive ($\sigma_u$ = 4600 MPa and E = 85.5 GPa [16]) with greater alumina content [16]. Glass fibre composites are used for piping in the chemical industry and for marine applications due to their high wear and corrosion resistance. Unfortunately, glass fibres are highly abrasive, and adversely affect the machinability of GFRP composites.
b. Kevlar is the commercial name for aramid fibres (aromatic polyamide) [1, 4, 16]. They are characterised by high tensile strength and tensile modulus ($\sigma_u$ = 3720 MPa and E = 63-143 GPa) together with low density (1.44 g/cm$^3$) [17]. Stiffness can be as high as 125 GPa and although very strong in tension, they have very poor compression and shear properties. In addition to their superior impact, creep and fatigue failure resistance, aramid fibres can maintain their mechanical properties between -200 and 200 $^o$C [4]. Kevlar fibres are mostly used to increase toughness in brittle matrices for pressure vessels, automotive brakes, clutch linings and gaskets [4]. Cutting of aramid fibre composites requires tools to have a high degree of edge sharpness and a small cutting edge radius as they are capable of sustaining large deformation in bending with subsequent spring-back causing fuzzing of the machined surface [12].
c. Carbon fibres were first introduced in the 1960's [1]. In addition to having a low density (~1.6 g/cm$^3$), they have a wide range of modulii and tensile strengths which can be up to 3 times the stiffness of steel and 15 times the strength of construction steel ($\sigma_T$ is up to 5000 MPa) [18]. Carbon fibres can be short or continuous with either a crystalline, amorphous or part crystalline structure. Commercial carbon fibres are produced from precursors

including polyacrylonitrile (PAN) or pitch [18, 19]. The manufacturing process of carbon fibres with any of the aforementioned precursors is almost identical. It involves initially burning the non-carbon elements such as oxygen, nitrogen, and others from the precursor fibre. They are subsequently placed in a furnace in an oxidising atmosphere to produce either carbon fibres (80-95 % carbon) or graphite fibres at higher temperature (99% carbon) [1]. The properties of the fibres are determined according to the rearrangement of carbon atoms in the furnace. The PAN-based fibre is the most commonly used precursor as pitch-based carbon fibres have lower compressive strengths. Carbon fibres are broadly classified into three categories, namely general purpose (GP), high performance (HP), and activated carbon fibres (ACF) [18]. The general purpose type is characterised by an amorphous and isotropic structure, low tensile strength, low tensile modulus and cost. Conversely, the high performance variant has relatively high strength and modulus but is considerably more expensive. With activated carbon fibres, the presence of a large number of open micro-pores which can act as adsorption points limits its use. They are however utilised to produce environmental protection equipment such as water treatment units and gas masks. Table 2.1 details properties of the different carbon fibre types while Table 2.2 presents properties of carbon fibres classified according to their tensile strength and strength/modulus ratio [18].

| Type | Diameter (μm) | Tensile strength (MPa) | Tensile modulus of elasticity (GPa) |
|---|---|---|---|
| General purpose (GP) | (7 – 15) | 700 | 40 |
| High performance (HP pitch) | (9 – 11) | 5000 | 350 |
| High performance polyacrylonitrile (HP PAN) | (4 – 8) | 2000 | 200-800 |
| Activated carbon fibres (ACF) | (7 – 15) | 200 | 1500 |

Table 2.1: Properties of various carbon fibre types [18]

| Type | Tensile modulus (GPa) | Strength to modulus ratio % |
|---|---|---|
| UHM (ultra high modulus) | > 500 | - |
| HM (high modulus) | > 300 | < 1 |
| IM (intermediate modulus) | < 300 | > 1 |
| LM (low modulus) | < 100 | Isotropic structure |
| HT (high strength) | Tensile strength > 3 GPa | 1.5 - 2 |

Table 2.2: Classification of carbon fibres based on their tensile strength and modulus [18]

#### *2.1.3.2 Matrix systems for FRP composites*

In FRP composites, the matrix is used to support and bond the reinforcement phase, transmit and distribute external applied loads to the reinforcement, control chemical and electrical composite properties and forestall any crack propagation [3]. In addition, as the matrix normally softens, melts or degrades at a lower temperature than the fibres, it governs the maximum operating temperature for the composite part (i.e. PMCs cannot be used near or above the glass transition temperature $T_g$, at which many of its physical properties change/degrade abruptly [1]). The matrix phase can be pure or mixed with other materials (additives) to improve its properties (e.g. increasing the allowable operating temperature, improving mechanical properties such as stiffness, strength and impact/wear resistance).

Two groups of matrix materials commonly employed in FRP composites are thermoset polymers (e.g. polyester, epoxy) and thermoplastic (e.g. polyamide, PEEK). Thermosets consist of long chains of hydrocarbon atoms held together by primary covalent bonds while thermoplastics have secondary bonds which are relatively weaker. Thermosets remain rigid when heated and are quite strong and stiff but have poor ductility due to the lack of atomic mobility and superior cross-linking between their randomly arranged molecules [2]. The polyester matrix is widely used due to its lower cost but is mainly employed in glass fibre composites. With carbon fibre based products, epoxies are usually selected for their lower shrinkage on curing, which allows high fabrication accuracy, superior mechanical properties and good environmental resistance. Epoxy resins can be used in various composite manufacturing techniques including press moulding, vacuum oven and autoclave curing processing, filament winding and resin transfer moulding. Since epoxies are relatively expensive and provide superior mechanical properties with moisture resistance, they are primarily employed for aerospace applications [1, 12]. Table 2.3 details the mechanical and thermal properties of a typical epoxy resin matrix used in CFRP composites against widely employed metallic materials such as cold drawn AISI 1020 steel and Al-7075-T6 aluminium alloy.

| Material | Epoxy resin | AISI 1020 steel (cold drawn) | Aluminium alloy (Al-7075-T6) |
|---|---|---|---|
| $\rho$ (g/cm$^3$) | 1.1 – 1.3 | 7.85 | 2.8 |
| E (GPa) | 2.6 – 3.8 | 207 | 71 |
| $\sigma_T$ (MPa) | 60 - 85 | 420 | 572 |
| Ductility (%) | 2 – 10 | 15 (minimum) | 11 |
| K (W/m$^o$C) | 0.17 – 0.2 | 51.9 | 130 |
| $C_p$ (kJ/kg$^o$C) | 1.05 | 0.48 | 0.96 |
| CTE ($10^{-6}$m/$^o$C) | 45 – 65 | 11.7 | 23.4 |
| $T_g$ ($^o$C) | 65 - 175 | - | - |

Table 2.3: Mechanical and thermal properties of epoxy resin against steel and aluminium [12]

*2.1.3.3 Description/nomenclature of FRP composite components*

The basic element of a continuous fibre composite part is a single unidirectional lamina/ply (shown in Figure 2.6), which behaves orthotropically [20]. This is typically fabricated either by prepregging, filament winding, pultrusion or resin transfer moulding (RTM) [1]. The properties of an individual lamina can be identified by the material supplier. These values provide the theoretical maximum for a given fibre/matrix volume of the individual lamina in the fibre direction, which in general is greater than those in the transverse direction. Mechanical property analysis gives the average properties of an individual ply based on its constituents, the relative amounts in the structure and the fibre/matrix bond [1, 4, 12]. The acceptable amount of voids in a composite component ranges between 1 and 5% of volume [12]. Voids reduce the overall density of the composite material and the difference between the actual and nominal/designed density is considered as the volume of voids present in the laminate [21].

The density for a composite part is calculated as follows [12]:

$w_c = w_f + w_m$ *weight balance* (1)

$\rho_c v_c = \rho_f v_f + \rho_m v_m$ *density x volume (weight)* (2)

$\rho_c = \rho_f V_f + \rho_m V_m$ *law of composite mixture* (3)

*Where;*

*Subscripts c, f and m refer to composite, fibre and matrix, respectively*

*w, v, $\rho$ and V refer to weight, volume, density and volume fraction, respectively*

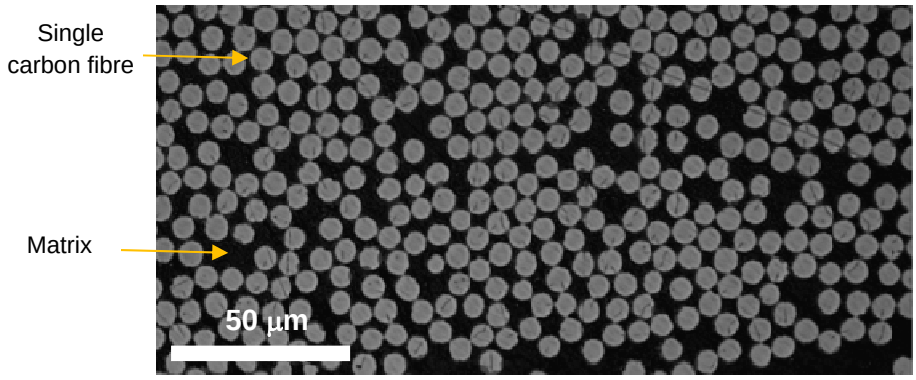


Figure 2.6: Microscopic image for cross sectioned CFRP laminate

Laminates are typically fabricated by stacking unidirectional or woven fabric layers at different fibre orientations according to the intended application [1]. For an *N* layer laminate, each ply has a distinct fibre orientation which is numbered from the top surface. The laminate is coded according to the angles of the reinforcing fibres within the plies from a reference axis ($0^o$), with either (+) and (-) signs representing the orientation (from the reference axis) of a single ply on the stack, as shown in Figure 2.7. The designation used for describing the stacking sequence of a FRP laminate includes brackets, parentheses, slashes and subscripts. Brackets "[ ]" are used to indicate all the fibre orientations present within a laminate (i.e. unit block) in accordance with the stacking sequence, while slashes "/" are used to separate layers or group of layers in a particular direction, designate repeated groups by a subscript *n*, where *n* is the number of repeated times and the subscript *s* (outside the brackets) denotes a symmetric laminate. A symmetric laminate should have an even number of plies with only half the layers quoted [3]. For example, $[0_2/90/90/0_2]_s$ refers to a laminate consisting of 12 plies, the first in the $0^o$ orientation and repeated twice and the laminate is symmetric with respect to a mid-plane. If the laminate is independent of fibre direction, or in other words, has equal number of plies at each principal fibre orientation (e.g. $[0/45/-45/90]_s$), it is known as a quasi-isotropic laminate structure.

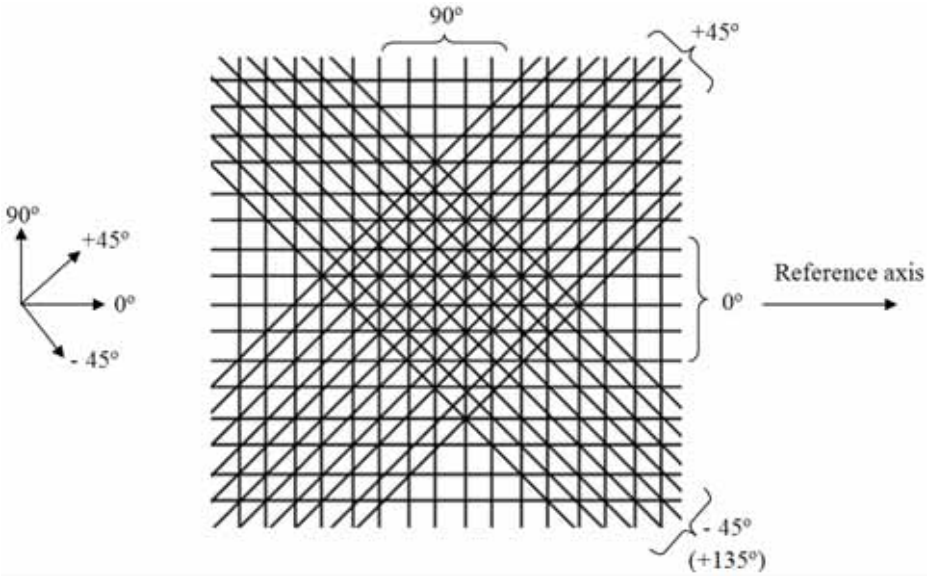


Figure 2.7: Different possible ply orientation for UD laminate layup

### 2.1.4 Carbon fibre reinforced plastic (CFRP) composites

#### *2.1.4.1 Manufacturing of CFRP*

As mentioned previously, various methods can be used for the manufacture of advanced composite components including vacuum bag moulding (oven cured), autoclave moulding, filament winding, press moulding, pressure bag moulding, thermal expansion moulding and pultrusion [12]. However, as oven and autoclave curing processes were the only methods used to fabricate workpieces for the current work, these are detailed in Appendix B.

#### *2.1.4.2 Properties of CFRP*

Carbon fibre reinforced plastic has relatively low thermal conductivity especially across the fibre direction (maximum of 1 W/mK as opposed to ~80 W/mK along the fibre direction) [22]. Table 2.4 details sample mechanical properties for a UD and woven carbon fibre composite laminate manufactured by the oven cured vacuum bag process. The unidirectional lamina has a 60% $V_f$ while the value is 55% for the fabric woven data. It is evident that the UD laminate has superior properties compared to the woven material. Table 2.5 details various mechanical properties for the most commonly used CFRP composites against equivalent GFRP and AFRP composites.

| Property | 145 gsm* 12k HTS5631 UD | 283 gsm 3k HTA5131 CF0604 5-HS Fabric |
|---|---|---|
| Tensile modulus (GPa) | 128.9 | 62.6 |
| Tensile strength (MPa) | 2159 | 927 |
| Compression modulus (GPa) | 123.2 | 59.4 |
| Compression strength (MPa) | 1330 | 729 |
| Flexural modulus (GPa) | 121.9 | 57.1 |
| Flexural strength (MPa) | 1958 | 1181 |
| * gsm is the fibre areal density in grams per square metre<br>12k indicates 12,000 fibres in each tow<br>5-HS fabric is five harness satin weave | | |

Table 2.4: Mechanical properties for carbon fibre laminate [5]

| FRP material | Tensile strength $\sigma_u$ (MPa) | Elastic modulus, E (MPa) | Strain to failure, $\varepsilon_u$ (%) | Density, $\rho$ (g/cm$^3$) |
|---|---|---|---|---|
| **CFRP** | | | | |
| Unidirectional ($V_f$ = 60%) High strength | 1,200 | 145,000 | 0.9 | 1.6 |
| Unidirectional ($V_f$ = 60%) High modulus | 800 | 220,000 | 0.3 | 1.6 |
| **GFRP** | | | | |
| Unidirectional ($V_f$ = 60%) | 1,000 | 45,000 | 2.3 | 2.1 |
| Woven cloth* | 100 - 300 | 10,000 – 20,000 | - | 1.5 - 2.1 |
| Chopped roving* (short fibres) | 50 - 200 | 6,000 – 12,000 | - | 1.3 – 2.1 |
| Sheet moulding compound* (short fibres) | 10 – 20 | 500 – 2,000 | - | 1.3 – 1.9 |
| **AFRP** | | | | |
| Unidirectional ($V_f$ = 60%) | 1,000 | 75,000 | 1.6 | 1.4 |
| * For these materials $V_f$ = 20 – 50% | | | | |

Table 2.5: Mechanical properties for the common CFRP laminates against GFRP and AFRP composites [2]

#### *2.1.4.3 Health and safety aspects*

Processing of CFRP requires special precautions/considerations due to the potential hazards presented by the dust and fumes produced during decomposition or cutting. The current body of evidence suggests that in all likelihood, carbon fibres are not carcinogenic but may cause irritation, coughing and pulmonary edema. Table 2.6 details the identification of general hazards relative to different composite material elements [23]. Critical values of exposure to carbon fibre and epoxy resin are presented in Table 2.7. Special precautions are usually required when handling CFRP which include:

- Electrical equipment, enclosures and circuits in or near areas where carbon fibres are used should be protected against infiltration or contact with airborne particles.
- Store carbon fibre products in original containers and avoid conditions that may generate carbon dust or lint.
- As with all industrial products, selection of specific personal protective equipment (e.g., gloves, disposable, clothing, respirators) and general control (e.g., local exhaust ventilation) depends upon the type of operation and exposure potential. To avoid ingestion incidental to handling, food and tobacco should not be present in the work area. Wash exposed skin areas with soap and water after contact.

| Composite component | Organ target | Possible health effect |
|---|---|---|
| Epoxy resins | Skin, lungs and eyes | Contact and allergic dermatitis, conjunctivitis |
| Carbon fibres | Skin and lungs | Skin and respiratory irritation, contact dermatitis (chronic interstitial lung disease) |

Table 2.6: Identification for expected hazards [23]

| Component | Type | Value |
|---|---|---|
| Carbon Fibre | ACGIH-TWA | 10 mg/m³ |
| | NIOSH-TWA | 3 fibres/cm³ for fibres less than or equal to 3.5 μm in diameter and greater than or equal to 10μm in length. |
| Formulated Epoxy Resin | TWA (Total) | 15 mg/m³ |
| | TWA (Respirable) | 5 mg/m³ |
| ACGIH: American Conference of Governmental Industrial Hygienists<br>NIOSH: The National Institute for Occupational Safety and Health<br>TWA: Time weighted average | | |

Table 2.7: Critical values of exposure [24]

Machining of FRP composites generally produce high emissions of dust and gases [25]. More specifically when cutting CFRP, clumps of material comprising resin with embedded fibres are normally produced. Commercially available engineering dust extraction systems are capable of filtering out particles down to 0.3 μm, which is much smaller than the size of typical carbon fibres which is ~6 μm diameter. Furthermore, as the diameter of these fibres are > 3 μm, they would not normally be respirable [26]. Additionally, in a study on aerosol emission when milling FRP, a maximum fibre concentration of ~3 mg/m$^3$ was reported, which was found to be within the safe respirable limit (5 mg/m$^3$) [25]. Additional information relating to material safety data sheet for CFRP can be found in Appendix C.

## 2.2 Titanium alloys

### 2.2.1 Introduction

Over the last few decades, the use of titanium and its alloys has expanded in many industrial sectors including automotive, aerospace, petroleum refining, pulp and paper, food processing and marine due to their superior properties [27]. These include high specific strength combined with exceptional fracture and corrosion resistance even under extremely aggressive environments [28]. Hardness and strength can generally be enhanced by increasing the alloying elements, albeit with a corresponding decrease in ductility [29]. Titanium alloys can be classified according to their alloying elements (stabilisers) and metallurgical features into three main groups namely, hexagonal close-packed α and near α alloys, body-centred cubic β alloys and α–β alloys [27]. Stabilisers are normally added to improve physical and mechanical properties of the alloy [30]. Table 2.8 details a list of commercial titanium alloys according to this classification system. The most commonly used group of titanium alloys is the α–β group.

| α and near α alloys | β alloys | α–β alloys |
|---|---|---|
| Ti-5Al-2.5Sn | Ti-3Al-8V-6Cr-4Mo-4Zr | Ti-6Al-4V |
| Ti-8Al-1Mo-1V | Ti-10V-2Fe-3Al | Ti-4Al-2Sn-4Mo-0.5Si |
| Ti-6Al-5Zr-0.5Mo-0.25Si | | Ti-6Al-2Sn |
| Ti-6Al-2Sn-4Zr-2Mo | | |

Table 2.8: A list of typical commercial titanium alloys

### 2.2.2 Properties and applications of Ti-6Al-4V

Alloy Ti-6Al-4V is generally regarded as the 'workhorse' of the titanium industry and accounts for ~ 60% of the total titanium alloy production [30-32]. Four heat treatments are typically used for Ti-6Al-4V including mill-annealed, recrystallise annealed, beta annealed or solution treated and aged [33]. The mill "partial" annealed alloy (general purpose treatment) is popular due to its moderate fracture toughness (66 $MPa.m^{1/2}$), high fatigue resistance and superior strength at relatively high operating temperatures (900 MPa at up to 400$^{o}$C) [33]. Ti-6Al-4V is widely used for applications such as rocket motor casings, aircraft components involving blades and discs for turbines and compressors, fuselage, wings, tail assembly structures, as well as for applications involving medical prosthetics/implants, chemical equipments, sports goods, forgings and fasteners, pressure vessels, marine components and steam turbine blades [30, 33-36].

## 2.3 Aluminium alloys

### 2.3.1 Introduction

Aluminium alloys are used for a broad range of applications in the aerospace, automotive and food processing sectors due to their superior combination of properties. These include low density (2.6 - 2.8 g/cm$^3$), coupled with relatively high strength (e.g. yield and ultimate strength of Aluminium 2014-T651 is 414 and 483 MPa, respectively) [30]. Aluminium alloys are classified using a numerical series designated by a four digit identification code in accordance with the International Alloy Designation System (IADS).

This classification divides aluminium alloys into groups based on the principal alloying elements as follows [30]:

- 1xxx: Pure unalloyed aluminium, used mainly in electrical and chemical industries.
- 2xxx: Copper is the principal alloying element and is widely used in the aircraft sector.
- 3xxx: Manganese is the prime alloying element, typically used for architectural applications.
- 4xxx: Silicon is the main alloying element, used for welding rods and brazing sheets.
- 5xxx: Magnesium is the principal alloying element, used in marine applications.
- 6xxx: Magnesium and silicon are the principal alloying elements and are widely used for marine and automotive applications.
- 7xxx: Zinc is the principal alloying element and is commonly used in aircraft structural components and high strength applications (strongest series alloys).
- 8xxx: Series of alloys with miscellaneous compositions, e.g. tin, lithium or iron.
- 9xxx: Reserved for future use.

In addition, each series is followed by a temper designation which typically comprises a letter followed by one to four digit numbers (e.g. Al-7150-T651, used for wing structures of the Boeing 767 and 757 planes [37]). This indicates the treatment of the alloy (e.g. F “as fabricated” and T “heat treated”) and the numbers refer to the secondary treatment used to influence properties [30].

### 2.3.2 Properties of Al-7050-T7651

Al-7050-T7651 is a high strength aluminium alloy commonly used in aircraft structures due to its high resistance to corrosion and stress-corrosion cracking, high fracture toughness and fatigue resistance. Table 2.9 lists the mechanical properties of Al-7050-T7651 alloy against Ti-6Al-4V.

| Property | Ti-6Al-4V | Al-7050-T7651 |
|---|---|---|
| Density ($g/cm^3$) | 4.43 | 2.83 |
| Hardness (HV) | 340 | 171 |
| Ultimate tensile strength | 950 MPa | 515 MPa |
| Yield strength | 830 MPa | 455 MPa |
| Modulus of elasticity | 114 GPa | 72 GPa |
| Shear modulus | 44 GPa | 27 GPa |
| CTE | 8.6 – 9.7 μm/mK | 25 μm/mK |
| Thermal conductivity | 6.7 W/mk | 154 W/mk |
| Chemical composition | 6% Al, >0.3% Fe, >0.2% O, 89-90% Ti and 4% V | 89% Al, 6% Zn, 2% Mg, 2% Cu and 1% other materials |

Table 2.9: Properties of Al-7050 and Ti-6Al-4V alloys [30, 34]

## 2.4 Machining of composites

### 2.4.1 Background

The machinability of composites differs from conventional materials and their alloys in many aspects such as chip formation, cutting tool requirements and operating parameters [38-40]. This is primarily due to the non-homogeneous and anisotropic nature of composites as well as the dissimilar mechanical and thermal properties of the reinforcement and matrix [2, 39, 41, 42]. For example, the different thermal expansion coefficients of the fibre and matrix material in FRP composites can result in thermal stresses causing deformation with a possibility of part damage. Separation of surface layer/delamination can also occur due to low interlaminate strength and high cutting forces [43]. Such detrimental forces can however be reduced/minimised through the proper selection of tool geometry/material and cutting parameters/conditions [12].

### 2.4.2 Machinability of FRP composites

Although the fabrication of FRP composites produces near net shape products, various machining operations including edge trimming, drilling, milling, routing, sawing etc. are often

still necessary to meet part quality/dimensional requirements and assembly needs [41-44]. Conventional machining of FRP composites requires tools with sharp cutting edges to cut/shear abrasive fibres effectively, while relatively low operating parameters are specified in order to achieve better surface quality and limit cutting temperatures [12]. Machining performance when cutting FRPs is dependent on the composite specification including fibre and matrix properties, fibre orientation, type of weave and curing conditions, in addition to appropriate selection of cutting parameters and tool materials/geometry [38, 39, 41, 42, 44-49].

#### *2.4.2.1 Effect of material properties*

Fibre orientation (commonly denoted by θ) has been found to be the main governing factor when cutting FRP's [50, 51]. It significantly affects cutting forces, torque, machined surface quality and chip formation [38, 39, 42, 48, 49]. Unlike metallic workpieces, material removal in FRP workpieces is typically the result of a series of mini-fractures owing to the brittleness of the material elements [52]. Wang et al. [48] were among the first to describe the various types of cutting mechanisms involved in chip formation observed when machining FRP composites and classified them into five categories, which were determined by the primary fibre orientation of the workpiece with respect to the cutting direction and tool rake angle. These were designated as delamination (Type I), fibre buckling (Type II), fibre cutting (Type III), deformation (Type IV) and shearing (Type V) [12, 48]. Type I was seen to occur when cutting parallel to the fibre direction ($\theta = 0^o$) with positive rake geometry as shown in Figure 2.8 (a). Following crack initiation at the tool tip, the damage propagates along the fibre/matrix interface. As the tool advances into the workpiece, the peeled layer slides up the rake face, causing it to bend in a manner similar to a cantilever. Bending-induced fracture then occurs ahead of the cutting edge perpendicular to the fibre direction. Small, discontinuous and irregular chips are typically produced under these conditions. Additionally, the cutting forces generally fluctuate with the repeated cycles of peeling, fibre bending, and fracture. Fibre buckling (Type II) however becomes prevalent when zero or negative rake angle tools are employed to cut along the fibre direction, see Figure 2.8 (b). Here, fibres are subjected to compressive loading along their axis resulting in buckling loads. Progress of the cutting edge causes cracks at the fibre/matrix interface and eventually fractures the fibres perpendicular to their axis under intense bucking. This also results in small discontinuous chips. While the fluctuation in cutting forces is smaller than that in Type I, the machined

surface is comparable. Fibre cutting or Type III mechanism occurs when θ is between $0^o$ and $90^o$, irrespective of tool rake angle. Here, the chip formation is a combination of fracture from compression induced shear across the fibre axis together with fibre/matrix interfacial shearing along the fibre direction. During compression, cracks are generated in the fibres above and below the cutting plane, with the latter remaining within the machined surface, see Figure 2.8 (c) and (d). Under these conditions, the chip morphology may be continuous or discontinuous. When cutting perpendicular to fibre orientation ($\theta = 90^o$), increasing inter-laminar shear leading to fracture of the chip segments along the fibre/matrix interface becomes the dominant chip formation mode (Type IV), see Figure 2.8 (e). Type V (shearing) occurs mainly at a fibre orientation of $105^o$–$150^o$ and is typically dominated by macro-fracture, see Figure 2.8 (f). As cutting progresses, severe fibre deformation occurs resulting in excessive inter-laminar shear along the fibre/matrix interface. Chip formation is then produced by the extensive elastic bending which results in cracks in both fibres and matrix producing relatively long chips. Here, the machined surface is irregular and the fibre ends have different lengths because fracture occurs at different points along their length. Elastic recovery also takes place following fibre shearing and leaves an irregular cut surface, see Figure 2.9 [49].

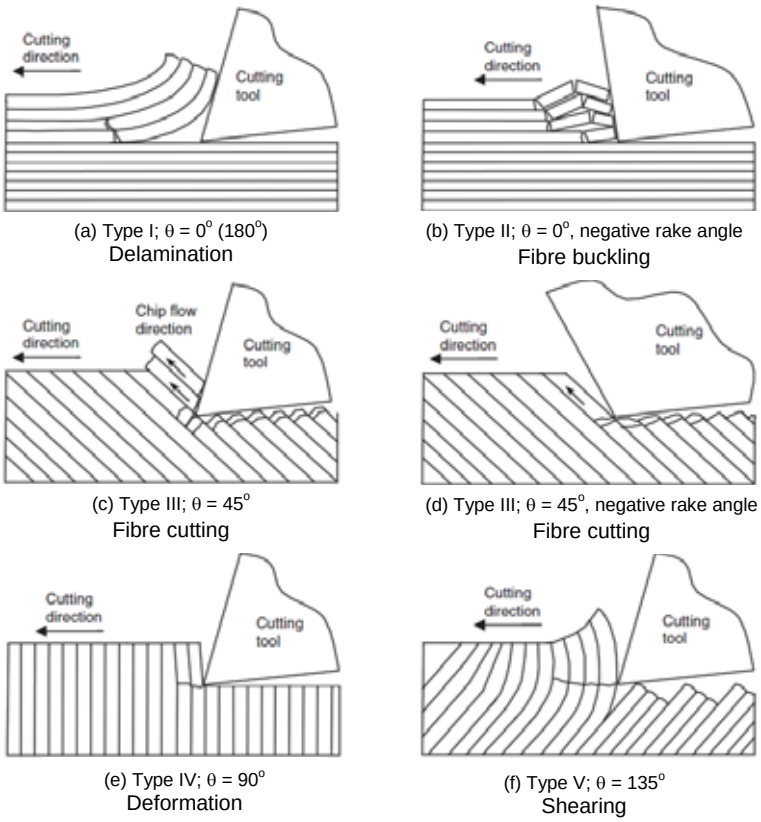


Figure 2.8: Cutting mechanisms in the orthogonal machining of FRP composites [48]

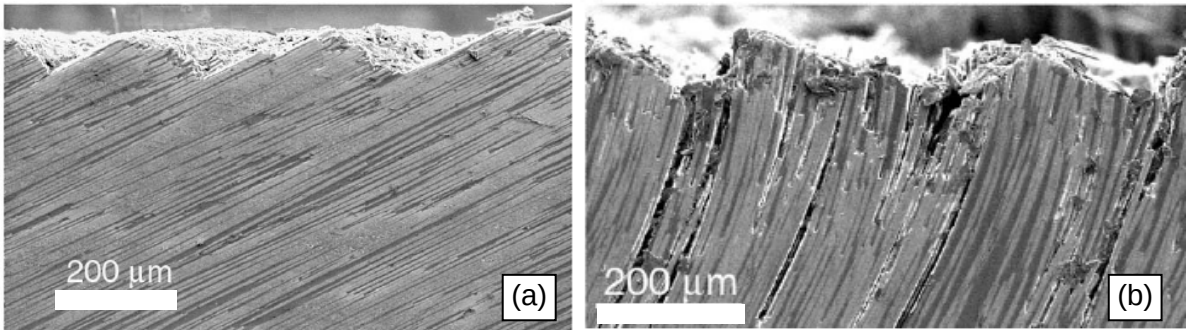


Figure 2.9: Microstructure when orthogonal cutting of graphite/epoxy composite: (a) $\theta = 150^{o}$ and 0.05 mm depth of cut and (b) $\theta = 120^{o}$ and 0.1 mm depth of cut [49]

Multidirectional (MD) FRP composites are commonly used in many applications similar to unidirectional laminates. When cutting MD composites, variations in cutting forces are common as the tool edge moves through different fibre angles throughout the composite workpiece [39]. The weave type also affects the machinability of FRP composites such that UD causes more damage in terms of the width of delaminated zone compared with a woven laminate when drilling CFRP [38].

#### *2.4.2.2 Effect of cutting conditions*

Feed rate has an overriding influence on cutting forces, which have been found to rise significantly with higher feed rates [38, 44, 47] for most machining processes. A high correlation has been reported between feed rate, thrust force and delamination when drilling GFRP [47]. Cutting speed on the other hand, has an overriding effect on tool life when turning CFRP using carbide tools [39, 46]. Increasing cutting speed and feed rate resulted in a rougher surface (up to 3 µm Ra) when milling CFRP whilst only feed rate was found to adversely affect workpiece delamination [45]. Feed rate also had a detrimental effect on surface roughness as an increase from 2 to 5 µm Ra was measured when the feed rate was raised from 0.05 to 0.25 mm/rev [41]. In contrast, cutting speed had no significant influence either on forces when drilling FRPs [38] or surface roughness when turning CFRP [41].

#### *2.4.2.3 Effect of tool materials/geometries*

Tool materials/geometries play an important role in relation to tool life and machined surface quality when cutting FRP composites. Polycrystalline diamond significantly outperformed WC tooling when employed in turning CFRP [41], see Figure 2.10. In separate studies, the use of CBN gave much longer life and lower surface roughness when turning CFRP than WC or conventional ceramic materials, (1.7 µm Ra for CBN whereas up to 4 µm

Ra for ceramic and WC) [46]. Employing positive rake angles also reduced surface roughness, especially when lower feed rates were used [41]. The use of standard point angle ($118^o$) increased the thrust force by 25% and reduced torque when drilling GFRP [44]. In contrast, when drilling GFRP, special drill formats including web thinning with an $85^o$ point angle and tripod "3 fluted" geometry drills also helped to reduce thrust force and hence delamination was controlled. Delamination factor, $F_d$ (detailed in the following section) was 1.04, 1.15 and 1.5 for tripod, web thinned tipped and conventional drills respectively [47].

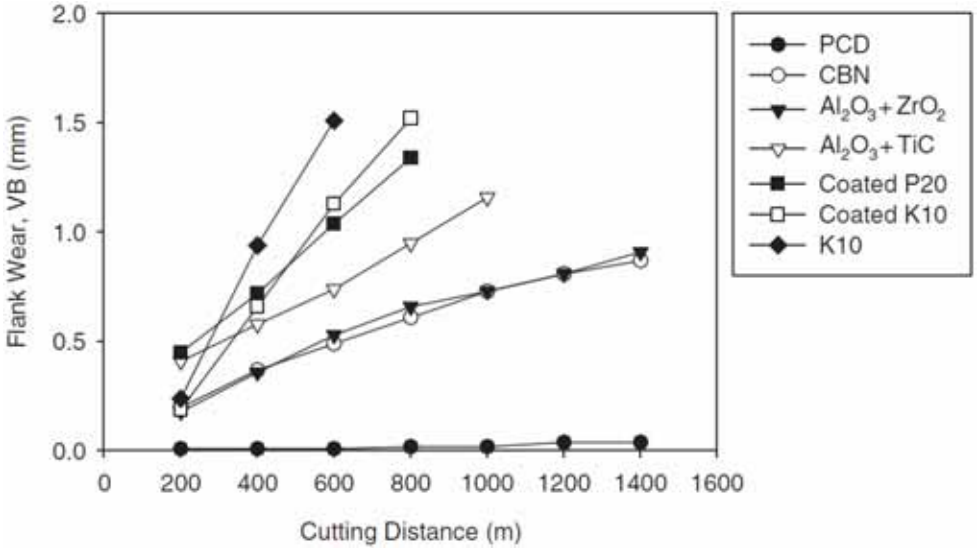


Figure 2.10: Flank wear results of different tool materials when turning CFRP [41]

## 2.5 Drilling of CFRP composites

### 2.5.1 Introduction

Standard twin lipped twist drills involving two main cutting edges and flutes are the most commonly used tools and are suitable of a wide range of applications. Other drill formats include step, candle, core, spade, centre, counter-boring and countersinking drills [53, 54]. Drill life is usually measured in terms of the number of holes produced prior to reaching the tool life criterion. Increasing tool wear produces greater levels of thrust force and torque, which can have a detrimental effect on hole quality/accuracy. Figure 2.11 depicts the terminology used for a standard twist drill.

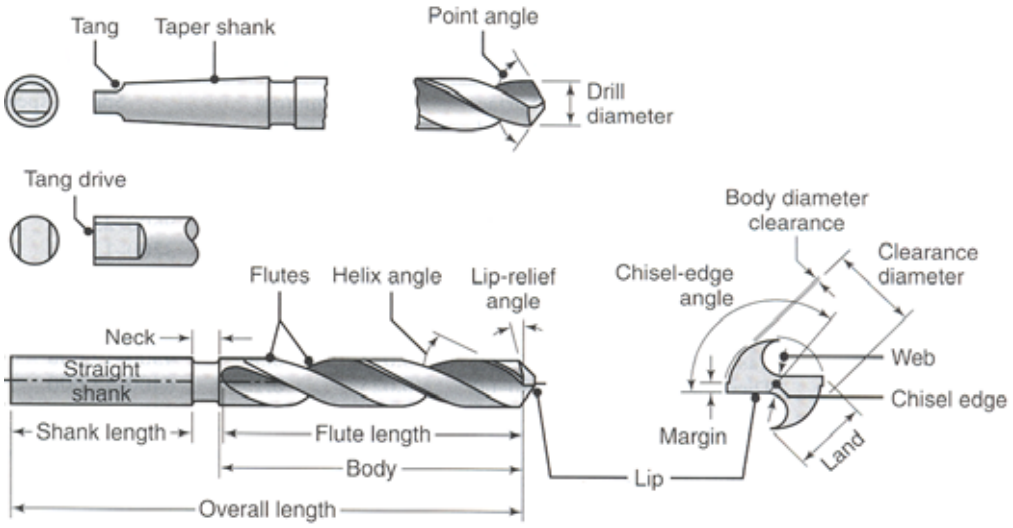


Figure 2.11: Twist drill terminology [53]

### 2.5.2 Twist drilling in CFRP

In many composite material related applications, mechanical joining methods are preferred to adhesive bonding due to the difficulty of disassembly for component inspection or repair, furthermore surface treatments may be required with the latter [20]. While incorporating holes in the part during the moulding stage would be desirable, it is generally unrealistic due to the inherent shrinkage that occurs in the curing stage and also as a consequence of the complexity of tooling, especially when many thousands of holes are involved (as is usually the case in small diameter hole-making) [55]. Difficulties are further exacerbated when considering complex shape components and the necessity of producing consistent laminate quality throughout the part (e.g. acoustic liners which are currently being developed for use in next generation aero-engine intake systems at GKN Aerospace, UK). Consequently, hole production is a key process in composite manufacture with drilling normally conducted as a post cure operation.

Drilling of CFRPs is not straightforward even with advanced diamond tooling as cutting is hampered by factors including fibre orientation and the type of weave [38, 56]. Since poor hole quality accounts for an estimated 60% of all part rejections [57], considerable attention should be given to all factors affecting the drilling of the composite material. Figure 2.12 shows a fishbone diagram that identifies all factors influencing output measures when drilling CFRP composites. Compared to more conventional workpiece materials, a larger number of factors must be considered when cutting CFRP due to the complexity of material structures,

due in part to the wide range of possible curing conditions. However, the factors in boxes have been highlighted for further investigation in small hole drilling of CFRP.

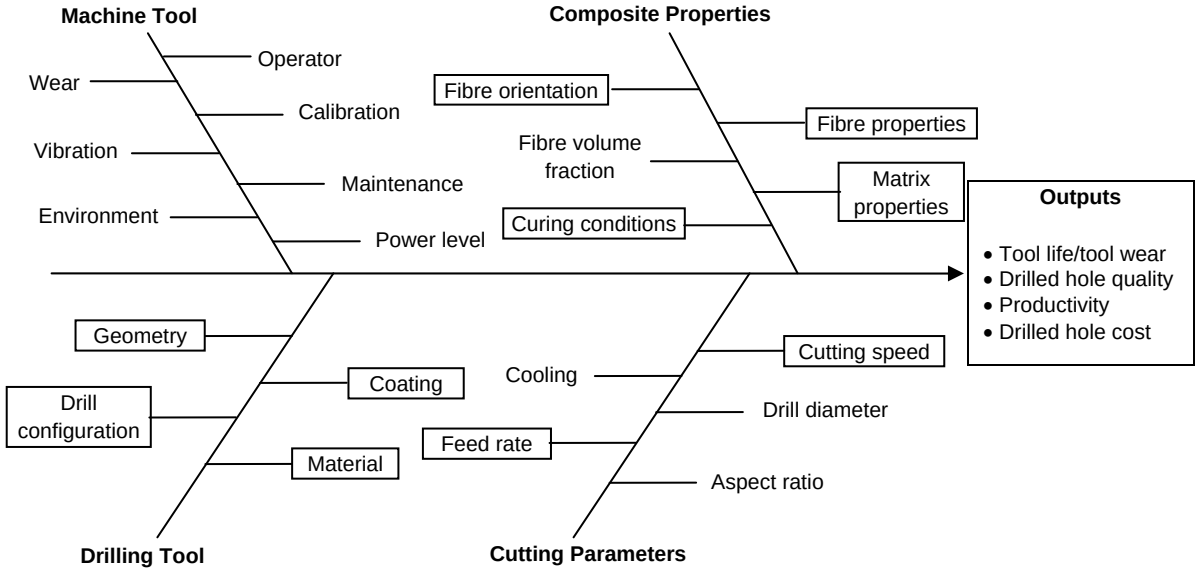


Figure 2.12: Fishbone diagram detailing factors affecting the drilling of CFRP

#### *2.5.2.1 Drilled hole quality*

Hole quality is arguably the most important measure when assessing drilling performance because it influences the service life of composite parts post assembly. Konig and Grass [43] described a methodology for assessing hole quality by classifying defects commonly associated with drilled holes in FRPs, see Figure 2.13. Here, quality criteria/categories include cracks, damage to surface layers, damage within a peripheral zone, workpiece surface roughness, hole roundness error and dimensional errors. Similarly, Abrao et al. [58] reviewed the main hole quality defects when drilling CFRP, which include surface delamination, fibre/resin pullout and inadequate surface roughness. Damage of surface layers is further subdivided into spalling, edge chipping, delamination and fuzzing. Additionally, defects when drilling CFRP composites have also been categorised not only in relation to the workpiece but also in relation to the tool [59]. Tool wear, the presence of powdery chips, workpiece surface delamination, internal delamination, fibre/resin pullout and decreased flexural strength significantly affect composite part strength and fatigue life. Whereas spalling was observed as the primary hole defect in a study by Zhang et al. [60], surface delamination was reported to be the dominant damage criterion when drilling CFRP in a number of other publications [52, 61-78]. Delamination is generally acknowledged to be the main reason for

stiffness/strength reduction in composite structures leading to catastrophic failure of the laminate under bending or shear loading conditions [58, 67]. Delamination can take two different forms, either push-out at the hole exit and/or peel–up at hole entry as illustrated in Figure 2.14. The former was found to be more severe and detrimental to component service life [71]. Peel up occurs at hole entry when the tool pulls away from the upper layer of the composite laminate resulting in separation and the formation of an entry delamination zone. As the drill approaches the bottom end of the hole, the uncut laminate thickness is no longer able to resist deformation and the tool acts like a punch which separates the thin uncut layer(s) from the remainder of the laminate [57]. Subsequently, push-out delamination initiates at the hole exit when the thrust force exceeds the interlaminar bond strength of the material [68]. Due to the high correlation observed between thrust force and delamination, Hocheng and Dharan [68] proposed relationships to calculate the critical thrust force at which the onset of push-out and peel-up delamination would occur, which are shown by Equation 4 and 5 respectively [68, 71].

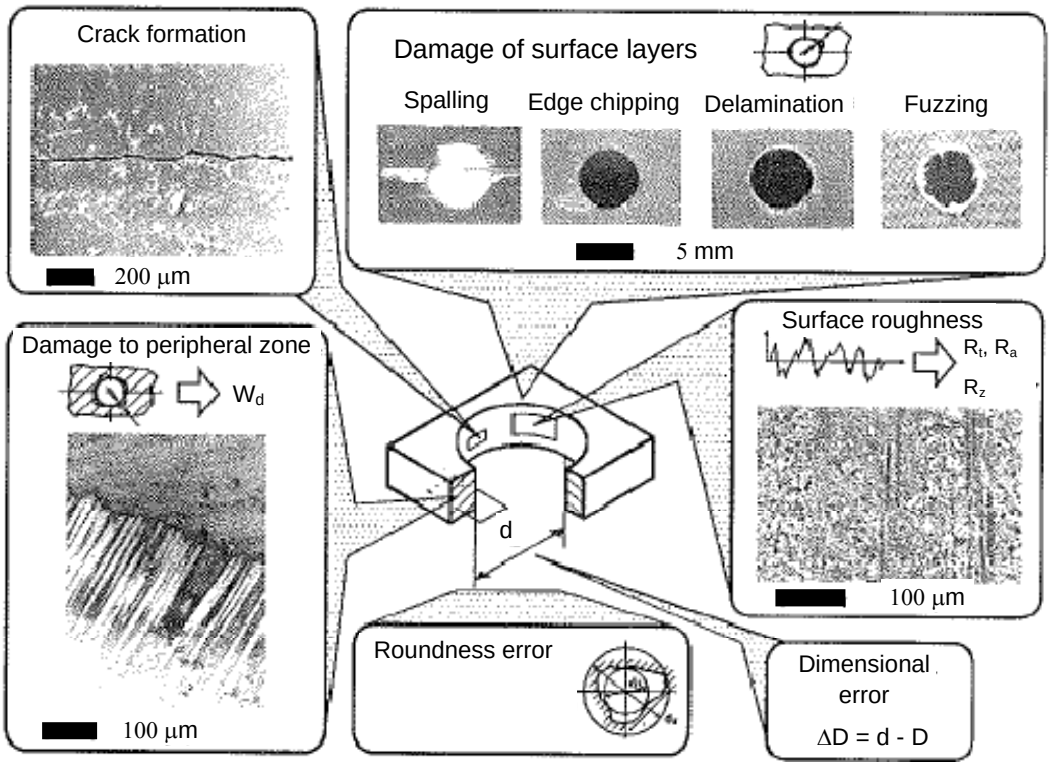


Figure 2.13: Quality criteria when drilling FRPs [43]

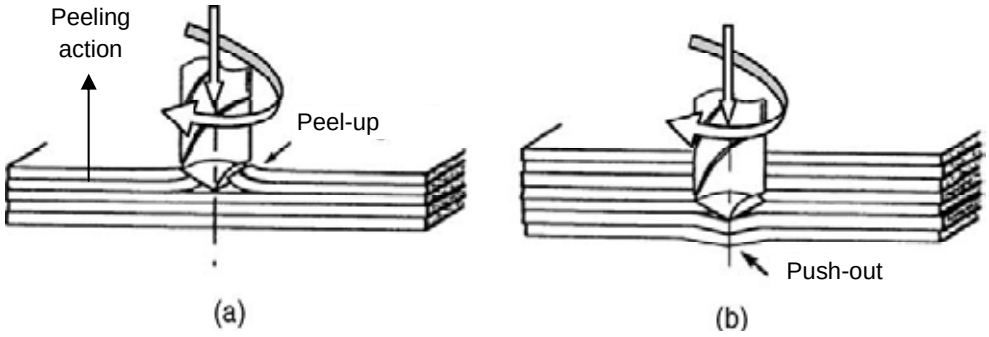


Figure 2.14: Delamination forms: (a) peel-up at entrance and (b) push-out at exit [68, 71]

$$F_A = \pi \left[\frac{8G_{1c}Eh^3}{3(1-v^2)}\right]^{1/2} \quad (4)$$

$$F_C = k\pi \left[\frac{8G_{1c}E(H-h)^3}{3(1-v^2)}\right]^{1/2} \quad (5)$$

where $F_A$ and $F_c$ are the critical thrust forces at which push-out and peel-up occurs respectively, $G_{1c}$ is the critical energy release rate for delamination, $E$ and $v$ are modulus of elasticity and Poisson's ratio, respectively, $h$ is the depth of material remaining to be cut under the tool, $H$ is the composite laminate thickness and $k$ is the peeling factor which is a function of the coefficient of friction between drill and workpiece and the drill helix angle.

Hole defects were also investigated by Zhang et al. [60] when drilling unidirectional and multidirectional CFRP using 4-facet point carbide drills (4.8 and 5.5 mm diameter tools). They found that spalling and fuzzing, as shown schematically in Figure 2.15, were the major exit defects, with spalling being more prominent. Additionally, the geometry of drill chisel and cutting edges were identified as the main cause of hole exit spalling which resulted in greater thrust force. An increase in operating parameters (rotational speed, feed rate/speed) and drill diameter further exacerbated spalling, with UD laminates seen to exhibit greater damage than MD laminates. A key finding of their work was the critical ratio of cutting speed to feed speed (both in units of mm/min) at which spalling was maintained below 1 mm. These were 5300 and 2800 for the UD and MD CFRP material respectively [60].

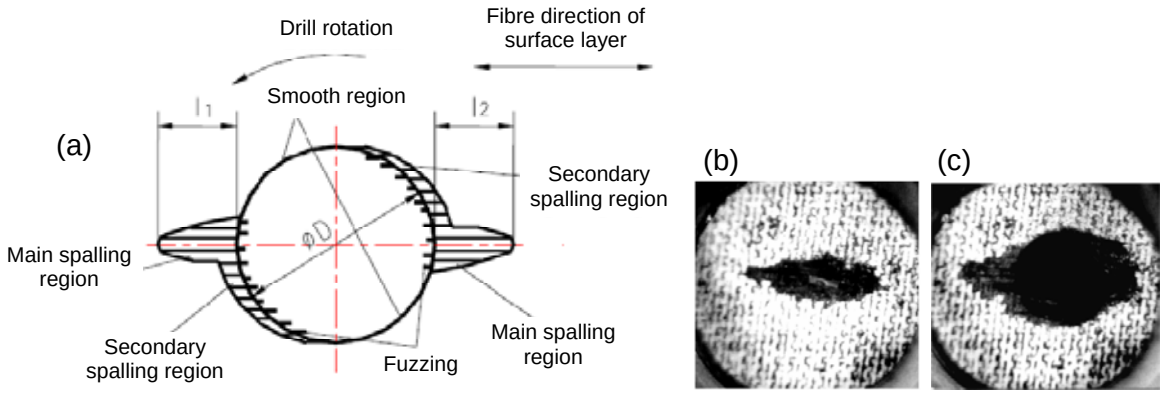


Figure 2.15: Spalling at exit surface when drilling MD CFRP: (a) schematic of spalling, (b) spalling at chisel edge penetration and (c) spalling after drilling [60]

Davim and Reis [62, 63] studied the delamination following drilling of woven CFRP using HSS and various cemented carbide drills. Their results were quantified in terms of a delamination factor ($F_d$), which is defined as the ratio between the maximum diameter of the damaged area to the required nominal diameter of the hole as illustrated in Figure 2.16. Their findings suggested that $F_d$ was larger with higher cutting speeds and feed rates, with the former being the more significant parameter affecting delamination. Conversely, when Tsao and Hocheng [73] investigated the effect of varying drill bits/configurations (conventional twin lipped, saw, and candlestick twist drills), cutting parameters and drill diameter on a similar workpiece material using Taguchi experimental design techniques, feed rate was highlighted as the most critical factor in terms of delamination when using conventional twist drills, while drill diameter was the significant factor with candlestick drills. With saw drills, feed rate, drill diameter and spindle speed were statistically significant, all three having approximately equal percentage contribution ratios (~ 33%). Chen [61] reported an increase in delamination factor with increasing number of holes drilled as outlined in Figure 2.17. Understandably, this was attributed to the growth in tool wear resulting in increased thrust force. Lin and Chen [70] found that during drilling of UD CFRP using carbide drills, improved hole quality was obtained when utilising low values of feed rate despite the relatively high cutting speeds used in the study. Enemuoh et al. [65] employed a combination of Taguchi experimental analysis and a multi-objective optimisation criterion to identify preferred drilling parameters (feed rate, cutting speed and drill point angle) with reference to delamination, surface roughness and thrust force. They observed that in order to produce delamination-free holes with good surface finish, high cutting speeds and low feed rates were necessary. Additionally, other researchers have found that in order to reduce entry

delamination, a combination of high cutting speed with small drill point angle and low feed rate is preferable when utilising cemented carbide drills [66].

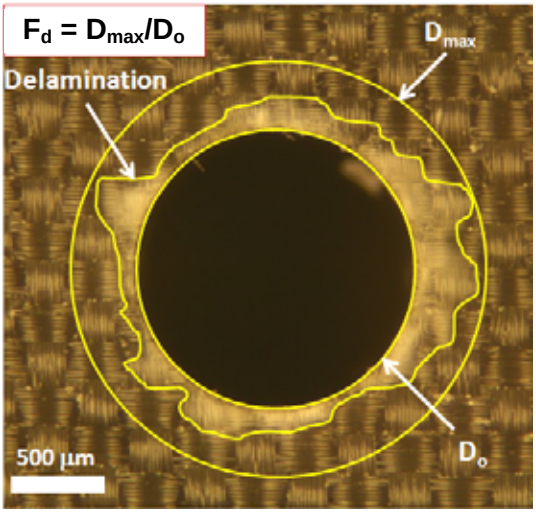


Figure 2.16: Schematic of delamination factor calculation

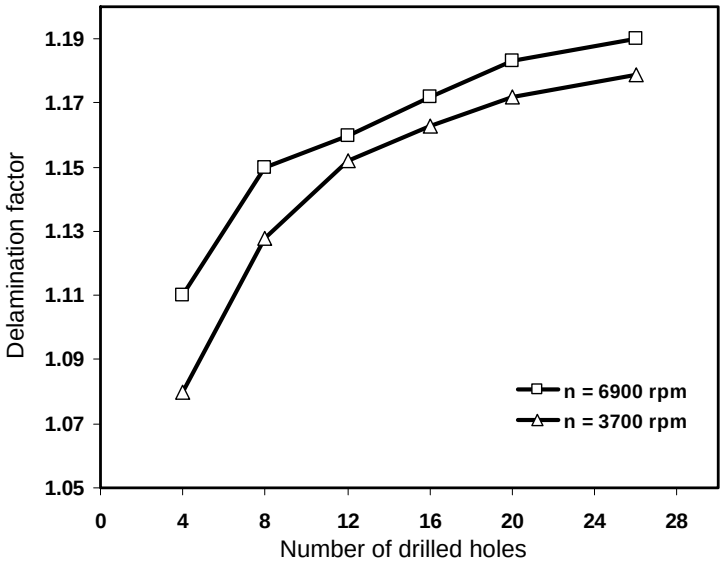


Figure 2.17: Correlation between delamination factor and number of drilled holes when using carbide drills for cutting CFRP [61]

The effect of tool wear on delamination when drilling 6 mm thick woven CFRP laminates was investigated by Tsao and Hocheng [79] using standard HSS twist drills under dry cutting conditions, at cutting speeds and feeds of 20, 30, 40 m/min and 10, 15, 20 mm/min respectively. Their findings showed that tool wear was the major factor affecting thrust force and hence delamination damage but also that the measured thrust force was greater than the predicted threshold for the onset of exit delamination as derived by Hocheng and Dharan [68].

More recently, work by Rawat and Attia [80] in drilling woven CFRP showed that even when using backup material on both sides, relatively high entry $F_d$ values were observed (up to 1.5 at 24 m/min and 0.8 mm/rev) and was attributed to the somewhat excessive feed rate used. Delamination was also evaluated by Davim et al. [64] who employed a digital image processing analysis technique when drilling CFRP laminates using conventional WC drills. The authors concluded that an 'adjusted' delamination factor ($F_{da}$) was more realistic, which was determined as a function of the actual/effective damage area. The advantage of the suggested measure is illustrated in Figure 2.18, where $F_d$'s for the two examples shown are identical, despite the obvious difference in damage. The calculation of the adjusted delamination factor is shown below:

$$F_{da} = \alpha \frac{D_{\max}}{D_o} + \beta \frac{A_{\max}}{A_o} \tag{6}$$

Where,

$$F_d = \frac{D_{\max}}{D_o} \tag{7}$$

$$\alpha + \beta = 1 \tag{8}$$

$$\beta = \frac{A_d}{(A_{\max} - A_{o)}} \tag{9}$$

$$F_{da} = F_d + \frac{A_d}{(A_{\max} - A_o)}.(F_d{}^2 - F_d) \tag{10}$$

where $A_o$ is the drilled hole area, $D_o$ the drilled hole diameter, $A_d$ the damaged area around hole, $A_{max}$ the maximum damage area, $D_{max}$ the maximum damage zone diameter, $F_d$ the traditional delamination factor, $F_{da}$ the adjusted delamination factor, $\alpha$ the traditional delamination factor weight, $\beta$ the ratio between the damaged area ($A_d$) and ($A_{max}$) - ($A_o$).

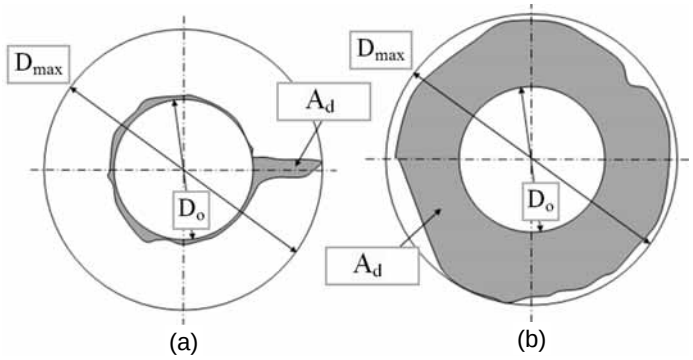


Figure 2.18: Examples of extreme delamination patterns when drilling FRP laminates: a) fine cracks and b) uniform damage area [64]

Tsao and Hocheng [69, 73, 74] carried out comprehensive investigations on the effect of different high speed steel drills on delamination when cutting CFRP. Diamond-plated core drills gave the lowest delamination damage followed by candlestick drills, saw drills and step drills, while the conventional twist drill produced the most damage as shown in Figure 2.19. All special drill types achieved higher values of critical feed rate before the onset of workpiece exit delamination compared to the conventional twist drill as illustrated in Table 2.10. In an investigation of tool materials and configurations, Davim and Reis [62, 63] reported that two flute cemented carbide helical drills introduced less damage than with four flute drills and that carbide products gave better performance compared to equivalent HSS tools. In addition, the brad & spur carbide drill design (similar to the candlestick configuration), produced less exit delamination than that for conventional helical flute drills. No reasons for this were given however it is likely that this was due to the avoidance of chisel edge 'push out'. In the Kungl Tekniska Hogskolan (KTH) drilling technique (analogous in part to trochoidal milling) detailed by Persson et al. [81], holes were machined axially and radially using a diamond coated core drill which is smaller in diameter than the required hole. They reported that the approach produced higher strength and fatigue life in composite parts when compared with results from drilling using conventional PCD tipped and carbide dagger drills. This was attributed to the reduction in thrust force due to the elimination of a stationary tool centre with little or no damage around the holes. In recent tests aimed at minimising induced exit delamination, Tsao [82, 83] introduced a new compound drill design known as the step-core drill with alternative step-core twist, step-core saw and step-core candlestick drills designs as shown in Figure 2.20. Results from his work showed that the former configuration exhibited less delamination and that a 0.74 diameter ratio between the internal

and external parts of the step-core drill gave lower delamination than with a corresponding 0.55 ratio tool.

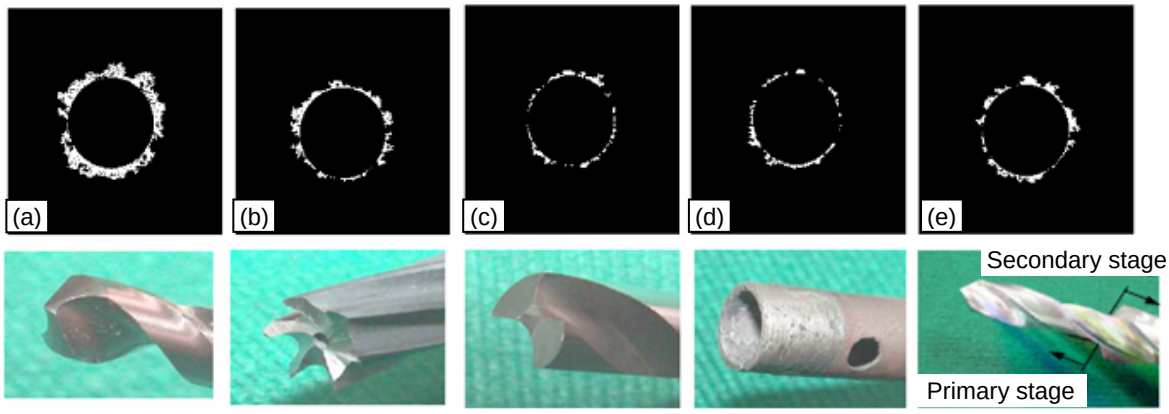


Figure 2.19: Various drill types/designs (diameter = 10 mm, spindle speed = 100 rpm, feed = 0.012mm/rev) (a) twist drill, (b) saw drill, (c) candlestick drill, (d) core drill, (e) step drill [69]

| **Drill bit** | **Critical feed rate (*$10^{-3}$ mm/rev)** |
|---|---|
| Core drill | 7.5 |
| Candlestick drill | 6.9 |
| Saw drill | 5.1 |
| Step drill | 4.9 |
| Twist drill | 4.7 |

Table 2.10: Critical feed rate for various drill bits [69]

(a) Step-core twist drill (b) Step-core saw drill (c) Step-core candlestick drill

Figure 2.20: Images for different step-core drills [82, 83]

Workpiece surface roughness when drilling CFRP can vary significantly depending on material properties, cutting conditions and tool geometries. In a study using candlestick drills, feed rate and spindle speed were the most influential parameters affecting the average surface roughness of drilled holes [84]. Hole surface roughness $R_a$ of up to 15 μm was measured following the drilling of CFRP using PCD drills and various carbide drills [85, 86]. Fibre orientation (with respect to feed direction) can also significantly affect surface roughness especially when $\theta = 135^o$, where fibres would be compressively loaded [38]. In terms of chip

morphology, the brittle nature of the epoxy and fibres regularly cause fibre breakage/pull out and matrix cracking during machining, and discontinuous chips are almost exclusively produced irrespective of the cutting conditions used [52].

#### *2.5.2.2 Cutting forces and torque*

The majority of published research has highlighted the strong correlation between thrust force and delamination, particularly at hole exit. Monitoring of thrust force has been shown to provide major benefits in drill wear assessment as well as minimisation of workpiece damage. Chen [61] reported that cutting speed had a negligible effect on thrust force and torque when drilling UD and MD CFRPs, while understandably, feed rate had a marked influence on both aspects, and was in agreement with study by Davim and Reis [62]. Similar results were also obtained by Tsao [82] and Won and Dharan [87] who analytically modelled the drilling of MD CFRP. Estimated thrust force results were in close agreement with experimentally measured data. Furthermore, the estimated allowable feed rate which resulted in damage free holes was 0.145 mm/rev when using 6.35 mm diameter carbide-tipped twist drills. This was because the thrust force was below the critical value for onset of exit delamination. Rawat and Attia [80] found that thrust force increased significantly with a decrease in cutting speed across the range of feed rate levels employed (0.02 – 0.8 mm/rev), while Jain and Yang [88] showed forces increasing significantly with drill diameter when cutting UD CFRP laminates using HSS drills. In work by Fernandes and Cook [89], thrust force and torque were shown to increase with spiral distance cut (associated with thicker material), which was understandable. A similar trend was obtained by Abrate and Walton [57] for thrust force in relation to the number of holes drilled, which was attributed to the chipping and wear of the cutting tool.

In an investigation of drilling UD laminates using HSS twist drills, Jain and Yang [90] found that chisel edge length had a significant influence on thrust force and workpiece delamination. Chen [61] found that larger point angles produced higher thrust forces with correspondingly lower torque levels, however both responses increased with an increase in web thickness, reduced helix angles and smaller chisel edge rake angles. Tsao and Hocheng [91] noted that core drills were preferable to twist drills as the thrust force tended to be uniformly distributed around the periphery rather than focussed at the drill centre and cutting edges, however manufacturing of small diameter core drills is extremely complex in practice. In terms of tool material, Wang et al. [92] reported that HSS drills induced higher thrust forces than carbide drills when drilling CFRP, however no indication was given as to why this

occurred. It is assumed that the results reflect the higher wear rate that would be expected with HSS. This was confirmed by tests undertaken by Malhotra [59] on 8 mm thick woven CFRP laminates using HSS and carbide drills with a feed rate ranging from 0.03 to 0.4 mm/rev. This suggested that carbide drills performed better than HSS drills in terms of tool wear and surface finish. Figure 2.21 shows thrust force and torque responses during the drilling of 4 mm thick quasi-isotropic CFRP and clearly identifies six distinct regions [93]. The work involved four straight fluted carbide drills incorporating a double point angle geometry. Maximum thrust force and torque occurred as the drill exited the laminate, although for the first few holes, maximum torque was registered when the second cutting edge corner (largest diameter location) entered the workpiece. In contrast to the profile obtained with the special tool design, thrust force increased steadily up to a constant value corresponding to steady state cutting when employing drills with standard geometries. This was followed by a sharp drop as the tool exited the hole. The torque was initially found to increase rapidly until the cutting edges engaged completely with the workpiece followed by a more gradual rise until a maximum value was reached owing to the increased friction between drill lands and hole wall [57]. Stone and Krishnamurthy [71] developed a neural network model to control thrust force (via variation of feed rate) when drilling a graphite/epoxy quasi-isotropic composite using PCD tipped drills. The model was trained during experimentation to forecast thrust force based on current and preceding feed rate levels together with previously measured thrust force data, which in turn resulted in the minimisation of workpiece delamination.

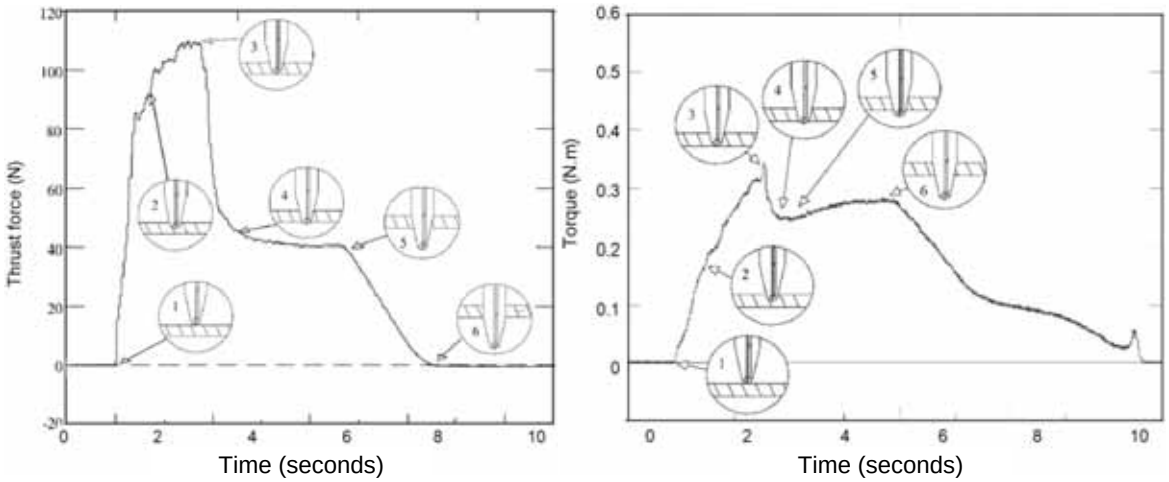


Figure 2.21: Thrust force and torque versus time plots for a single cutting operation [93]

#### *2.5.2.3 Methods for reduction of drilling forces*

It is evident that thrust force has a major influence on the incidence of delamination when drilling CFRP and extensive research has been carried out aimed at reducing drilling forces and hence workpiece damage. A widely employed strategy is the use of smaller pre-drilled/pilot holes prior to the main drilling cycle, such as that suggested by Won and Dharan [94] involving carbide tipped twist drills in combination with HSS pilot tools for drilling woven CFRP. The introduction of an initial pilot hole reduced the thrust force by ~ 65% during the subsequent primary drilling cycle as illustrated in Figure 2.22, due to the absence of interaction between the workpiece material and twist drill chisel edge. In addition, this approach allowed higher feed rates to be utilised without significant increase in thrust force, as shown in Figure 2.23. An investigation into the use of backup material (2 mm thick aluminium plate) revealed that delamination was inhibited when drilling woven CFRP using both saw and core drills, see Figure 2.24 [95]. Furthermore, such an arrangement permitted the use of higher feed rates and greater productivity before the onset of delamination, although at the expense of higher thrust forces. Additionally, Wang et al. [92] reported a reduction in thrust force of more than 50% when utilising vibration assisted drilling (at frequencies ranges from 100 to 500 Hz) with both carbide and HSS drills. They attributed this to changes in the mechanics of chip formation and the subsequent effect on cutting energy. A similar conclusion was reported by Arul et al. [96], see Figure 2.25. Special drill configurations were also tested by Piquet et al. [97], aimed at minimising the induced thrust force when drilling carbon epoxy composites. The work involved the use of straight fluted WC drills having three cutting edges with measurements of thrust force, torque and hole inlet/exit damage. The results showed that the bespoke drills produced less hole inlet/exit damage compared to conventional twin lipped twist drills together with reduced roundness error due to lower cutting edge loading.

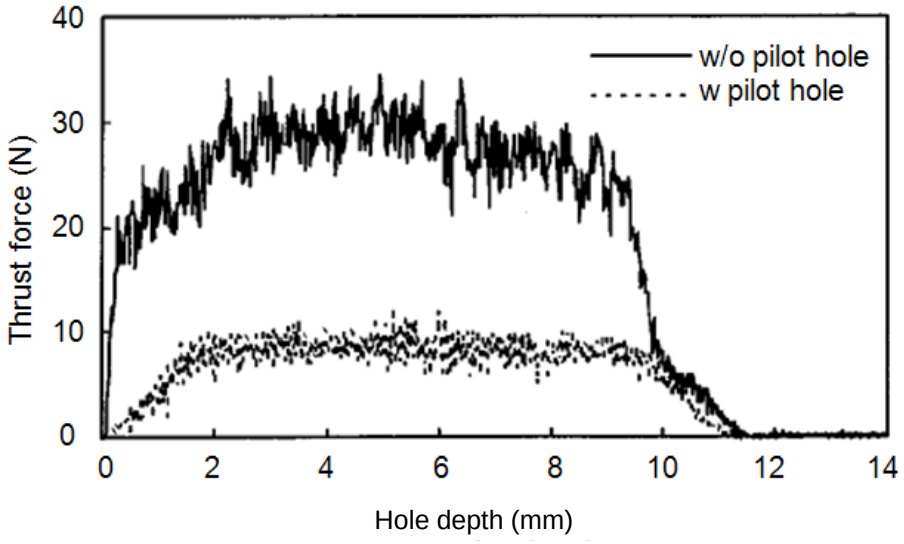


Figure 2.22: Thrust force curves with and without pilot hole [94]

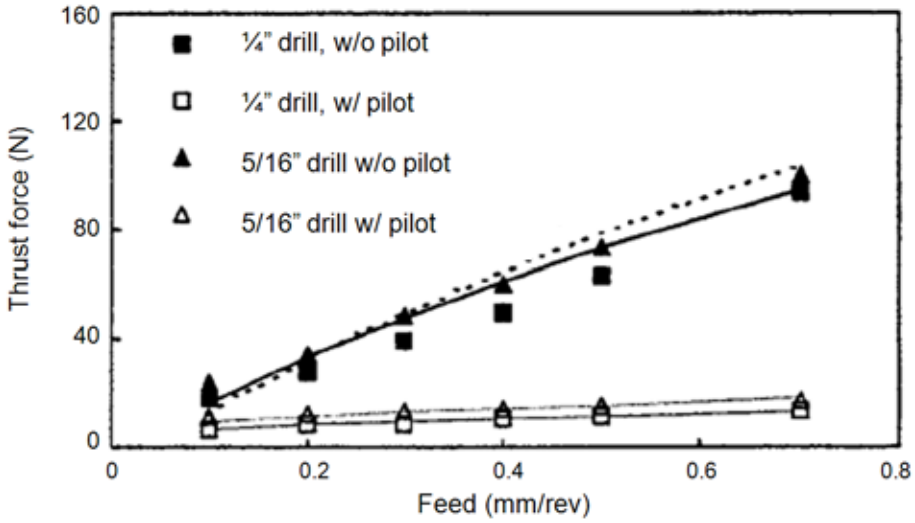


Figure 2.23: Measured and estimated thrust force values when drilling CFRP [94]

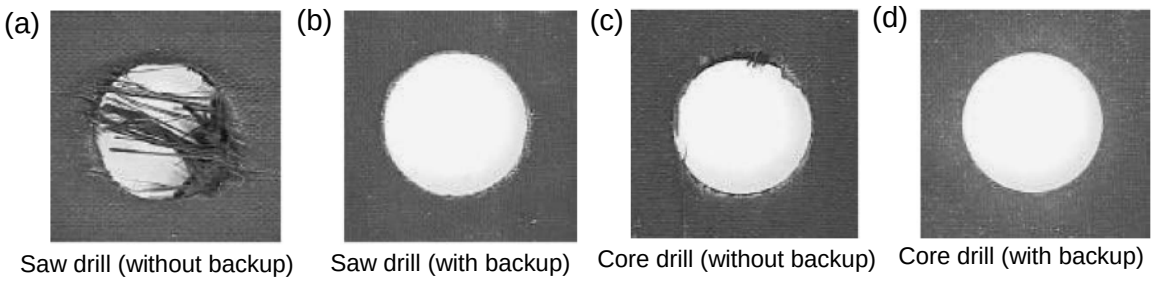


Figure 2.24: Drilling induced delamination (1000 rpm, 0.016 mm/rev): a, c: drilling without backup - b, d: drilling with backup [95]

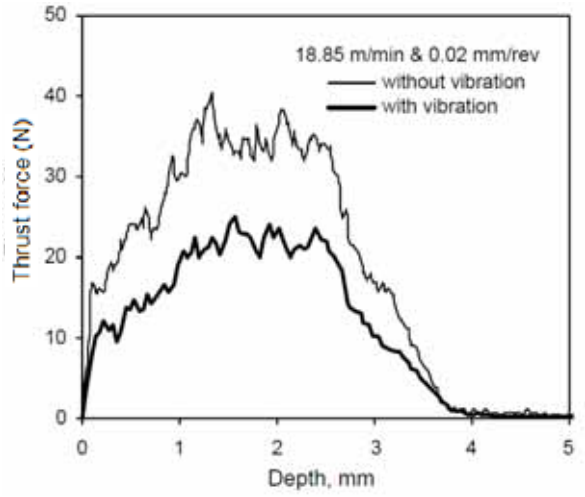


Figure 2.25: Comparison between thrust force when vibration assisted and conventional drilling [96]

#### *2.5.2.4 Tool life/tool wear and cutting temperature*

The most commonly used criterion to determine end of tool life is maximum flank wear ($VB_{Bmax}$) and is typically between 0.3 - 0.6 mm for metals, however there is no established tool wear criterion in relation to cutting FRPs composites [12]. When drilling CFRP, both flank and chisel edge wear is evident, which increases with the number of drilled holes, the former at a higher rate. The principal tool wear mechanism experienced when cutting FRP composites is abrasion with micro-chipping often present as a secondary wear mode [12]. Abrasion occurs when hard workpiece particles progressively indent/erode tool surfaces and remove tiny amounts of material from the cutting tool. In the case of FRPs, this is attributed to the highly abrasive fibres within the material. The presence of micro-chipping is generally a result of force oscillations due to the composites inhomogeneous nature. Unlike metal machining, diffusion wear is rarely seen when cutting FRPs due to the relatively low temperatures and pressures involved [98]. Gross fracture and edge chipping can also occur under interrupted cutting conditions due to the variation of mechanical properties between the reinforcement and matrix phase [12, 98]. The typical wear pattern observed however when cutting FRPs is severe edge rounding of the tool [12, 99] as shown in Figure 2.26.

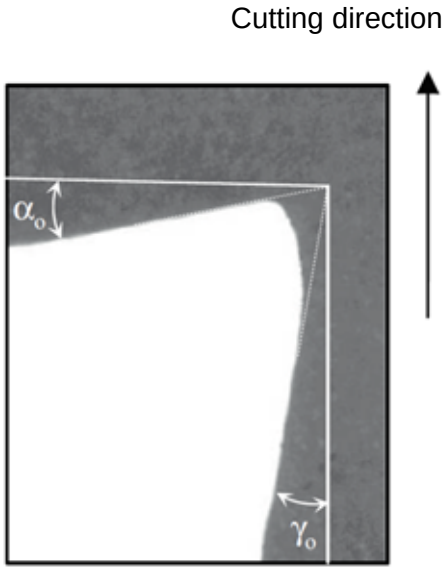


Figure 2.26: A cross section of a replica from a cutting edge when machining FRPs ($\alpha_o$ is the rake angle and $\gamma_o$ is the clearance angle) [12]

Davim and Reis [63] found negligible wear on carbide drills compared to HSS tools when drilling 4 mm thick CFRP plate, with the latter producing a wear scar of 0.012 mm after relatively few holes. Results from experimental work undertaken by Lin and Chen [70] relating to the effect of cutting speed on tool wear when drilling UD and MD CFRP laminates were comparable. Cutting speed ranged from 210 to 850 m/min whereas feed rate varied between 0.03 and 0.07 mm/rev using 7 mm WC conventional and multi-faceted drills. Both drill geometries however showed a significant decrease in tool life with increasing cutting speed. When using coated tungsten carbide drills, Murphy et al. [93] reported that TiN and diamond like carbon (DLC) coatings had no beneficial effect on reducing either delamination or thrust forces when drilling MD CFRP as detailed in Figure 2.27. Surprisingly, literature on the use of brazed and veined PCD or even CVD diamond coated tools for drilling composites is relatively scant, however the limited amount of published data indicates that superior workpiece surface roughness, lower workpiece damage and longer tool life when machining both UD and MD CFRP can be expected when compared with carbide and HSS tools [16, 48, 49]. Additionally, there is evidence that special drill configurations and geometries such as core, candlestick, straight flute and saw drills can provide significant tool life advantages [69, 100].

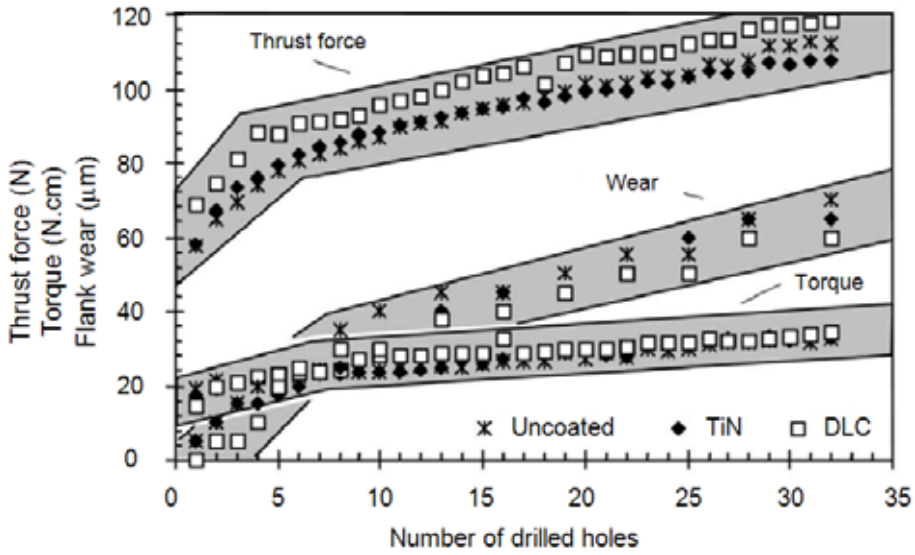


Figure 2.27: Effect of number of drilled holes on tool wear, thrust force and torque for uncoated, TiN and DLC coated drills when drilling CFRP [93]

Cutting temperatures exceeding 1000$^{o}$ C are not uncommon when machining metallic materials such as high strength nickel based super-alloys and titanium alloys, which have a highly detrimental effect on tool life [101, 102]. Considerably lower tool-workpiece interface temperatures are produced when machining FRP composites [61, 103], with the heat generated typically distributed at a ratio of 0.5:0.25:0.25 to the tool, workpiece and chip respectively [57]. No significant temperature change was recorded by Masuda et al. [103] when turning CFRP using WC tools despite the doubling of cutting speed from 100 to 200 m/min (increase from 220 to 260$^{o}$C). However, when drilling MD CFRP using HSS drills, flank surface temperatures increased significantly (generally ranging between 60 to 300$^{o}$C) with reducing feed rate and increasing cutting speed [61]. As feed rate was varied between 0.05 to 0.4 mm/rev at a cutting speed of ~ 23 m/min, the recorded temperature changed from ~120 to 60$^{o}$C respectively while for cutting speed, an increase from 40 to 200 m/min caused a rise in temperatures ranging from ~120 to 300$^{o}$C at a constant feed rate of 0.05 mm/rev, see Figure 2.28. Similar results were obtained by Rawat and Attia [80], where a flank surface temperature of up to 300 $^{o}$C was measured when drilling woven CFRP using two-fluted uncoated carbide drills at a feed rate and cutting speed of 0.06 mm/rev and 235 m/min, respectively.

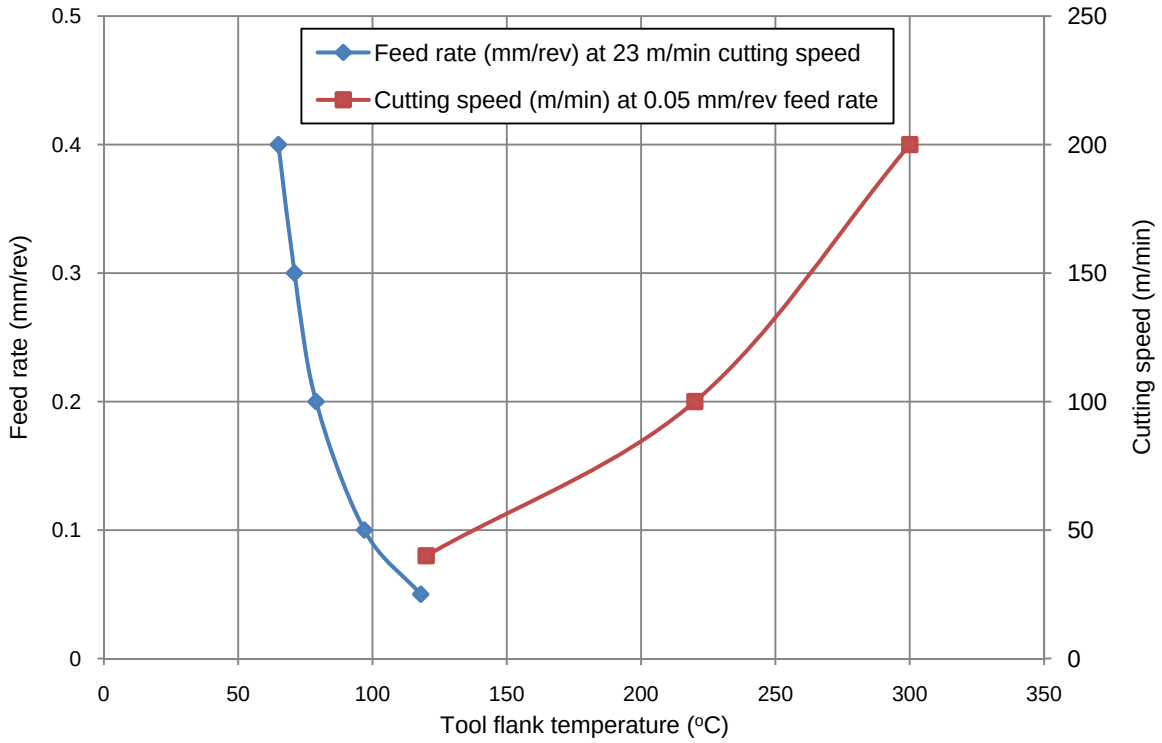


Figure 2.28: Flank temperature when drilling CFRP versus feed rate and cutting speed [61]

### 2.5.3 Alternative techniques for cutting small holes in FRP

The production of small holes less than 3 mm diameter is of considerable interest in many industries/applications, not least in the manufacture of printed circuit boards (~ 1 mm diameter), acoustic panels in aerospace components (~ 1.5 mm diameter), sports products and in medical prostheses (< 1 mm diameter). In addition to conventional twist drilling operations, a number of non-conventional machining processes including waterjet machining and laser drilling are also employed. Conventional drilling of small diameter holes in carbon fibre composites requires the use of moderate to high spindle speeds to achieve good hole quality. The majority of studies on the drilling of small holes in composites have involved glass fibre reinforced plastics with comparatively limited research conducted on CFRP. Drilling of 1 mm diameter holes in woven GFRP was investigated by Aoyama et al. [104] and Ogawa et al. [105]. Their results included surface roughness which was measured against edge position angle γ (the relative angle between the cutting direction and fibre direction as shown in Figure 2.29). Here, roughness value was found to be a maximum (~ 50 μm $R_{max}$) at an edge position angle of $\gamma = 30^{o}$. Furthermore, surface roughness typically increased with feed rate and rotational speed. The variation in $R_{max}$ in different fibre orientation reduced significantly as

the number of drilled holes increased as shown in Figure 2.30 (a) while hole damage increased with the latter, see Figure 2.30 (b).

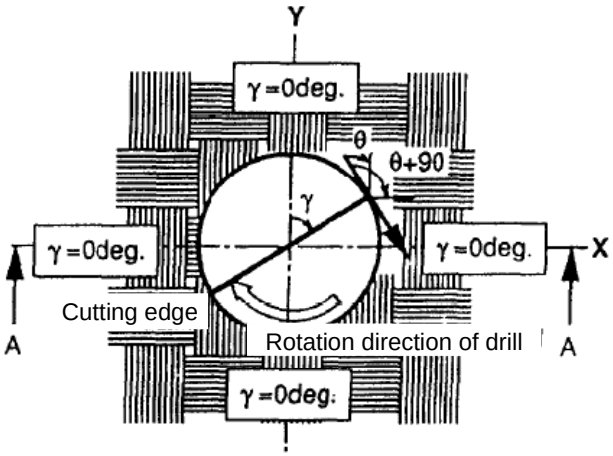


Figure 2.29: The definition of the edge position angle (γ) [104]

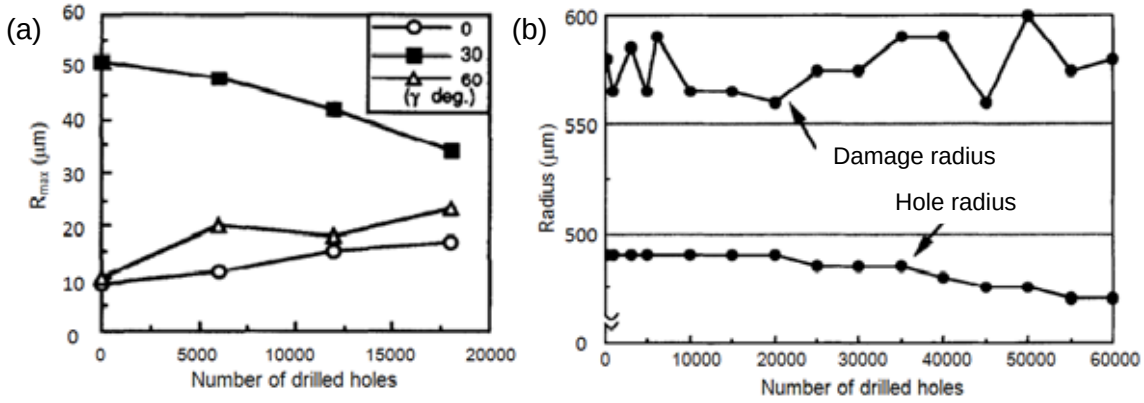


Figure 2.30: Number of drilled holes versus: (a) surface roughness and (b) hole damage [104]

Inoue et al. [106] evaluated the drilling of 1.6 mm thick woven GFRP using 0.4 – 5 mm diameter cemented carbide drills under high rotational speeds of up to 80,000 rpm and feed rates up to 0.05 mm/rev. Their results showed that the ratio of drill radius to yarn width was a significant factor affecting tool life. A maximum damage width of ~ 30 μm occurred at γ of $45^{o}$ – $60^{o}$ for the first hole while the anisotropy around the drilled hole decreased with increasing tool wear and number of holes. When using a 1 mm diameter drill, the damage width was approximately constant at all edge position angles following the $8000^{th}$ hole as detailed in Figure 2.31. Aoyama et al. [107] investigated the internal damage produced when drilling glass/epoxy printed wiring boards (PWB) using 1 mm diameter drills at a constant rotational speed of 5000 rpm and feed rate ranging between 5 and 63 μm/rev. Aluminium and bakelite plates were employed as stiffeners on the top and bottom surfaces respectively to

prevent drill run-out with the primary aim of minimising delamination at hole entry and exit. Internal damage width was seen to increase with the rise of surface roughness, fibre bundle thickness and feed rate. For the same fibre bundle thickness, a maximum damage width of ~100 μm occurred at an edge position angle of $\gamma = 45^{o}$, which was consistent with the conclusion of Inoue et al. [106].

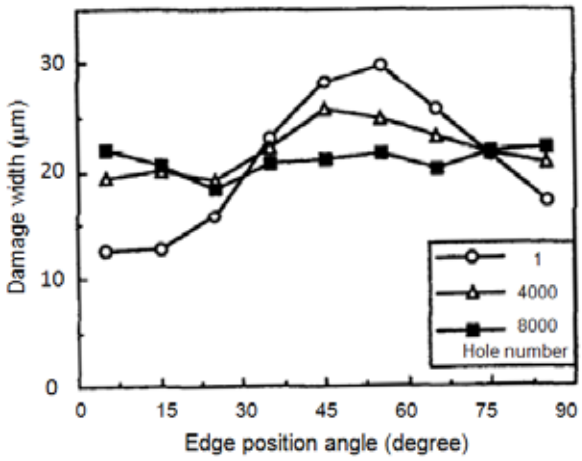


Figure 2.31: Damage width around the drilled hole (1 mm diameter, 80000 rpm and 50 μm/rev feed) [106]

Small hole production in CFRP was investigated by Wang et al. [92] using 0.5 mm diameter HSS and carbide drills, which were employed at a constant rotational speed of 22,000 rpm (35 m/min cutting speed) and feed speed of 50 mm/min. Low levels of thrust force were produced compared with results for larger drill diameters previously detailed in Section 2.5.2.2, and ranged from 2 to 4 N and 6 to 10 N for the HSS and carbide drills respectively.

Fibre reinforced plastics have also been machined using various non-conventional techniques although results to date have shown limited success especially in terms of machining time and production costs. It is therefore not surprising that such processes have yet to be adopted in industry to cut CFRP despite certain advantages/benefits.

A number of researchers have investigated the feasibility of using waterjet machining for the cutting of FRPs. An obvious advantage is the lack of thermal damage however, severe delamination and chipping is still present at hole exit, in addition to the relatively high cost and power consumption of the process. Shanmugam et al. [108] showed that abrasive waterjet (AWJ) machining produced superior surface roughness (6 - 7 μm Ra) compared to plain waterjet cutting of graphite epoxy composites (12 - 15 μm Ra). Kerf taper angles ($4^{o}$ – $6^{o}$),

burr formation and high surface waviness were the main problems recorded by Wang [109] when AWJ was utilised to cut a 3 mm thick polymer matrix composite material. Similarly, Lemma et al. [110] reported that average surface roughness varied between 3 and 8 μm Ra when cutting 10 mm thick UD GFRP laminates, while Miller [111] successfully employed micro-abrasive waterjet machining involving a 50 μm diameter jet to profile carbon fibre composites.

Vibration assisted drilling with frequencies ranging between 100 and 600 Hz was used to reduce thrust force (by ~50%) and minimise hole damage especially at the hole exit [92]. Arul et al. [96] succeeded in producing approximately 50 holes in 5 mm thick GFRP with HSS drills when using vibration assisted drilling while only 30 holes were achieved with conventional drilling for the same level of tool wear. In work by Linbo et al. [112] involving the drilling of 2 mm diameter holes in CFRP using HSS drills, machining and vibration variables were continuously altered during operation in response to the detected thrust force level. This technique succeeded in reducing exit delamination by over 50% compared to conventional vibration drilling.

Laser machining is another potential non-traditional process capable of drilling FRP composites, however, precise control of the focus position, feed rate and gas flow are required. Understandably, thermal damage is a key consideration in relation to the matrix phase where burning generates smoke and fumes. The process is also expensive due to the high power consumption and use of expensive gases (helium and argon), in addition to low productivity. Laser drilling was utilised by Young and O' Driscoll [113] to produce 50 μm diameter holes in 1.25 mm thick UD and woven CFRP, which resulted in a reduction of up to 30% of the workpiece specimen's stiffness based on subsequent tensile and compression tests. An area of resin damage (burn out) was present surrounding each hole as illustrated in Figure 2.32. Tagliaferri et al. [114] performed tests using a $CO_2$ laser with a 0.25 mm beam diameter to cut various composite materials including aramid, glass and graphite. In contrast to the glass and aramid based materials, the graphite/polyester composites experienced poor uniformity and surface morphology. This was attributed to the high vaporisation temperature and thermal conductivity of the fibres compared to the matrix material.

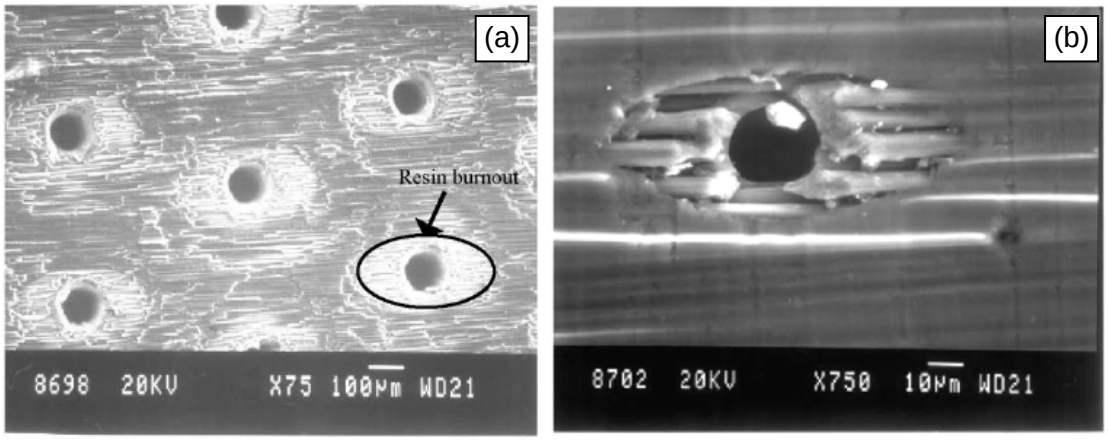


Figure 2.32: SEM image of perforated UD CFRP with resin damage on: (a) drilling side and (b) exit side [113]

The formation of a heat affected zone (HAZ) is one of the main limitations of laser cutting which has been shown to cause matrix recession/decomposition, disorientation and distortion of fibres, as well as delamination [115-117]. Pan and Hocheng [118] investigated the formation of a HAZ following laser grooving of 8 mm thick UD carbon/epoxy composite plates. Cutting was performed both in parallel and perpendicular to the fibre axis directions. Thermal damage led to poor assembly tolerances and long term deterioration. Furthermore, irregular holes that were slightly larger in diameter along the fibre direction were obtained. This was possibly due to the higher thermal conductivity of the composite parallel to the fibre axis, as shown in Figure 2.33 (a) [119]. Additionally, the matrix volatilised in the vicinity of the hole close to the top surface, allowing fibres in that region to curve upwards as highlighted in Figure 2.33 (b). Further analysis revealed a depleted matrix region together with a marked degree of fibre swelling, as an increase in hole diameter of up to 50% was observed, see Figure 2.33 (c). Other limitations and drawbacks when laser drilling FRPs include charred material [120], generation of smoke and fumes, elliptical hole sections, larger diameter exit holes, discontinuities in the profile at interfaces between adjacent layers [121], swelling of carbon fibres in the heat affected zone adjacent to drilled holes (fibre diameter increase ~ 50%) [119], taper angle of the kerf surface [122] and reduction of tensile and compression strength of the drilled part [113].

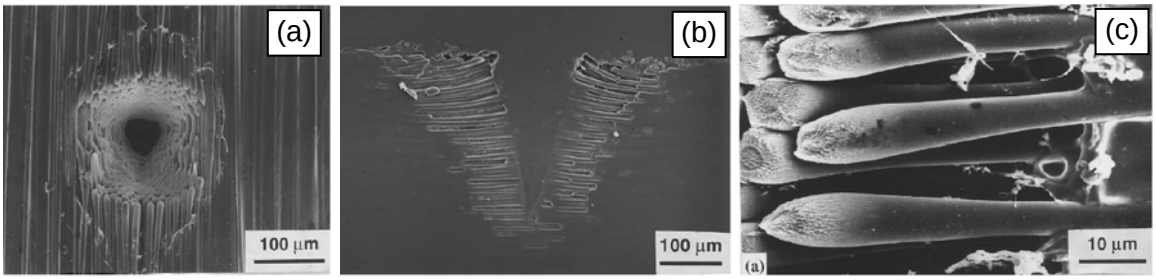


Figure 2.33: Various workpiece defects when laser drilling of CFR thermoplastic composites [119]

Although ultrasonic machining (USM) can be used for producing small features/holes in hard/brittle materials such as glass, ceramics, precious stones, etc, it is not a preferred technique for the machining of CFRP due to a number of limitations [123]. Problems associated with USM mainly relate to the accuracy of the setup and dynamics of the equipment [124], with low productivity a major shortcoming particularly in respect of single hole production [100]. In an investigation involving ultrasonic drilling of carbon fibre reinforced silicon carbide composites, Hocheng et al. [125] reported low material removal rate (2 – 10 $mm^3$/sec), where a 4.5 mm diameter x 2.35 mm deep hole took 15 seconds to produce. Delamination and fibre splintering was still apparent with the occurrence more severe at hole exit, see Figure 2.34. Additionally, tool wear was also cited as a problem (axial tool wear of up to 38.9 μm per hole), which caused changes in the resonance frequency of the tool and high values of hole clearance (up to 0.35 mm per hole with coarse abrasive grit). Unlike laser machining however, ultrasonically drilled holes are typically free of heat affected zones as well as thermal stresses and can be more economical than waterjet and laser drilling for simultaneous multi-hole production [125].

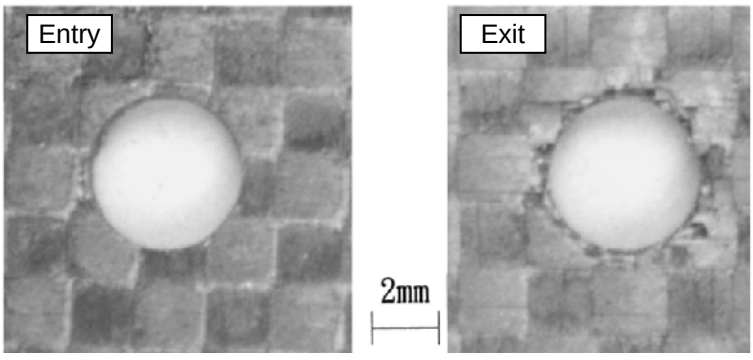


Figure 2.34: Entry/exit quality when ultrasonic drilling of CFR Si/C [125]

### 2.5.4 Modelling the drilling of FRP composites

The use of modelling techniques to investigate the drilling of fibre-reinforced composites has been the subject of considerable research in recent years. Although, the majority have involved analytical and empirical schemes, a few have utilised the finite element (FE) method to simulate drilling of fibre-reinforced laminates. Many models have been developed for the prediction of critical thrust force at which the onset of delamination occurs. These have included push-out and peel-up for hole exit and entry respectively [68] and linear fracture mechanisms by Tsao and Chen [126].

A comprehensive analysis based on the law of energy conservation and linear elastic fracture mechanisms was performed when drilling fibre reinforced laminates using various drill types including saw, candlestick, core, step, core-saw and standard twist drills in order to estimate the critical thrust force triggering the onset of delamination [69, 127, 128]. Findings showed that special drill types gave higher levels of critical thrust forces than standard twist drills which allowed the use of larger feed rates and hence improved productivity. The influence of pilot holes on delamination when drilling fibre reinforced laminates has been analytically modelled by Tsao and Hocheng [129]. The use of a pilot hole significantly reduced the thrust force by 25 – 50%, which was more than the reduction of the critical thrust (~ 11%). In related work, Tsao and Hocheng [95] developed an analytical model to predict critical thrust force when drilling of CFRP using backup material. They found that under such circumstances, higher levels of critical thrust force were predicted, which meant that greater feed rates could be employed while still maintaining delamination free holes. The effect of increasing drill eccentricity was studied analytically and was predicted to lower the critical thrust force, which necessitated to use of lower feed rates in order to avoid delamination [130]. More recently, Tsao [72] modelled the influence of inaccurate tool regrinding on workpiece delamination when drilling FRPs and found that drill deviation from its nominal geometry reduced the critical thrust force level and hence operational productivity. Empirical models based on experimental data have also been developed to estimate thrust force and torque when drilling CFRP [131]. In terms of computational techniques, a FE based simulation to predict the critical thrust force for the onset of delamination when drilling of quasi-isotropic CFRP was developed by Zitoune and Collombet [132]. The results from their model showed agreement with experimentally measured data. Predictive FE models for thrust force and torque have also been developed by Singh et al. [44] when drilling UD-GFRP. The

model was used to study the effect of drill point angle on drilling induced damage with outputs suggesting that a $90^{o}$ drill point angle produces less damage compared to drills with angles of $104^{o}$ and $118^{o}$.

## 2.6 Machining of titanium alloys

### 2.6.1 Overview

Titanium and its alloys are generally considered to have poor machinability [29] owing to their low thermal conductivity (7 W/mK for Ti-6Al-4V compared to 50.7 W/mK for AISI 1045 steel, [133]), high chemical reactivity, relatively low modulus of elasticity (114 GPa for Ti-6Al-4V) and high tensile strength (950 MPa for Ti-6Al-4V). The main problems associated with the machining of titanium alloys can be summarised as follows [134];

- High chemical reactivity resulting in diffusion and welding of the workpiece material to the cutting edge leading to rapid tool wear, chipping and premature tool failure.
- Poor dissipation of heat during cutting producing high tool/workpiece interface temperatures even at moderate cutting speeds.
- Retention of strength at elevated temperatures.
- Localised shear strains in the chip leading to the formation of serrated chips. Such chip morphologies can cause vibration/high frequency dynamic forces which coupled with high cutting temperatures produce micro-fatigue loading on the cutting tool resulting in severe flank wear and tool failure.
- High stresses due to the small chip/tool contact length (typically a third of that compared to cutting steel at similar conditions).

### 2.6.2 Cutting temperature when machining titanium alloys

Although alloying elements (e.g. aluminium and vanadium) present in titanium materials are incorporated to improve mechanical properties, varying the amounts of additives can however raise cutting temperatures [29]. An example of this was reported by Freeman [135] where the allowable cutting speed was reduced from 91 m/min to 53 m/min when oxygen content was raised from 0.13% to 0.2% (in order to maintain a cutting temperature of $900^{o}$C). Workpiece/tool interface temperatures of ~$1100^{o}$C are not unusual when machining Ti-6Al-4V alloy and 70 - 80% of the heat produced is conducted to the tool due to the low

thermal conductivity of the workpiece, see Figure 2.35 [27]. In comparison, the ratio when machining steels is approximately 50:50.

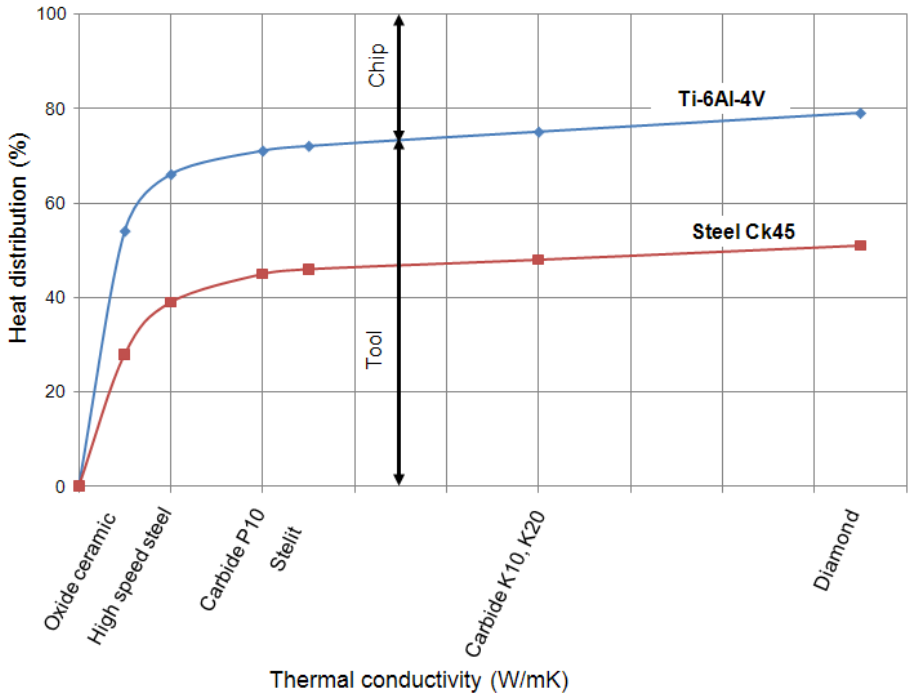


Figure 2.35: Distribution of thermal load when machining titanium and steel [27]

### 2.6.3 Tool wear when machining titanium alloys

The common modes of tool failure when cutting titanium alloys include notching, crater and flank wear, micro chipping and catastrophic edge fracture [134]. The inherent chemical reactivity of titanium alloys with all cutting tool materials has often resulted in dissolution/diffusion wear being the dominant wear mechanism, in addition to attrition and plastic deformation [136]. Uncoated cemented carbide (6% Co and WC grain size of 0.8 - 1.4 μm) and high speed steel tools are generally recommended for the cutting of titanium alloys with hardmetal coatings such as TiN and TiCN providing no significant benefits [134]. An investigation by Nabhani [136] showed that a TiN/TiC coating layer was rapidly removed when machining titanium alloy TA48, which exposed the WC substrate to crater wear. The performance of conventional ceramic tools ($Al_2O_3$) when machining titanium alloys is similarly poor due to their low thermal conductivity, low fracture toughness and chemical affinity with titanium [27, 133]. Limited research on using PCD has shown encouraging results with lower wear rates reported compared to other cutting tool materials when maintaining cutting temperatures below a critical threshold [134]. Conversely, Narutaki et al.

[133], showed that PCD performed poorly when used for machining titanium alloys due to their low fracture toughness and high chemical reactivity.

### 2.6.4 Cutting conditions when machining titanium alloys

In general, cutting speed has the most significant effect on the machinability of titanium alloys. High clearance and negative rake angles are generally preferred when cutting titanium alloys in order to reduce the contact between the tool flank face and workpiece. The use of cutting fluids are recommended, which act not only as a coolant to reduce tool and workpiece temperatures but also as a lubricant, thus lowering cutting forces and the incidence of chips welding onto tool cutting edges [134]. This also enables the use of higher cutting speeds when turning alloys such as Ti-6Al-4V [133]. Although most researchers recommend the application of cutting fluids when machining titanium alloys, studies employing dry cutting and minimum quantity lubrication (MQL) have received increased attention due to environmental and economic considerations [137, 138].

### 2.6.5 Chip formation and surface integrity when machining titanium alloys

Chip morphology has been found to be highly dependent on cutting speed, with discontinuous chips produced at low speed (60 m/min), and serrated chips at higher cutting speed (120 m/min) when turning Ti-6Al-4V [139]. Researchers have also reported continuous-serrated chips at 75 m/min cutting speed at low and high feed rates when turning the same alloy [140], see Figure 2.36. The formation of serrated chips was attributed to the high dynamic/cyclic cutting force while a continuous chip was associated with the static force component.

The quality or integrity of the workpiece surface/subsurface after machining can play a significant role in terms of the functional performance of a component, with heat affected zones, variations in hardness, micro cracks etc. adversely affecting fatigue performance. Such flaws must be avoided/minimised, particularly with safety critical components [14]. In terms of workpiece microhardness when turning Ti-6Al-4V, Che-Haron and Jawaid [141] highlighted an increase of ~ 20% in surface hardness at test cessation (up to 410 HV), which extended up to 0.5 mm beneath the machined surface. This was ascribed to the work/strain hardening effect when using worn tooling.

Average surface roughness (Ra) decreased from 1.4 to 1.04 μm as cutting speed was increased from 55 to 90 m/min when dry turning of Ti-6Al-4V using uncoated carbide tools

[142]. A further increase in cutting speed however (110 m/min) resulted in severe tool wear which in turn produced a poorer surface finish (up 3.5 μm Ra). The lower wear rate experienced by PCD tools translated to a superior Ra of 2 μm when cutting annealed TA48 titanium alloy compared with 11 μm Ra when using TiC/TiC-N/TiN coated carbide tools [136].

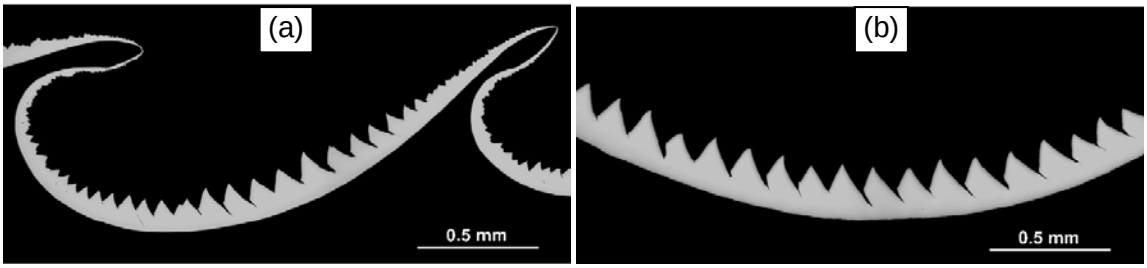


Figure 2.36: Continuous-serrated chips produced from turning Ti-6Al-4V at 75 m/min cutting speed and feed rate of: (a) 0.05 mm/rev and (b) 0.28 mm/rev [140]

### 2.6.6 Drilling of Ti-6Al-4V

A substantial body of research focusing on the drilling of Ti-6Al-4V has been carried out over the last few decades to investigate the effect of cutting conditions, tool geometries/materials and cutting environment on hole quality and process productivity [143-148]. In general, use of cutting fluid is deemed essential [144-147], however several studies have been conducted to evaluate the feasibility of dry or minimum quantity lubrication (MQL) machining [143, 144, 148]. Various types of burr formation were reported when dry drilling including rolled-back (at high feed rate and cutting speed) and uniform burrs, see Figure 2.37 (a). In contrast, only uniform burrs either with or without attachments (caps and rings) were observed when wet cutting as shown in Figure 2.37 (b) [144]. Burr height typically varied from 0.1 - 0.15 mm when operating at cutting speeds of 6 – 10 m/min and feed rates of 0.05 – 0.2 mm/rev with wet cutting [144], while higher values of up to 0.3 mm were measured under dry cutting conditions at 50 m/min and 0.07 mm/rev [143]. In addition, Dornfeld et al. [144] reported that a combination of tools with $30^{o}$ and $130^{o}$ helix and point angles respectively with high pressure coolant produced shorter burrs.

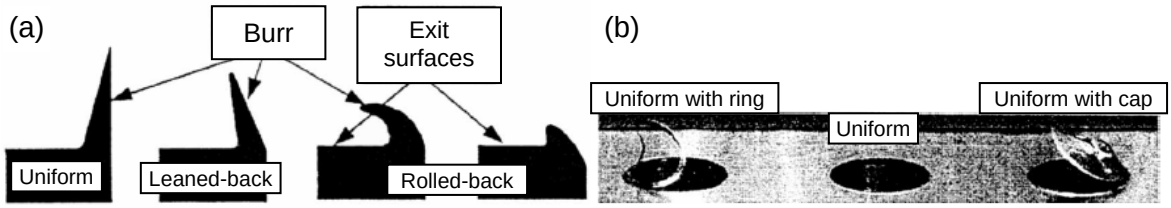


Figure 2.37: Burr types formed in: (a) dry cutting and (b) wet cutting [144]

When wet drilling through 20 mm thick Ti-6Al-4V using 6 mm diameter tools, Sharif and Rahim [147] reported that TiAlN coated drills outperformed their uncoated WC counterparts. The former produced longer tool life (25 holes at 25 m/min and 7 holes at 45 m/min) compared to the latter which wore very rapidly (only 1 hole at 25 m/min). This was attributed to the likely formation of a thin $Al_2O_3$ film that thermally insulated the cutting tool and reduced friction at the tool/workpiece interface. Increasing cutting speed had an adverse effect on tool life although Ra was generally below 1.3 μm regardless of the operating conditions. The difference in cutting temperature when drilling under MQL and wet conditions were studied using thermocouples embedded in the Ti-6Al-4V workpiece by Zeilmann et al. [148]. A temperature of 450$^{o}$C was recorded when operating at a cutting speed of 15 m/min, which increased to 550$^{o}$C when the speed was doubled to 30 m/min. Conversely, when flood coolant was employed via through holes in the tool, a temperature of 150$^{o}$C at 30 m/min was measured, which only increased to 300$^{o}$C at 50 m/min. In related studies by Li et al. [145] and Li and Shih [146] involving the use of ultra high cutting speeds (up to 183 m/min with feed rates up to 0.15 mm/rev) when drilling 6.35 mm thick Ti-6Al-4V plates with a special drill design (spiral point having 0.72 mm web thickness as opposed to 0.45 mm for conventional twist drills), extremely high cutting temperatures approaching 1210$^{o}$C were generated even for the first hole drilled under dry conditions. This value dropped by almost 50% to 651$^{o}$C when employing internal tool coolant. Maximum tool life of 204 holes was obtained at a cutting speed and feed rate of 91 m/min and 0.1 mm/rev respectively. In general, the spiral point drill performed better against the conventional twist drill in terms of tool life, thrust force, torque, workpiece surface roughness and burr height. This special drill however was not suitable for machining FRP composites as thinner web dimensions are typically required to reduce the effect of chisel edges on thrust force and hence minimise delamination. With regard to tool coatings, use of CrCN and TiAlN [148] led to moderately reduced cutting temperatures (~100$^{o}$C less) which was in agreement with results by Sharif and Rahim [147]. The lower coefficient of friction provided by the coatings was thought to be the

most likely reason for the observation. Reduction of thrust forces was also evident at higher cutting temperatures and reflected softening of the workpiece material. Additionally, adhesion (smearing) on hole surfaces was reported owing to the presence of plastic deformation at high cutting temperatures (> 500$^{o}$C) [148]. Smearing was also found on the drill rake face when dry cutting as shown in Figure 2.38 [143].

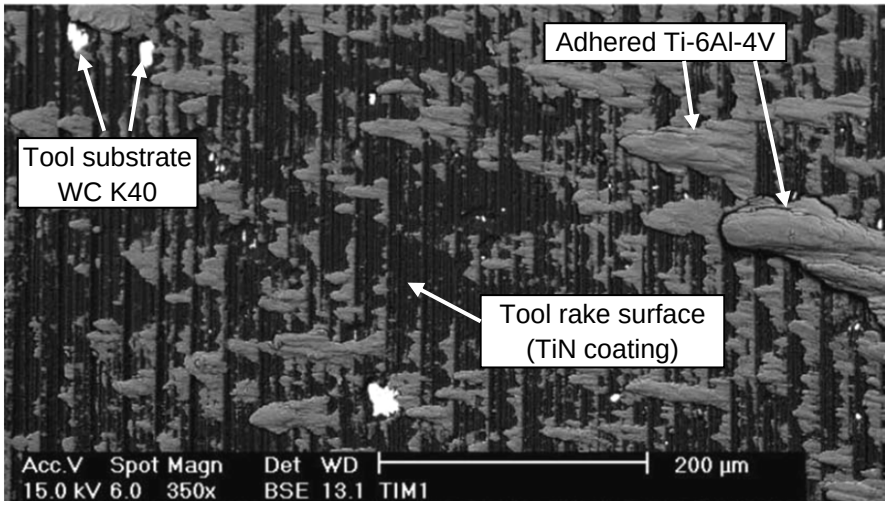


Figure 2.38: SEM image of drill rake face (15 holes) [143]

Canter et al. [143] investigated the effects of varying cooling frequency when dry drilling of Ti-6Al-4V. This involved directing compressed air to the tool and workpiece either after each hole (condition I) or following every 8 holes (condition II) drilled. The former arrangement (condition I) gave a threefold increase in tool life compared to the latter.

## 2.7 Machining of aluminium alloys

Aluminium alloys are generally considered easy to machine in terms of tool life, cutting force, material removal rate, chip formation and surface roughness [29]. The melting point of aluminium alloys range between 530 – 670$^{o}$C depending on additive content [30] and consequently the temperatures generated during machining are insufficient to cause any significant damage to carbide tools, even when dry cutting, although the use of cutting fluids when drilling aluminium alloys is still recommended in order to minimise cutting temperatures, reduce adhesion and facilitate chip transport. More problematic is the relatively high coefficient of thermal expansion of ~18-25 µm/mK linked with the high thermal conductivity (~154 W/mK) for aluminium alloys. A temperature variation of ~200$^{o}$C will cause a 50 µm change in the dimension of a 10 mm workpiece and can result in difficulties with achieving product tolerances. Typical problems encountered when cutting aluminium

alloys include significant burr formation particularly when using high feed rates together with poor lubrication [149], difficulties with swarf evacuation leading to tool clogging when dry drilling [150], and built-up edge formation/loss of cutting edge sharpness under low cutting speeds conditions (< 25 m/min) [151]. The maximum tool-chip interface temperature when dry drilling aluminium AA2024 was found to be ~80$^{o}$C at low cutting speeds (25 m/min), which rose up to 220$^{o}$C at 300 m/min [152]. On the tooling front, various coatings including DLC and TiC have been shown to provide superior performance in terms of tool life and hole quality compared to uncoated tools when drilling various aluminium alloys [149, 152-154]. The anti-sticking property of DLC coatings lead to much longer drill life (i.e. 150 holes was achieved compared to 50 holes using HSS tools) in addition to lower thrust force and torque (i.e. 2 N.m as opposed to 4 N.m using HSS tools at test cessation) [154, 155]. In general, small and discontinuous chips are desirable when drilling aluminium alloys in order to avoid clogging difficulties associated with long swarf, which promote increased torque and cutting temperatures leading to drill failure [156]. While Al-7050 alloy is used in the current work as workpiece material (Phase 3), published information on its machinability is extremely limited. An investigation by Tang et al. [157] however evaluated the effect of tool flank wear on residual stresses induced during milling of Al-7050 material. Wear had a significant influence on residual stresses as even small levels of flank wear caused either tensile and compressive stresses between -20 to 20 MPa, while higher wear levels at test cessation (0.25 mm flank wear on carbide cutter) produced tensile residual stresses on the machined surface of up to 127 MPa. Cutting temperatures and corresponding forces of up to 200$^{o}$C and 360 N respectively were also measured as the tool was worn.

## 2.8 Drilling of multilayered composite/metallic materials

### 2.8.1 Background

The combination of CFRP with titanium and/or aluminium to form multilayered material stacks has gained prominence in recent years. This is especially true for applications such as aerospace structures subject to extreme mechanical loads [14]. Joining of these materials typically requires the production of fastener holes. At present, such holes for wing and tail plane components are manufactured via a multi-shot routine which necessitates pre-drilling of each individual layer followed by a deburring cycle [55]. The stack is then assembled and temporarily held together (mechanically) prior to hole reaming. The disparity

in workpiece mechanical properties (e.g. different elastic modulus, thermal expansion coefficient etc.), often presents an obstacle towards achieving the required tolerance levels. Problems encountered when cutting these dissimilar materials typically include severe tool wear, heat induced damage, large hole size, roundness deviation and the presence of metallic burrs [158]. Therefore, relatively low cutting speeds involving manual drilling together with low feed rates are usually employed, which in turn results in extensive fabrication times (typically of the order of several minutes per hole). In addition, the high tool wear rates encountered when drilling CFRP and titanium further impacts on process productivity.

### 2.8.2 Drilling of metallic/composite stacks

Contrary to the extensive information on the machining of CFRP's, published data on the drilling of two or three layer metal/composite materials is somewhat limited. The available literature however indicates that the main challenge when drilling composite/titanium stacks relates to the excessive tool wear induced by the titanium layer as well as damage caused by the metallic chips on the hole surface of the composite section [14, 57]. Drilling of graphite composite/titanium stacks were investigated by Kim and Ramulu [158] and Ramulu et al. [159]. Here, the performance of 5 mm diameter HSS and carbide drills were evaluated over a range of operating parameters including feed rates of 0.02 and 0.3 mm/rev and rotational speeds from 660 to 5440 rpm (10 – 85 m/min). In general, carbide tools outperformed HSS equivalents in terms of lower thrust force and torque, longer tool life (35 drilled holes compared with 4 holes using HSS drills [159]), reduced burr height and smoother surface finish on both Ti and composite materials. The surface roughness (Ra) of the titanium alloy surface was found to be 5 and 2 μm as opposed to 14 and 6 μm for the composite layer when HSS and carbide drills were used respectively [159]. Additionally, the thrust force and torque profiles show several distinct regions as the tool moves through the stack, with the maximum value obtained when the drill was completely engaged in the titanium layer, see Figure 2.39. The height of burrs produced on the titanium layers increased with higher cutting speeds and lower feed rates. When carbide drills were employed, entry and exit height were up to 0.15 mm (at 10 m/min and 0.25 mm/rev) and 1 mm (at 40 m/min and 0.08 mm/rev) respectively [158, 159]. Optimum parameters of 0.08 mm/rev feed rate and 660 rpm (10 m/min) were reported for drilling 12.4 mm thick graphite/titanium stacks with carbide drills [159].

Heat generation leading to severe matrix degradation with a corresponding reduction in tool life [158, 159] is a major concern when machining stacks. In a recent study by Kim and Ramulu [160], the influence of curing methods (autoclave or induction heating) for graphite polymer composite workpieces which were backed on both sides with 140 μm thick titanium foils, was investigated when drilling using carbide tools. Similar results in terms of force (450 N), torque (70 N.cm), specific cutting energy and hole size were found, regardless of the curing technique. The drilled surface on the composite produced by induction heating was however smoother than the autoclaved material, which may in part be due to the higher levels of matrix smearing [160]. Here, the common hole defects observed included burr formation, delamination, fibres pullout etc., see Figure 2.40.

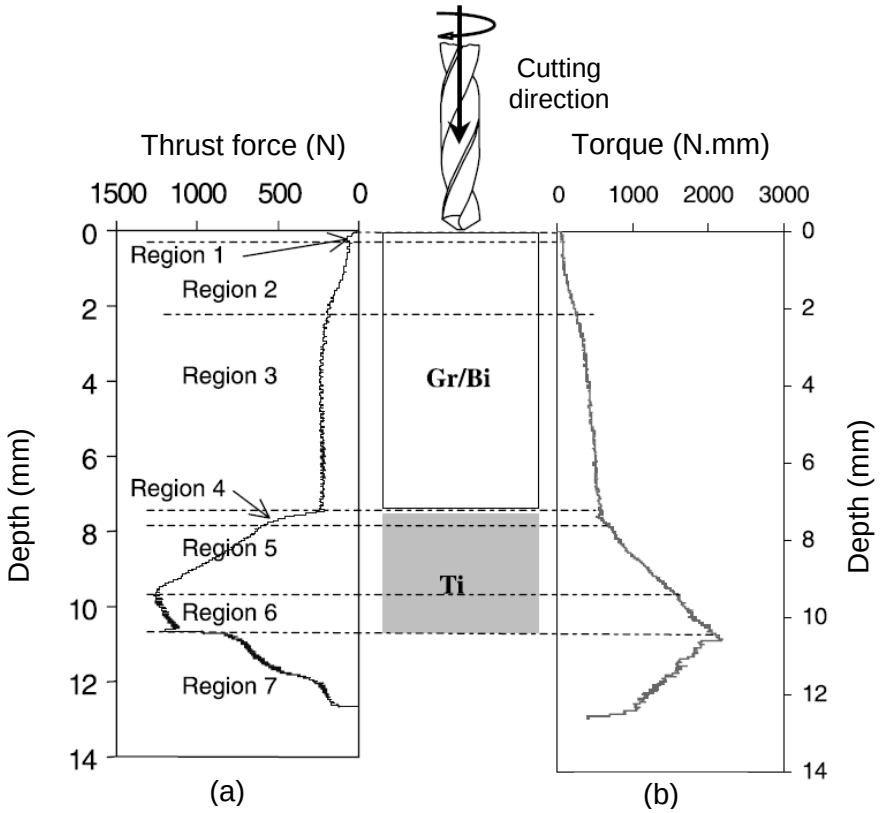


Figure 2.39: (a) Thrust force and (b) torque profiles versus drilling depth when using HSS drill with 660 rpm and 0.2 mm/rev feed rate [159]

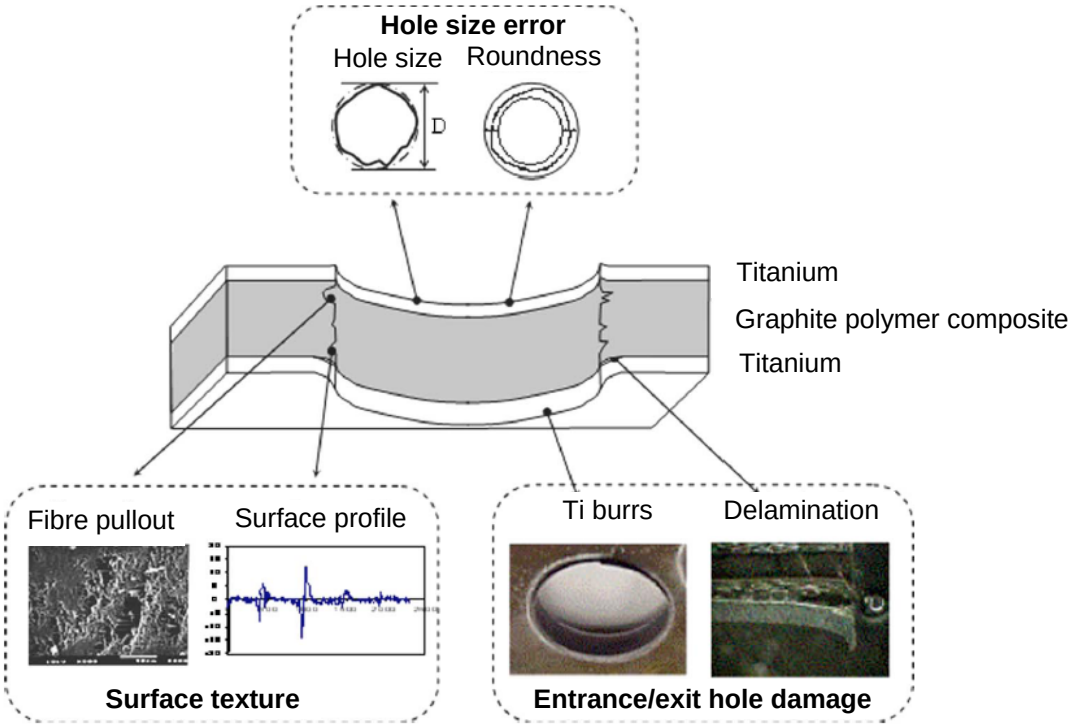


Figure 2.40: Some hole quality parameters in drilling graphite/titanium hybrid composites [160]

Drilling of composite/aluminium stacks (comprising 4.2 mm CFRP laminates followed by a 3 mm layer of Al 2024) was recently studied by Zitoune et al. [161], using different sizes of uncoated WC tools. Thrust force and torque on both CFRP and aluminium layers generally increased with higher feed rate and cutting speed, however at high spindle speeds, thrust force when machining the CFRP layer decreased. This was attributed to the large amount of heat generated, which reduced the epoxy's resistance to cutting. Additionally, drill diameter had a significant influence on thrust force as a result of larger chisel edge dimensions (e.g. 0.6 mm chisel edge length for 4 mm drill diameter while it was 1.6 mm for 8 mm drill diameter) leading to an increase in chip cross sectional area. The effect of chisel edge (60 % contribution) was consistent with the findings by Won and Dahran [94]. Similarly, chip breakability when drilling the CFRP/aluminium stack was improved when using drills with diameters > 6 mm at a feed rate of 0.1 mm/rev [161]. Results reported by Zitoune et al. [161] also suggest that cutting force values are only stable/acceptable within the first 30 – 60 holes, and that high surface roughness Ra values of between 4 μm to 8 μm (feed rate of 0.05 - 0.15 mm/rev) are produced in the CFRP. The corresponding Ra in the Al layer was up to 3 μm, but unfortunately this exceeds the typical industrial upper limit which is 1.6 μm and 3.2 μm for metallic and composite surfaces respectively [162].

A key paper by Brinksmeier and Janssen [163] describes some of the difficulties associated with through drilling of multilayer Al/CFRP/Ti stacks using uncoated and coated tungsten carbide tools. These include low tool life (~ 30 holes), clogging of drill flutes due to poor evacuation of continuous titanium chips from the bottom layer and severe damage/erosion of the CFRP hole surface caused by sharp Ti swarf, see Figure 2.41. Aluminium built-up edge formation on the main cutting lips combined with excessive tool wear was also observed to adversely affect the machined hole quality. Support offered to the CFRP laminate by the Al and Ti plates is anticipated to inhibit delamination of the composite surfaces during drilling in accordance with data reported by Tsao and Hocheng [95], where use of a backup layer (2 mm thick Al plate) was seen to impede the progress of laminate failure. Additionally, reduced burr formation on the titanium and aluminium material at the interface with the CFRP layer can also be expected [164]. No tests however were performed to evaluate the influence of stack arrangement/drilling sequence (i.e. machining commenced from Ti layer rather than Al) on process performance.

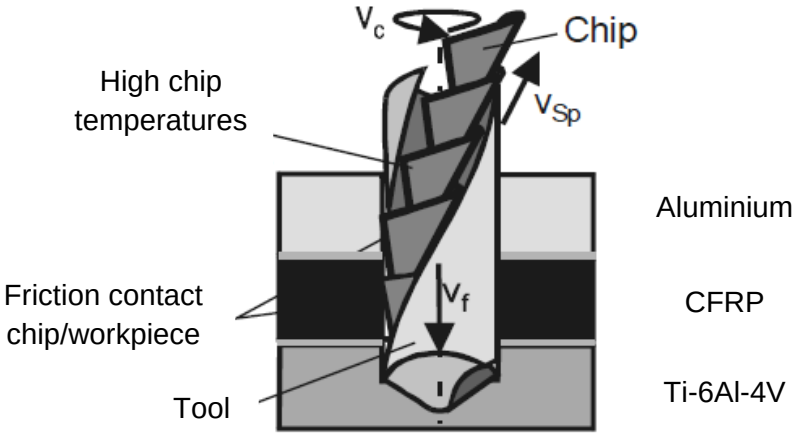


Figure 2.41: Chip removal problem when drilling Ti-6Al-4V in a metallic/composite stack [163]

## 2.9 Cutting tool materials and coatings

### 2.9.1 Introduction

There are numerous different tool materials with a wide range of properties, performance levels and cost available for various machining applications. The choice of tool material is governed by several factors including workpiece specification, productivity requirements, product design, machine tool condition and tooling cost. Generally, desirable characteristics for cutting tools include high hot hardness, good thermal conductivity, good

chemical inertness relative to the workpiece material, high toughness and fatigue resistance together with high compressive, tensile and shear strength [27]. Tool materials are commonly classified into three main groups in accordance with their mechanical properties (e.g. hardness, toughness, strength, etc.) namely high speed steels (HSS), cemented carbides and ceramic/superhard materials [165]. Of these, cemented carbides are the most widely used due to their favourable balance of properties in terms of toughness and hardness/abrasion resistance which cannot be matched by other materials, see Figure 2.42 [166]. While possessing superior toughness, the main limitation of HSS tools is their relatively low hardness and moderate strength, which make them unsuitable for cutting highly abrasive materials such as FRPs [12]. Therefore, no further details of HSS tools will be presented in the following sections.

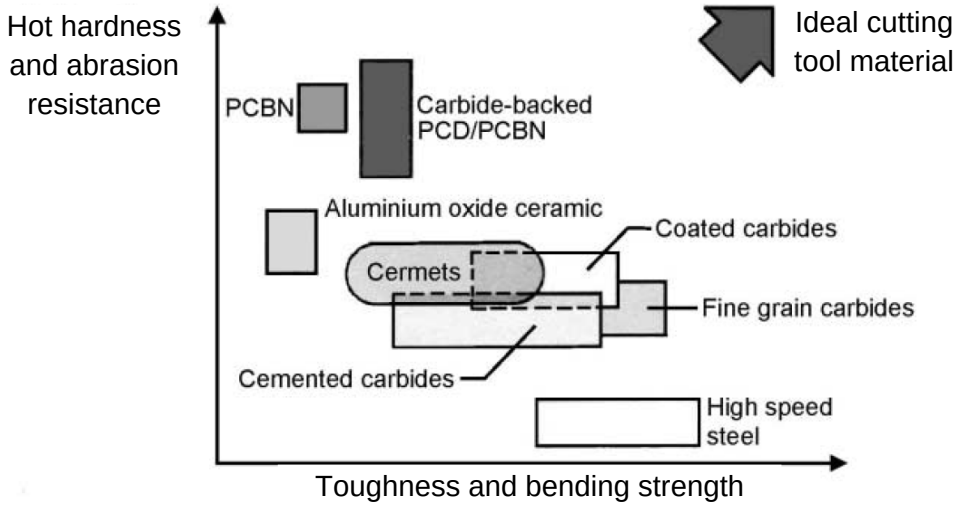


Figure 2.42: The relationship between toughness and hardness for various cutting tool materials [166]

### 2.9.2 Tungsten carbide tools

Cemented tungsten carbide (WC) tools comprising hard carbide particles (mainly WC) are 'held together' by a metallic binder (mainly Co although other elements can also be present), which is generally in a liquid phase at the sintering temperature of above 1300$^{o}$C [12, 167]. The cobalt content is typically between 4 – 12 %, depending on the grade of carbide [29, 167]. Mechanical/physical properties of WC-Co tool materials are highly dependent on the cobalt content and carbide grain size [29, 165, 167], see Table 2.11. In general, a smaller grain size results in higher hardness and wear resistance while both hardness and compressive strength also improve with lower cobalt content [12, 29].

Therefore, submicron/fine grain sized carbides are preferred for the machining composites in order to withstand abrasion attack from the reinforcement [12].

| Co % | Mean WC grain size (μm) | Hardness (HV) | Transverse rupture strength (MPa) | Compressive strength (MPa) | Young's modulus (GPa) | Fracture toughness ($MPa.m^{1/2}$) |
|---|---|---|---|---|---|---|
| 3 | 0.7 | 2020 | 1000 | - | - | - |
| | 1.4 | 1820 | - | - | - | 8 |
| 6 | 0.7 | 1800 | 1750 | 4550 | - | - |
| | 1.4 | 1575 | 2300 | 4250 | 630 | 10 |
| 9 | 0.7 | 1670 | 2300 | - | - | - |
| | 1.4 | 1420 | 2400 | 4000 | 588 | 13 |
| | 4.0 | 1210 | 2770 | 4000 | - | - |
| 15 | 0.7 | 1400 | 2770 | - | 538 | - |
| | 1.4 | 1160 | 2600 | 3500 | - | 18 |

Table 2.11: Properties of WC-Co tool materials [29]

### 2.9.3 CVD diamond and DLC coatings

The chemical vapour deposition (CVD) process involves a gas-phase chemical reaction such as methane, nitrogen, aluminium chloride or titanium tetrachloride etc. in an excess of hydrogen above a solid surface such as a carbide cutting tool, and is typically performed at temperatures of 800-1100$^{o}$C [167, 168]. Several microns of a single layer or multilayer coating which can include hardmetals (TiC, TiN etc.) and diamond are deposited on the tool surface in order to improve their wear resistance [12]. Diamond, with its unrivalled hardness level (10,000 HV), relatively low coefficient of friction (0.03), high thermal conductivity (2000 W/mK at room temperature), low chemical reactivity (except ferrous workpieces) and high tensile and compressive strength [168, 169] make it an ideal material for the machining of nonferrous high strength/abrasive materials. The properties of the diamond or hardmetal layer are determined to a large extent by the gas mixing ratio (typically the precursor gas is $CH_4$ which is diluted in an excess of hydrogen by 1-2% volume) and the preparation temperature of the tool surface (1000 – 1400 K) [168]. The main limitation of the CVD diamond coating process however is the poor adhesion of diamond due to the presence of cobalt in the carbide tool substrate [29]. In order to improve coating adhesion, cobalt has to be either removed or stabilised by the formation of inert chemical compounds. Here, the typical procedure involves two etching steps comprising an initial tool substrate surface roughing, which is typically performed mechanically by sandblasting followed by chemical pre-treatment to deplete or dissolve cobalt and form $CoSO_4$ and Co-oxides [166, 170].

CVD diamond coated tools have been evaluated by a number of researchers for cutting composite materials with somewhat encouraging results [169, 171]. The optimum thickness of the CVD diamond coating was found to be 9 – 10 μm, which outperformed a 6 μm thick layer (30% longer tool life) when used for the turning of CFRP [170]. In terms of drilling, CVD diamond coated tools (e.g. CCDia Fiberspeed from Cemecon, Germany) produced 500 holes in CFRP compared to 90 holes with uncoated carbide drills under comparable operating conditions. Corresponding hole quality of H8 was achieved with the CVD coated tools, which was not replicated by either the uncoated or PVD coated drills [13]. Davim and Mata [169] measured lower cutting forces with CVD diamond coated tools compared to WC and PCD inserts when turning composites although the surface roughness produced was approximately the same. Further benefits of CVD diamond coatings compared to equivalent solid ultrahard tool materials is their lower cost (~ 30% cheaper than brazed PCD) and relative ease of implementation on complex tool geometries (i.e. helical fluted small drills and end mills) [12, 169].

Diamond-like carbon (DLC) is a mixture of hard carbon atoms (diamond and graphite are commonly referred to as $sp^3$ and $sp^2$ hybrid carbon based bonded arrangements respectively) which are linked together in an amorphous structure similar to natural diamond [172, 173], with comparable mechanical/physical properties [172, 174-176]. Unlike CVD diamond products, DLC coatings are produced using the physical vapour deposition (PVD) technique involving sputter deposition or an ion-beam system operating at significantly lower temperatures (up to 500$^{o}$C) [175], which does not cause any difficulties with the cobalt binder in carbide tools. The PVD process also results in a finer microstructure, greater toughness and reduced substrate deterioration [12]. The hardness of DLC depends primarily on the $sp^3$ element concentration in the mixture. Where the element concentration approaches 100%, the coating hardness approximates that of natural diamond (8000 – 10000 HV), but drops by ~50% (3000 – 5000 HV) when the $sp^3$ diamond concentration is reduced to ~ 15 – 20% [173]. DLC layer thickness is typically of the order of several microns, whereas diamond coatings can be up to 18 μm. To date, the use of DLC coated tools for the machining of metal matrix composites [173] or FRP composites [93] is still limited. Despite their superior properties, Murphy et al. [93] found limited benefits in using DLC coatings over uncoated tools in terms of tool wear when drilling CFRP.

### 2.9.4 Polycrystalline diamond (PCD) drills

Synthetic polycrystalline diamond is produced by sintering diamond grits (2 – 50 μm) at high temperatures and pressures of 1500 $^{o}$C and 60 GPa respectively [177]. A metal catalyst/binder (mainly cobalt) is used to promote diamond inter-growth and ensure a suitably dense product [178, 179]. The resulting material typically has high hardness (8000 – 10000 HV) with more uniform mechanical properties than natural diamond. Polycrystalline diamond blanks are normally produced in a disc format up to 75 mm diameter with a 0.5 – 0.7 mm thick diamond layer bonded onto a WC substrate. The various insert shapes are produced by fabricating tools using segments/sectors of PCD cut from the initial disc or blank [166]. The properties of PCD tools depend upon the diamond grain size, the degree of diamond inter-growth together with the quantity and distribution of the catalyst material [178]. Contrary to tungsten carbide tools, larger diamond grit products have higher hardness while finer grains are preferred when edge sharpness is of importance [178, 180]. At temperatures of above ~800$^{o}$C the diamond reverts to graphite and consequently cutting temperatures must not be allowed to exceed this level [179]. Since the cutting temperatures of FRP composites are generally below this figure, PCD tools can potentially be successfully employed.

PCD tools are widely utilised for the machining non-ferrous workpiece materials [86, 166, 180, 181] while their use for ferrous material is prohibited because of reaction with ferrite at high operating temperatures resulting in a back-transformation to graphite. Ramulu et al. [180] observed uniform flank wear, edge rounding, cracking and chipping when using PCD tools to cut graphite/epoxy composites. When turning Al/SiC MMC's, PCD tooling was able to achieve a tool life of 5 min when operating at a cutting speed of 1000 m/min, as opposed to 0.2 min reported for WC tools, working at a considerably lower cutting speed of 50 m/min. Ding et al. [181] also suggests that when turning Al/SiC MMC's, PCD exhibited a marked reduction in flank wear and surface roughness compared with various grades of PCBN, see Figure 2.43. This was attributed to their higher abrasion and fracture resistance together with a lower affinity for adhesion with aluminium based materials. Despite the superiority of PCD tools in terms of tool life and machined quality, their capital cost is generally considerably higher than other tool materials [178]. Additionally, their use is only recommended when the dominant wear mechanism is abrasion [166].

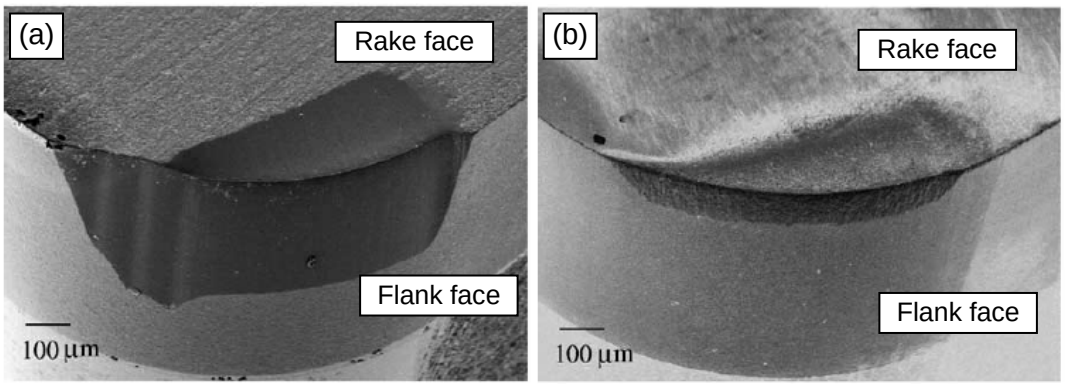


Figure 2.43: (a) PCBN and (b) PCD tools used to machine Al-SiC MMC at 50 m/min without coolant [181]

## 2.10 Statistical experimental design techniques

### 2.10.1 Introduction

An experiment can be defined as a test or series of tests where changes are made to the input variables of a process to observe and identify the reasons for variation in the resulting output response [182]. Statistical experimental design is the process of planning an experiment such that appropriate data can be collected and statistically analysed in order to draw valid conclusions. Different methods allow the investigation of numerous factors (variables) simultaneously and economically in order to identify their effects on the experimental results and determine the 'best/preferred' combination of factors under specific experimental conditions. Experimental design can be broadly classified into two categories; full and fractional factorial. A full factorial design is one where the levels of one factor are evaluated against each level of every other factor, and the arrangement provides all possible effects and interactions, however the scale of testing can be prohibitive. For instance, an assessment of 4 factors, each at 4 levels would necessitate 246 experiments (full factorial array) excluding any replications. A more realistic approach, particularly for initial screening/ rationalisation purposes, would be to employ a fractional factorial which requires significantly fewer tests (for the last example, a small orthogonal array such as an L16 could be used for investigating the main factor effects), but still provide acceptable confidence in the results. The Taguchi methodology [183] is one such approach, which employs main effects and interaction plots together with analysis of variance (ANOVA) to calculate the relative influence of individual test factors and the corresponding sensitivity of the associated levels in relation to selected response measures (e.g. tool life, surface roughness, cutting force etc.).

### 2.10.2 Taguchi experimental design procedure

It is suggested that a simple step-by-step approach to experimental design can be implemented without an expert background in statistics [184]. This results in a set of procedures that initially involves selecting a suitable orthogonal array (OA) from a set of standard designs (e.g. L4, L8, L16, L32 for two and four levels factors & L12, L18 for two and three levels combination & L9, L27 for three levels factors), followed by assignment of factors into the OA using linear graphs or assignment tables and finally analysis of the experimental data. The best factor combination is extracted from a one-shot experiment followed by a confirmation run in order to validate the results. Useful sets of orthogonal arrays, linear graphs and assignment tables are presented by Taguchi [185]. The main limitation of the technique is that it underestimates the importance of factor interaction effects, although Taguchi implies that their effects can be eliminated by correctly specifying the response variable and carefully selecting corresponding design factors and levels [184].

### 2.10.3 Overview of analysis of variance (ANOVA) technique

For analysing experimental results, the analysis of variance (ANOVA) technique can be used to interpret experimental data and make necessary decisions. ANOVA is a statistically based, objective decision making tool for detecting differences in the average performance of a group of factors examined [183]. As its name suggests, the procedure involves partitioning the total variability of a response into its individual components. In essence, the technique compares the variability in the mean of an individual factor with the inherent experimental error. A confirmation experiment, especially when a fractional factorial design has been applied, is used in order to validate the conclusions drawn from the analysis [183]. More details can be found in the reference by Ross [183].

# 3. EXPERIMENTAL WORK

The research involved three main phases of experimental testing. Phase 1 and 2 investigated the drilling of small diameter holes (1.5 mm) in thin sheet CFRP laminates while Phase 3 involved one-shot drilling (6.35 mm diameter holes) of multilayer workpiece stacks comprising titanium, CFRP and aluminium. Each phase was further divided into appropriate sub-phases as listed below:

Phase 1A: Preliminary small hole drilling of CFRP and the influence of peel ply layers
Phase 1B: Effect of tool geometry and operating parameters
Phase 2A: Effect of composite material, fibre orientation and machining parameters
Phase 2B: Evaluation of diamond based coatings
Phase 3A: Preliminary drilling trials in separate CFRP and Ti workpiece and multilayer stacks
Phase 3B: Impact of stack arrangement and performance of PCD tools
Phase 3C: Effect of tool coatings and operating parameters

The following sections detail the workpiece materials, tooling and equipment used in the trials together with a comprehensive description of the experimental procedure and associated test arrays.

## 3.1 Workpiece materials

Carbon fibre reinforced plastic (CFRP) composite laminates were used throughout Phase 1 and 2 trials while Phase 3 work utilised stack material comprising CFRP sandwiched between Ti-6Al-4V and Al-7050. All workpiece materials were supplied by GKN Aerospace (UK).

### 3.1.1 CFRP composite laminates for Phase 1 and 2 tests

All CFRP workpiece materials used in Phase 1 and 2 tests were manually laid up with 12 pre-impregnated (prepreg) layers each measuring 0.25 mm thick to provide ~3 mm thick symmetric CFRP plates. Woven glass scrims (100 μm thickness) were applied to both sides of all plates with a further 100 μm thick peel ply sheet comprising J2 (HS013) MF Nylon overlayed prior to curing, which was retained during drilling (except for Phase 1A tests). All prepregs employed carbon fibres approximately 6 – 8 μm in diameter with a toughened epoxy

matrix/resin and were produced (by GKN) from different manufacturers. Workpiece test specimens were subsequently cut into 120 mm x 120 mm plates in order to fit a specially designed jig with clearance holes. All the composite laminates used in Phase 1 involved unidirectional (UD) prepregs (MTM44-1/HTS) but with different lay-up and curing conditions employed for Phase 1A and 1B respectively, see Table 3.1 for details. For Phase 2, three different prepreg/resin systems (from different manufacturers) encompassing both UD and woven fibre arrangements were evaluated, see Table 3.2. Figure 3.1 shows cross sectional micrographs of the fibre orientation seen in UD and woven laminates respectively.

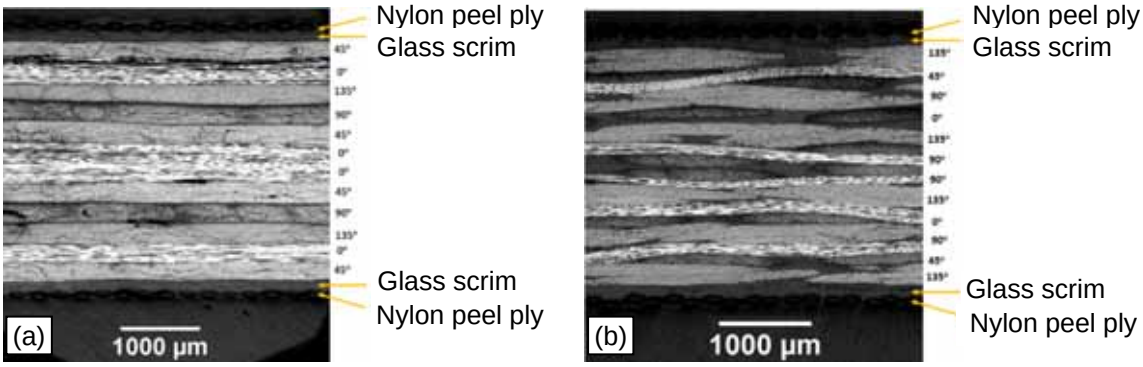


Figure 3.1: Cross section micrographs of: (a) UD and (b) woven MTM44-1/HTS OC laminates with associated fibre orientation

| **Phase 1A** | |
|---|---|
| **Prepreg supplier** | Advanced Composite Group (ACG) |
| **Prepreg specifications** | |
| Reinforcement | Toho Tenax HTS 12K, 268gsm, 1/4 mm, UD, 1.76g/cm$^3$(ρ) |
| Matrix | ACG MTM44-1 1.18g/cm$^3$ (ρ) |
| Fibre/resin code | ACG MTM44-1/HTS-268-12K ($V_f$ = 56.5%) |
| **Fibre weave type** | Unidirectional (UD) |
| **Fibre orientation (lay-up)** | $(45^o/0^o/135^o/90^o/45^o/0^o)_s$* |
| **Curing conditions** | |
| Ramp rate | 1$^o$C/min at vacuum pressure of 0.9 bar |
| Curing | Oven cured with a step dwell of 80°C for 30 minutes then heat up to 135°C |
| **Phase 1B** | |
| **Curing conditions** | |
| Initial curing | Oven cured with a heating rate of 1°C/min with a step dwell at 80°C for 30 minutes followed by a heating rate of 1°C/min to 135°C which was maintained for 4 hours, all held at a minimum vacuum pressure of 27"Hg (0.914 bar) |
| Post curing | Heating rate of 2.5°C/min to 135°C followed by a slower heating rate of 0.2°C/min to 180°C and held for 2 hours. Free standing with no vacuum applied |
| All other factors same as in Phase 1A | * The subscript "s" indicates the laminate is symmetric |

Table 3.1: Details of workpiece materials for Phase 1 tests

| **Properties common between all materials used in Phase 2** | | | |
|---|---|---|---|
| Fibre orientation | UD | $(45^o/0^o/135^o/90^o/45^o/0^o)_s$* | |
| | Woven | $(135^o/45^o/90^o/0^o/135^o/90^o)_s$* | |
| **Material** | **Phase 2A** | | |
| 977-2/HTS | **Prepreg supplier** | Cytec Engineered Materials | |
| | **UD prepreg specifications** | Reinforcement | Toho Tenax HTS 12K, 268gsm, 1/4 mm, UD, 1.76g/cm$^3$ (ρ) |
| | | Matrix | Cytec 977-2 1.31 g/cm$^3$ (ρ) |
| | | Fibre/resin code | 977-2/HTS-268-12K ($V_f$ = 59%) |
| | **Woven prepreg specifications** | Reinforcement | Toho Tenax HTA, 2x2 twill, 285gsm, 1.8g/ cm$^3$ (ρ) |
| | | Matrix | Cytec 977-2 1.31 g/cm$^3$ |
| | | Fibre/resin code | Cytec 977-2/HTS-285-6K 2x2 twill ($V_f$ = 55%) |
| | **Curing conditions** | Autoclave cured with a heating rate between 0.5 and 3.5$^o$C/min and held for 180 minutes at 180°C. 100 psi (7 bar) pressure during cure. | |
| 8552/AS4 | **Prepreg supplier** | Hexcel | |
| | **UD prepreg specifications** | Reinforcement | Hexcel AS4, 145gsm, 1.79g/cm$^3$ (ρ) |
| | | Matrix | Hexcel 8552 1.3g/cm$^3$ (ρ) |
| | | Fibre/resin code | Hexcel 8552/AS4-145-12K ($V_f$ = 58.5%) |
| | **Woven prepreg specifications** | Reinforcement | Hexcel 3K AS4 286gsm 5HS |
| | | Matrix | Hexcel 8552 1.3g/cm$^3$ (ρ) |
| | | Fibre/resin code | Hexcel 8552/AS4-286-5HS ($V_f$ = 55%) |
| | **Curing conditions** | Autoclave cured with a heating rate of 1-3$^o$C/min to 110$^o$C with a dwell for 60 minutes. Heating at 1-3$^o$C to 180$^o$C with a dwell for 2 hours. 100 psi (7 bar) pressure during curing. | |
| MTM44-1/HTS | **Prepreg supplier** | Advanced Composite Group (ACG) | |
| | **UD prepreg specifications** | Reinforcement | Same as in Phase 1A |
| | | Matrix | |
| | | Fibre/resin code | |
| | **Woven prepreg specifications** | Reinforcement | Toho Tenax 3K, HTS 5131, 283gsm, CF0604 5HS fabric |
| | | Matrix | ACG MTM44-1 1.18g/cm$^3$ (ρ) |
| | | Fibre/resin code | ACG MTM44-1/HTS-283-5HS ($V_f$ = 55%) |
| | **Curing conditions** | | |
| | Initial curing | Same as in Phase 1B | |
| | Post curing | | |
| * The subscript "s" indicates the laminate is symmetric | | | |

Table 3.2: Details of workpiece materials for Phase 2 tests

### 3.1.2 Ti/CFRP/Al stacks for Phase 3 tests

Each material in the stack had a nominal thickness of 10 mm and was bonded together using a strong film adhesive (3M AF163) which helped to ensure that cutting forces and exit/entry hole damage were not adversely affected by material separation. For the primary tests, the 30 mm thick workpiece specimens were cut into 120x120 mm blocks, see Figure 3.2. A limited number of test blocks were also assembled using an interfay sealant (PR 2001B2-BA1002) instead of the adhesive, which were cut into 17 mm wide strips and bolted together at each end with M6 screws to prevent breakup of the stack during drilling. This enabled thrust force and hole accuracy analysis to be undertaken at different levels of tool wear, as well as easy disassembly of the stack workpiece samples for evaluation of hole quality and interface damage.

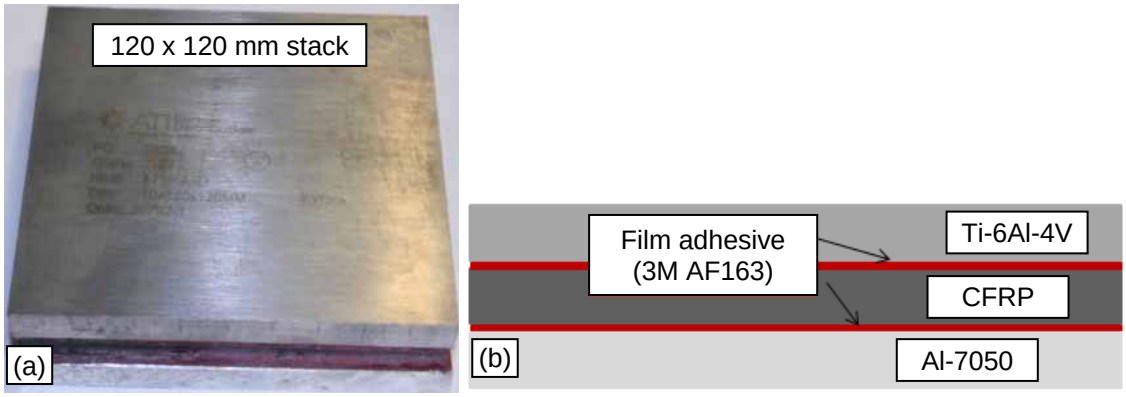


Figure 3.2: (a) Ti/CFRP/Al stacks and (b) cross section schematic

#### *3.1.2.1 CFRP composite laminates*

Quasi-isotropic UD CFRP laminates formed of 36 prepreg layers (~ 10 mm thick) were used. The prepregs were of the type supplied by ACG (see Table 3.1 for matrix and fibre specification/properties) with a ~100 μm thick glass scrim layer applied on both sides of the plates in order to prevent galvanic corrosion as well as minimise the incidence of drill breakage. Table 3.3 details the mechanical properties of the CFRP laminates following the curing process [55].

| Property | Value | Property | Value |
|---|---|---|---|
| Density | 1.6 g/cm$^3$ | Shear strength (interlaminal) | 14 MPa |
| Hardness | 60-65 Barcol | CTE | Up to 25 μm/m$^o$C |
| Ultimate tensile strength | 2000 MPa | Modulus of elasticity | 150 GPa (yield) |
| Thermal conductivity | 1 W/mK perpendicular & 70 W/mK parallel to fibre direction | | |
| Fibre volume fraction | 0.5 - 0.6 | | |

Table 3.3: Mechanical properties of the CFRP laminates post curing [55]

*3.1.2.2 Titanium - Ti-6Al-4V alloy*

The titanium employed was an alpha-beta alloy with an elemental composition of 90% titanium, 6% aluminium and 4% vanadium. The plates were annealed according to MIL-T-9046 specifications. Table 3.4 shows typical properties of the Ti-6Al-4V workpiece material [32].

| Property | Value | Property | Value |
|---|---|---|---|
| Density | 4.43 g/cm$^3$ | Shear modulus | 44 GPa |
| Hardness | 350 HV | Shear strength | 550 MPa |
| Ultimate tensile strength | 950 MPa | CTE | 9.2 μm/m$^o$C |
| Modulus of elasticity | 115 GPa | Thermal conductivity | 7 W/mK |

Table 3.4: Mechanical properties of Ti-6Al-4V alloy [32]

*3.1.2.3 Aluminium - Al-7050 alloy*

A relatively high strength aluminium alloy – Al-7050-T7651 AMS 4050 was used as the third layer in the stacks. This grade is typically used in aircraft structures due to its high resistance to exfoliation corrosion and stress-corrosion cracking, high fracture toughness and fatigue resistance. Table 3.5 lists the mechanical properties of the Al-7050 alloy [30].

| Property | Value | Property | Value |
|---|---|---|---|
| Density | 2.83 g/cm$^3$ | Shear modulus | 27 GPa |
| Hardness | 171 HV | Shear strength | 324 MPa |
| Ultimate tensile strength | 552 MPa | CTE | 25 μm/m$^o$C |
| Modulus of elasticity | 72 GPa | Thermal conductivity | 153 W/mK |
| Chemical composition | 89% Al, 6% Zn, 2% Mg, 2% Cu and 1% other elements | | |

Table 3.5: Mechanical properties of Al-7050 alloy [30]

## 3.2 Tool geometries, materials and coatings

Phase 1 and 2 experimental work involved tooling to produce 1.5 mm diameter holes. A range of uncoated and coated (TiN, amorphous carbon and CVD diamond) twin lipped tungsten carbide (WC) drills with varying geometry were evaluated. For Phase 3 trials, 6.35 mm diameter drills were employed and involved uncoated and coated WC together with polycrystalline diamond (PCD) products. Further details of tools and coatings are given in the following sections.

### 3.2.1 Small diameter carbide drills for Phase 1 and 2

Two different drill types were used, (i) conventional twist drill and (ii) stepped drill, which were manufactured from 90% WC and 10% cobalt composition by Dixi Polytool (Le Locle, Switzerland), see Figure 3.3. The former had a constant diameter of 1.5 mm over the length of the tool (shank and fluted sections) while the latter comprised a 3 mm long pilot section of 1 mm diameter connected to a 1.5 mm diameter sizing portion, see Figure 3.4. Four different tool geometries were employed with two helix angles ($24^o$ and $30^o$) and two point angles ($118^o$ and $140^o$). The performance of a physical vapour deposition (PVD) TiN coating was evaluated in Phase 1 while various advanced coatings were tested in Phase 2. These included a PVD diamond like carbon (DLC) coating together with chemical vapour deposition (CVD) diamond coatings from 3 different manufacturers. Details of material composition, physical properties and supplier information of all the coatings used are given in Table 3.6 while Table 3.7 provides a summary of the drills including cost.

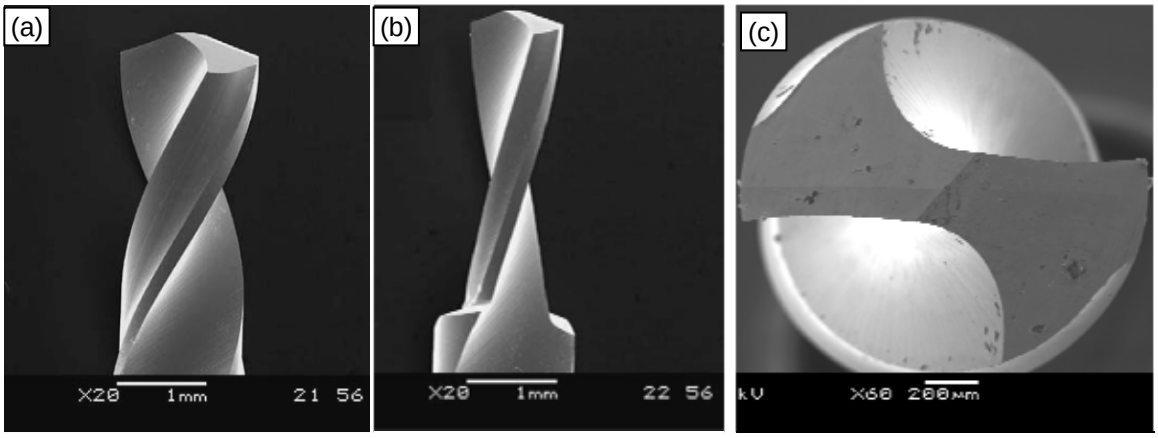


Figure 3.3: SEM images for: (a) conventional twist drill, (b) stepped drill and (c) end view for conventional drill used for Phase 1B tests

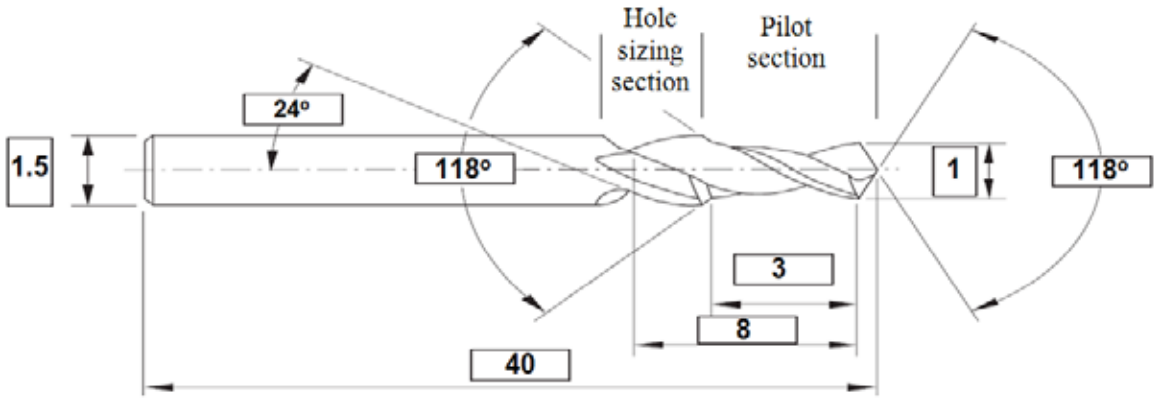


Figure 3.4: Stepped drill geometry used in the test programme (All dimensions in mm and all angles in degrees)

| **Coating type** | **TiN** | **DLC** | **Rhobest diamond** | **Diamond plus** | **Diamond fibre speed** |
|---|---|---|---|---|---|
| **Coating material** | Titanium nitride | taC* | Nanocrystalline diamond | CrCN + DLC | Nanocrystalline Diamond |
| **Micro hardness (HV)** | 2300 | 5300 | Up to 10000 | 2800 | 10000 |
| **COF†** | 0.5 | | 0.03 | | |
| **Max. operating temp. ($^{o}$C)** | 560 | 500 | NA | 500 | 700 |
| **Coating technique** | PVD | PVD | CVD | CVD | CVD |
| **Supplier** | Dixi Polytool, Switzerland | Argor-Aljba, Switzerland | ρ-Best coating, Austria | Cemecon, Germany | Cemecon, Germany |
| * tetrahedral amorphous carbon | | | † COF: coefficient of friction | | |

Table 3.6: Specification for coating materials used in Phase 1 and 2

| Phase and number of tools used | Drill description | Tool coating | Cost per drill |
|---|---|---|---|
| **Phase 1a** 2 drills | DIXI 1126, *P*=118°, H=30° | Uncoated | £6.20 |
| **Phase 1b** 36 drills | DIXI 1130, *P*=118°, H=24° | Uncoated | £6.65 |
| | | TiN | £8.40 |
| | DIXI 1130, *P*=118°, H=30° | Uncoated | £7.00 |
| | DIXI 1130, *P*=140°, H=24° | TiN | £8.40 |
| | DIXI 1130, *P*=140°, H=30° | Uncoated | £7.00 |
| | | TiN | £8.68 |
| | DIXI 1501, *P*=140°, H=24° | Uncoated | £15.05 |
| | | TiN | £17.50 |
| | DIXI 1501, *P*=140°, H=30° | Uncoated | £15.05 |
| | DIXI 1501, *P*=118°, H=30° | TiN | £17.50 |
| | DIXI 1501, *P*=118°, H=24° | Uncoated | £15.05 |
| **Phase 2a** 40 drills | DIXI 1501, *P*=118°, H=24° | Uncoated | £10.50 |
| | DIXI 1130, *P*=118°, H=24° | Uncoated | £6.65 |
| **Phase 2b** 40 drills | DIXI 1130, *P*=118°, H=24° | Uncoated | £4.80 |
| | | DLC | £8.40 |
| | | Rho-best | £24.00 |
| | | Diamond plus | £46.40 |
| | | Diamond fibre speed | £28.80 |
| **Notes**<br>*P*: point angle, H: helix angle.<br>All drills had 40 mm total length and 8 mm maximum cutting length.<br>Drills coded DIXI 1130 and 1126 were conventional twist drills.<br>Drills coded DIXI 1501 were stepped drill geometry and had the same point & helix angles on both pilot and sizing sections. | | | |

Table 3.7: Small diameter carbide drills used in Phase 1 and 2 test programme

### 3.2.2 Drills for Phase 3 test programme

Initial trials involved the benchmarking of a novel straight fluted (0° helix angle) 'domed' PCD drill designed and fabricated by Element Six (E6 – Ireland) against commercially available multilayer TiN/TiAlN PVD coated WC drills from Sandvik Coromant. The carbide tools recommended for composite/Ti drilling were the R840-0635-50-A1A (6.35 mm diameter) and R846-0680-50-A1A (6.8 mm diameter as the R846 series was not available in 6.35 mm and has different cutting edge geometry), see Figure 3.5. The domed PCD drills consisted of cylindrical PCD blanks (92% diamond –14 μm grain size and 8% Co) with a 'hemispherical' end, which was brazed onto carbide shafts and ground to the required geometry, see Figure 3.6. Drills for mainstream testing were supplied by Unimerco and included uncoated tungsten carbide together with CVD diamond and C7 coated tools and

brazed PCD tools, see Figure 3.7 for drills used in Phase 3C. The CVD diamond coating (CCDia FiberSpeed) produced by Cemecon in Germany had a hardness of 10000 HV and operating limit of 700°C while the C7 product (proprietary to Unimerco) consisted of a nano-composite structure with nano-crystalline AlTiN grains embedded in an amorphous matrix of silicon nitride ($Si_3N_4$). This coating had an oxidation limit of 1100°C and a hardness of 45 GPa (4600 HV). The brazed PCD drills employed sandwich tipped 10 μm grain PCD blanks from MegaDiamond which were subsequently inserted into a pre-machined slot at the end of a carbide drill. This ensured that the chisel edge and major cutting edges of the tool were composed of PCD, see Figure 3.8. In addition, the performance of a modified domed PCD drill (helical flutes instead of straight) was also evaluated, see Figure 3.9. All drills were twin fluted and incorporated internal coolant holes with corresponding helix and point angles of 30° and 130°, respectively (except for the brazed PCD drills, where the values were 20° and 135°).

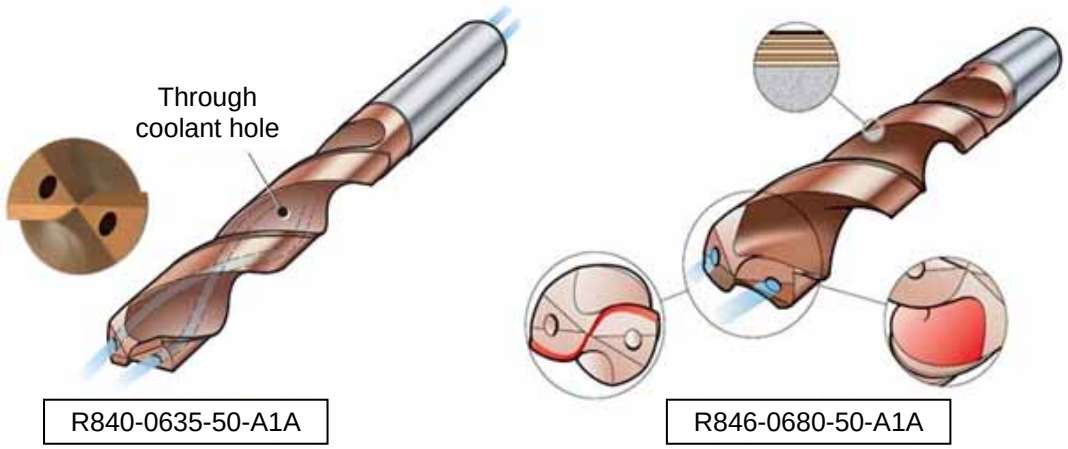


Figure 3.5: Sandvik drills used in Phase 3A tests (Courtesy of Sandvik Coromant)

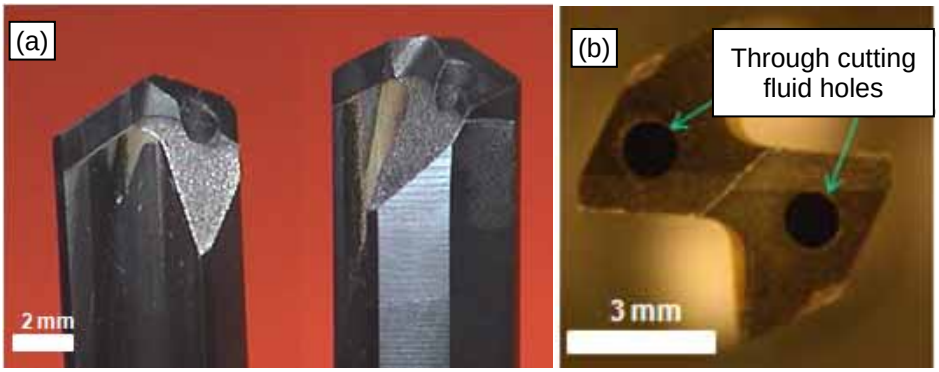


Figure 3.6: Straight fluted PCD drills used in Phase 3A: (a) side view and (b) end view

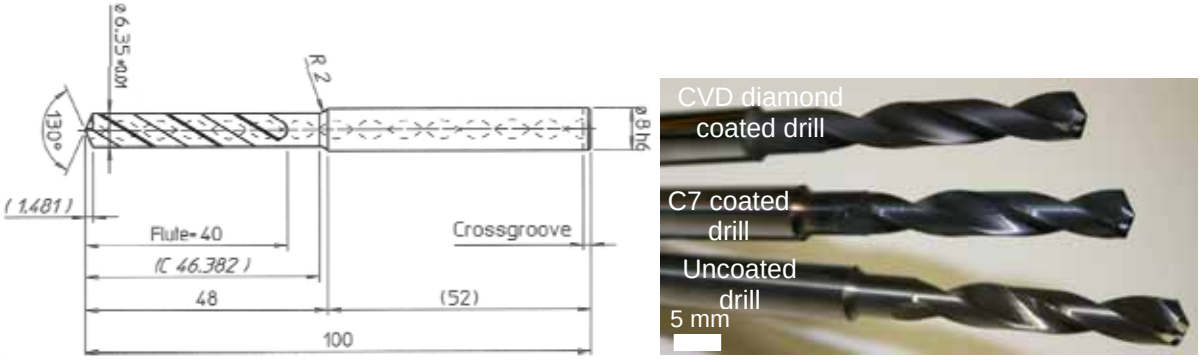


Figure 3.7: Uncoated and coated WC drills used in Phase 3 and supplied by Unimerco

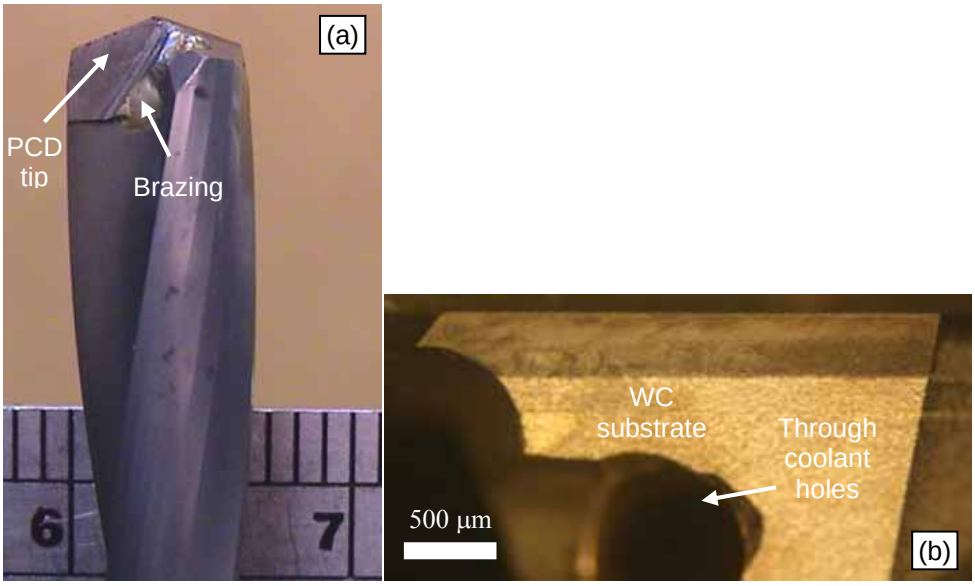


Figure 3.8: Brazed PCD drill used in Phase 3B: (a) side view and (b) end view

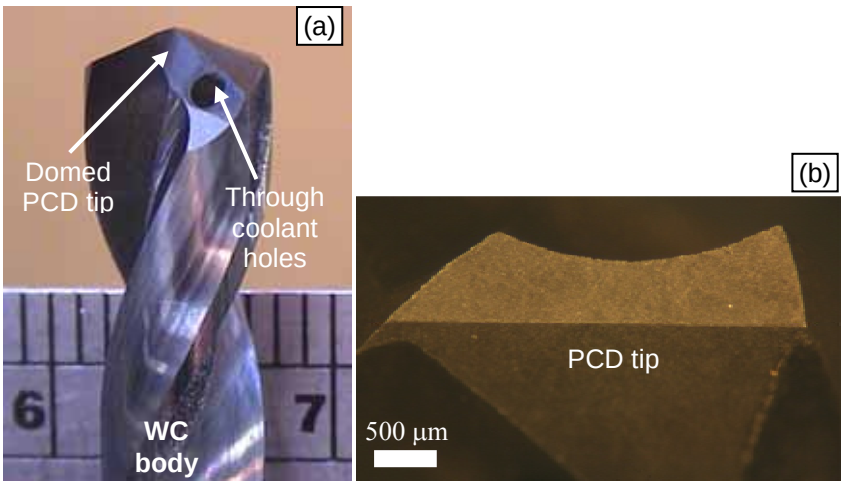


Figure 3.9: Helical fluted domed PCD drill used in Phase 3B: (a) side view and (b) end view

## 3.3 Equipment

### 3.3.1 Machine tool and cutting fluid application

#### *3.3.1.1 Matsuura FX-5 high speed machining centre*

All tests were carried out on a Matsuura FX-5 vertical high speed CNC machining centre (see Figure 3.10) which has a variable speed spindle capable of up to 20,000 rpm rated at 15 kW and a corresponding maximum feed rate of 15 m/min. The machine was fitted with a Renishaw touch trigger probe for tool length setting and also equipped with a Dustomat 15 extraction system (supplied by Filtermist Ltd) and able to remove airborne CFRP particles ≥ 0.3 μm, see Figure 3.11. A full specification of the unit is given in Table 3.8. Two extraction points were installed with the system, the first via a direct connection which was placed on the ceiling of the machine guard while the second used an adjustable self-supporting lock-line.

#### *3.3.1.2 Cutting fluid application*

All tests in Phase 1 and 2 were carried out dry, however, Phase 3 tests were performed using two different cutting environments; flood coolant and spray mist. The flood coolant involved a water/oil emulsion containing a 7-8 % volume solution of Hocut 3380 mineral oil. This was kept constant and monitored using an Atago N1 refractometer. The cutting fluid was delivered to the cutting zone via a retrofit "through coolant" spindle adaptor (6000 rpm maximum) incorporating a BT40 tool holder. A flow rate of 30 litres per minute and corresponding pressure of 70 bar (7 MPa) was used. An externally delivered spray mist environment was generated using a Jet Thrust two fluid (coolant and lubricant) system, supplied by Freddy Products Ltd. Soluble oil coolant and mineral oil lubricant stored in separate tanks were pumped to a mixing jet at a pressure of 0.7 bar (0.07 MPa), which was subsequently discharged through a front nozzle having a 5 mm diameter orifice using compressed air (3 – 4 bar), to produce a fine particle spray. In the current work, the coolant utilised was a fully synthetic fluid incorporating a corrosion inhibitor diluted in water to provide a 7 – 8% volume solution, while the lubricant was a special purpose mineral oil blended with a high performance additive.


Figure 3.10: Matsuura FX5 high speed machining centre


Figure 3.11: Filtermist Dustomat 15 extraction unit

| Parameter | Value |
|---|---|
| Filter surface size | 3.5 $m^2$ |
| Minimum chip size can be drawn | 0.3 μm |
| Dust collection bin | 100 L |
| Dimensions (mm) | 1230*530*1757 |
| Extraction rate | 720 $m^3$/hr |
| Approximate total cost (£) | £ 6000 |

Table 3.8: Characteristics of the dust extraction system

*3.3.1.3 Experimental setup*

The 3 mm thick CFRP specimens used in Phase 1 and 2 testing were held in a bespoke drilling jig with an array (25x25) of pre-fabricated 3 mm diameter clearance holes. Figure 3.12 shows a schematic of the jig design and associated experimental setup. Figure 3.13 details examples of the experimental arrangement employed in Phase 3 work when using (a) the through coolant adaptor (shown here during the force measurement procedure) and (b) spray mist unit, respectively. Similarly, the 30 mm high stack workpiece material was clamped onto a custom made drilling fixture with 9 mm diameter clearance holes to allow unsupported through hole drilling and a simulation of industrial practice.

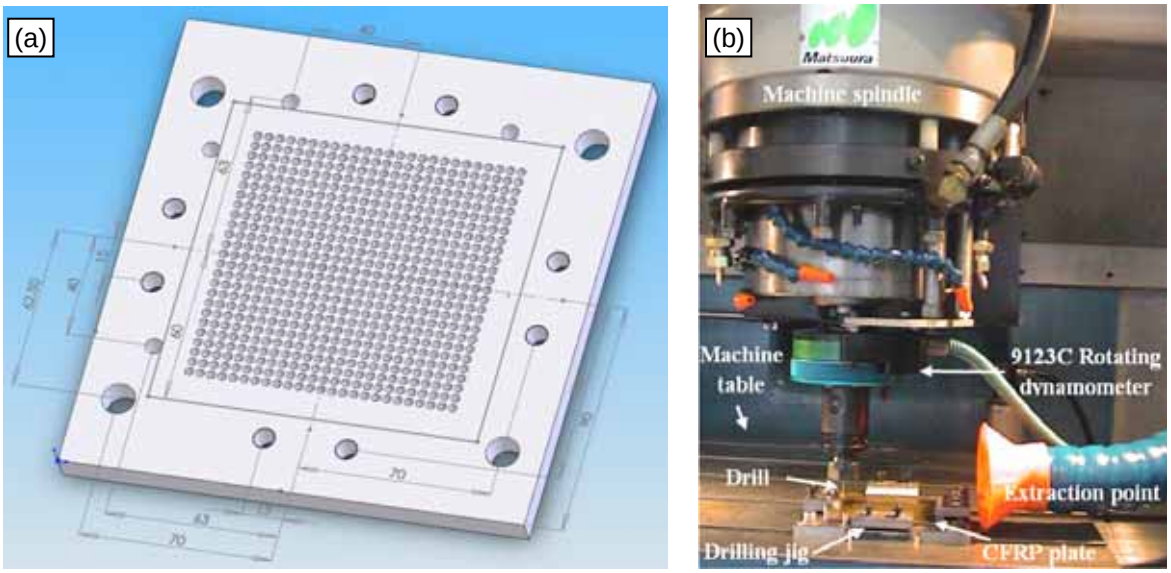


Figure 3.12: (a) Drilling jig and (b) experimental setup in Phase 1 and 2 testing

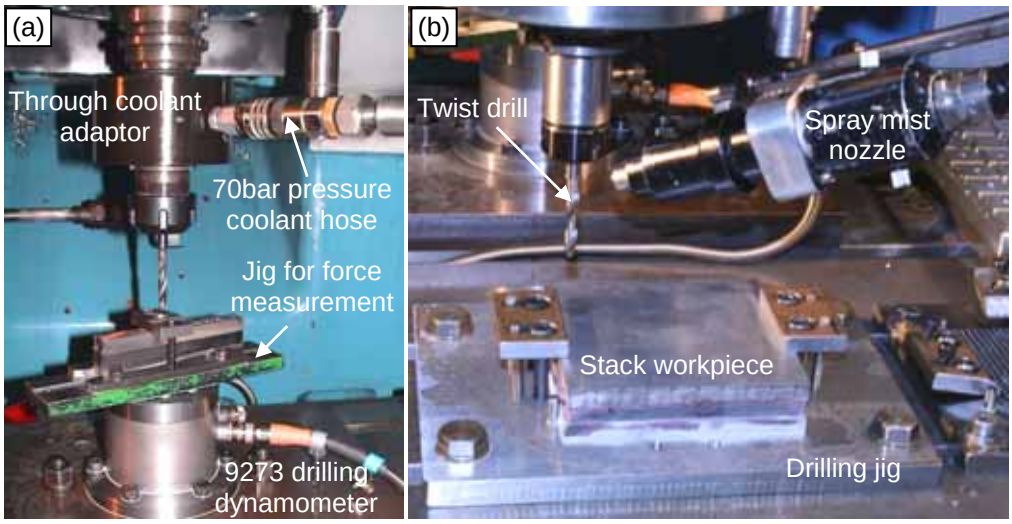


Figure 3.13: Experimental setup for Phase 3 tests: (a) through coolant adaptor with force measurement and (b) spray mist unit

### 3.3.2 Force measurement

Two fully calibrated Kistler Instruments piezoelectric force dynamometer systems were employed for the research. A 4-component rotating dynamometer (RD) type 9123C was used throughout Phase 1 and 2 experiments to evaluate thrust force and torque exerted on the cutting tool. The RD had an upper operating limit of 10,000 rpm and was equipped with a Sandvik Varilok quick release tool holder. For Phase 3 tests however, forces and torque were measured using a type 9273 drilling dynamometer due to the use of the through coolant adaptor. Signals recorded from both the rotating and static drilling dynamometers were processed through appropriate charge amplifiers (models 5223A and 5011A, respectively)

before being channelled through an A/D board connected to a PC for subsequent analysis using Dynoware software. Figure 3.14 shows the respective dynamometers and charge amplifiers used during the test programme.

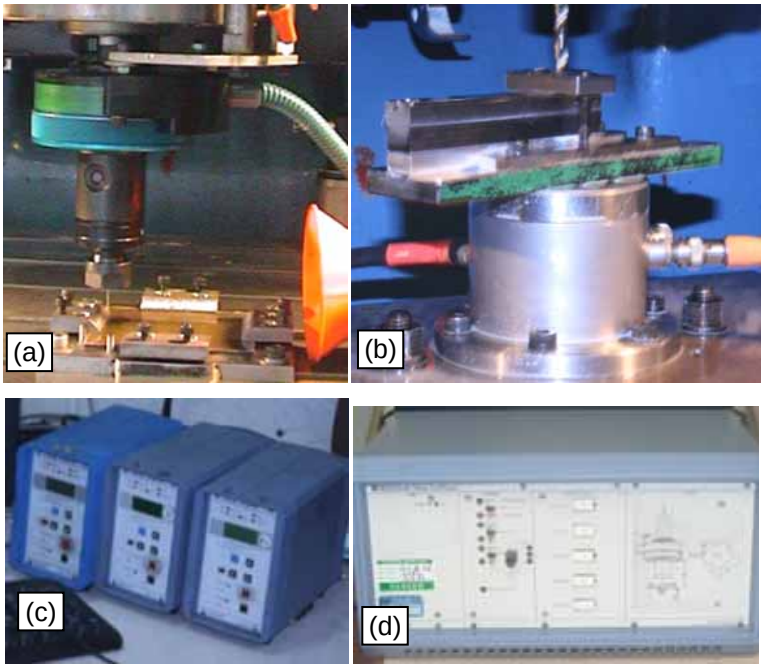


Figure 3.14: (a) 9123C Kistler rotating force dynamometer, (b) 9273 Kistler drilling dynamometer, (c) 5011A charge amplifiers connected to a PC running Dynoware and (d) 5223A charge amplifier used with the RD

### 3.3.3 Tool wear, workpiece delamination and chip analysis

Tool wear was measured using a WILD M3Z toolmaker's microscope having a XY digital micrometer platform (0.001 mm resolution); see Figure 3.15 which shows the typical wear measurement setup. A special tilting rotating table was modified and mounted on the measuring platform in order to accommodate the through coolant adaptor arrangement. When stepped drills were employed (Phase 1B and 2A), tool wear assessment was performed on the cutting lips of the pilot section only due to its high correlation with forces and delamination, which is detailed in Section 4.3.3. Additionally, SEM analysis of worn cutting lips (pilot and step) showed that the pilot cutting lips were subject to comparable levels of wear as with the step (see Figure 3.16) however, the former was easier to measure. Therefore, the accuracy of the final hole was measured and correlated with tool life measured at the cutting lips of the pilot drill section.

Digital photographs of new/worn drills, swarf from various workpiece materials and hole entry/exit delamination were captured using a high resolution Nikon EOS 400D digital camera (10 Mega pixels) attached to the microscope. These were subsequently processed with digital imaging software (Omnimet 8.7) for analysis.

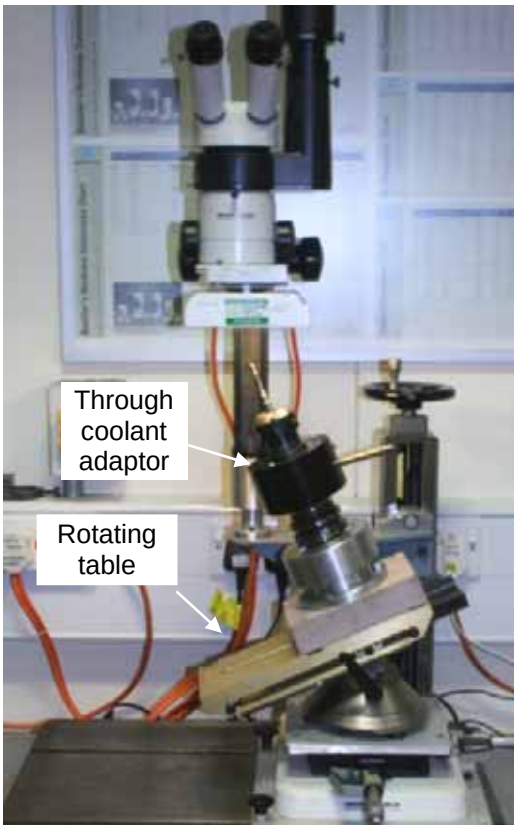


Figure 3.15: Tool wear measurement setup

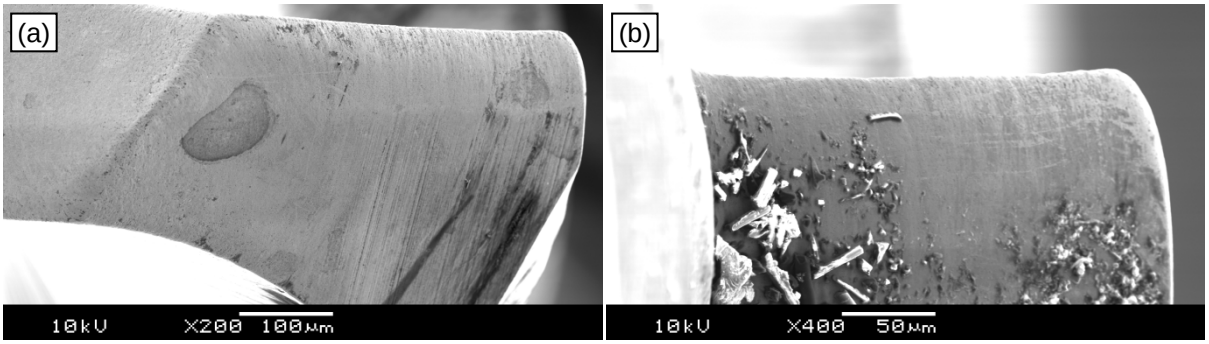


Figure 3.16: SEM images of typical worn cutting lip of: (a) pilot and (b) step drill sections

### 3.3.4 Hole diameter, cylindricity and out of roundness measurement

The small diameter drilled holes (nominally 1.5 mm) were measured using a 3 axis DEA Mistral coordinate measuring machine (CMM) equipped with a Renishaw head and 1

mm diameter ruby ball stylus (product code: A-5003-1325) as shown in Figure 3.17 (a). Final hole diameter was determined by measurement at three axial positions; 0.5, 1.5 and 2.5 mm from hole entry, as shown in Figure 3.17 (b). Twenty seven points were taken for each hole axial position and replicated twice with an average calculated. The diameter of the larger holes (6.35 mm) together with associated geometrical characteristics including cylindricity and out of roundness (ovality) was assessed using a Taylor Hobson Talyrond series 300 system, see Figure 3.18. Hole diameter and geometrical characteristics for the stacks was assessed by measurement at three axial positions; 2, 5 and 8 mm from hole entry for each material layer.

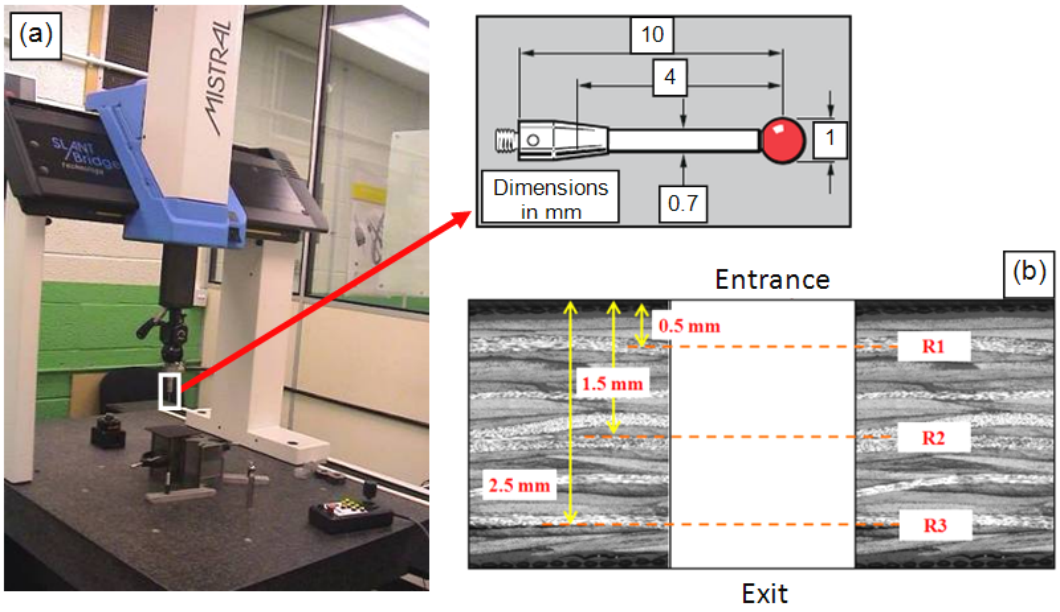


Figure 3.17: (a) 3 axis DEA Mistral coordinate measuring machine (CMM) with a 1 mm ruby ball stylus and (b) measurement positions for each material layer

Figure 3.18: Taylor Hobson Talyrond series 300

### 3.3.5 Surface roughness and burr height assessment

Following geometrical analysis of the drilled holes, the 3 mm thick CFRP plates and 30 mm thick Ti/CFRP/Al specimens were sectioned using an Agie-Charmilles Robofil FI 240ccs 5-axis CNC wire EDM machine. Hole surface roughness evaluation was primarily performed for Phase 1A and Phase 3C specimens on a Taylor Hobson Talysurf series 120L laser interferometric transducer, which produced both 2D and 3D surface topography plots (Ra and Sa). This was done using a standard conisphere diamond tipped stylus of 2 μm radius at 0.8 mm cut off length over a 4 mm evaluation length. In addition, the machine was also used to measure entry and exit burr heights on the Ti and Al material from Phase 3C tests, see Figure 3.19. 3D maps were only produced of samples from tests which showed the highest tool life.

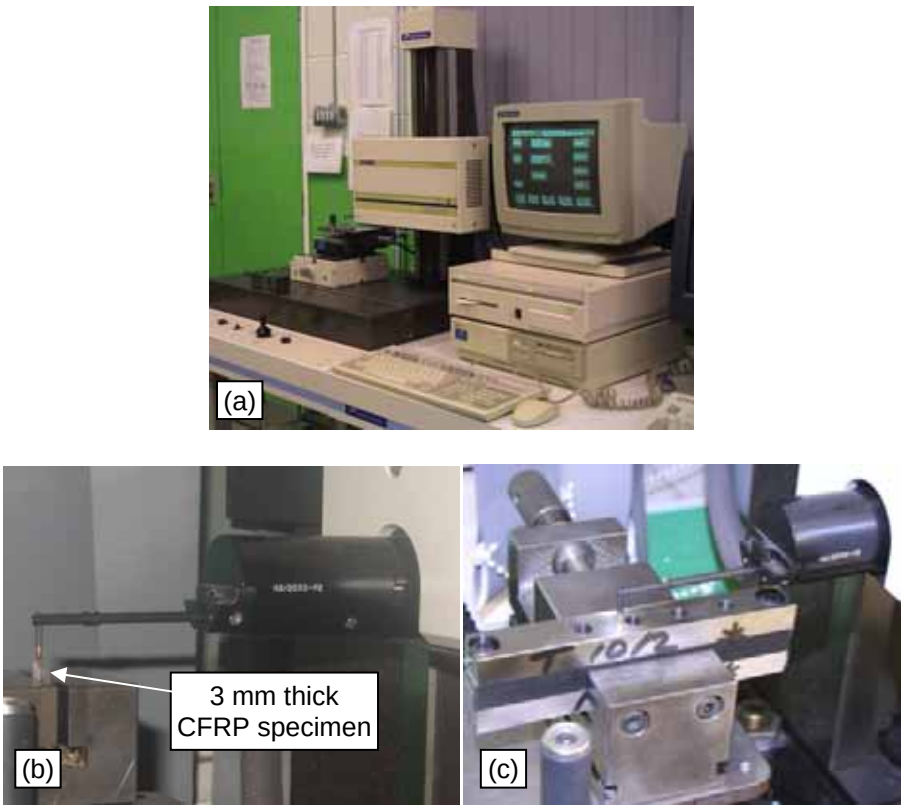


Figure 3.19: (a) Taylor Hobson Talysurf 120L, (b) setup for Ra and (c) setup for burr height measurement

### 3.3.6 Hole surface integrity analysis and microscopy

Microstructural analysis of CFRP specimens used in Phase 1 and 2 were sectioned using a band saw followed by cold mounting in an epoxy resin. In Phase 3 tests, Al and Ti samples for microhardness evaluation were hot mounted in Bakelite using a Buehler Simpliment 2 mounting press; see Figure 3.20 (a). All mounted specimens (from Phase 1 – 3) were ground

and polished using a Buehler Alpha 2 grinder-polisher shown in Figure 3.20 (b) using appropriate regimes. Optical investigation of microstructural alterations in CFRP was undertaken on Leica DMLM microscope fitted with a *PixeLINK* camera, as shown in Figure 3.20 (c) while a JOEL 6060 scanning electron microscope (SEM) was also used for assessing hole quality and cutting tool edges. Due to the relatively poor electrical conductivity of CFRP, specimens were gold coated using a sputter coater (model SC 7640) prior to analysis, see Figure 3.21.

Micro-hardness measurements of cross sectioned holes in the Al-7050 and Ti-6Al-4V layers were undertaken using a Mitutoyo HM-124 micro-hardness with a Knoop indenter at a load of 25g over a 15 second dwell time. The bulk hardness/baseline value of each material was initially determined from an average of five random measurements taken at different positions of the specimen. A hardness depth profile was obtained by taking measurements at appropriate intervals (average of 3 readings at each depth level) starting at 10 μm from the machined surface and extending up to 1000 μm.

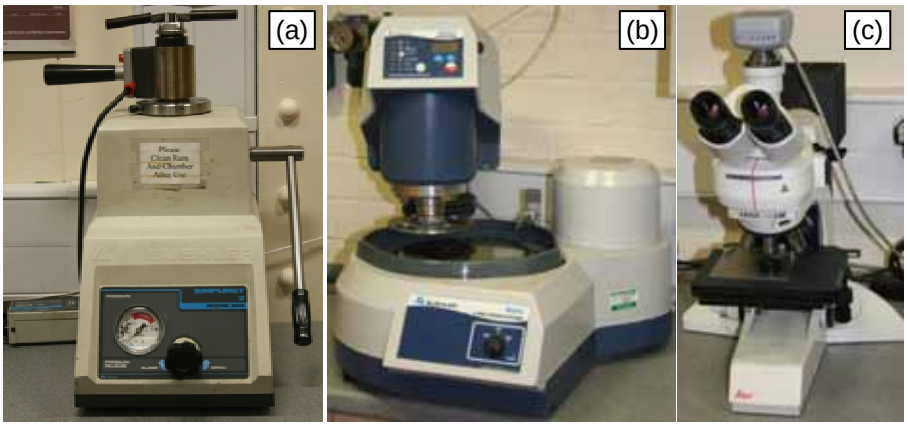


Figure 3.20: (a) Buehler mounting press, (b) Buehler grinder-polisher and (c) Leica DMLM microscope

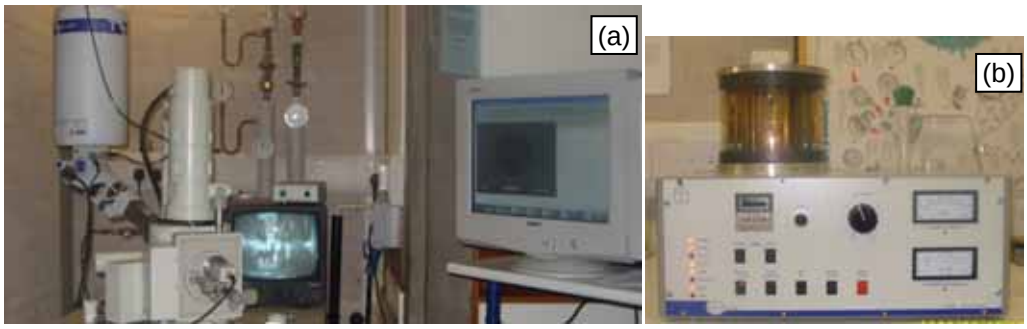


Figure 3.21: (a) JOEL 6060 Scanning electron microscope (SEM) and (b) sputter coater (SC 7640)

## 3.4 Experimental design and test arrays

The following sections describe the experimental procedure and associated test arrays used in the 3 experimental phases.

### 3.4.1 Phase 1A: Preliminary small hole drilling of CFRP and the influence of peel ply layers

Peel ply sheets assist the bleeding of volatiles and air from the laminate during curing as well as helping to prevent surface contamination which would jeopardise secondary bonding. In a production environment, this layer is generally removed from the composite surfaces prior to the drilling operation. Two comparative tests between CFRP laminates with the peel ply layers retained and removed were performed to assess their effect on hole entry and exit delamination, tool wear, thrust force, torque, hole accuracy and surface roughness. The experiments were performed using uncoated conventional twist drills with geometry as detailed in Section 3.2.1. Tests wear halted when the maximum flank wear $VB_B$ reached 100 μm. Table 3.9 details the test parameters including tooling and composite material employed.

| Fixed factors | Levels |
|---|---|
| Cutting speed | 45 m/min (9600 rpm) |
| Feed rate | 0.15 mm/rev (1440 mm/min) |
| Drill diameter | 1.5 mm |
| Drill format | Conventional twin lipped twist drill (DIXI 1126) |
| Drill material | Uncoated WC |
| Workpiece material | ACG carbon fibre reinforced plastics |
| Workpiece thickness | 3 mm |
| Cutting medium | Dry |

Table 3.9: Fixed factors and their corresponding levels for Phase 1A

### 3.4.2 Phase 1B: Effect of tool geometry and operating parameters

Phase 1B aimed to establish the influence of process parameters and drill geometry/material on key output measures including tool life, productivity, geometrical accuracy and workpiece integrity (fibre pullout, delamination, etc.). The experimental work utilised a fractional factorial design involving a modified L12 Taguchi orthogonal array. This considered variation in six process control variables (factors) including drill type, coating, point angle, helix angle, cutting speed and feed rate; each at two levels as shown in Table 3.10. Experiments were performed in a random order with a confirmation test performed in

accordance with results from the statistical analysis. Table 3.11 shows the modified Taguchi orthogonal array.

| Factors | Level 1 | Level 2 |
|---|---|---|
| Drill type (A) | Conventional | Stepped |
| Surface condition (B) | Uncoated | TiN |
| Point angle ($^o$) (C) | 118 | 140 |
| Helix angle ($^o$) (D) | 24 | 30 |
| Cutting speed (m/min) (E) | 15 | 45 |
| Feed rate (mm/rev) (F) | 0.1 | 0.2 |

Table 3.10: Process control variables for Phase 1B

| Exp. No. | Drill type (A) | Surface condition (B) | Point angle ($^o$) (C) | Helix angle ($^o$) (D) | Speed m/min (rpm) (E) | Feed mm/rev (mm/min) (F) |
|---|---|---|---|---|---|---|
| 1 | Stepped | Uncoated | 140 | 24 | 15 (3200) | 0.1 (320) |
| 2 | Stepped | TiN | 118 | 30 | 15 (3200) | 0.1 (320) |
| 3 | Conventional | TiN | 140 | 24 | 45 (9600) | 0.1 (960) |
| 4 | Stepped | Uncoated | 140 | 30 | 15 (3200) | 0.2 (640) |
| 5 | Stepped | TiN | 118 | 30 | 45 (9600) | 0.1 (960) |
| 6 | Stepped | TiN | 140 | 24 | 45 (9600) | 0.2 (1920) |
| 7 | Conventional | TiN | 140 | 30 | 15 (3200) | 0.2 (640) |
| 8 | Conventional | Uncoated | 140 | 30 | 45 (9600) | 0.1 (960) |
| 9 | Conventional | Uncoated | 118 | 30 | 45 (9600) | 0.2 (1920) |
| 10 | Stepped | Uncoated | 118 | 24 | 45 (9600) | 0.2 (1920) |
| 11 | Conventional | TiN | 118 | 24 | 15 (3200) | 0.2 (640) |
| 12 | Conventional | Uncoated | 118 | 24 | 15 (3200) | 0.1 (320) |

Table 3.11: A modified OA L12 for process control variables (A–F) and their corresponding levels for Phase 1B

Minitab software (version 15.1.20.0) was used to perform statistical analysis and produce main effects plots. Tool wear was measured in accordance with ISO 8688-2 with an end of test criterion of 100 μm maximum flank wear ($VB_B$max). This was based on the lip/cutting edge on new drills having a grind width of 100 – 120 μm. Micrographs of the drills both in the new and worn condition were taken together with photographs of hole entry and exit in the CFRP in order to evaluate workpiece delamination/damaged. The latter was quantified using a parameter known as the delamination factor ($F_d$), which is defined as the ratio of maximum damage diameter ($D_{max}$) to drilled hole diameter ($D_o$), see Figure 3.22 and

Equation (1). Entry and exit delamination were evaluated for both first and last holes drilled. Thrust force, drilling torque and flank wear measurements were recorded at intervals of ~300 holes. All tests were performed dry.

$$F_d = D_{max} / D_o \quad (3)$$

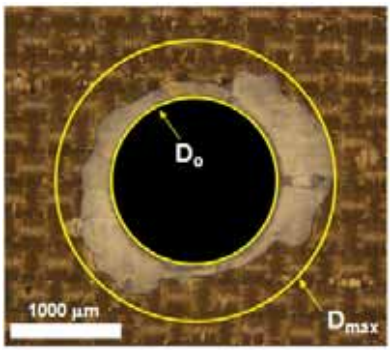


Figure 3.22: Measures used in calculating the delamination factor

### 3.4.3 Phase 2A: Effect of composite material, fibre orientation and machining parameters

This phase comprised a 4 factor (1 at 3 levels and 3 at 2 levels, shown in Table 3.12) full factorial experimental design which entailed 24 runs, as shown in Table 3.13. The control variables considered were prepreg type (977- 2/HTS autoclave cured, 8552/AS4 autoclave cured and MTM44-1/HTS oven cured), prepreg form (UD & woven), drill feed rate (0.2 and 0.4 mm/rev) and drill type (conventional and stepped geometry). Table 3.14 details factors which were kept constant. These were selected based on results from Phase 1B which identified the preferred cutting speed and drill geometry/material. Trials where drills experienced catastrophic fracture were replicated. Tool flank wear was measured according to ISO 8688-2 and tests were halted when the maximum $VB_B$ reached 100 µm or catastrophic tool failure occurred. Thrust force and torque were also recorded at intervals of ~300 holes. Final hole diameter was measured according to the procedure detailed in section 3.3.4.

| Level | Prepreg type (A) | Prepreg form (B) | Feed rate (mm/rev) (C) | Drill type (D) |
|---|---|---|---|---|
| 1 | Cytec (977-2/HTS) AC | UD | 0.2 (1920 mm/min) | Conventional |
| 2 | Hexcel (8552/AS4) AC | Woven | 0.4 (3840 mm/min) | Stepped |
| 3 | ACG (MTM44-1/HTS) OOAC | | | |

Table 3.12: Phase 2A process control variables and levels

| Test no. | (A) | (B) | (C) | (D) |
|---|---|---|---|---|
| 1 | 977-2/HTS AC (1) | UD (1) | 0.2 (1) | Conventional (1) |
| 2 | 8552/AS4 AC (2) | UD (1) | 0.2 (1) | Conventional (1) |
| 3 | MTM44-1/HTS OOAC (3) | UD (1) | 0.2 (1) | Conventional (1) |
| 4 | 977-2/HTS AC (1) | Woven (2) | 0.2 (1) | Conventional (1) |
| 5 | 8552/AS4 AC (2) | Woven (2) | 0.2 (1) | Conventional (1) |
| 6 | MTM44-1/HTS OOAC (3) | Woven (2) | 0.2 (1) | Conventional (1) |
| 7 | 977-2/HTS AC (1) | UD (1) | 0.4 (2) | Conventional (1) |
| 8 | 8552/AS4 AC (2) | UD (1) | 0.4 (2) | Conventional (1) |
| 9 | MTM44-1/HTS OOAC (3) | UD (1) | 0.4 (2) | Conventional (1) |
| 10 | 977-2/HTS AC (1) | Woven (2) | 0.4 (2) | Conventional (1) |
| 11 | 8552/AS4 AC (2) | Woven (2) | 0.4 (2) | Conventional (1) |
| 12 | MTM44-1/HTS OOAC (3) | Woven (2) | 0.4 (2) | Conventional (1) |
| 13 | 977-2/HTS AC (1) | UD (1) | 0.2 (1) | Stepped (2) |
| 14 | 8552/AS4 AC (2) | UD (1) | 0.2 (1) | Stepped (2) |
| 15 | MTM44-1/HTS OOAC (3) | UD (1) | 0.2 (1) | Stepped (2) |
| 16 | 977-2/HTS AC (1) | Woven (2) | 0.2 (1) | Stepped (2) |
| 17 | 8552/AS4 AC (2) | Woven (2) | 0.2 (1) | Stepped (2) |
| 18 | MTM44-1/HTS OOAC (3) | Woven (2) | 0.2 (1) | Stepped (2) |
| 19 | 977-2/HTS AC (1) | UD (1) | 0.4 (2) | Stepped (2) |
| 20 | 8552/AS4 AC (2) | UD (1) | 0.4 (2) | Stepped (2) |
| 21 | MTM44-1/HTS OOAC (3) | UD (1) | 0.4 (2) | Stepped (2) |
| 22 | 977-2/HTS AC (1) | Woven (2) | 0.4 (2) | Stepped (2) |
| 23 | 8552/AS4 AC (2) | Woven (2) | 0.4 (2) | Stepped (2) |
| 24 | MTM44-1/HTS OOAC (3) | Woven (2) | 0.4 (2) | Stepped (2) |

Table 3.13: Phase 2A full factorial test array

| Fixed factors | Levels |
|---|---|
| Cutting speed | 45 m/min (9600 rpm) |
| Drill geometry | Twin lipped twist drill $118^{o}$ point angle and $24^{o}$ helix angle |
| Drill material | Uncoated WC |
| Workpiece thickness | 3 mm |
| Cutting environment | Dry |

Table 3.14: Phase 2A fixed factors and levels

### 3.4.4 Phase 2B: Evaluation of diamond based coatings

Work here was designed to investigate the performance of various CVD diamond and diamond like carbon (DLC) coatings in comparison with conventional uncoated tungsten carbide (WC). Coating specification and suppliers are detailed in Section 3.2.1. A full factorial test array was initially considered which entailed 40 tests with 3 control variables (drill coating material at 5 levels, feed rate at 4 levels and prepreg type at 2 levels), see Table 3.15. However preliminary tests using CVD diamond coatings showed no benefits over uncoated or DLC coated drills and therefore they were only tested at 2 levels of feed rate. The final test matrix employed is detailed in Table 3.16. A fixed cutting speed of 47 m/min (10,000 rpm) was used for all tests while feed rate was varied between 0.1 (1000 mm/min) and 0.4 mm/rev (4000 mm/min). Results from Phase 2A highlighted that the relatively high feed rate of 0.4 mm/rev was feasible when using conventional twist drills. Similar helix and point angles were used for both standard/conventional and stepped WC twin lipped twist drills, which were $24^{o}$ and $118^{o}$ respectively. Tool wear was measured at appropriate intervals with an end of test criterion of 100 μm $VB_{B}$max or tool catastrophic failure. Limited SEM analysis was performed for both new and worn tools as well as the workpiece material. Thrust force, torque and hole entry/exit delamination were measured in accordance with the procedure used previously in Phase 1B and 2A.

| **Factors** | **Levels** | | | | |
|---|---|---|---|---|---|
| | **1** | **2** | **3** | **4** | **5** |
| Coating material (A) | Uncoated | DLC | Rhobest diamond coating | Diamond plus | Diamond fibre speed |
| Feed rate mm/rev (mm/min) (B) | 0.1 (1000) | 0.2 (2000) | 0.3 (3000) | 0.4 (4000) | |
| Prepreg type (C) | UD MTM | Woven 977-2 | | | |

Table 3.15: Phase 2B process control variables and their corresponding levels

| Test number | Coating material (A) | Feed rate (B) (mm/rev) | Prepreg type (C) |
|---|---|---|---|
| 1 | Uncoated WC | 0.1 | UD MTM |
| 2 | | | Woven 977-2 |
| 3 | | 0.2 | UD MTM |
| 4 | | | Woven 977-2 |
| 5 | | 0.3 | UD MTM |
| 6 | | | Woven 977-2 |
| 7 | | 0.4 | UD MTM |
| 8 | | | Woven 977-2 |
| 9 | Diamond like carbon (DLC) | 0.1 | UD MTM |
| 10 | | | Woven 977-2 |
| 11 | | 0.2 | UD MTM |
| 12 | | | Woven 977-2 |
| 13 | | 0.3 | UD MTM |
| 14 | | | Woven 977-2 |
| 15 | | 0.4 | UD MTM |
| 16 | | | Woven 977-2 |
| 17 | Rhobest diamond coating | 0.2 | UD MTM |
| 18 | | | Woven 977-2 |
| 19 | | 0.4 | UD MTM |
| 20 | | | Woven 977-2 |
| 21 | Diamond plus | 0.2 | UD MTM |
| 22 | | | Woven 977-2 |
| 23 | | 0.4 | UD MTM |
| 24 | | | Woven 977-2 |
| 25 | Diamond fibre speed | 0.2 | UD MTM |
| 26 | | | Woven 977-2 |
| 27 | | 0.4 | UD MTM |
| 28 | | | Woven 977-2 |

Table 3.16: Phase 2B test array

### 3.4.5 Phase 3A: Preliminary drilling trials in separate CFRP and Ti workpieces and multilayer stacks

Phase 3A involved initial experimental trials to determine the performance of a novel straight fluted domed PCD tipped drill (designed and fabricated by Element Six) against an off-the-shelf WC tool (Sandvik R840) when machining thick sections of CFRP and Ti workpieces. This comprised drilling 6.35 mm diameter holes in separate ~10 mm thick UD 977-2 CFRP laminates and 18 mm thick Ti-6Al-4V plates. Cutting speed was fixed at 80 m/min and 40 m/min for CFRP and Ti respectively while feed rate was kept constant at 0.1 mm/rev for all tests. Tool flank wear ($VB_B$ in accordance with ISO 8688-2) was measured

with tests halted when average flank wear reached 0.3 mm or when 1200 holes were produced. A further test was carried out on drilling through a combined CFRP/Ti stack (held together using a mechanical jig) under similar operating parameters using a R846 Sandvik WC drill which was recommended for composite/metallic workpieces. Table 3.17 details the test matrix. All tests were conducted wet with 70 bar through coolant. Thrust force, torque, surface roughness (Ra) and burr height were determined as comparative performance measures.

| Test no. | Drill used | Drill diameter | Material cut | WP thickness (mm) | Cutting speed (m/min) (rpm) |
|---|---|---|---|---|---|
| 1 | E6 domed PCD | 6.35 | CFRP | 9 | 80 (4000) |
| 2 | Sandvik R840 | 6.35 | CFRP | 9 | 80 (4000) |
| 3 | Sandvik R840 | 6.35 | Ti | 18 | 40 (2000) |
| 4 | E6 domed PCD | 6.35 | Ti | 18 | 40 (2000) |
| 5 | Sandvik R846 | 6.8 | CFRP/Ti | 9+18 | 84/42 (4000/2000) |

Table 3.17: Drilling test matrix for Phase 3A

### 3.4.6 Phase 3B: Impact of stack arrangement and performance of PCD tools

Following the preliminary trials in Phase 3A, experiments involving one shot drilling through multilayer 30 mm thick stacks of Al, CFRP and Ti were performed. Tests were planned involving C7 and CVD diamond coated WC drills together with brazed PCD and modified domed PCD tools (helical flute). Drilling commenced from the Al-7050 section and progressed through the CFRP and Ti layers in line with industrial practice, see Figure 3.23. Due to the significant difference in mechanical properties of the different workpiece materials, a dual level cutting speed was employed during drilling, with that for Al and CFRP being higher than that for the Ti. The initial levels for control variables are shown in Table 3.18. Four levels for both cutting speed and feed rate were selected. Unfortunately the performance of all tools, even at lowest operating parameters was poor with severe noise in force signals as well as the poor coolant transport to the titanium layer. A number of tests were then carried out with the drilling commencing from the Ti layer (Test 9 – 11). All tests in Phase 3B were performed wet. Table 3.19 details the final array for Phase 3B.

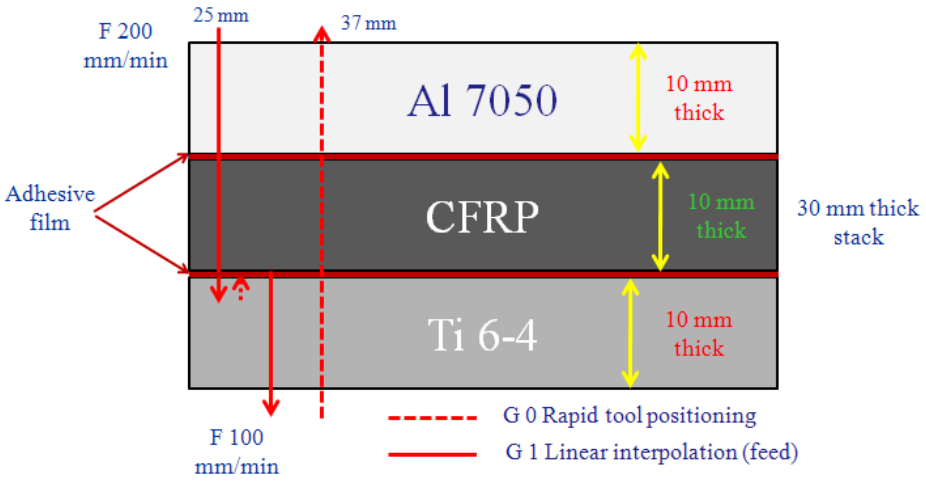


Figure 3.23: Drilling arrangement when cutting Al/CFRP/Ti stacks

| **Factors** | **Levels** | | | |
|---|---|---|---|---|
| | **1** | **2** | **3** | **4** |
| Drill type (A) | C7 coating WC | CVD diamond coating WC | Brazed PCD | E6 Domed PCD |
| Cutting speed (B) (m/min) | 60/20 (3000/1000 rpm) | 80/30 (4000/1500 rpm) | 100/40 (5000/2000 rpm) | 120/50 (6000/2500 rpm) |
| Feed rate (C) (mm/rev) | 0.05 | 0.1 | 0.15 | 0.2 |
| Environment condition (D) | Wet | Spray mist | | |

Table 3.18: Initial plan for Phase 3B control factors and levels

| **Test no.** | **Drill used** | **Cutting speed (m/min)** | **Feed rate (mm/rev)** |
|---|---|---|---|
| **Tests performed with Al/CFRP/Ti material order** | | | |
| 1 | C7 coated WC | 60/20 | 0.05 |
| 2 | C7 coated WC | 80/30 | 0.1 |
| 3 | C7 coated WC | 100/40 | 0.15 |
| 4 | C7 coated WC | 120/50 | 0.2 |
| 5 | CVD diamond coated WC | 80/30 | 0.2 |
| 6 | CVD diamond coated WC | 100/40 | 0.05 |
| 7 | CVD diamond coated WC | 120/50 | 0.1 |
| 8 | Brazed PCD | 80/30 | 0.05 |
| **Tests performed with Ti/CFRP/Al material order** | | | |
| 9 | CVD diamond coated WC | 30/80 | 0.1 |
| 10 | Brazed PCD | 20/60 | 0.1 |
| 11 | Domed PCD (E6) | 40/100 | 0.05 |

Table 3.19: Drilling tests conducted for Phase 3B

### 3.4.7 Phase 3C: Effect of tool coatings and operating parameters

Phase 3C comprised a fractional factorial design based on a L18 Taguchi orthogonal array (OA) involving variations in environment condition, drill coating, cutting speed and feed rate as shown in Table 3.20. Table 3.21 details the corresponding OA with the respective parameter levels. In terms of drill type, C7 and CVD diamond were tested alongside an equivalent uncoated WC tool. The cutting speed when drilling through CFRP and Al was twice that utilised for the Ti material. Three levels of cutting speed and feed rate were investigated, which were selected based on results from Phase 3A and 3B and the limited published literature [163]. Figure 3.24 shows the stack arrangement used, where cutting commenced from the titanium layer. Tests were carried out wet using the through coolant adaptor (specifications provided in Section 3.3.1.2) or using spray mist. Tool life criterion was identical to that employed in Phase 3B while thrust force and torque were measured at intervals of ~10-30 holes for all tests. Hole geometrical characteristics, burr height and surface roughness were only assessed for tests which produced more than 150 drilled holes in addition to the longest tool life obtained with spray mist. Final hole diameter was measured at the mid position for every layer. Cylindricity error for the entire stack (based on 9 axial positions) and for the individual layers were also obtained (3 axial positions/layers, similar to roundness positions). Hole entry and exit burr height for the Al and Ti layers were recorded while hole edge quality for all materials was assessed. The surface roughness (Ra) was measured at three positions within each layer of the stack and then averaged. Chips from the various workpiece materials were collected and photographed for analysis. Microhardness measurement for the Al and Ti holes was performed only for two tests which demonstrated the longest tool life.

| **Factor** | **No of levels** | **Levels** | | |
|---|---|---|---|---|
| Environment condition (A) | 2 | Wet | Spray mist | |
| Drill type (B) | 3 | Uncoated WC | CVD diamond coating WC | C7 coating WC |
| Cutting speed (C) Ti/CFRP/Al (m/min) | 3 | 20/40 (1000/2000 rpm) | 40/80 (2000/4000 rpm ) | 60/120 (3000/6000 rpm) |
| Feed rate (D) (mm/rev) | 3 | 0.05 | 0.10 | 0.15 |

Table 3.20: Process control variable and levels for Phase 3C

| Test | Environment condition (A) | Coating (B) | Cutting speed (C) (m/min) | Feed rate (D) (mm/rev) |
|---|---|---|---|---|
| 1 | Wet (1) | Uncoated (1) | 20/40 (1) | 0.05 (1) |
| 2 | Wet (1) | Uncoated (1) | 40/80 (2) | 0.1 (2) |
| 3 | Wet (1) | Uncoated (1) | 60/120 (3) | 0.15 (3) |
| 4 | Wet (1) | CVD coated (2) | 20/40 (1) | 0.05 (1) |
| 5 | Wet (1) | CVD coated (2) | 40/80 (2) | 0.1 (2) |
| 6 | Wet (1) | CVD coated (2) | 60/120 (3) | 0.15 (3) |
| 7 | Wet (1) | C7 coated (3) | 20/40 (1) | 0.1 (2) |
| 8 | Wet (1) | C7 coated (3) | 40/80 (2) | 0.15 (3) |
| 9 | Wet (1) | C7 coated (3) | 60/120 (3) | 0.05 (1) |
| 10 | Spray mist (2) | Uncoated (1) | 20/40 (1) | 0.15 (3) |
| 11 | Spray mist (2) | Uncoated (1) | 40/80 (2) | 0.05 (1) |
| 12 | Spray mist (2) | Uncoated (1) | 60/120 (3) | 0.1 (2) |
| 13 | Spray mist (2) | CVD coated (2) | 20/40 (1) | 0.1 (2) |
| 14 | Spray mist (2) | CVD coated (2) | 40/80 (2) | 0.15 (3) |
| 15 | Spray mist (2) | CVD coated (2) | 60/120 (3) | 0.05 (1) |
| 16 | Spray mist (2) | C7 coated (3) | 20/40 (1) | 0.15 (3) |
| 17 | Spray mist (2) | C7 coated (3) | 40/80 (2) | 0.05 (1) |
| 18 | Spray mist (2) | C7 coated (3) | 60/120 (3) | 0.1 (2) |

Table 3.21: L18 OA in real variable values

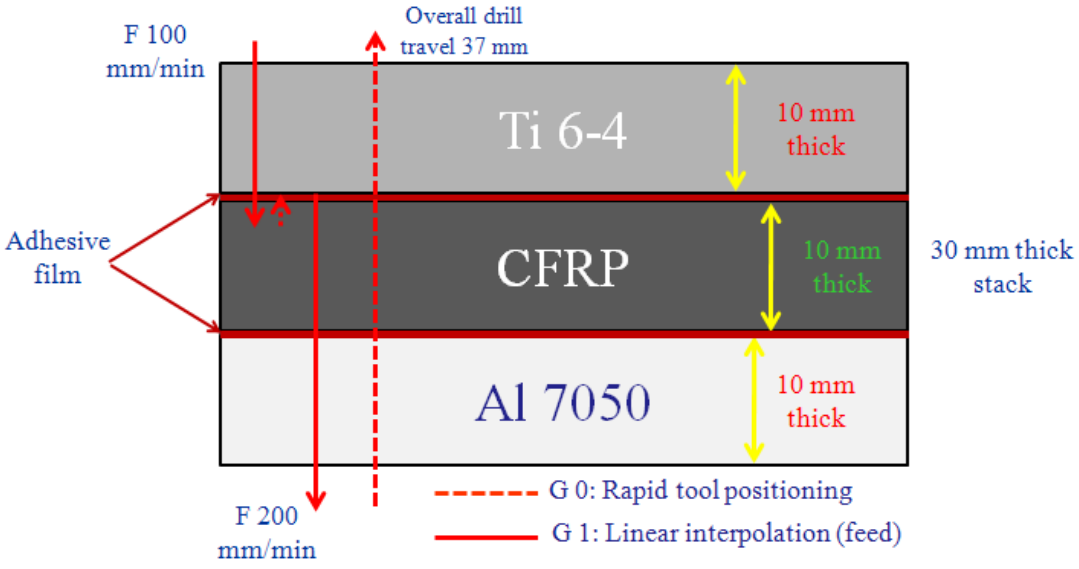


Figure 3.24: Drilling arrangement when cutting Ti/CFRP/Al stacks

# 4. RESULTS AND DISCUSSION

## 4.1 Phase 1A: Preliminary small hole drilling of CFRP and the influence of peel ply layers

Figure 4.1 shows the progression of entry and exit delamination factor against number of drilled holes for tests performed with the nylon peel ply backed CFRP material. Workpiece delamination was understandably found to be greater at the hole exit compared to entry due to the lack of support to prevent matrix/fibre fracture during tool breakout. At cessation of the trial, hole entry and exit showed an $F_d$ of 1.30 and 1.35 respectively. In contrast, the test carried out on laminates without the peel ply layer experienced severe workpiece damage in the form of fuzzing, incomplete fibre cutting and edge chipping both at hole entry and exit in addition to delamination, see Figure 4.2. Unfortunately, the damage was such that it prevented the evaluation of delamination factor for specimens without the peel ply layers.

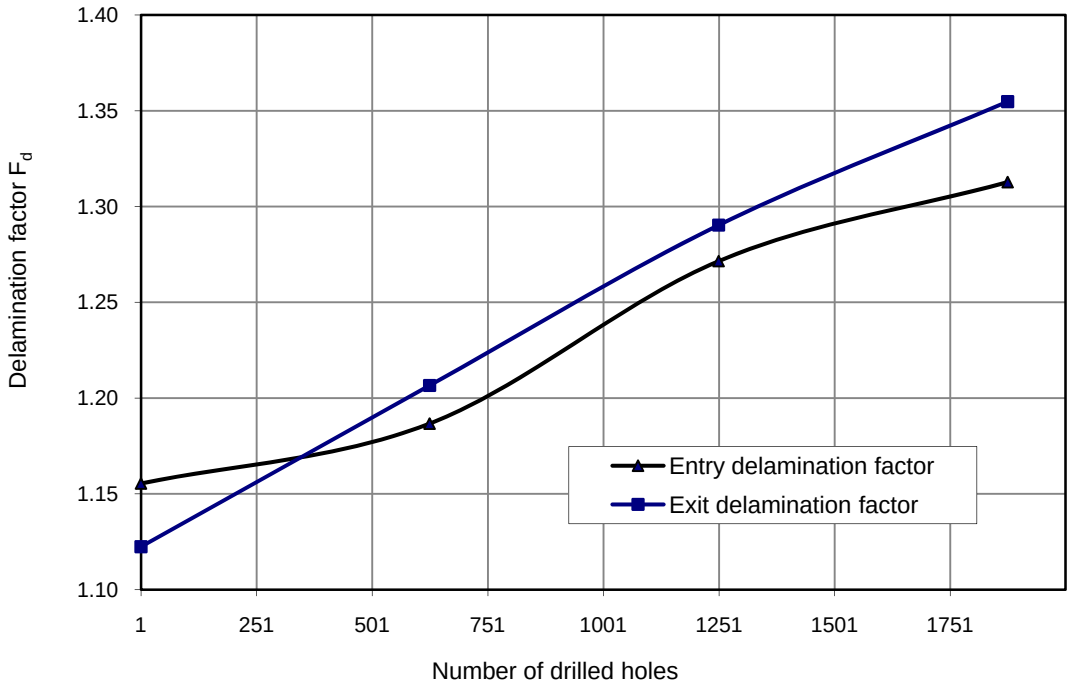


Figure 4.1: Entry/exit delamination factor for drilling with peel ply layer

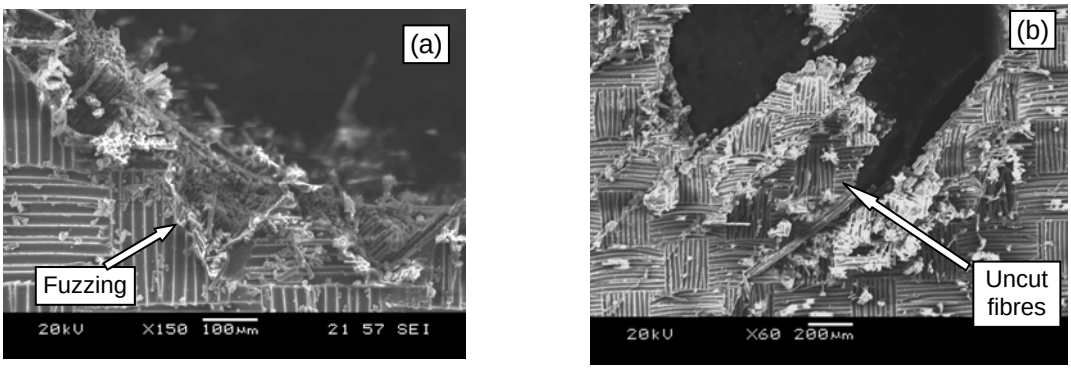


Figure 4.2: (a) Entry damage for the 1250$^{th}$ hole and (b) Exit damage (fraying) of the 625$^{th}$ hole for un-backed materials

A comparison of hole quality obtained when drilling workpieces with and without the peel ply layer at various points of the test is shown in Figure 4.3 and Figure 4.4. The CFRP with the nylon layer maintained excellent hole edge integrity even after 1250 holes however the situation was markedly different with the non peel ply specimens. Here, fuzzing was the primary defect observed at hole entry, while substantial edge chipping was present at the exit after only several holes. The benefits accorded by the peel ply layer are analogous to the advantages/benefits provided when employing backup material during the drilling of FRP composites, as detailed in the results by Tsao and Hocheng [95].

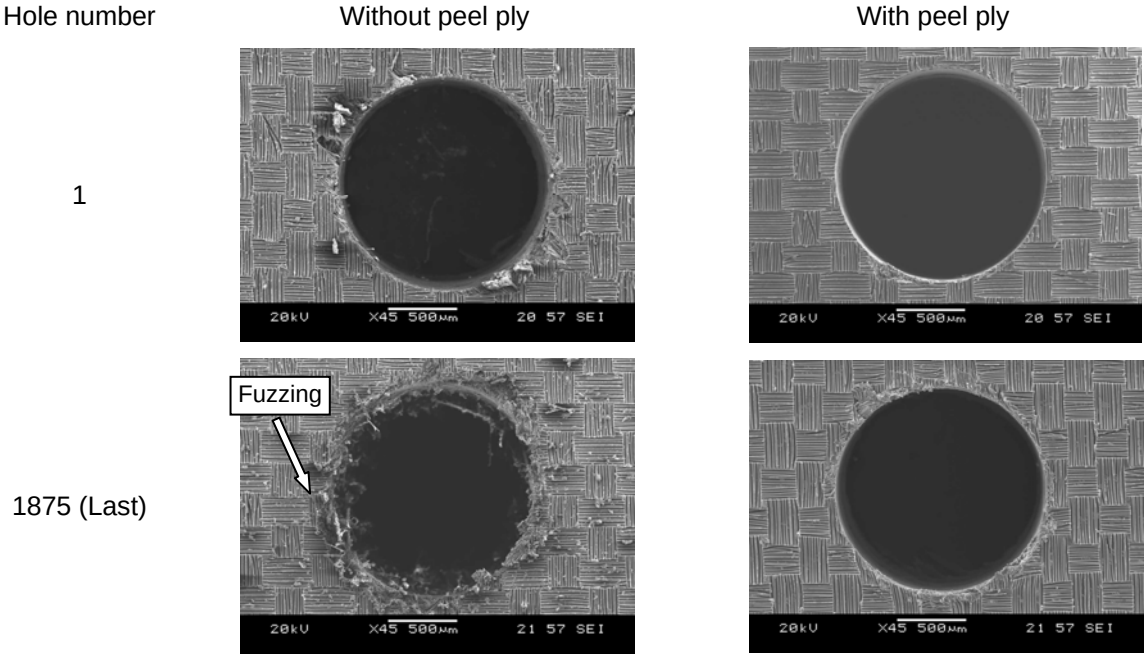


Figure 4.3: SEM images showing progression of damage at hole entry

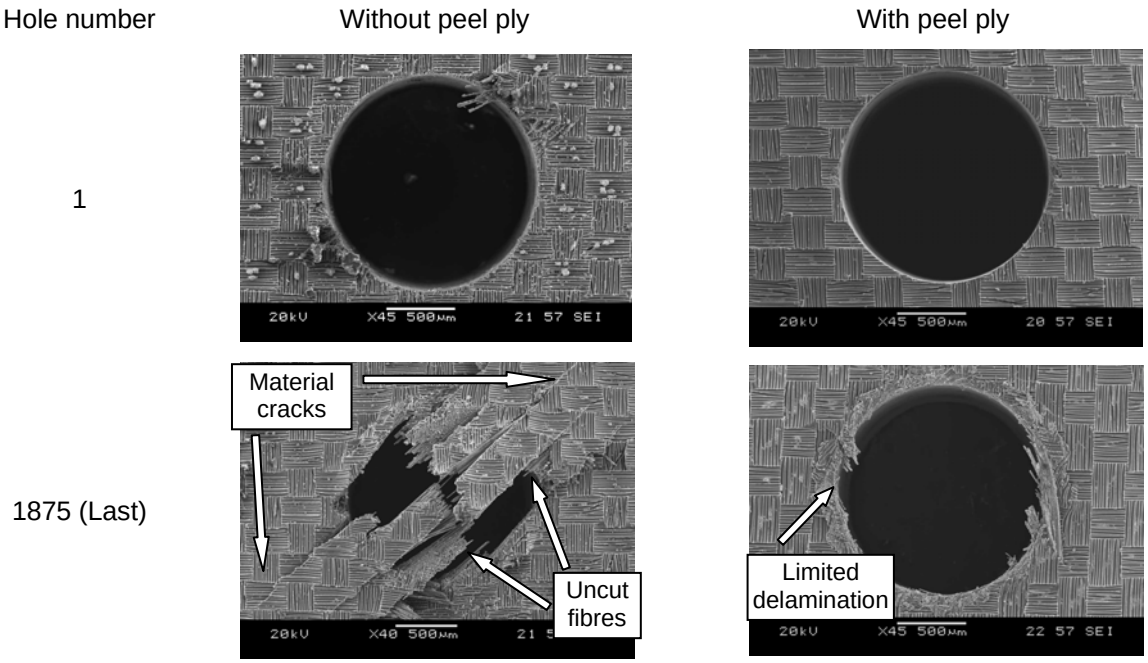


Figure 4.4: SEM images showing progression of damage at hole exit

Drill flank wear was measured at regular intervals of ~ 150 holes during each test. Figure 4.5 details the progression of tool flank wear with number of holes drilled for the backed and un-backed CFRP material. While wear progression followed a similar trend in both tests, the wear rate was somewhat higher in the case where a peel ply was employed. This can be attributed to the cumulative increase in workpiece material thickness of 375 mm over 1875 holes as a result of the peel ply layer (~ 200 μm per hole). An additional 5 μm of flank wear was observed at the end of the tests. SEM images of new and worn WC conventional twist drills following drilling of the backed and un-backed materials are shown in Figure 4.6. Blunting/rounding of the cutting and chisel edges due to abrasion was the principal wear mode. Trials carried out with the peel ply samples revealed a greater tendency for the resulting chips (composed of fibre and matrix elements) to adhere onto the secondary flank of the tool, owing to the melting/softening of the nylon layer.

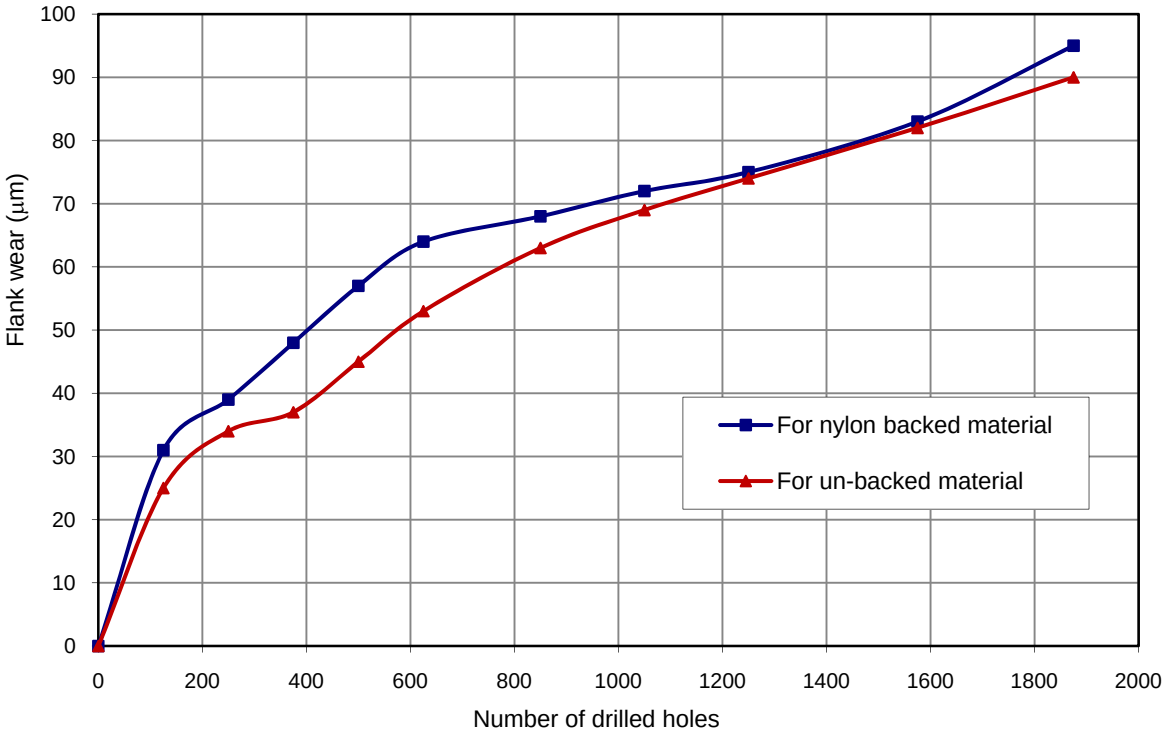


Figure 4.5: Flank wear for drilling nylon backed and un-backed CFRP materials

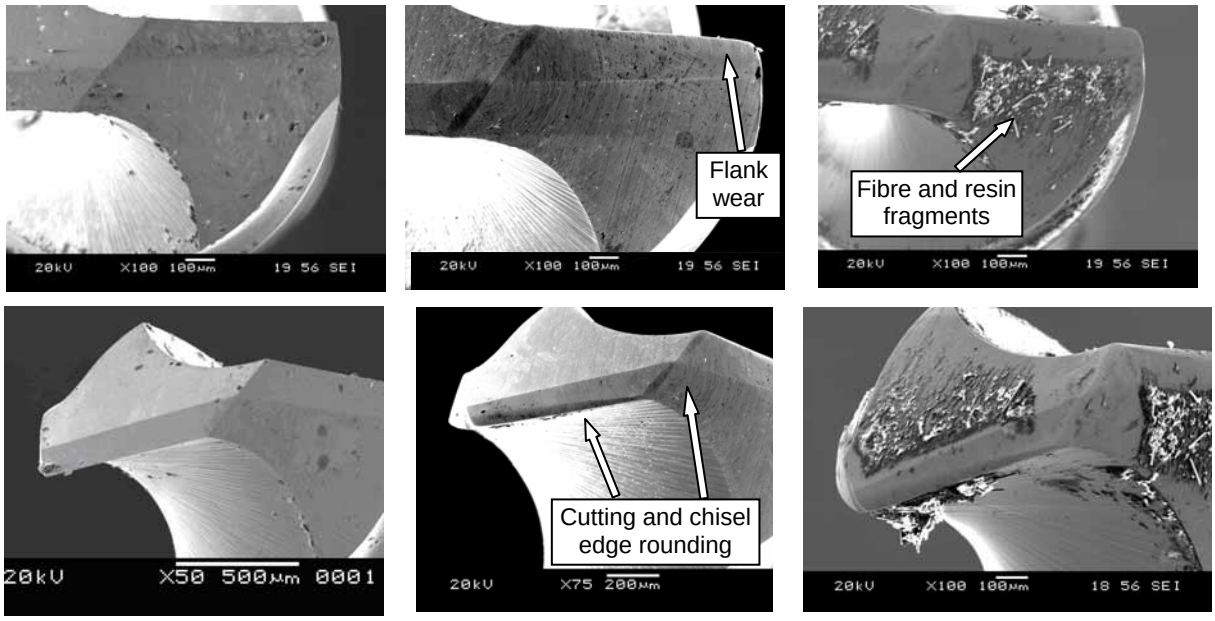


(a) (b) (c)

Figure 4.6: WC drills: (a) new, (b) used for drilling un-backed CFRP and (c) used for nylon backed CFRP

Figure 4.7 (a) shows the thrust force values recorded when drilling peel ply backed and un-backed CFRPs respectively. Typically, the forces were seen to double from the start (26 – 29 N) to the end (49 – 52N) of the tests in both cases. On average, the absence of the peel ply layer also reduced thrust forces by approximately 10%. This corresponded to the higher tool wear levels associated with the nylon backed material as previously indicated. Dimensional error refers to the difference between the required/nominal hole diameter (1.5 mm) and the actual hole dimension produced. Here, the use of a peel ply layer presented no significant effect on dimensional error as the measured diameter values were approximately similar over the test duration for both material conditions; see Figure 4.7 (b). As expected, the size of the holes decreased as the experiment progressed, which reflected the reduction in drill diameter as a result of tool wear. Despite this, the percentage dimensional error was extremely small, in the region of ~ 2% (maximum of ~ 30 µm undersize) after 1875 holes. This was deemed to be within the acceptable limits of tolerance for some of the applications envisaged.

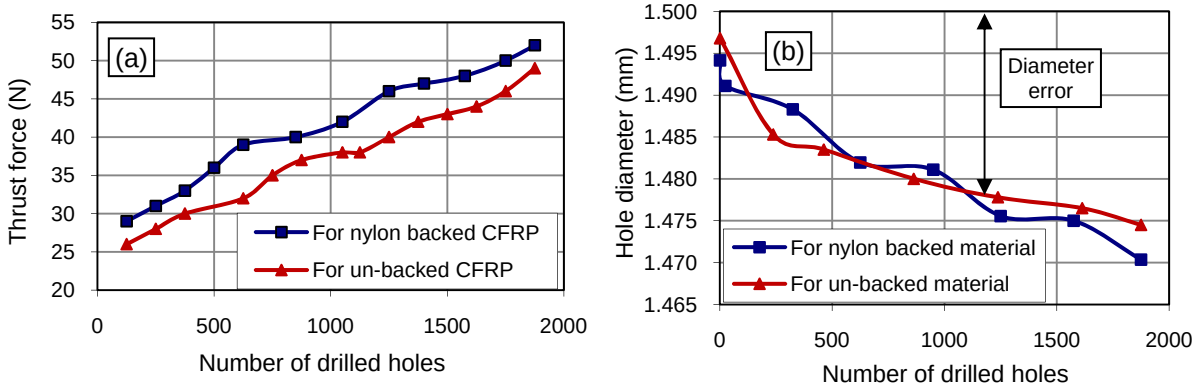


Figure 4.7: (a) Thrust force and (b) hole diameter versus number of drilled holes for backed and un-backed CFRP

In terms of hole surface quality, the average surface roughness (Sa) was relatively low (< 0.8 µm) for the first ~ 30 holes, irrespective of the material drilled. This was most likely due to the sharpness of cutting edges with new tools. The surface roughness however quickly deteriorated with a two fold increase after approximately 625 holes, in line with tool wear progression, see Figure 4.8. This steep rate of decline in surface quality subsequently stabilised, with only a further very small increase in surface roughness up to test cessation, see Figure 4.9. Despite an obvious trend in the data, there is nonetheless concern regarding the reliability and value of surface roughness as a performance measure due to the inhomogeneous and fibrous nature of the composite material.

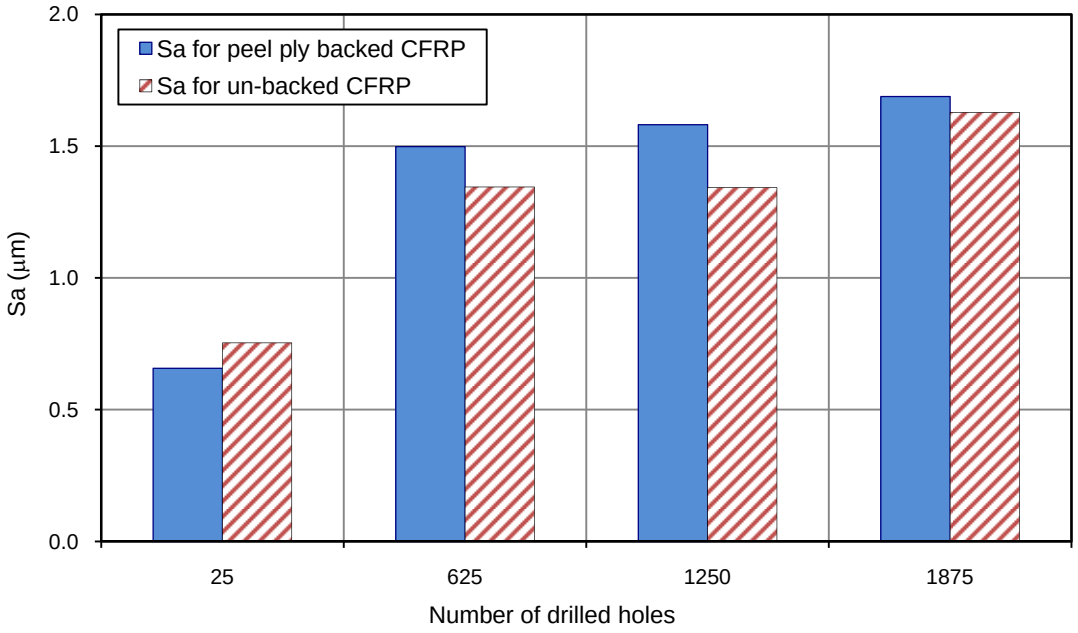


Figure 4.8: Average surface roughness for drilling backed and un-backed CFRP materials

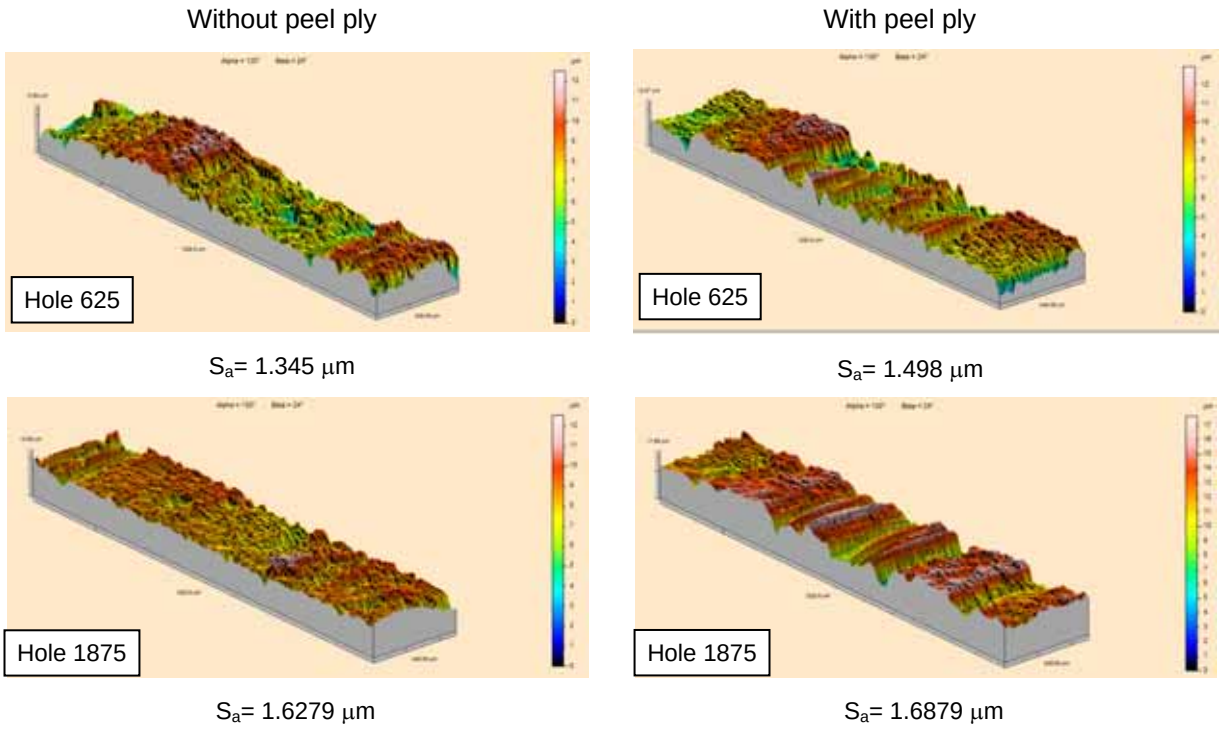


Figure 4.9: 3D topography maps for un-backed (left) and backed (right) materials

SEM analysis revealed that greater levels of damage occurred at the position where fibre orientation was 135°, see Figure 4.10 (a). In this direction, fibres fractured at different positions along their length and hence produced irregular surfaces. This was in agreement with previous research on orthogonal cutting of FRP composites by Wang et al. [48]. Additionally, hole edge quality was also adversely affected as some of the fibres were deflected during cutting which sprang back when the tool was retracted as shown in Figure 4.10 (b).

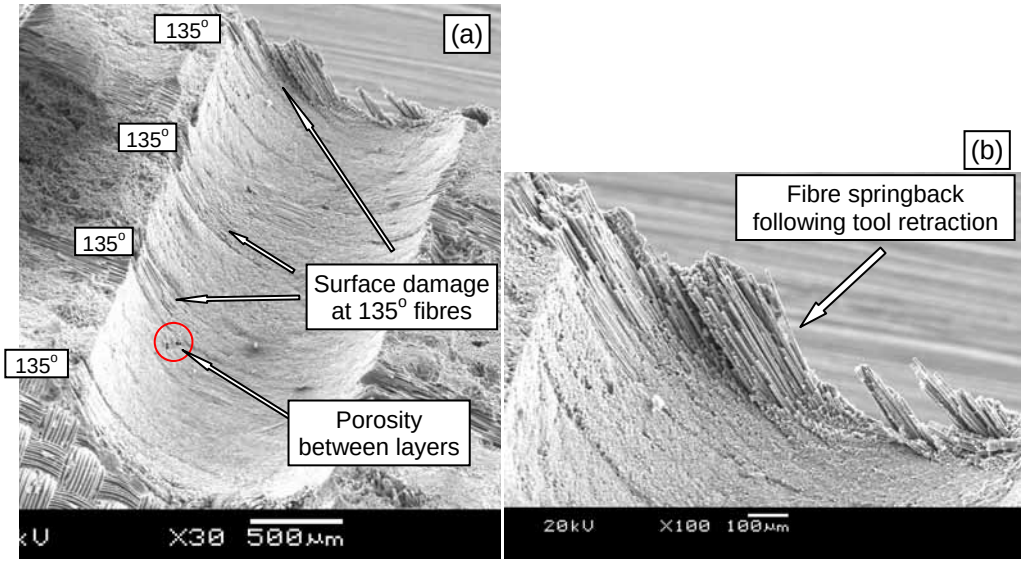


Figure 4.10: (a) Various forms of damage at the cut surface and (b) incompletely cut fibres

## 4.2 Phase 1B: Effect of tool geometry and operating parameters

### 4.2.1 Tool wear and tool life

Flank wear and chisel edge wear were observed in all tests and were dominant wear features. The former was measured during each test at intervals of ~200 holes, and a typical gradual increase observed. Figure 4.11 shows drill wear plots for all tests. The graphical data follow conventional trends seen when cutting a wide range of materials. The close proximity in results for the two cutting edges reflects the good geometrical accuracy of the drills. Figure 4.12 shows sample photographs for new and worn tools used in the experimentation at two different test combinations. The typical flank wear evolution of drills can be seen in Figure 4.13. The level of flank wear varied over the drill lip cutting edge with the maximum scar associated with the location of highest cutting speed (drill corner). No chisel edge or cutting

edge fractures occurred in any of the tests, and all tools showed similar wear patterns at test cessation, see Figure 4.14. Additionally, peeling of the coating (Figure 4.15) from the main cutting edge and chisel edge rounding were also observed in tests. The findings are in agreement with results by Faraz et al. [99] who reported that edge rounding is the dominant wear mode when machining CFRP composites due to the highly abrasive nature of the fibres.

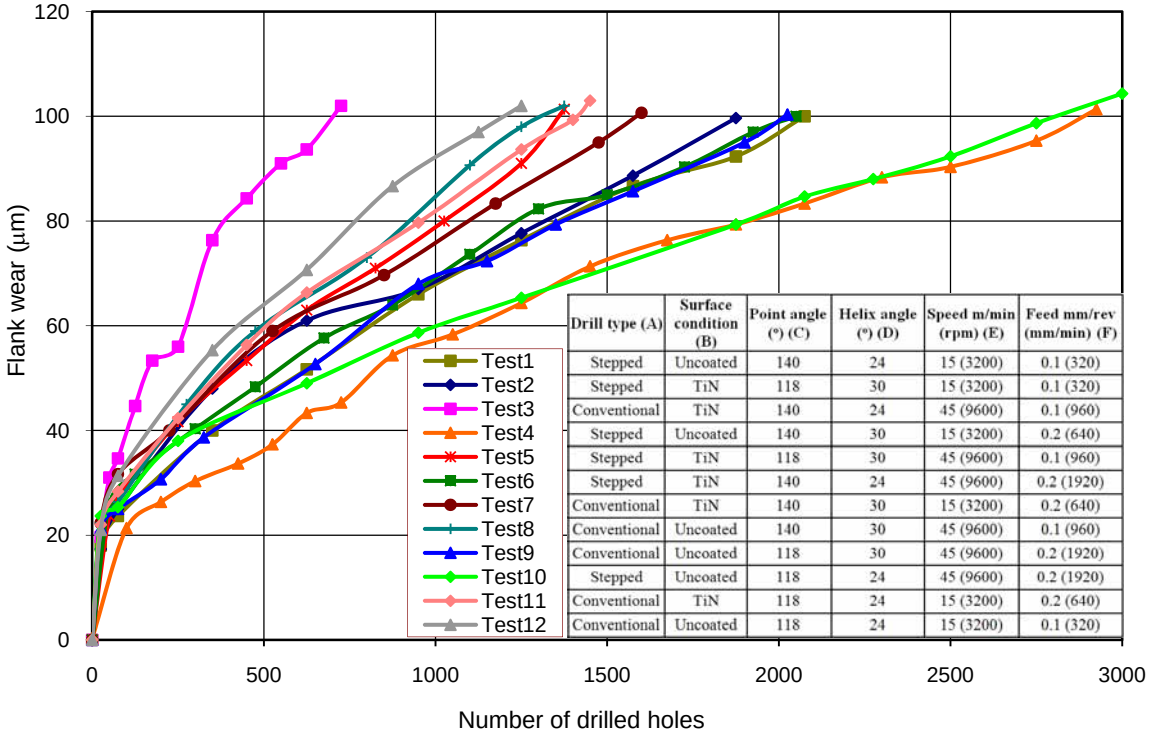


| Drill type (A) | Surface condition (B) | Point angle (°) (C) | Helix angle (°) (D) | Speed m/min (rpm) (E) | Feed mm/rev (mm/min) (F) |
|---|---|---|---|---|---|
| Stepped | Uncoated | 140 | 24 | 15 (3200) | 0.1 (320) |
| Stepped | TiN | 118 | 30 | 15 (3200) | 0.1 (320) |
| Conventional | TiN | 140 | 24 | 45 (9600) | 0.1 (960) |
| Stepped | Uncoated | 140 | 30 | 15 (3200) | 0.2 (640) |
| Stepped | TiN | 118 | 30 | 45 (9600) | 0.1 (960) |
| Stepped | TiN | 140 | 24 | 45 (9600) | 0.2 (1920) |
| Conventional | TiN | 140 | 30 | 15 (3200) | 0.2 (640) |
| Conventional | Uncoated | 140 | 30 | 45 (9600) | 0.1 (960) |
| Conventional | Uncoated | 118 | 30 | 45 (9600) | 0.2 (1920) |
| Stepped | Uncoated | 118 | 24 | 45 (9600) | 0.2 (1920) |
| Conventional | TiN | 118 | 24 | 15 (3200) | 0.2 (640) |
| Conventional | Uncoated | 118 | 24 | 15 (3200) | 0.1 (320) |

Figure 4.11: Drill wear graph for all tests (based on the maximum flank wear criterion)

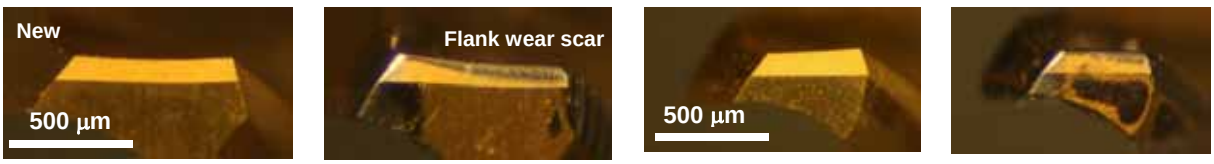


(a) Test 11, conventional drill, TiN coated (b) Test 5, stepped drill, TiN coated

Figure 4.12: New and worn drills for Test 5 and Test 11

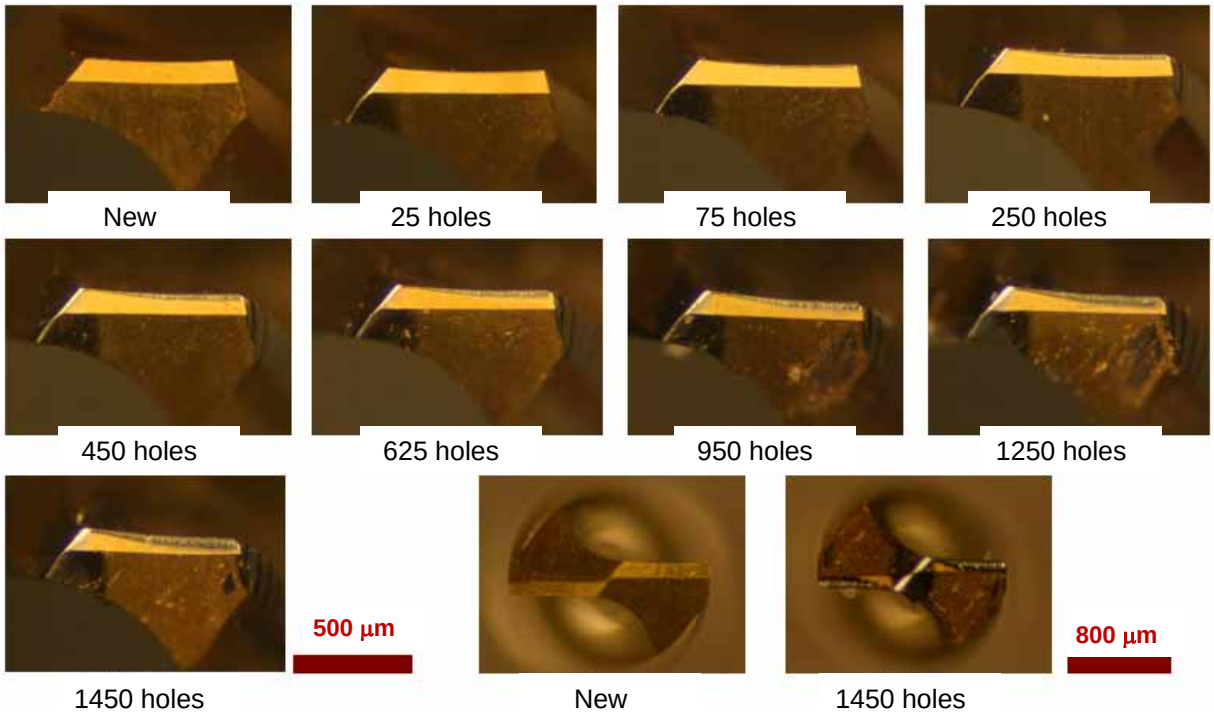


Figure 4.13: Drill flank wear evolution for Test 11 (TiN conventional drill, 118°, 24°, 15 m/min and 0.1 mm/rev)

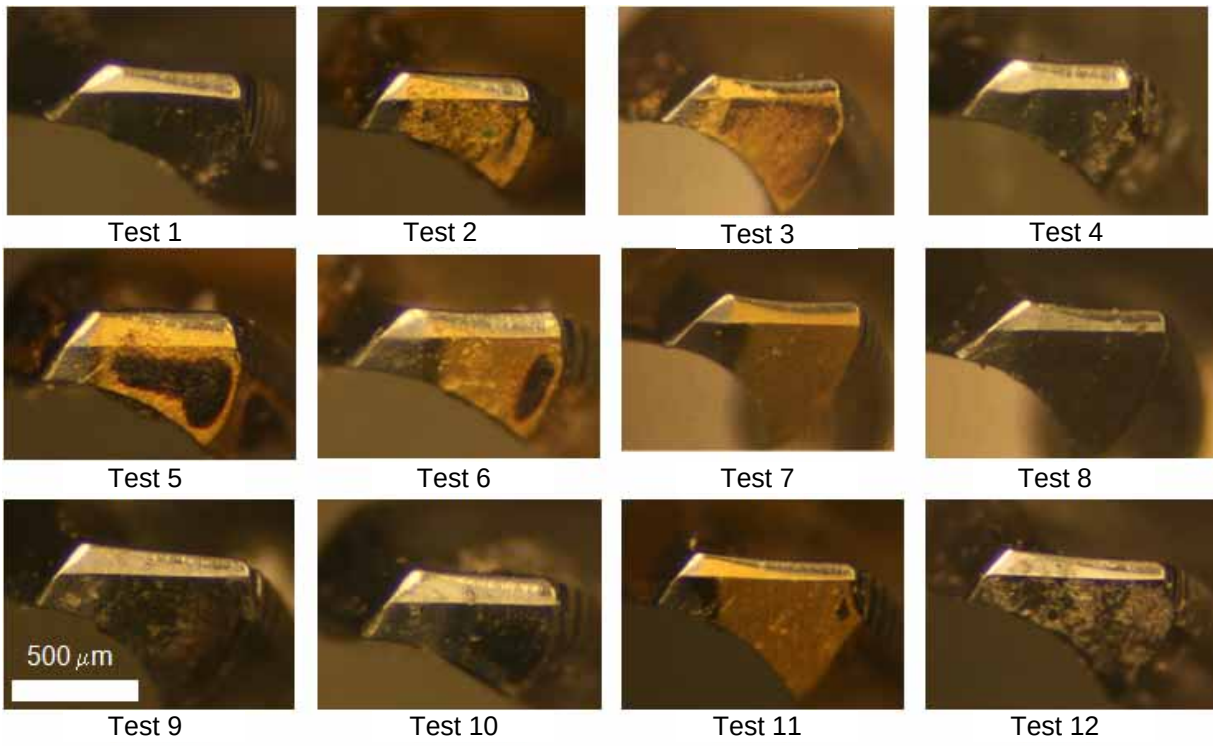


Figure 4.14: Drill wear pattern for all tests at end of tool life

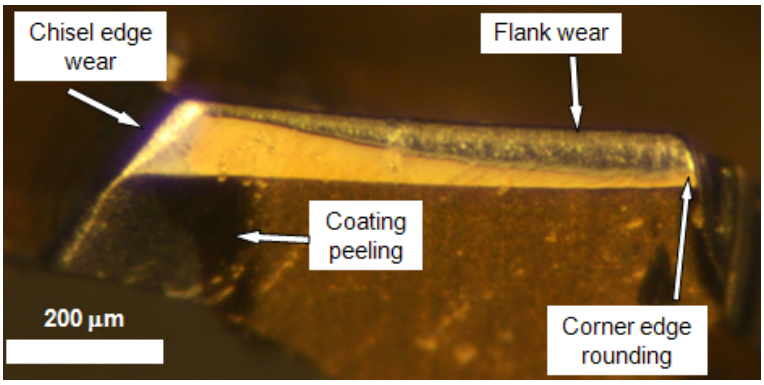


Figure 4.15: Drill wear details for Test 11 after 1450 holes (conventional drill, TiN coating, 118$^{o}$ helix angle, 24$^{o}$ point angle, 15 m/min cutting speed and 0.2 mm/rev feed rate)

Figure 4.16 shows the main effects plot for tool life. In general, tool life ranged between 700 and 2900 holes with the statistical analysis showing that the main contributing factors were drill type and feed rate, each having high PCR's of 37.2% and 32.6% respectively, while tool surface condition was also significant but with a more moderate PCR of 20%, see Table 4.1. Essentially the results showed that higher tool life could be obtained when employing a stepped drill, higher feed rate and an uncoated tool. Stepped drills are preferred as they exhibited higher productivity compared to conventional twist drills. In the present work their use contributed to a significant reduction in thrust force during second stage drilling (when the 1.5 mm diameter sizing section was involved in cutting) due to the lack of interaction between the chisel edge and workpiece material. This corresponds with published data by Tsao and Hocheng [69, 73-74]. As feed rate was increased, contact time between the cutting tool and workpiece material reduced, resulting in a reduction in the spiral distance cut, anticipated lower cutting temperatures and hence tool wear. The longer tool life achieved with the uncoated drills was however somewhat unexpected but may have been due to the sharper cutting edges present in comparison with the coated tools. In any event, the ~10% error level associated with tool life evaluation was within acceptable limits, suggesting all important factors had been considered as well as measurements performed accurately.

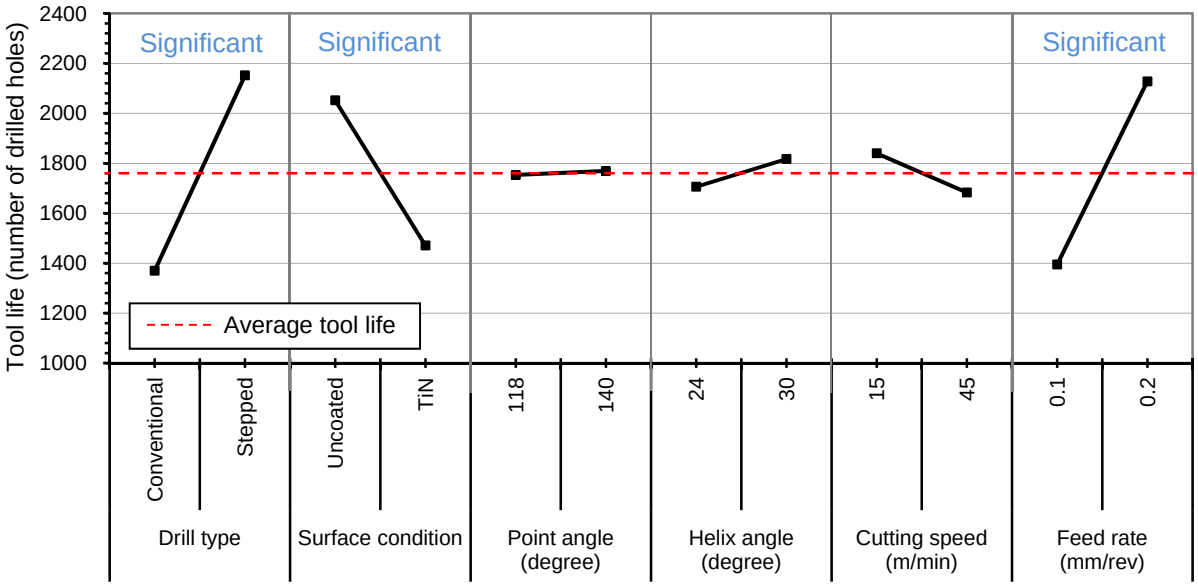


Figure 4.16: Main effects plot, means for tool life (Phase 1B)

| Factor | DF | SS | Exp SS | F | P | PCR |
|---|---|---|---|---|---|---|
| **Drill type** | 1 | 1829102 | 1765947 | 50.20 | 0.001* | 37.21 |
| **Surface condition** | 1 | 1012102 | 948947 | 27.78 | 0.003* | 19.99 |
| **Point angle (°)** | 1 | 752 | -62403 | 0.02 | 0.891 | 0 |
| **Helix angle (°)** | 1 | 36852 | -26303 | 1.01 | 0.361 | 0 |
| **Cutting speed (m/min)** | 1 | 74419 | 11263.6 | 2.04 | 0.212 | 0.23 |
| **Feed rate (mm/rev)** | 1 | 1609669 | 1546514 | 44.18 | 0.001* | 32.59 |
| **Error** | 5 | 182160 | | | | ***10.18*** |
| **Total** | 11 | 4745056 | | | | |

DF = Degrees of freedom
SS = Sum of squares
Exp SS = Expected sum of squares
* Significant at the 5% level

F = F-test value
F calculated for all factors = 6.61
P = Probability
PCR = Percentage contribution ratio

Table 4.1: ANOVA results for tool life (Phase 1B)

### 4.2.2 Thrust force and torque

Figure 4.17 shows the thrust force profile for a typical hole drilled using (a) conventional and (b) stepped drill geometries at identical cutting speed and feed rate (45 m/min and 0.1 mm/rev respectively) levels. When using conventional drill geometry, the force signal recorded was as expected [57]. With the stepped drill however, the thrust force profile principally comprised two regions, which corresponded to the operation of the pilot section of 1 mm diameter and sizing region (1.5 mm diameter) respectively. A significant reduction in maximum thrust force (~ 42%) was observed with an anticipated drop in stress acting on tool edges. This explains the greater performance in terms of longer tool life

obtained when the stepped drill was utilised. Additionally, the thrust force fluctuations experienced over the workpiece depth were the result of tool edges passing through different fibre orientations as well as the different properties between fibres and matrix. The findings are in agreement with results by Bhatnagar et al. [39] who reported that thrust force behaves in a cyclic fashion when machining FRP composites. Figure 4.18 shows the respective thrust force and torque data for tests producing the highest tool life (Test 4 and 10), with the remaining results presented in Appendix D. A typical gradual increase in both responses with number of holes drilled was seen as a result of regular cutting edge wear [57, 89].

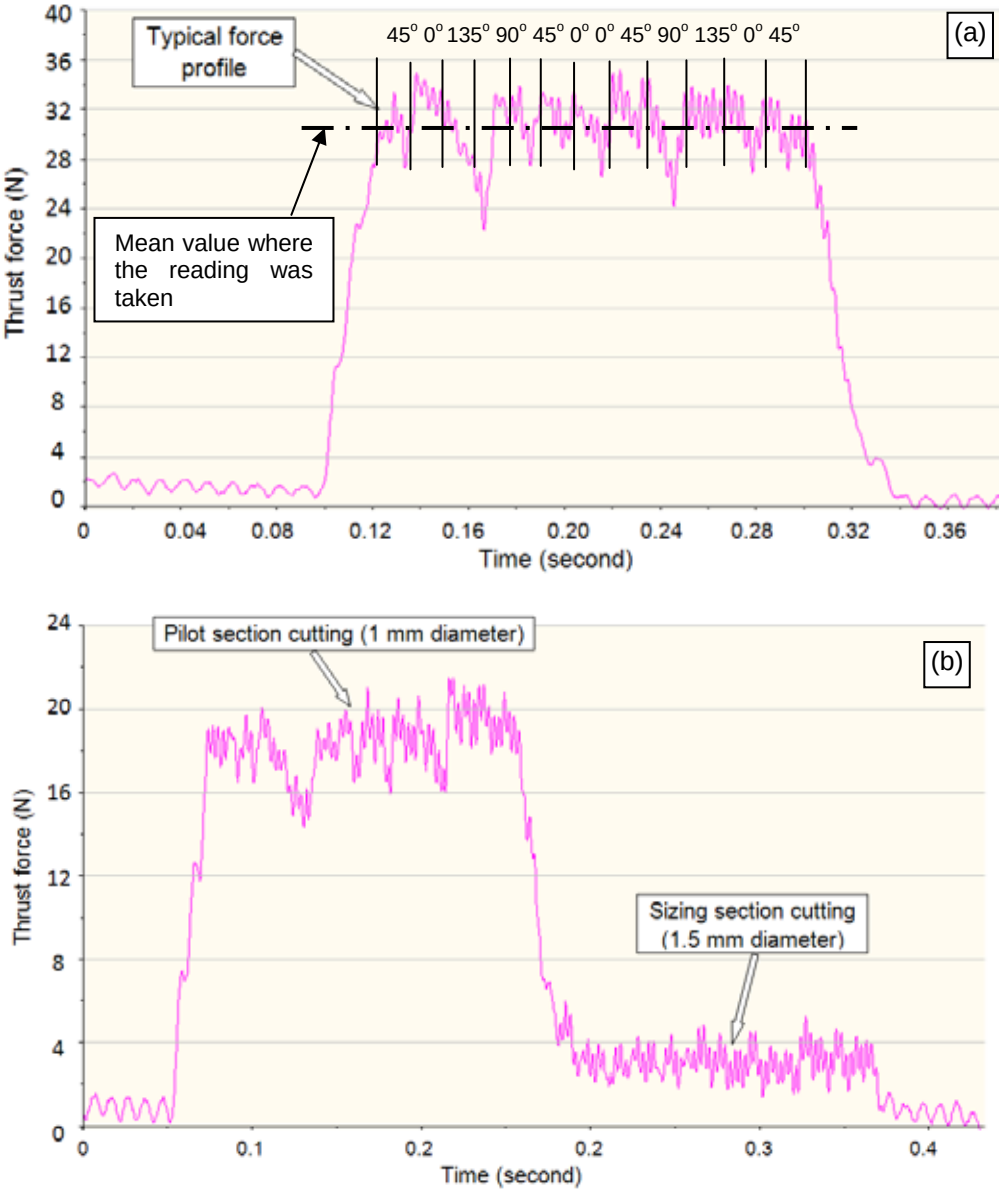


Figure 4.17: Thrust force profile for the first hole drilled using (a) conventional drill and (b) stepped drill (Test 3 and 5 respectively)

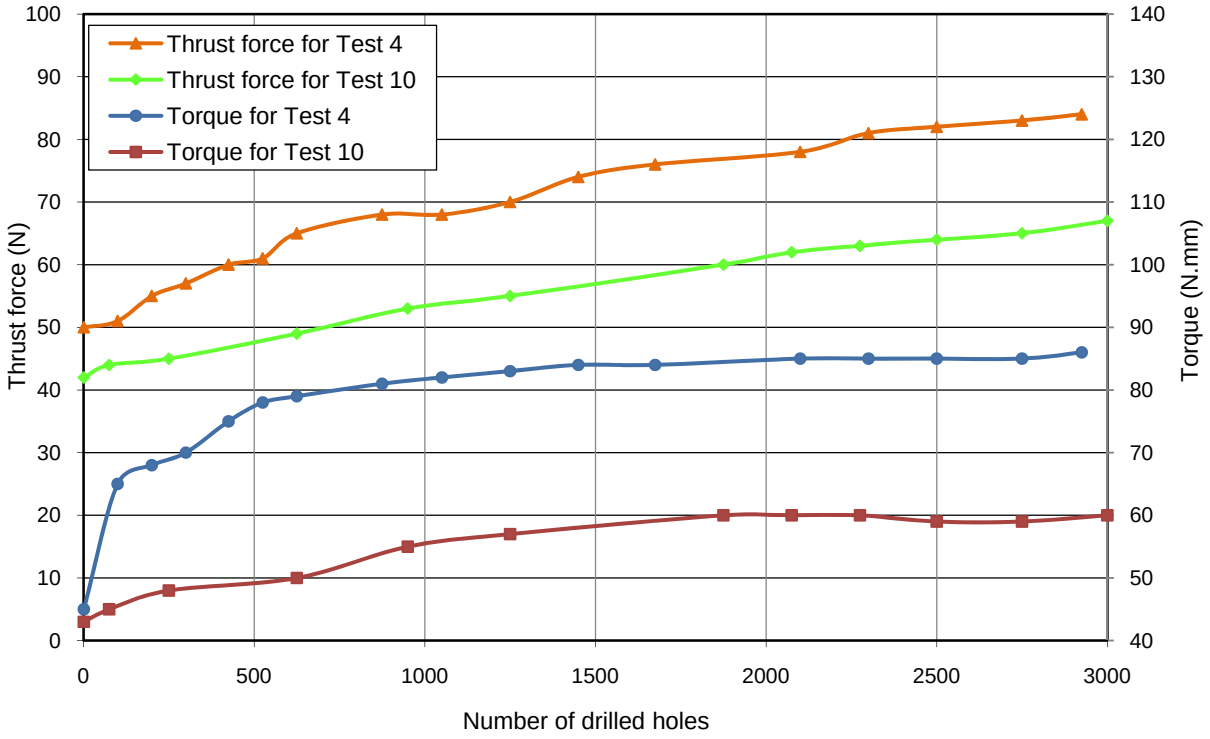


Figure 4.18: Thrust force and torque results for tests showing the highest tool life

Figure 4.19 and Table 4.2 show the main effects plot and corresponding ANOVA results relating to means for thrust force at cession of tests, which were typically below 100 N (38 – 93 N). Understandably, feed rate had the most influential effect with the highest PCR of 61.8% followed by drill type at 25.5%. This was in line with other studies on drilling CFRP (albeit involving larger hole diameters) [61, 62]. Surface condition and point angle were also found to be significant at the 5% level although their PCR's were relatively small (7.4% and 1.6%, respectively).

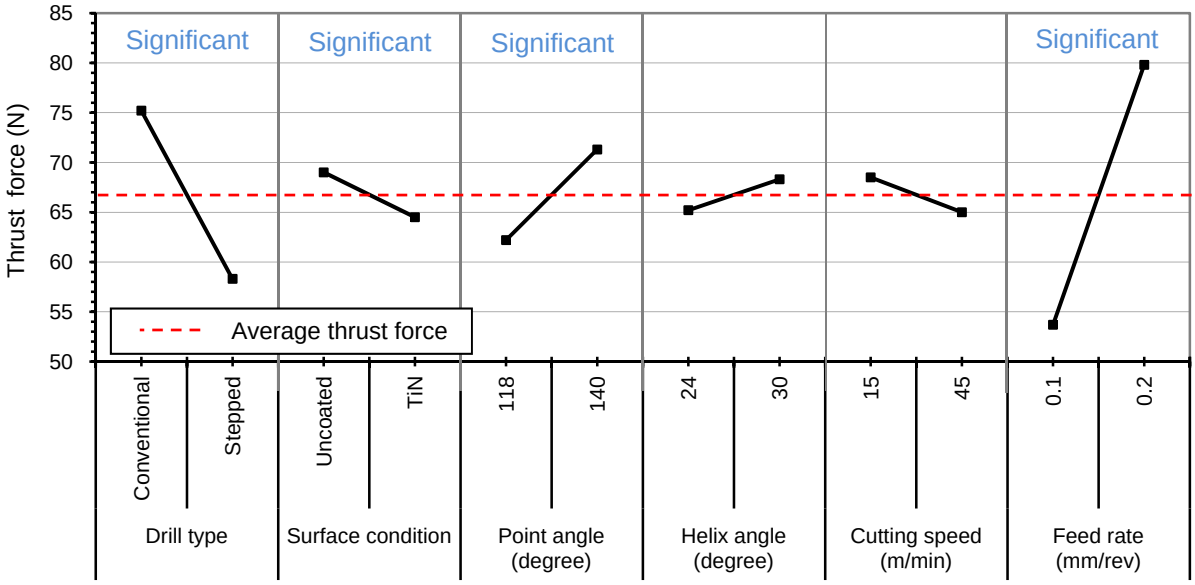


Figure 4.19: Main effects plot, means for thrust force (Phase 1B)

| Factor | DF | SS | Exp SS | F | P | PCR |
|---|---|---|---|---|---|---|
| **Drill type** | 1 | 850 | 843.92 | 139.7 | 0.00* | 25.46 |
| **Surface condition** | 1 | 60.75 | 54.67 | 9.98 | 0.025* | 1.65 |
| **Point angle (°)** | 1 | 252.08 | 245.99 | 41.43 | 0.001* | 7.42 |
| **Helix angle (°)** | 1 | 30.08 | 23.99 | 4.94 | 0.077 | 0.72 |
| **Cutting speed (m/min)** | 1 | 36.75 | 30.67 | 6.04 | 0.057 | 0.92 |
| **Feed rate (mm/rev)** | 1 | 2054.1 | 2048 | 337.6 | 0.000* | 61.79 |
| **Error** | 5 | 30.42 | | | | ***2.02*** |
| **Total** | 11 | 3314.25 | $F_{table} = 6.61$ | | | |

Table 4.2: ANOVA results for thrust force at the last hole drilled (Phase 1B)

In terms of torque results, cutting speed was the main contributory factor with a PCR of 53.7%, while feed rate and drill type had moderate effects of 21.6% and 11.6% respectively see Figure 4.20 and Table 4.3. Torque increased with feed rate and conversely as cutting speed decreased. This can be attributed to the greater rubbing associated with lower cutting speeds while the use of higher feed rate increased the un-deformed chip thickness producing higher forces and torque.

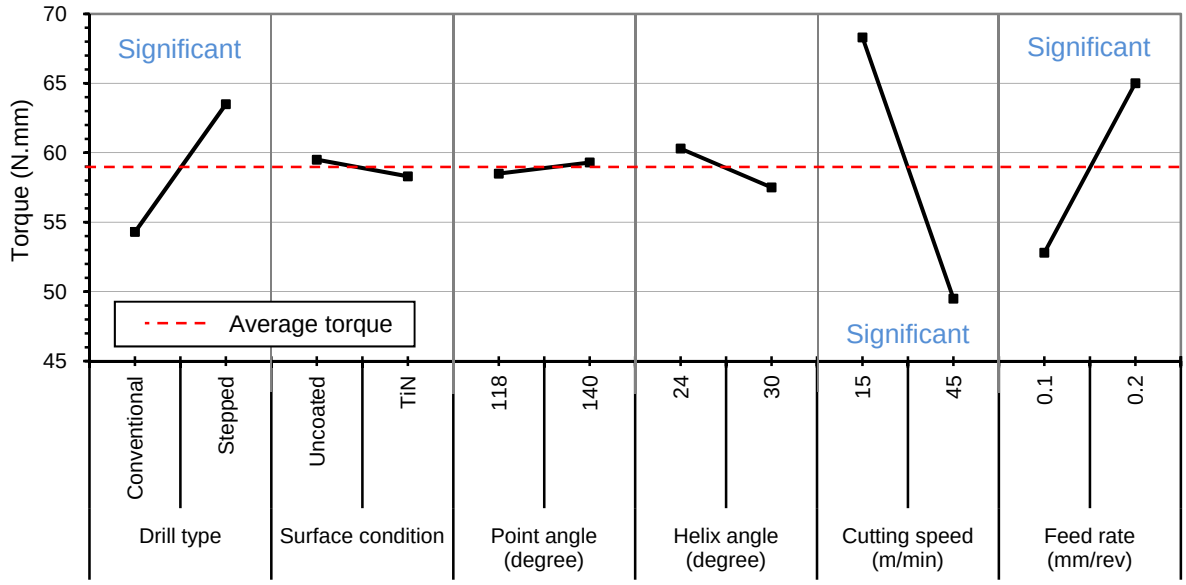


Figure 4.20: Main effects plot, means for torque (Phase 1B)

| Factor | DF | SS | Exp SS | F | P | PCR |
|---|---|---|---|---|---|---|
| **Drill type** | 1 | 252.08 | 224.4 | 9.10 | 0.029* | 11.63 |
| **Surface condition** | 1 | 4.08 | -23.6 | 0.15 | 0.717 | 0 |
| **Point angle ($^o$)** | 1 | 2.08 | -25.6 | 0.07 | 0.795 | 0 |
| **Helix angle ($^o$)** | 1 | 24.08 | -3.6 | 0.87 | 0.394 | 0 |
| **Cutting speed (m/min)** | 1 | 1064.08 | 1036.4 | 38.48 | 0.002* | 53.73 |
| **Feed rate (mm/rev)** | 1 | 444.08 | 416.4 | 16.04 | 0.010* | 21.59 |
| **Error** | 5 | 138.42 | | | | ***13.05*** |
| **Total** | 11 | 1928.92 | $F_{table} = 6.61$ | | | |

Table 4.3: ANOVA results for drilling torque (Phase 1B)

### 4.2.3 Drilled hole quality and damage

Figure 4.21 shows sample SEM images of hole exit for Test 9 at various periods during the trial. Only minor damage in the form of fuzzing on hole edges can be seen even after more than 2000 holes owing to the supportive action provided by the peel ply layer. The apparent weave pattern shown corresponds to the peel ply surface which was removed post drilling. The superior edge quality obtained in respect of both hole entry and exit for first holes drilled in all tests is shown in Figure 4.22. This can be attributed to the low thrust force levels and sharp cutting edge conditions during early stages of the experiment. Damage in the form of delamination, spalling, fuzzing and edge chipping/fracture (typical damage shapes when drilling FRPs [43]) however developed as drilling progressed, and was further exacerbated during the last several hundred holes, similar to that detailed in Figure 4.23. This suggests a correlation between increasing flank wear and thrust force with respect to hole quality/damage. Delamination was found to be the dominant form of hole surface damage and was further assessed quantitatively using optical microscopy.

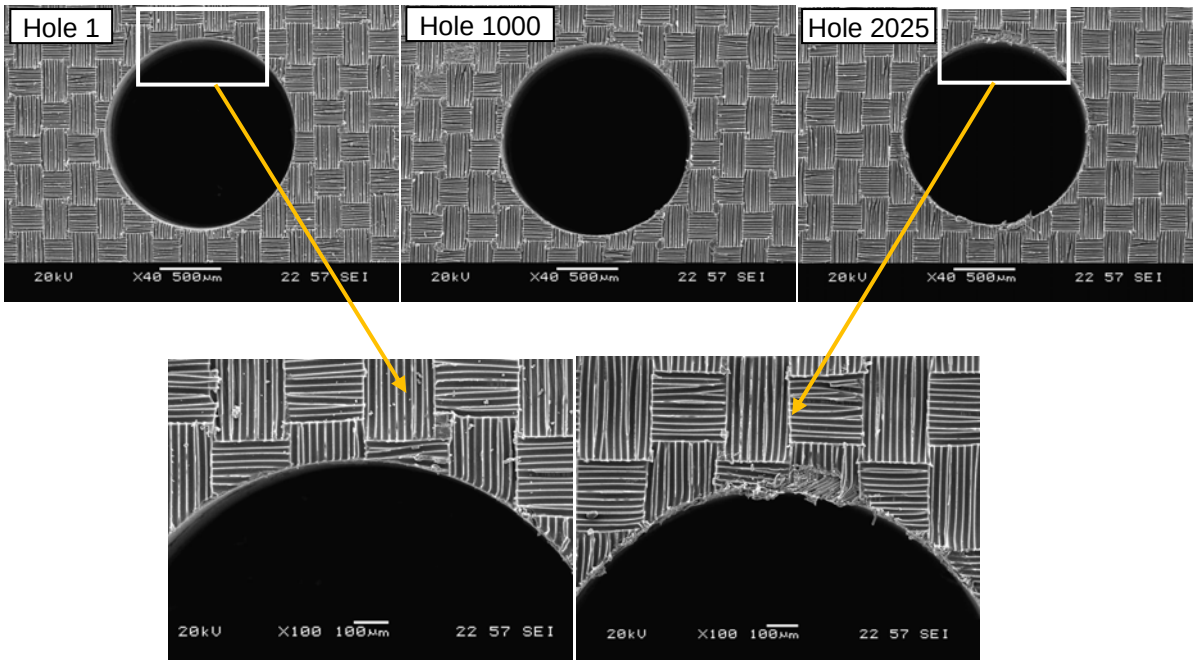


Figure 4.21: SEM images for hole exit (Test 9)

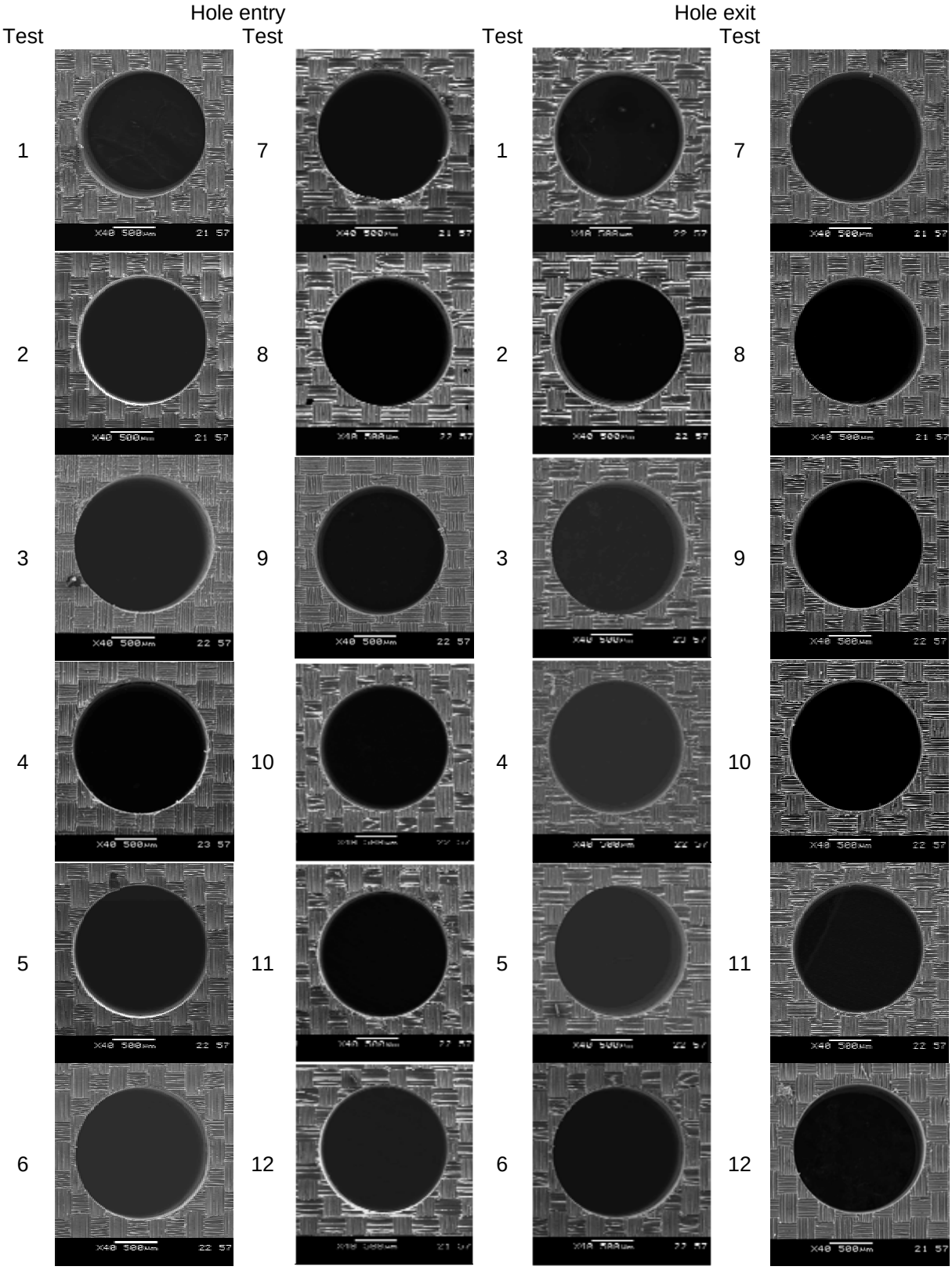


Figure 4.22: Hole entry and exit at first hole

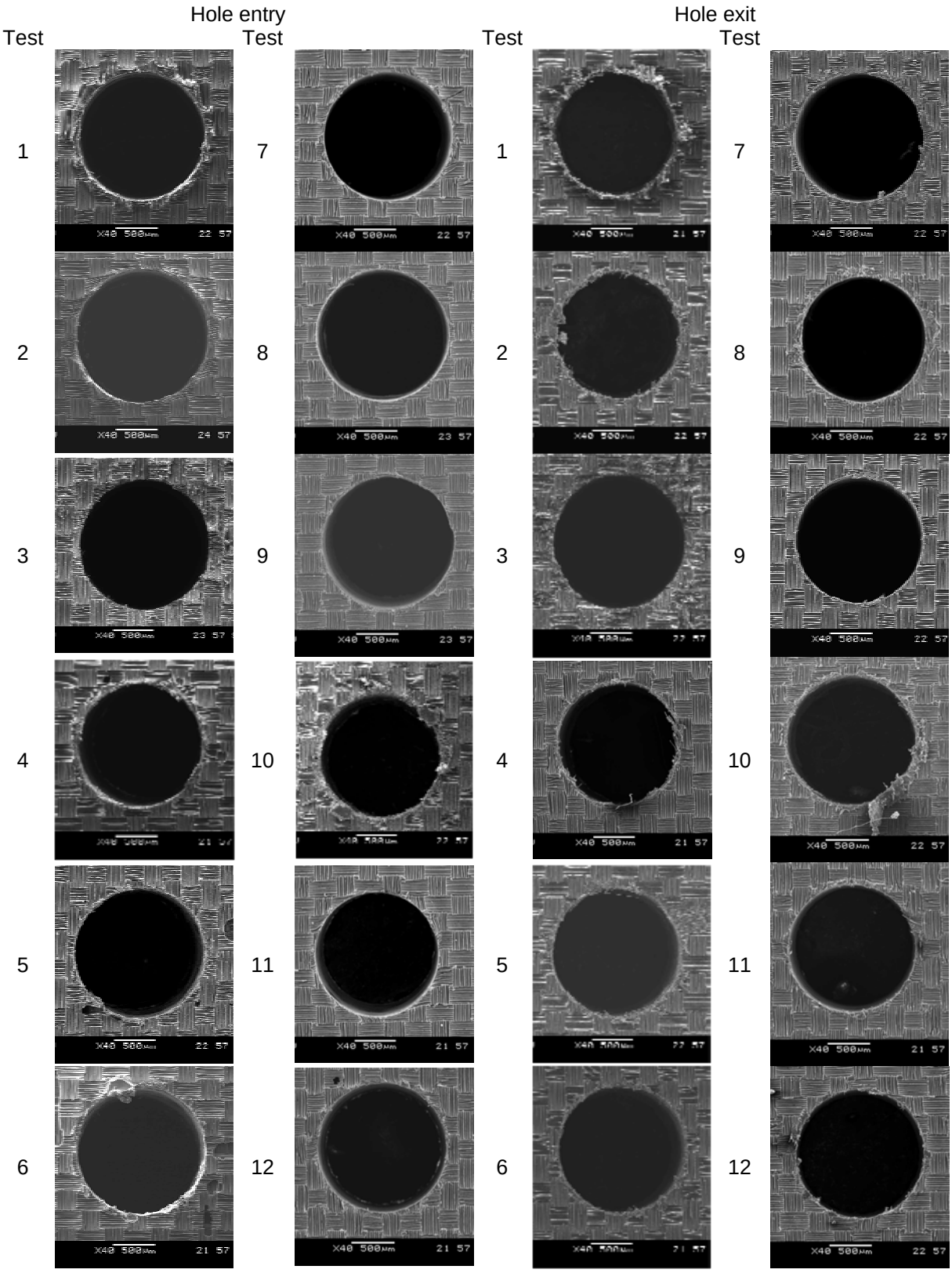


Figure 4.23: Hole entry and exit at last hole (all to the same flank wear criterion)

Figure 4.24 - Figure 4.25 and Table 4.4 - Table 4.5 show the main effects plots and associated ANOVA results for entry delamination factor ($F_d$) during the first and last hole respectively. Feed rate was the main parameter which influenced entry delamination factor for the first hole with a PCR of 78% while helix angle was also significant but with a low contribution of 5.75%. For the last hole, drill type and feed rate were the main contributing factors affecting entry $F_d$, each providing PCR values of ~ 47 and 31%, respectively. A larger $F_d$ was however obtained with stepped drills and higher feed rates for the last hole drilled. The latter was most probably attributed to the higher thrust force generated [68, 71].

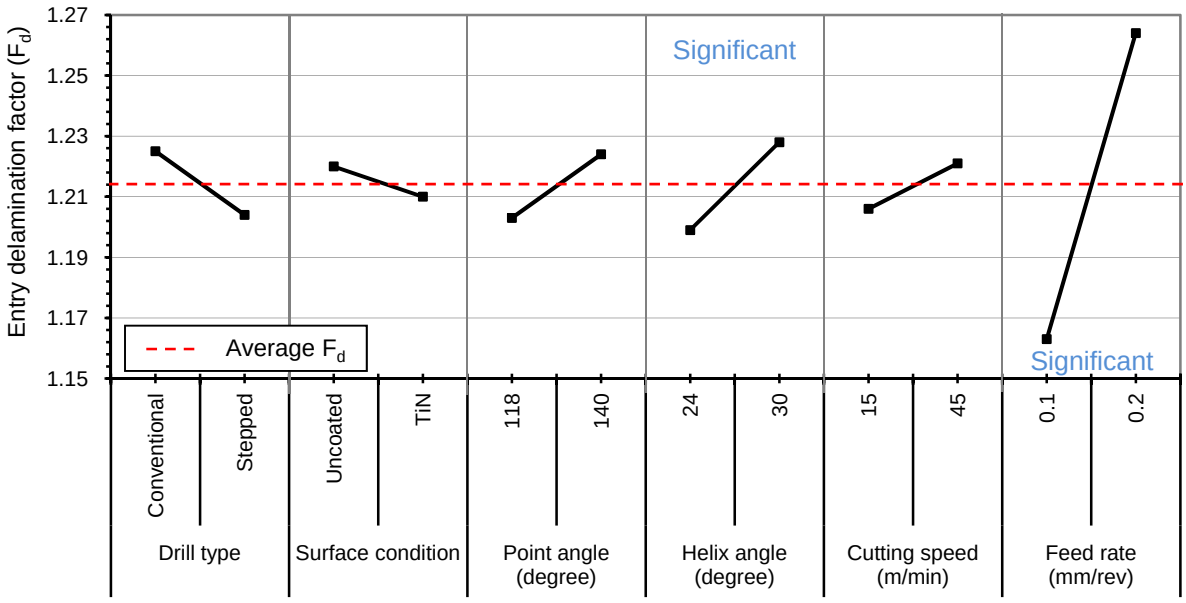


Figure 4.24: Main effects plot, means for entry $F_d$ for the first hole (Phase 1B)

| Factor | DF | SS | Exp SS | F | P | PCR |
|---|---|---|---|---|---|---|
| **Drill type** | 1 | 0.00163 | 0.00127 | 4.56 | 0.086 | 3.33 |
| **Surface condition** | 1 | 0.00013 | -0.00022 | 0.38 | 0.566 | 0.00 |
| **Point angle (°)** | 1 | 0.00129 | 0.00093 | 3.6 | 0.116 | 2.43 |
| **Helix angle (°)** | 1 | 0.00256 | 0.00220 | 7.14 | 0.044* | 5.75 |
| **Cutting speed (m/min)** | 1 | 0.00061 | 0.00026 | 1.71 | 0.247 | 0.67 |
| **Feed rate (mm/rev)** | 1 | 0.03027 | 0.02991 | 84.51 | 0.000* | 78.12 |
| **Error** | 5 | 0.00179 | | | | 9.71 |
| **Total** | 11 | 0.03829 | $F_{table} = 6.61$ | | | |

Table 4.4: ANOVA results for entry $F_d$ for the first hole (Phase 1B)

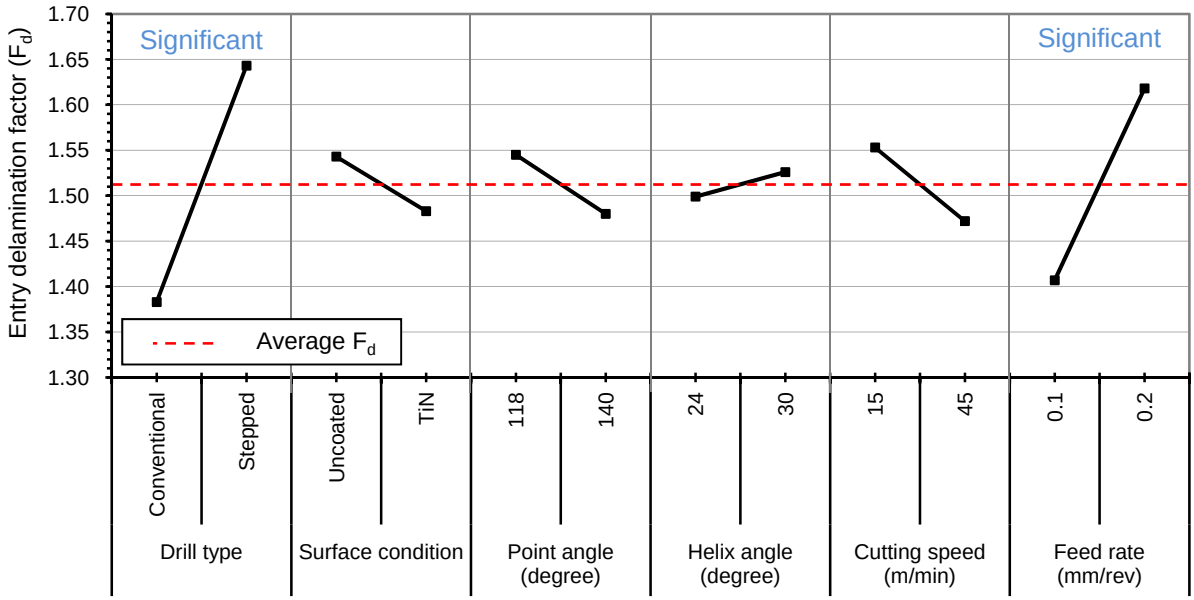


Figure 4.25: Main effects plot, means for entry $F_d$ for the last hole (Phase 1B)

| Factor | DF | SS | Exp SS | F | P | PCR |
|---|---|---|---|---|---|---|
| **Drill type** | 1 | 0.20317 | 0.19652 | 30.54 | 0.003* | 47.25 |
| **Surface condition** | 1 | 0.01071 | 0.00406 | 1.61 | 0.26 | 0.98 |
| **Point angle (°)** | 1 | 0.01275 | 0.00610 | 1.92 | 0.225 | 1.47 |
| **Helix angle (°)** | 1 | 0.00216 | -0.00449 | 0.32 | 0.594 | 0.00 |
| **Cutting speed (m/min)** | 1 | 0.01986 | 0.01321 | 2.99 | 0.145 | 3.18 |
| **Feed rate (mm/rev)** | 1 | 0.13397 | 0.12731 | 20.14 | 0.006* | 30.61 |
| **Error** | 5 | 0.03326 | | | | 16.52 |
| **Total** | 11 | 0.41588 | $F_{table} = 6.61$ | | | |

Table 4.5: ANOVA results for entry $F_d$ for the last hole (Phase 1B)

In terms of exit delamination, feed rate similarly had the largest influence in relation to the first hole drilled with an associated PCR of ~45% (see Figure 4.26 and Table 4.6) while point angle and cutting speed were the significant contributing factors affecting the exit $F_d$ for last hole drilled with PCR's of 24 and 20%, respectively (see Figure 4.27 and Table 4.7). Despite the fact that exit $F_d$ was generally found to be higher than that for hole entry, the mean value obtained for both was marginally lower at hole exit compared to corresponding entry positions. This was probably due to the presence of nylon peel ply and glass scrim layer, which helped to constrain fibre push out and minimised workpiece deflection/bursting at the exit. In general, average $F_d$ was ~1.5 for last hole drilled, however with Test 4 (longest tool life with ~ 2900 holes produced), entry and exit delamination factors were 1.88 and 1.62 respectively. Unfortunately, the level of error in respect of exit $F_d$ analysis was relatively high

both for first and last hole drilled (~ 54% and 31.5% respectively). Such levels are much higher than the ~15% deemed acceptable with Taguchi experiments [183] and were felt due to measurement difficulties/accuracy.

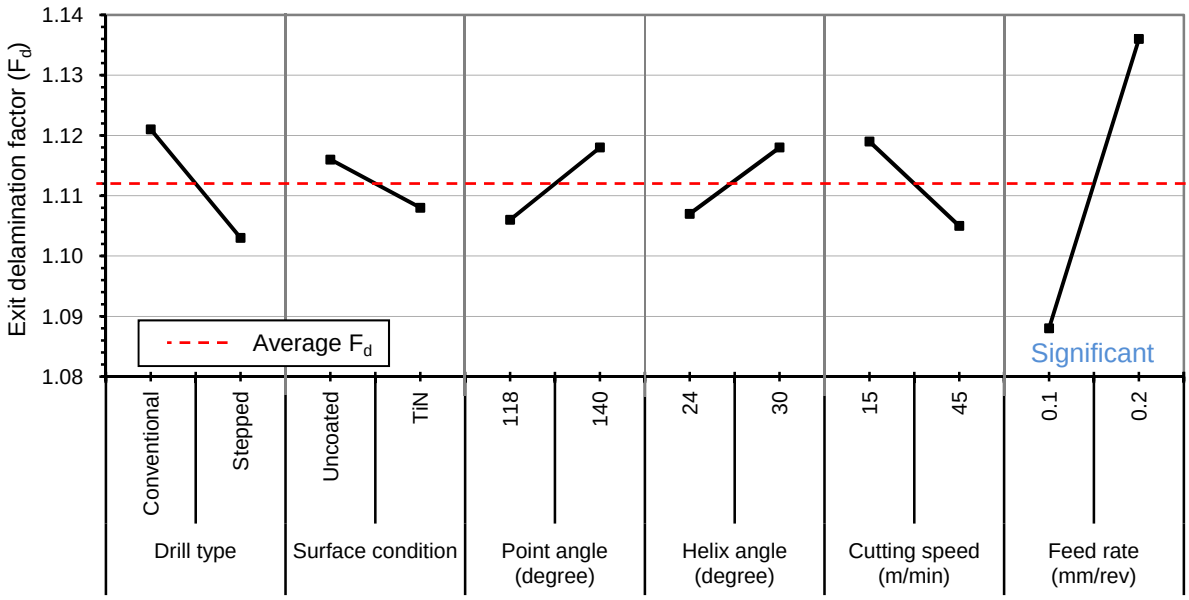


Figure 4.26: Main effects plot, means for exit $F_d$ for the first hole (Phase 1B)

| Factor | DF | SS | Exp SS | F | P | PCR |
|---|---|---|---|---|---|---|
| **Drill type** | 1 | 0.00103 | 0.00020 | 1.24 | 0.316 | 1.42 |
| **Surface condition** | 1 | 0.00019 | -0.00064 | 0.23 | 0.653 | 0.00 |
| **Point angle (°)** | 1 | 0.00047 | -0.00036 | 0.57 | 0.484 | 0.00 |
| **Helix angle (°)** | 1 | 0.00036 | -0.00047 | 0.44 | 0.537 | 0.00 |
| **Cutting speed (m/min)** | 1 | 0.00070 | -0.00013 | 0.84 | 0.402 | 0.00 |
| **Feed rate (mm/rev)** | 1 | 0.00706 | 0.00623 | 8.51 | 0.033* | 44.65 |
| **Error** | 5 | 0.00415 | | | | 53.93 |
| **Total** | 11 | 0.01395 | $F_{table} = 6.61$ | | | |

Table 4.6: ANOVA results for exit $F_d$ for the first hole (Phase 1B)

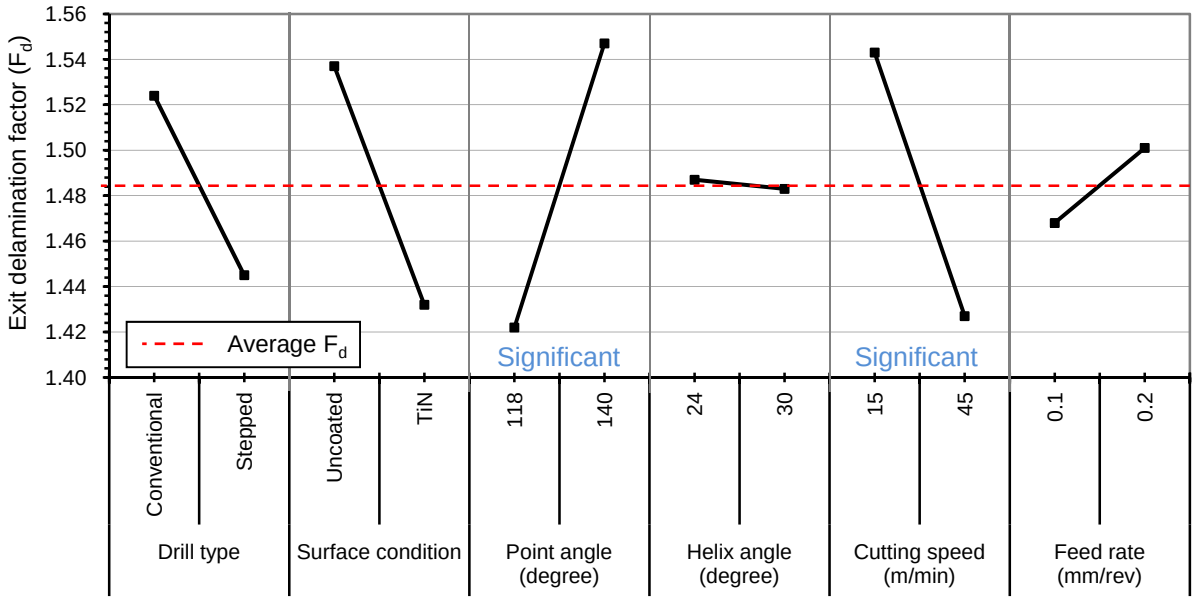


Figure 4.27: Main effects plot, means for exit $F_d$ for the last hole (Phase 1B)

| Factor | DF | SS | Exp SS | F | P | PCR |
|---|---|---|---|---|---|---|
| **Drill type** | 1 | 0.01894 | 0.01334 | 3.38 | 0.125 | 7.80 |
| **Surface condition** | 1 | 0.03305 | 0.02744 | 5.9 | 0.06 | 16.05 |
| **Point angle ($^o$)** | 1 | 0.04716 | 0.04156 | 8.41 | 0.034* | 24.30 |
| **Helix angle ($^o$)** | 1 | 0.00006 | -0.00555 | 0.01 | 0.924 | 0.00 |
| **Cutting speed (m/min)** | 1 | 0.04047 | 0.03487 | 7.22 | 0.043 | 20.39 |
| **Feed rate (mm/rev)** | 1 | 0.00330 | -0.00231 | 0.59 | 0.478 | 0.00 |
| **Error** | 5 | 0.02803 | | | | 31.46 |
| **Total** | 11 | 0.17101 | $F_{table} = 6.61$ | | | |

Table 4.7: ANOVA results for exit $F_d$ for the last hole (Phase 1B)

Drilling with the peel ply attached significantly reduced the occurrence of surface damage such as fuzzing and severe delamination (see Figure 4.28), however the subsequent removal of this layer sometimes caused additional damage around the drilled hole and occasionally left small segments of peel ply debris, see Figure 4.29. Fibre/matrix cracking, porosity and layer separation were seen on the inner hole surfaces, and were present even during the early stages of drilling, see Figure 4.30. The helical pattern of damage shown in Figure 4.30 (b) confirms that the machined surfaces are irregular and that their quality is highly dependent on fibre orientation angle as reported by Wang et al. [48]. The poor thermal conductivity of CFRP is a contributory factor in relation to resin melt which typically occurs at 300 - 400$^o$C, however damage may occur at lower temperature associated with the onset of

plastic deformation. Limited cutting temperature measurements were carried out and are detailed in Appendix E. Results showed that the maximum cutting temperature when drilling CFRP under the cutting conditions used was 250$^{o}$C.

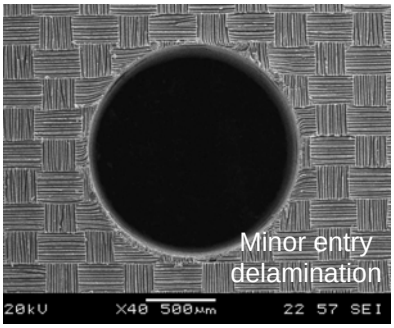


(a) Test 11, hole entry, hole number 1000

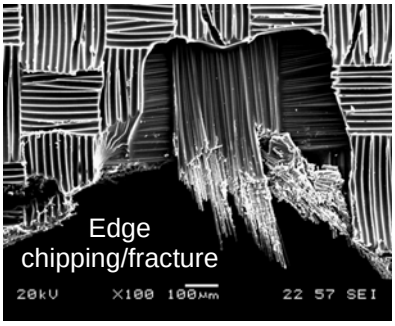


(b) Test 6, hole entry, hole number 1250

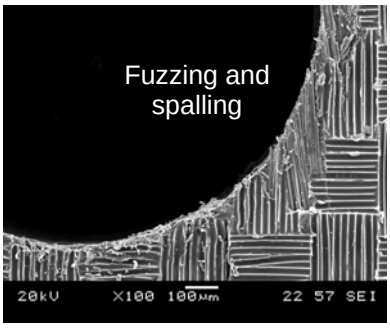


(c) Test 8, hole exit, hole number 1375

Figure 4.28: Various types/configurations of damage produced when drilling CFRP

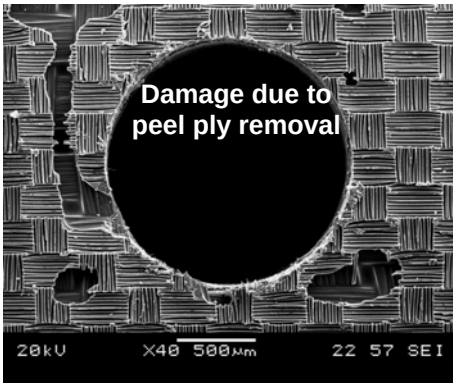


(a) Test 6, hole entry, hole number 1000

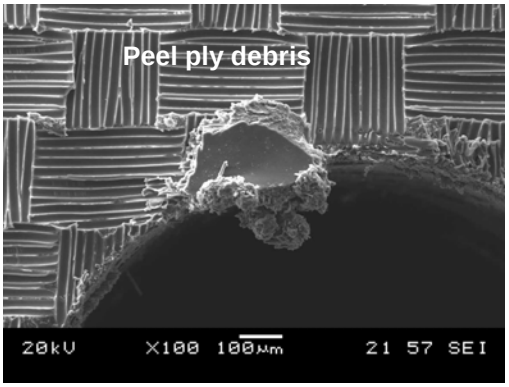


(b) Test 6, hole entry, hole number 2050

Figure 4.29: Damage caused by removal of the peel ply layer

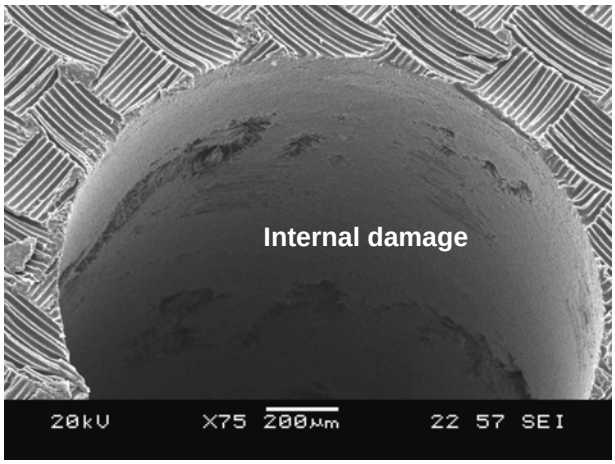


(a) Test 11, from hole exit, hole number 250

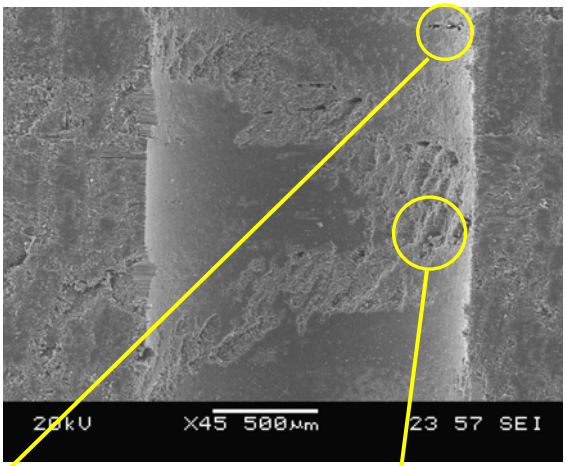


(b) Test 3, sectioned hole, first hole

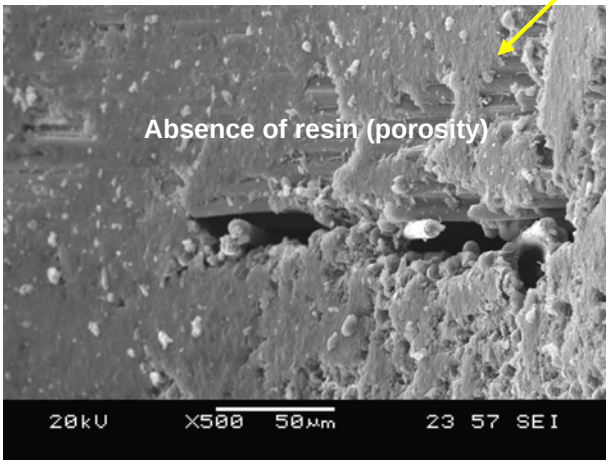


(c) Absence of resin between layers (porosity)

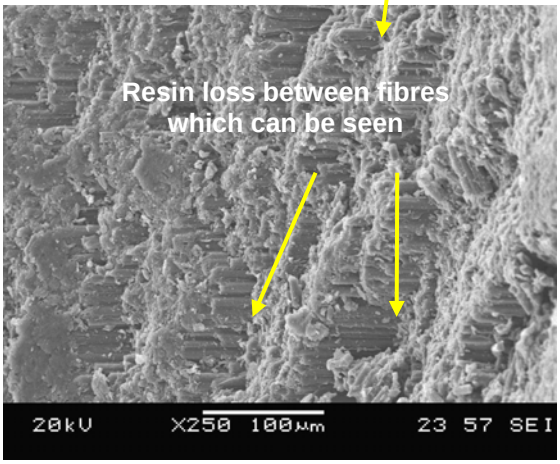


(d) Resin loss

Figure 4.30: Internal hole damage forms

### 4.2.4 Hole size measurement

Measurement of hole diameter showed all holes to be undersize compared to the nominal drill dimension by up to 2.8% upon reaching the tool life criterion, see Figure 4.31. The main effects plot and ANOVA results for hole diameter following test cessation are shown in Figure 4.32 and Table 4.8 respectively. The data revealed that drill type and feed rate were the principal factors affecting hole size with associated PCR's of ~ 27.8 and 25.5%. Cutting speed and point angle were also statistically significant albeit with lower contribution ratios. Average tool life when conventional drills were employed was shorter than that when using stepped drills (1370 and 2152 holes respectively), which probably resulted in less drill land wear and consequently produced better hole accuracy.

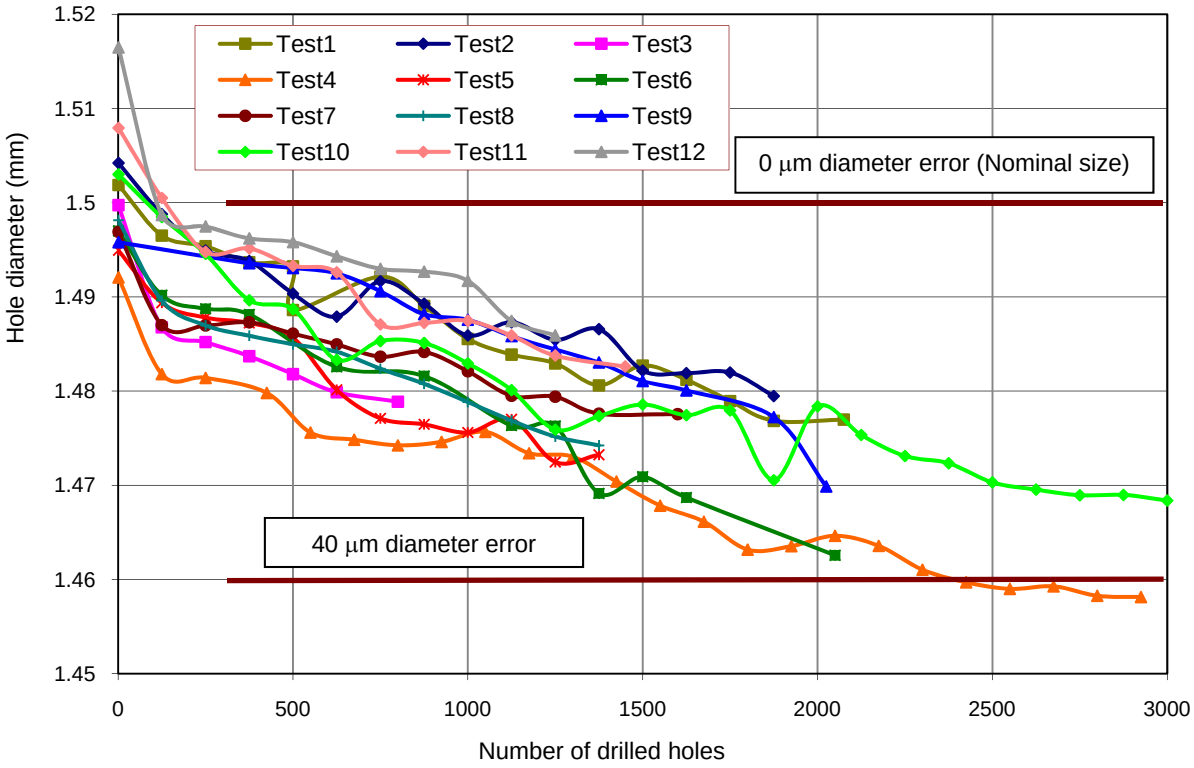


Figure 4.31: Hole diameter results (Phase 1B)

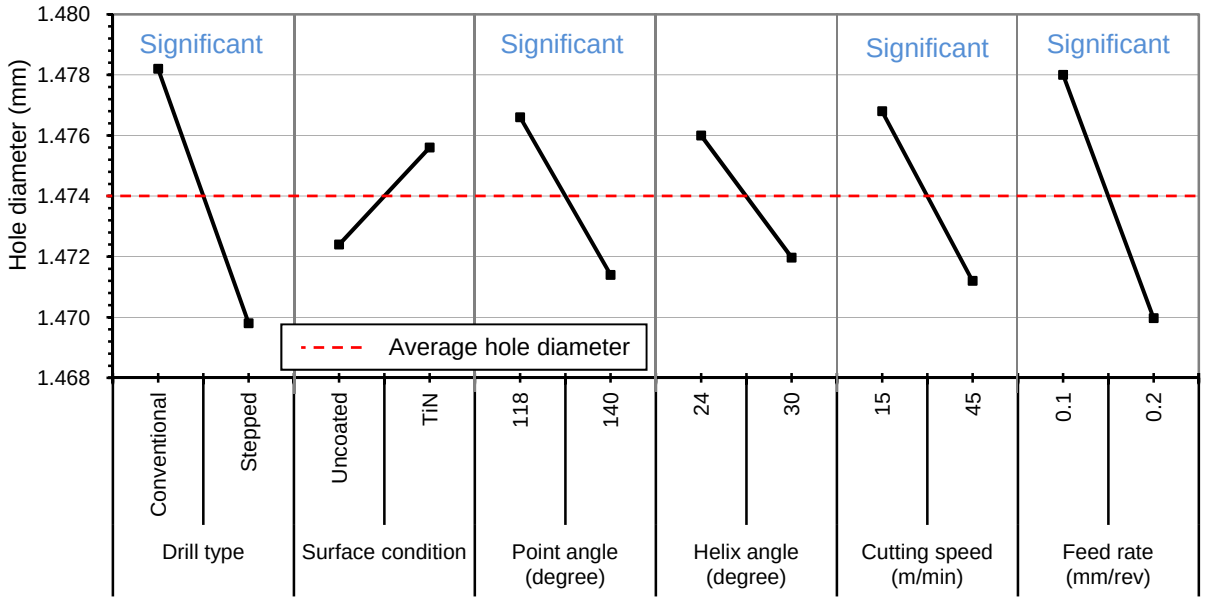


Figure 4.32: Main effects plot, means for hole diameter (Phase 1B)

| Factor | DF | SS | Exp SS | F | P | PCR |
|---|---|---|---|---|---|---|
| **Drill type** | 1 | 0.0002117 | 0.00020002 | 18.13 | 0.008* | 27.83 |
| **Surface condition** | 1 | 0.000032 | 0.00002032 | 2.74 | 0.159 | 2.827 |
| **Point angle ($^o$)** | 1 | 0.0000801 | 0.00006842 | 6.86 | 0.047* | 9.52 |
| **Helix angle ($^o$)** | 1 | 0.0000488 | 0.00003712 | 4.18 | 0.096 | 5.164 |
| **Cutting speed (m/min)** | 1 | 0.0000941 | 0.00008242 | 8.06 | 0.036* | 11.468 |
| **Feed rate (mm/rev)** | 1 | 0.0001936 | 0.00018192 | 15.58 | 0.01* | 25.312 |
| **Error** | 5 | 0.0000584 | | | | 17.876 |
| **Total** | 11 | 0.0007187 | $F_{table} = 6.61$ | | | |

Table 4.8: ANOVA results for hole diameter (Phase 1B)

### 4.2.5 Confirmation test

The maximum tool life (corresponding to the preferred factor levels of A2, B1, C2, D2, E1, and F2) achieved during the experiment was 2900 holes/tool. A confirmation test was performed using the above conditions in order to validate results from the statistical analysis (L12 OA). The responses considered include tool life, thrust force and delamination factors for hole entry and exit. The confidence interval (95%) for results of the confirmation test was calculated using the following equation;

$$\text{Confidence interval} = \sqrt{F_\alpha(1,\upsilon_e)V_e[(1/n_{eff})+(1/r)]}$$

$F_\alpha$ = tabulated F value for a 95% confidence interval

$\upsilon_e$ = degrees of freedom associated with the error/residual

$V_e$ = mean sum of square associated with the error/residual

$r$ = sample size for the confirmation experiment

$$n_{eff} = \frac{Total\ number\ of\ observations}{1 + [\text{total degrees of freedom associated with items used in estimating mean}}$$

$F_\alpha = 6.61,\ V_e = 36432$ and $r = 1$

$$n_{eff} = \frac{12}{1+6} = 1.7143$$

Confidence interval = 2900 + / - 617 and confidence limits = 2282 *and* 3517 holes

Following the confirmation test, the number of drilled holes obtained was 3075 holes, which was within the confidence interval calculated, indicating that the experiment was statistically acceptable. Thrust force and torque during the first hole were 41 N and 50 N.mm respectively which increased to 68 N and 80 N.mm following the last hole drilled. A corresponding delamination factor $F_d$ for last hole drilled of 1.65 was obtained for both hole entry and exit, which was comparable to that observed in the mainstream testing for hole exit ($F_d = 1.62$) and marginally lower than that for hole entry ($F_d = 1.85$).

## 4.3 Phase 2A: Effect of composite material, fibre orientation and machining parameters

### 4.3.1 Tool wear and tool life

Figure 4.33 details evaluation of flank wear results for experiments using stepped drills while Figure 4.34 shows data obtained with conventional drills. Trials carried out at the lower feed rate (0.2 mm/rev) displayed typical 'steady' wear progress (flank & chisel edge wear) up to the maximum flank wear criterion. Figure 4.35 shows corresponding tool life end point comparisons. The majority of stepped drills tested at a feed rate of 0.4 mm/rev were observed to experience catastrophic failure (fracture) while all tests carried out at 0.2 mm/rev or using conventional geometry reached the tool life criterion via gradual progression of tool flank wear, see Figure 4.36. Despite this however, the longest tool life (3750 holes) was obtained when machining woven MTM44-1/HTS OC laminates at the higher feed rate level using stepped geometry. A similar result (up to 3250 holes) was also recorded in the tests involving UD 977-2/HTS AC and MTM44-1/HTS OC materials drilled at 0.4 mm/rev feed rate using stepped and conventional drills, respectively. In addition, the effect of prepreg form on tool life was only prominent when employing a higher feed rate using stepped geometry (up to a 44 fold increase in tool life between UD & woven).

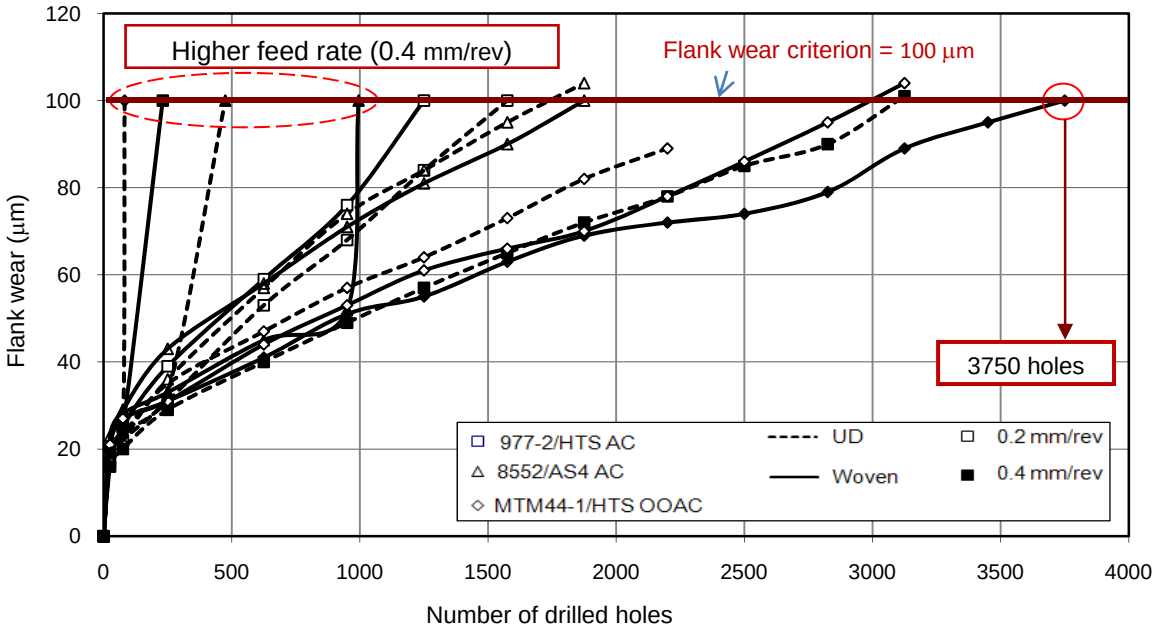


Figure 4.33: Flank wear curves for tests carried out using stepped drills

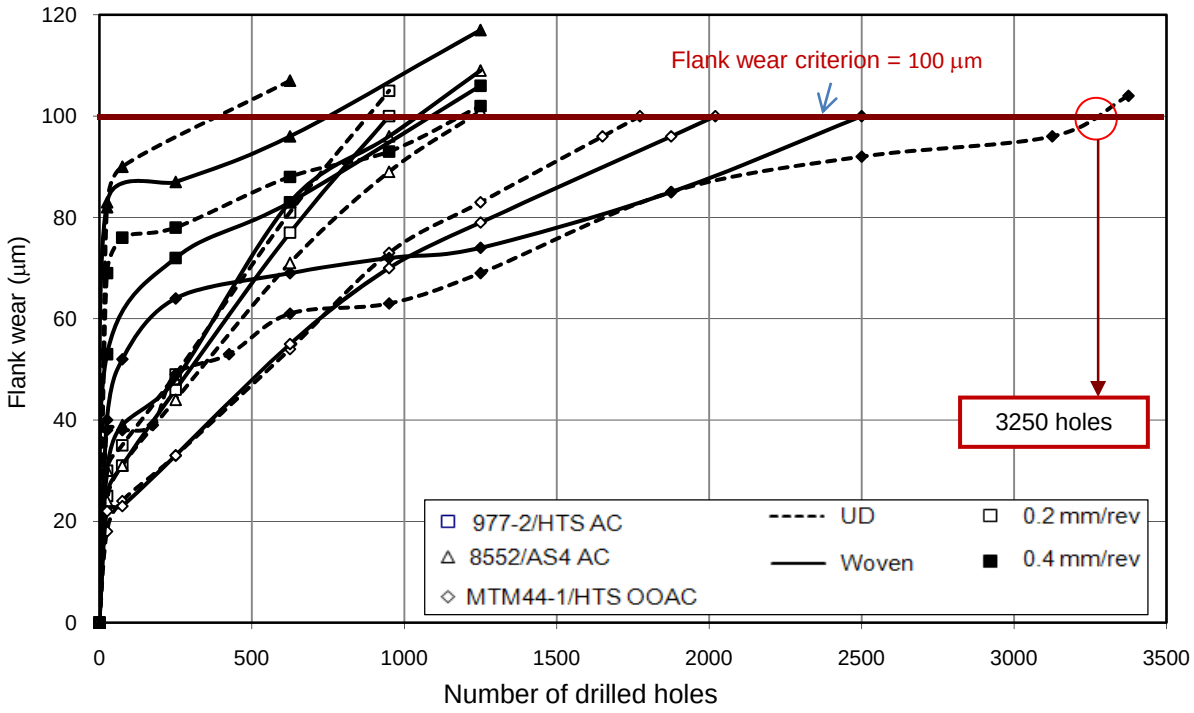


Figure 4.34: Flank wear curves for tests carried out using conventional drills

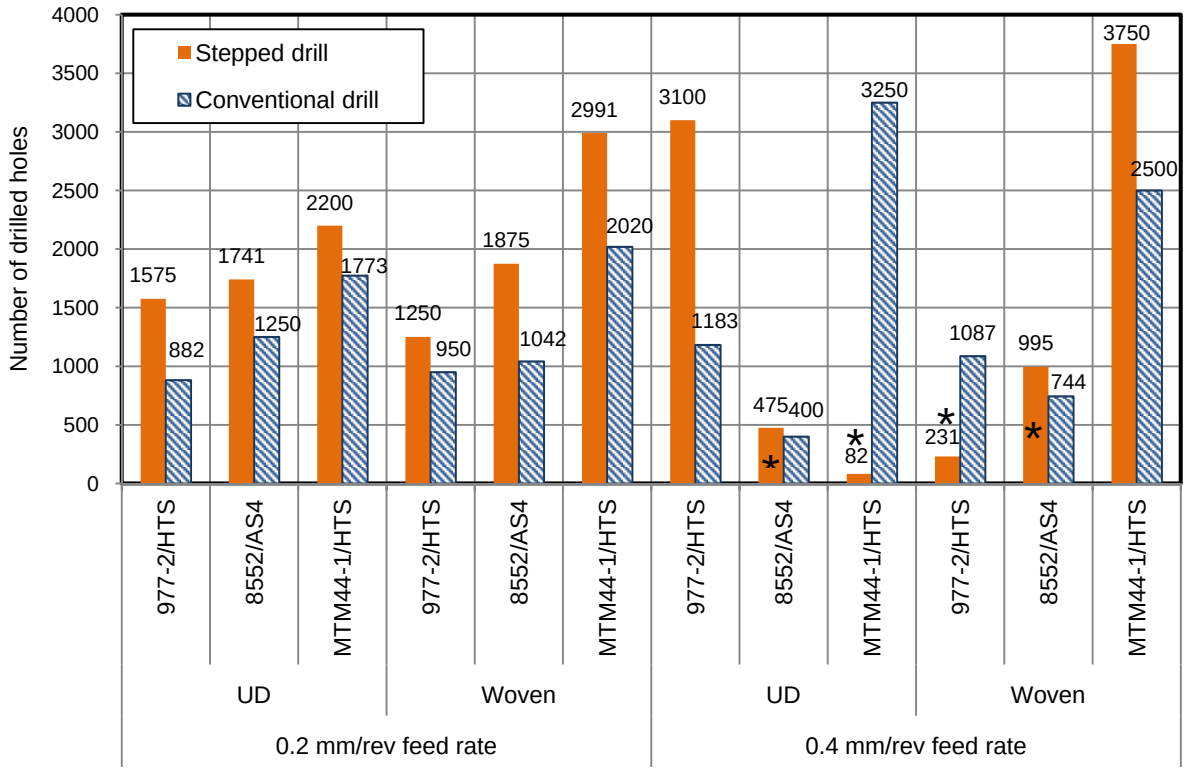


Figure 4.35: Tool life in terms of number of drilled holes (* tests experienced tool fracture)

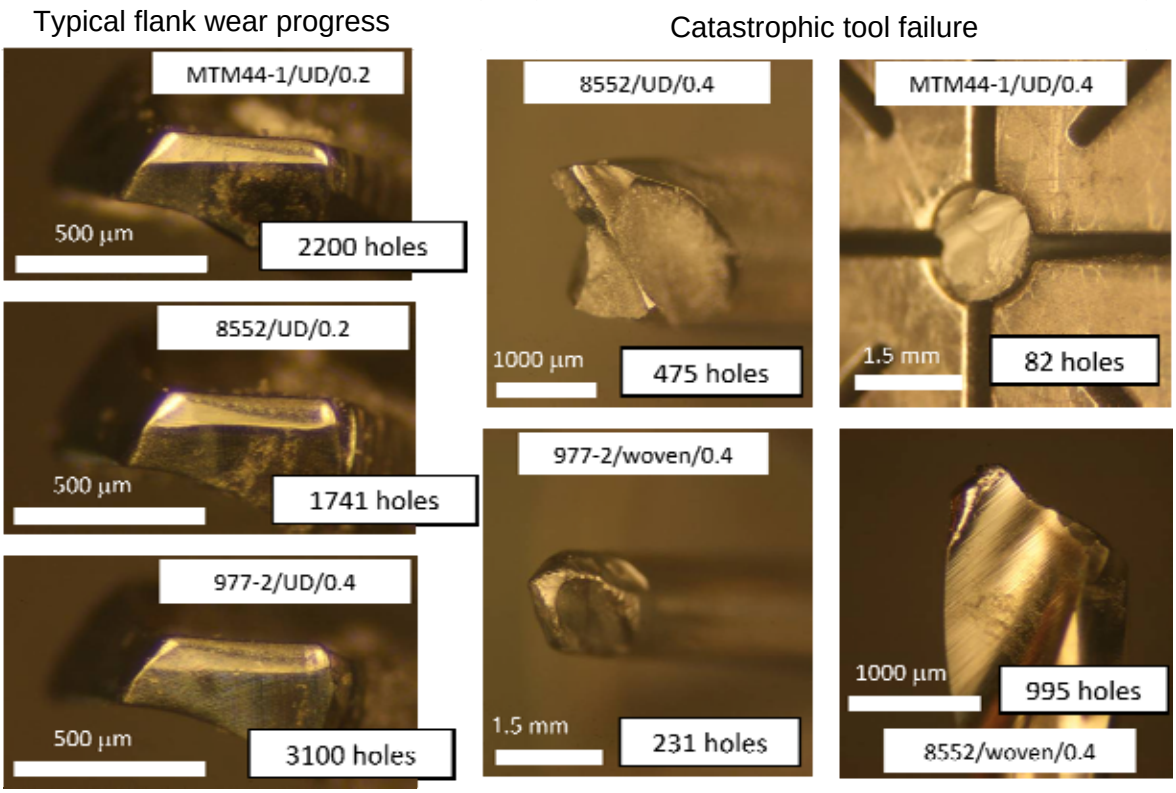


Figure 4.36: Micrographs of tool at test cessation (tests performed using the stepped drills)

The main effects plot shown in Figure 4.37 indicates that best tool life/highest number of holes drilled would be obtained when drilling woven MTM44-1/HTS OC prepreg composites at low feed rate using stepped drill. The associated analysis of variance (ANOVA) however showed that only prepreg type was statistically significant at the 5% level with a PCR of 24%, but there was an unusually high level of error (~75%), see Table 4.9. The reason for this was probably due to the premature failure of drills in several tests performed at high feed rates. Replication of the tests where tool fracture occurred also yielded similar outcomes on each occasion. Taking into account the fact that most of the failures occurred in the pilot portion of the stepped drill, it was surmised that the strength of the 1 mm diameter section was probably insufficient to withstand the machining conditions imposed by operating at a feed rate of 0.4 mm/rev. The above hypothesis was further reinforced by the fact that the tool fractures observed when stepped drills were employed were not mirrored in comparative tests employing conventional twist drills (1.5 mm diameter throughout). The findings were at odds with published data by Tsao and Hocheng [69, 73 – 74] where stepped drills were used successfully to cut CFRP, however significantly lower feed rates were employed (up to 0.03 mm/rev).

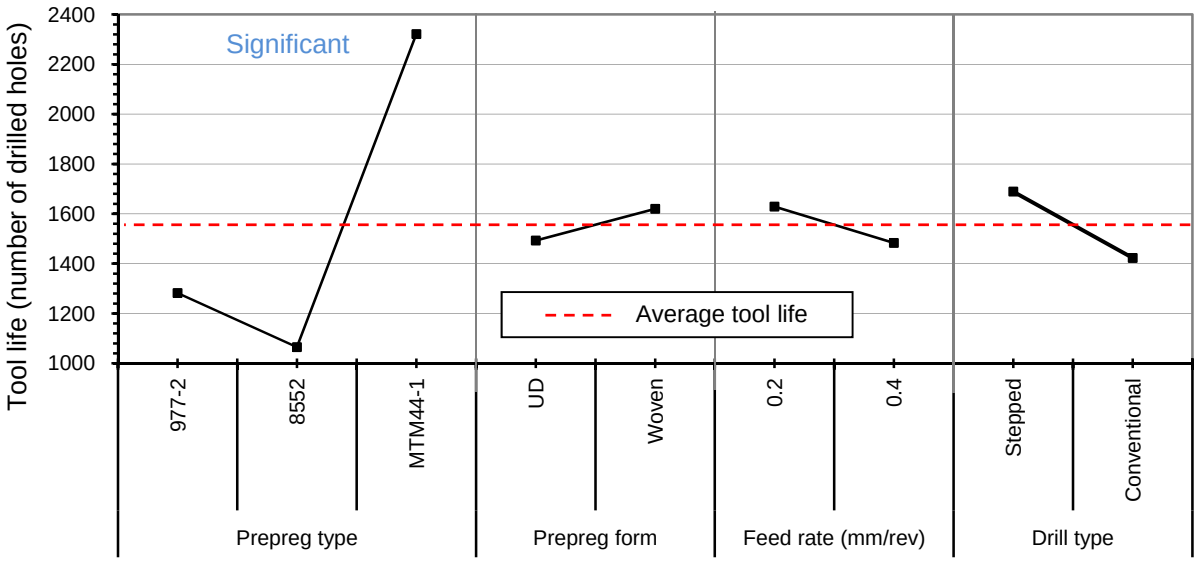


Figure 4.37: Main effects plot, means for tool life (Phase 2A)

| Factor | DF | SS | Exp SS | F | P | PCR |
|---|---|---|---|---|---|---|
| **A (prepreg type)** | 2 | 7204937 | 5536231 | 4.32 | 0.029* | 24.21 |
| **B (prepreg form)** | 1 | 96774 | -737579 | 0.12 | 0.737 | 0.00 |
| **C (feed rate mm/rev)** | 1 | 127896 | -706457 | 0.15 | 0.7 | 0.00 |
| **D (drill type)** | 1 | 422411 | -411942 | 0.51 | 0.486 | 0.00 |
| **Error** | 18 | 15018352 | | | | 75.79 |
| **Total** | 23 | 22870370 | | | | |

Table 4.9: ANOVA results for tool life (Phase 2A)

At 0.2 mm/rev feed rate, stepped drills produced longer tool lives compared with conventional geometry while at feed rate of 0.4 mm/rev, unpredictable tool life was obtained due to the premature tool fracture. In terms of the influence of prepreg form, average tool life for woven laminates was marginally higher than that for UD. An investigation of the different CFRP laminate lay-up structures revealed a generally higher fibre density/concentration in the UD configurations compared to the woven arrangements, see Figure 4.38. It is likely that this led to increased interaction between the tool and abrasive fibres during drilling, resulting in lower tool life as seen with the majority of UD laminates in contrast to their woven counterparts. The presence of extensive voids/cavities in the woven composites was expected to cause a reduction in inter-laminar strength and abrasiveness, however their incidence would be lower following high pressure autoclave curing of the 977-2/HTS AC and 8552/AS4 AC laminates. In contrast, the MTM44-1/HTS OC laminates were simply oven cured under atmospheric pressure. This, coupled with the relatively low fibre tensile strength and modulus (2159MPa / 129GPa as opposed to 4480MPa / 231GPa for the 8552/AS4 AC laminate), as

well as the inconsistency of the composite structure (porosity etc.), was thought to partially account for the unexpectedly high tool life seen when drilling the woven MTM44-1/HTS OC workpiece using both drill geometries.

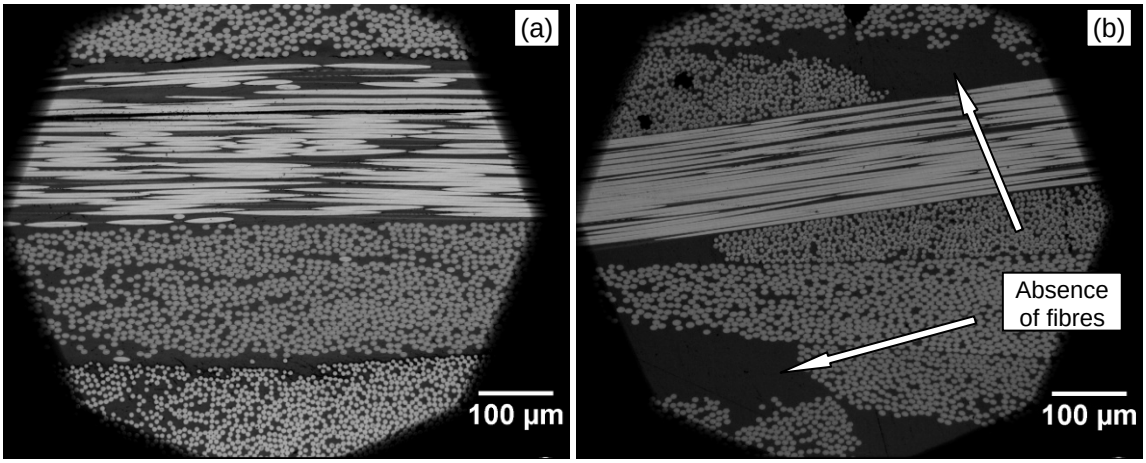


Figure 4.38: Subsurface microscopic analysis of (a) UD and (b) woven 8552/AS4 AC

### 4.3.2 Thrust force and torque

For tests performed using the stepped drill geometry, thrust force and torque results were based on the average value measured during cutting with the pilot section (part B, Figure 4.39) due to its higher contribution to workpiece delamination (explained further in Section 4.3.3). This concurred with the hypothesis by Won and Dharan [94], who determined that the pilot section of a stepped drill contributed ~ 65% of the total thrust force during cutting. For the conventional geometry, thrust force and torque results were based on an average value when the tool was completely engaged with the workpiece. Figure 4.40 and Figure 4.41 detail thrust force results recorded following the first and last holes drilled respectively. In the former case, thrust forces were generally found to be constant around ~ 45 N when a feed rate of 0.2 mm/rev was used, irrespective of the prepreg material or its associated prepreg form. These forces however increased by up to two fold (ranging between 40 N and 90 N) when operating at the higher feed rate level, and had a detrimental effect on hole quality in terms of workpiece delamination/damage (detailed further later in Section 4.3.3). As expected, last hole thrust forces were substantially higher (by an average of ~75%) due to the incidence of tool wear, in particular for drills which reached the maximum wear criterion.

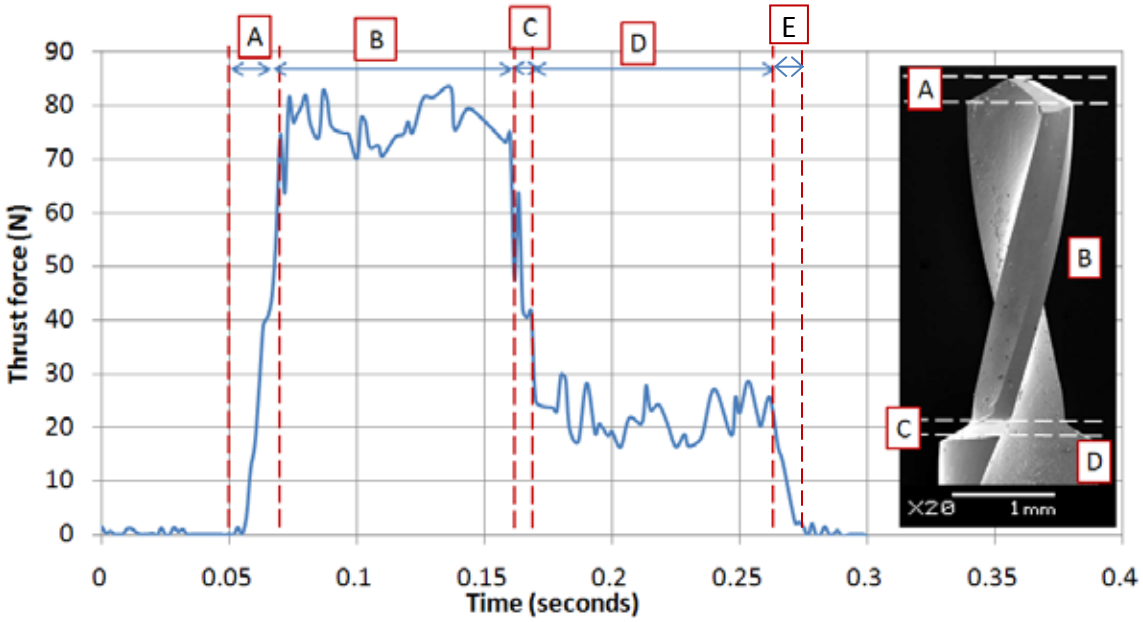


Figure 4.39: Typical force diagram for a single hole drilled using a stepped drill in woven 8552/AS4 AC laminate at 0.2 mm/rev

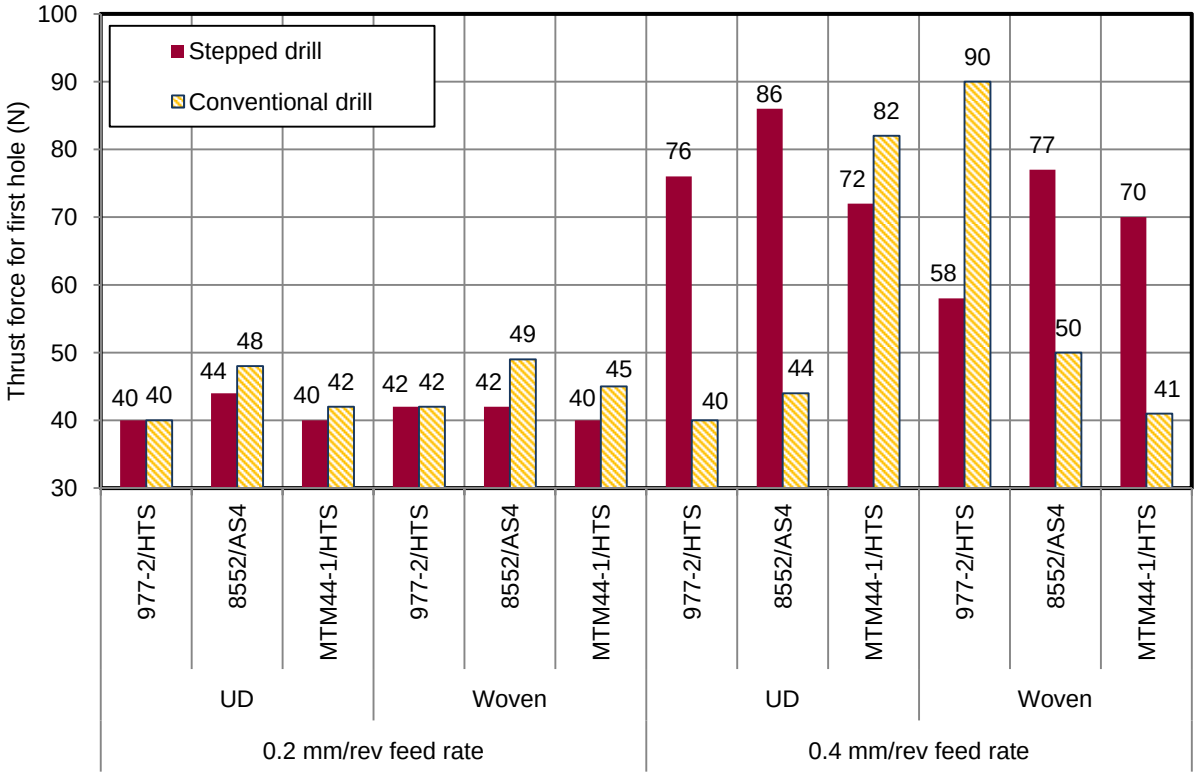


Figure 4.40: Thrust force results for the first hole drilled (Phase 2A)

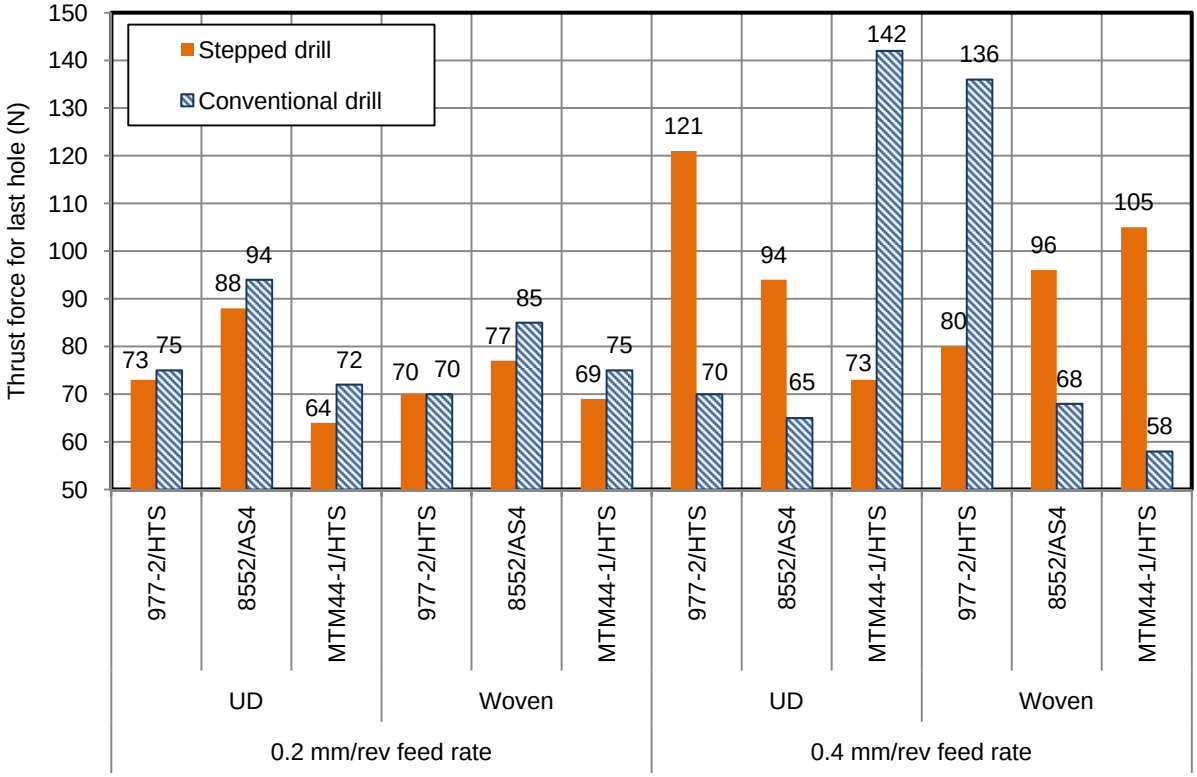


Figure 4.41: Thrust force results for the last hole drilled (Phase 2A)

The main effects plot and corresponding ANOVA table for first hole thrust force is shown in Figure 4.42 and Table 4.10 respectively. Drill feed rate had an overriding influence with a percentage contribution ratio of 42.53%, while the effect of prepreg type & form were largely negligible. This was not unexpected and broadly agreed with data previously reported by several researchers [61, 82 and 87]. With the exception of feed rate which had a 10% PCR, variation in factor levels for the last hole thrust force, (see Figure 4.43) produced a negligible change in the measured response and none of the factors evaluated were found to be statistically significant at the 5% level. Unfortunately, the analysis of variance also revealed a higher than acceptable error level for both first and last hole thrust force which was probably due to suspected interactions between variables as well as the premature failure of the drills in several tests conducted at high feed rates.

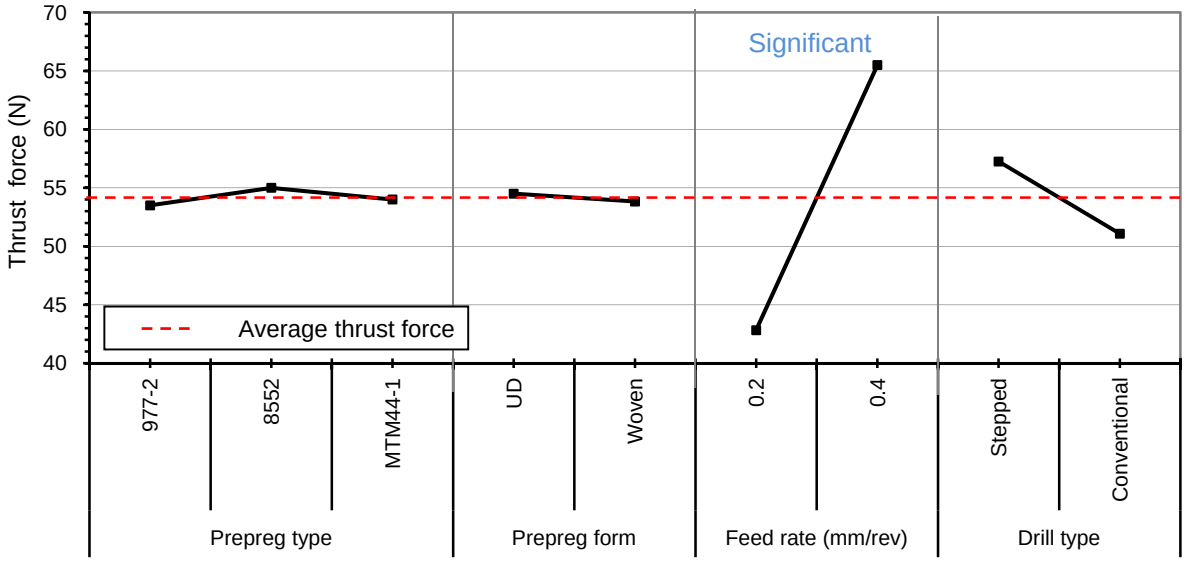


Figure 4.42: Main effects plot, means for thrust force (first hole)

| Factor | DF | SS | Exp SS | F | P | PCR |
|---|---|---|---|---|---|---|
| **A (prepreg type)** | 2 | 9.3 | -376.533 | 0.02 | 0.976 | 0.00 |
| **B (prepreg form)** | 1 | 2.7 | -190.217 | 0.01 | 0.908 | 0.00 |
| **C (feed rate mm/rev)** | 1 | 3082.7 | 2889.783 | 15.98 | 0.001* | 42.53 |
| **D (drill type)** | 1 | 228.2 | 35.28333 | 1.18 | 0.291 | 0.52 |
| **Error** | 18 | 3472.5 | | | | 56.95 |
| **Total** | 23 | 6795.3 | | | | |

Table 4.10: ANOVA results for thrust force (first hole)

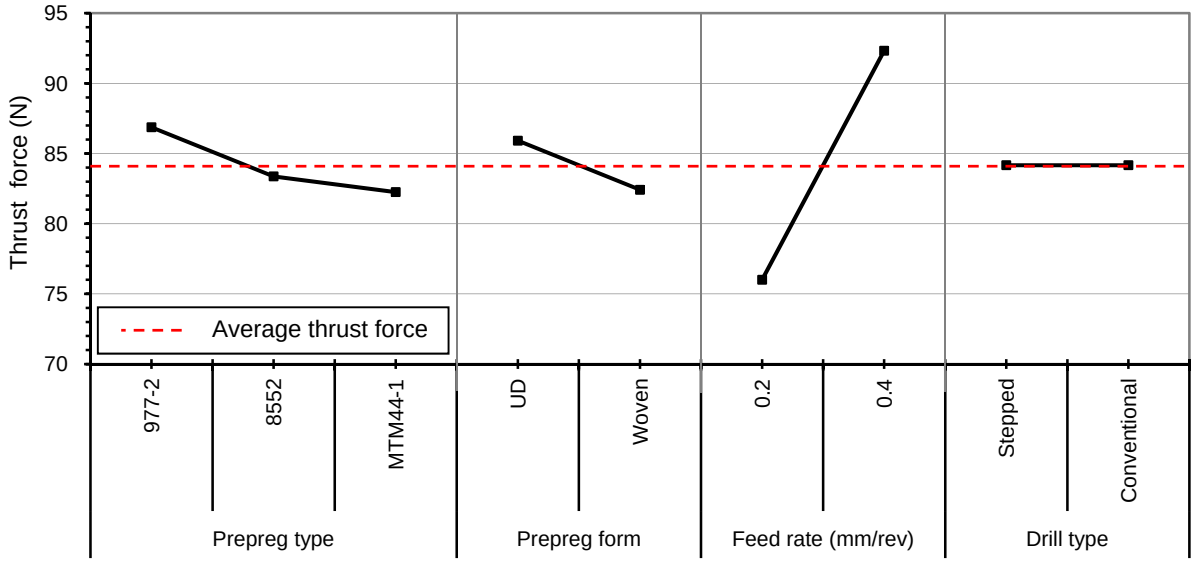


Figure 4.43: Main effects plot, means for thrust force (last hole)

The maximum torque level did not exceed 65 and 95 N.mm over the range of parameters tested for stepped and conventional drills respectively, see Figure 4.44. A larger cutting area was the likely reason for the higher values associated with conventional drill geometry. None of the factors or interactions relating to torque were found to be significant at the 5% level however prepreg type and drill type showed greater variation, see Figure 4.45. This corresponded to findings detailed in Section 4.2 where cutting speed was shown to have an overriding influence on drilling torque over other variables.

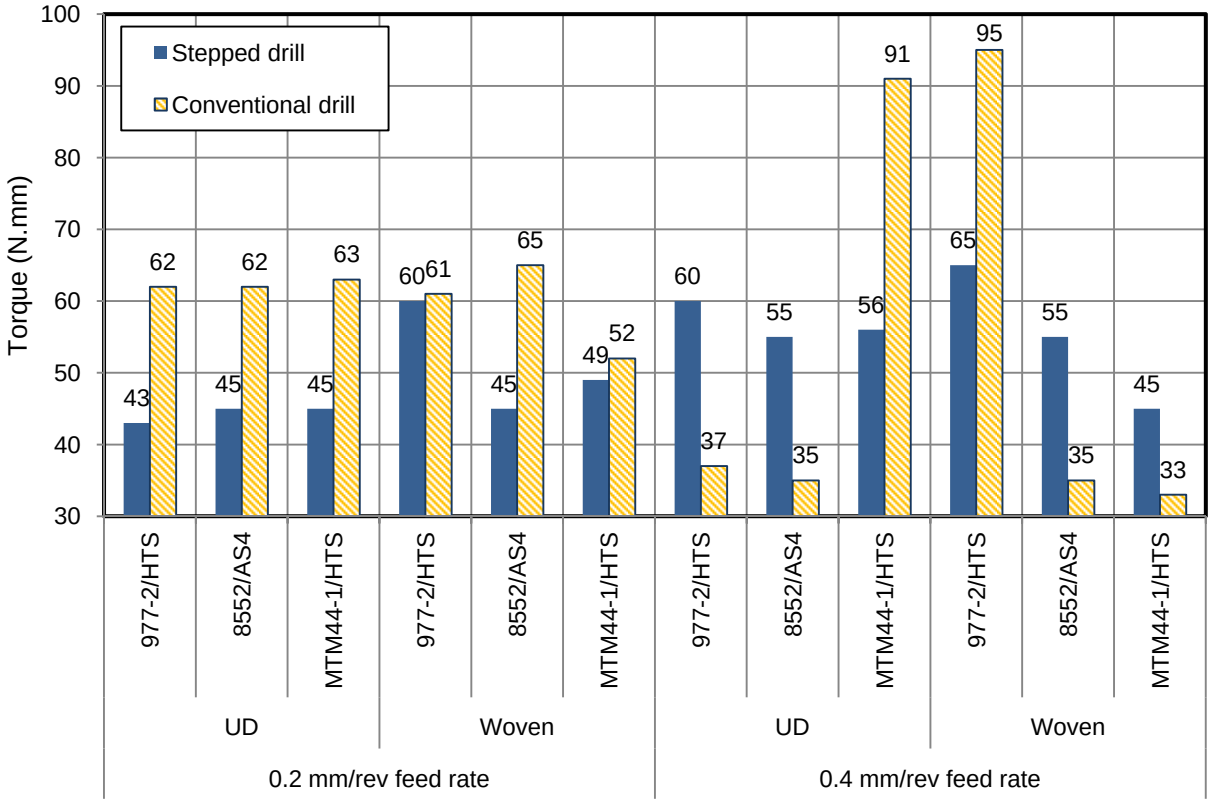


Figure 4.44: Drilling torque results (Phase 2A)

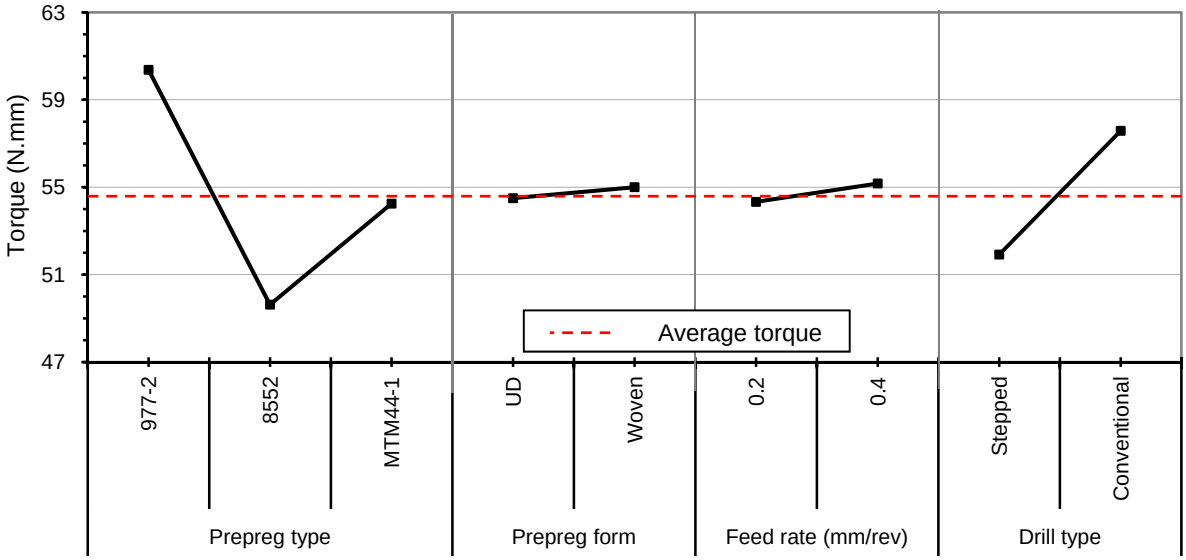


Figure 4.45: Main effects plot, means for torque (Phase 2A)

### 4.3.3 Drilled hole quality and damage

Entry and exit delamination were evaluated for both the first and last holes drilled. Figure 4.46 - Figure 4.49 detail the calculated delamination factors at the entry and exit. In general, delamination factor was found to be marginally greater at hole exit with a maximum of 2.1 obtained when cutting UD 977-2/HTS using a stepped drill and 8552/AS4 AC using conventional geometry at 0.4 mm/rev. $F_d$ was up to 1.95 at hole entry for the experimental parameters employed. Hole edge quality also largely deteriorated with respect to the increasing number of holes produced, in particular at hole exit, which agreed with results obtained by Chen [61]. This was in part due to the decline in drill edge sharpness which caused an elevation in thrust forces, as described in Section 4.3.2.

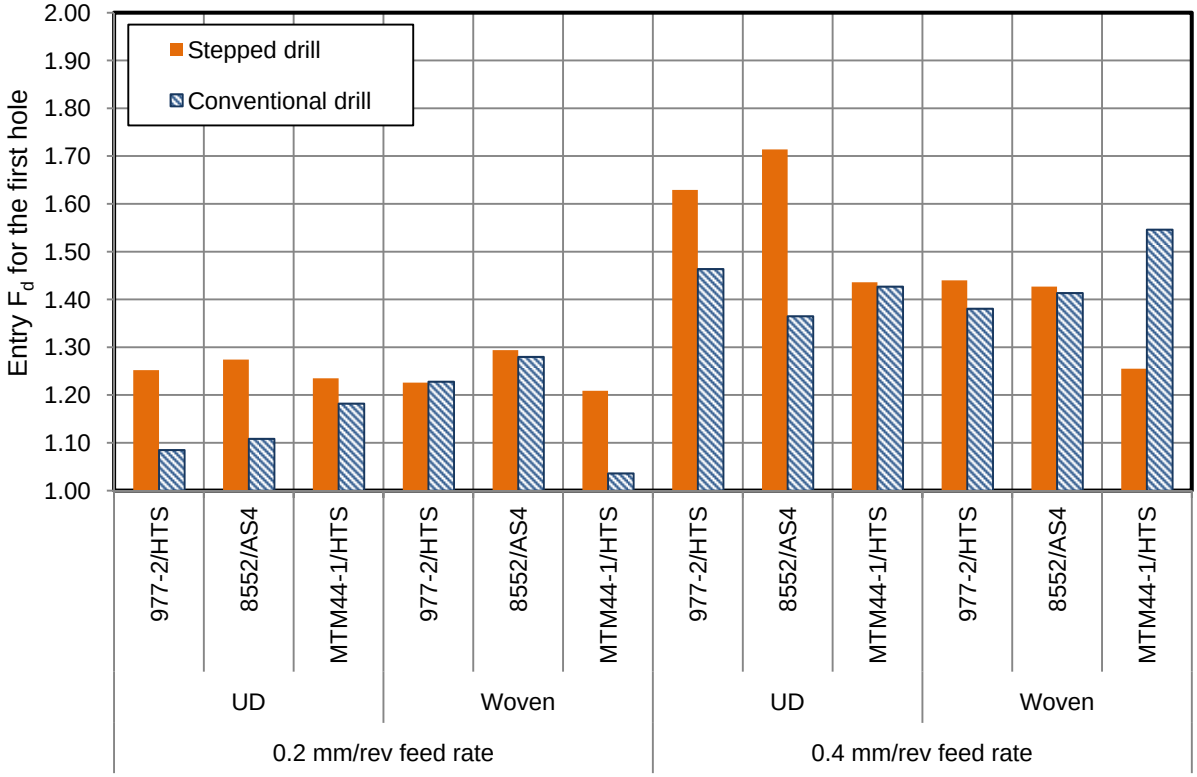


Figure 4.46: Entry delamination factor results for first hole drilled (Phase 2A)

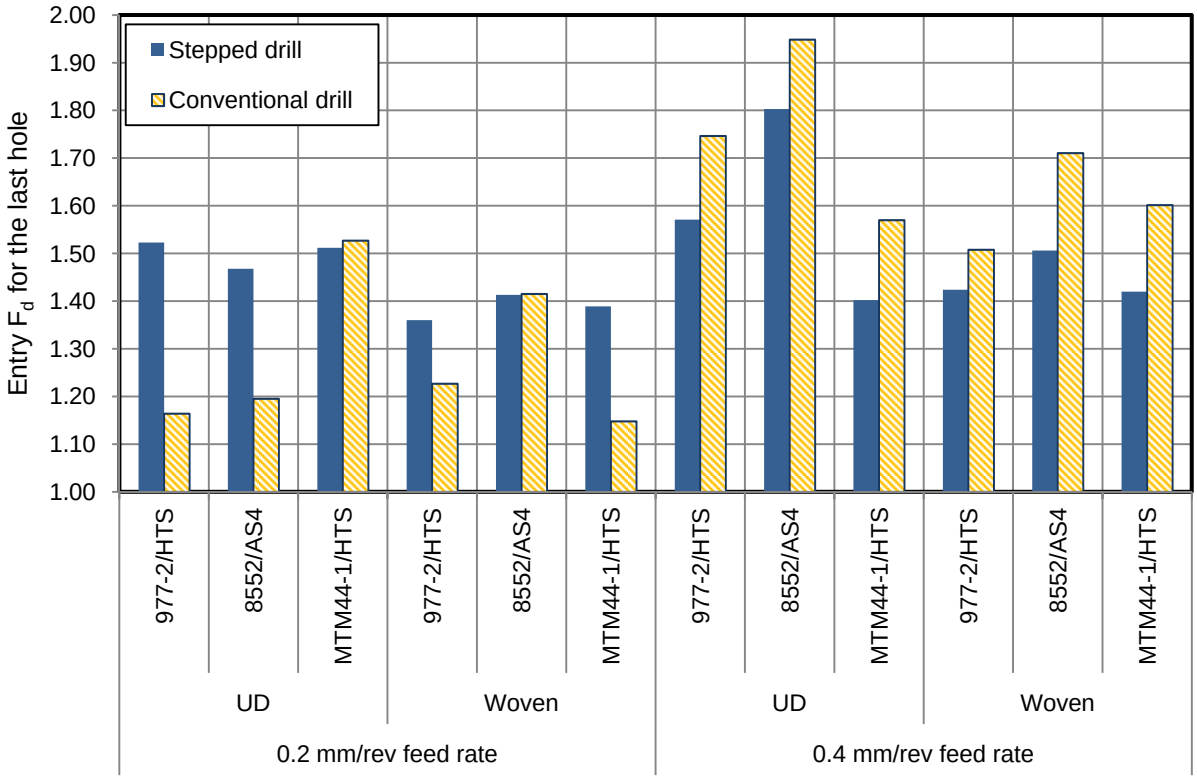


Figure 4.47: Entry delamination factor results for last hole drilled (Phase 2A)

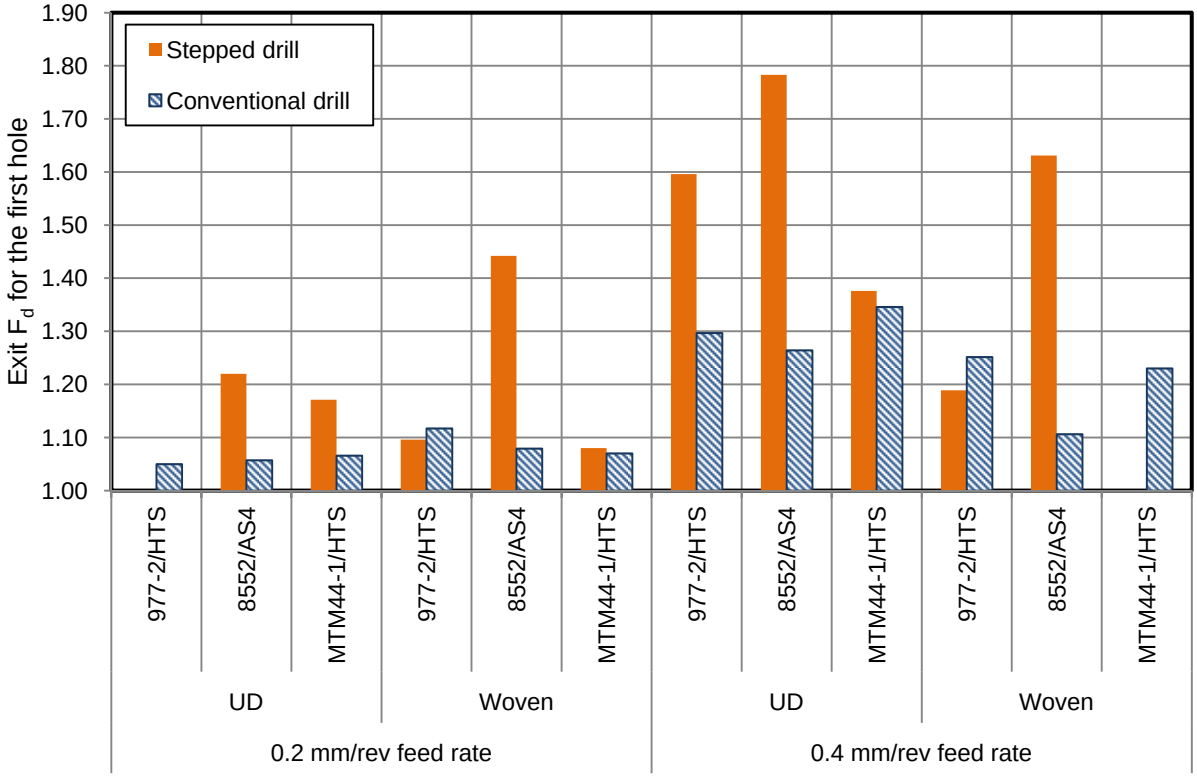


Figure 4.48: Exit delamination factor results for first hole drilled (Phase 2A)

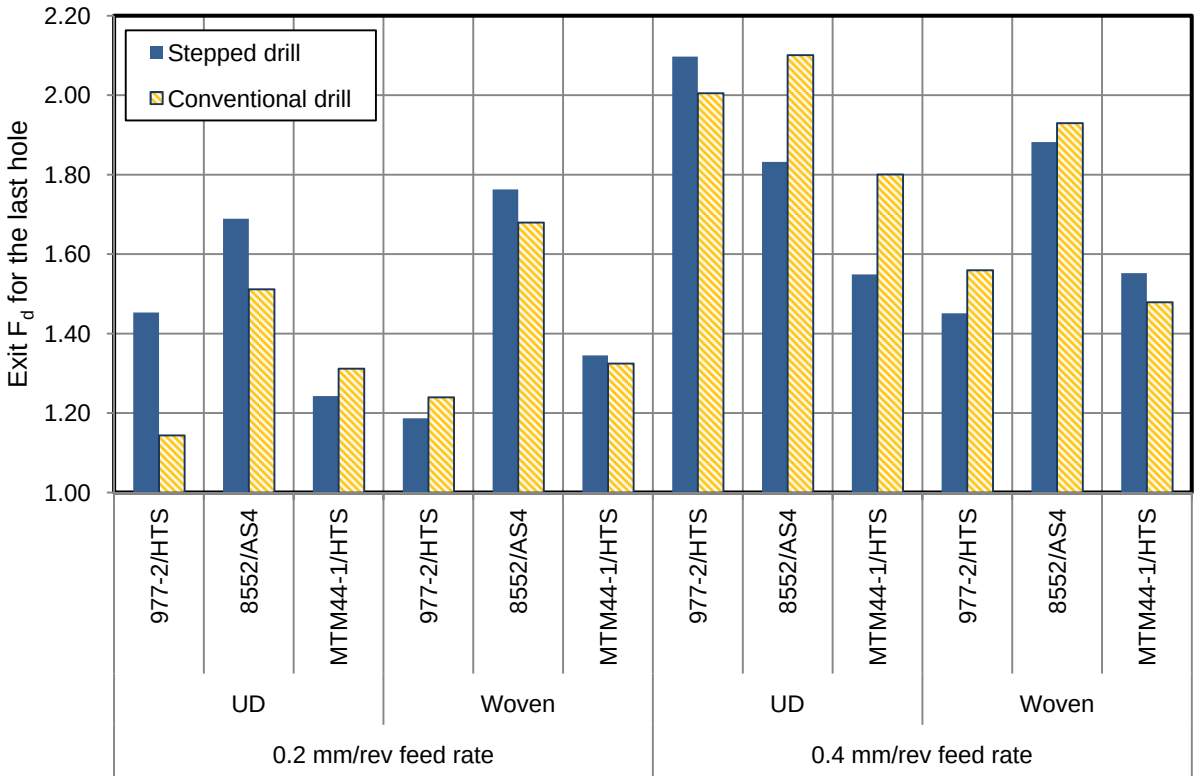


Figure 4.49: Exit delamination factor results for last hole drilled (Phase 2A)

A closer inspection of the results from first holes drilled showed the $F_d$ to be in most cases lower at hole exit compared to corresponding entry positions. This fact is clearly illustrated by the micrographs detailed in Figure 4.50. This was in line with the finding of Section 4.2.3 where average $F_d$ results were marginally higher associated with hole entry. The presence of nylon peel ply layers which essentially function as backup/support material, was thought to increase the critical thrust force level at which the onset of delamination occurred thereby inhibiting the progress of fibre push out. Superior or comparable delamination factor values were also obtained in certain instances at the exit side of the last holes drilled with the lower feed rate. As the feed rate was increased from 0.2 to 0.4 mm/rev however, there was a sharp decline in composite integrity around hole entry and exit for all laminate types. The only exceptions where higher $F_d$ occurred with a 0.2 mm/rev feed rate was at the hole exit of 8552/AS4 AC prepregs. This was despite the higher thrust forces generated when drilling at high feed rate. In terms of the composite resin system, the 8552/AS4 prepregs experienced the worst level of damage even with new tools when operating at 0.4 mm/rev feed rate, especially at the exit position, see Figure 4.51. This was almost similar for both the UD and woven laminates. No significant variation in terms of damage was seen for the two drill geometries employed, see Figure 4.52. This was in line with thrust force results detailed in Section 4.3.2, which were comparable when using either stepped or conventional drills.

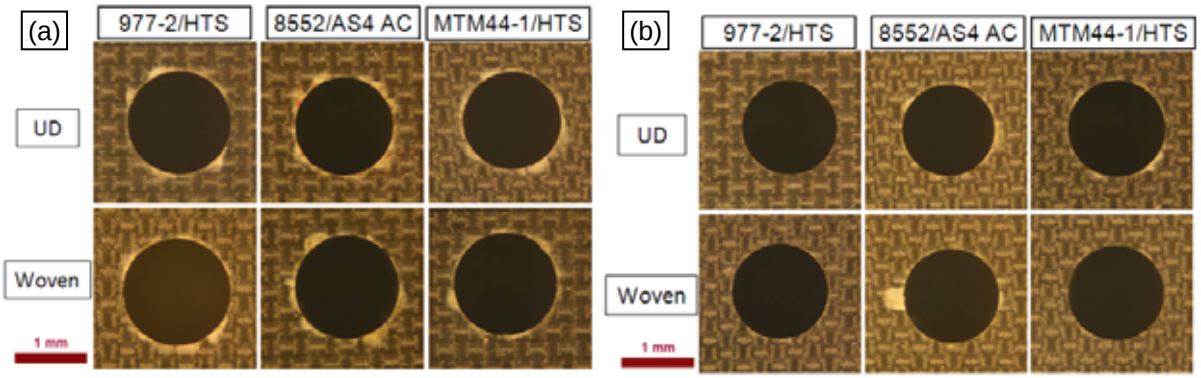


Figure 4.50: Delamination for: (a) hole entry and (b) hole exit at 0.2 mm/rev feed rate for first drilled hole (stepped drill)

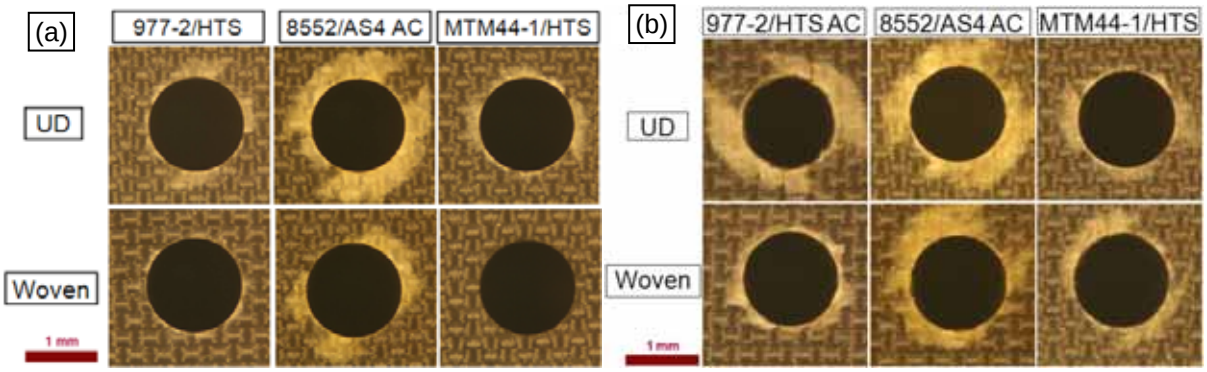


Figure 4.51: Exit delamination at 0.4 mm/rev feed rate for: a) the first and b) the last drilled hole (stepped drill)

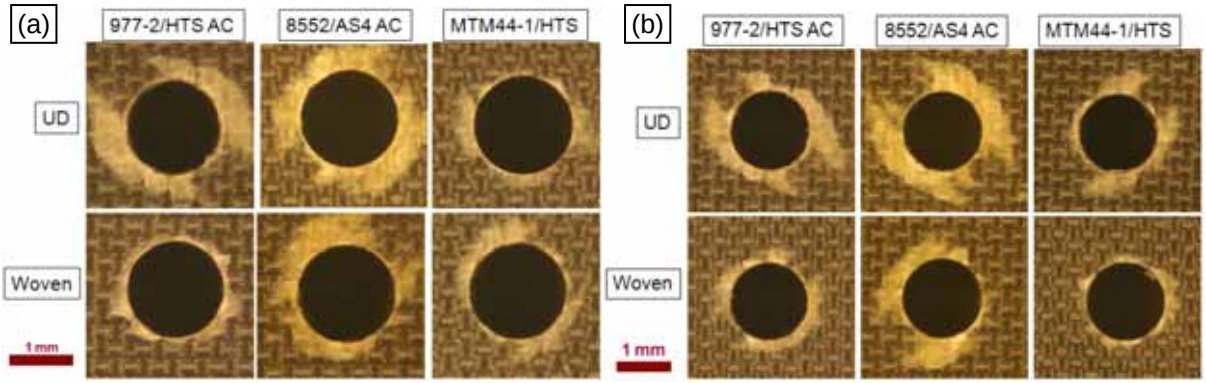


Figure 4.52: Exit delamination at 0.4 mm/rev feed rate for: a) stepped and b) conventional drill (last drilled hole)

In general, the contribution of the pilot section (1 mm diameter) of the drill on the thrust force was more significant than the step portion (1.5 mm diameter). As shown previously, the latter only produced a force signature approximately 30% of that for the pilot (see Figure 4.39). This agreed with published data by Jain and Yang [90] who reported that the chisel edge of a drill typically contributes about 50-70% of the thrust force generated. In addition, checks on measurement of delamination diameter after the pilot operation compared with that following final sizing with the step portion of the drill, indicated that the majority of damage (up to ~ 90%), was due to the action of the pilot section of the drill. In connection with this, Figure 4.53 shows a hole produced using the pilot portion of the drill only and the corresponding damage produced. The average diameter of damage following final hole sizing (1.5 mm) is also indicated, and it can be seen that the majority of damage was already present prior to operation with the step section.

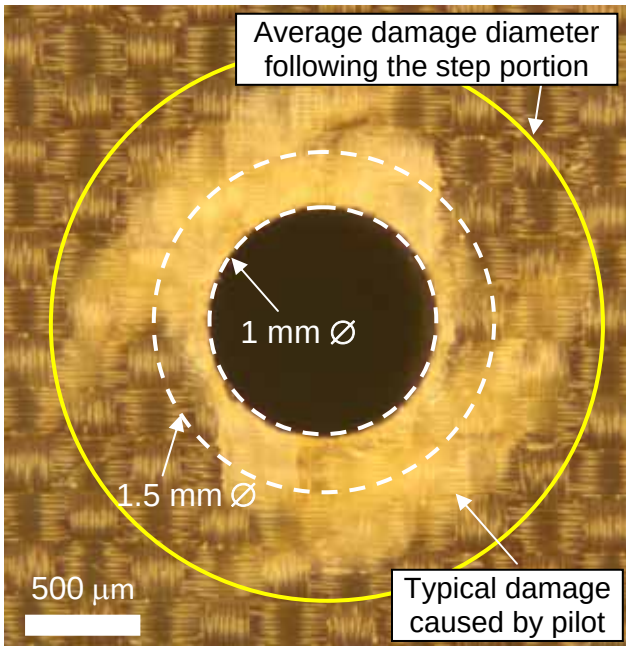


Figure 4.53: Extent of delamination caused by pilot portion of drill

Subsequent statistical analysis however showed near identical results in relation to the influence of process variables on entry/exit delamination for both first and last drilled holes. Main effect plots for calculated delamination factor pointed to the lowest $F_d$ being obtained when drilling woven MTM44-1/HTS OC composites at 0.2 mm/rev feed rate using conventional drills (or either geometries for the last hole drilled), see Figure 4.54 - Figure 4.57. Average delamination factor for the last hole drilled was 1.48 and 1.59 for entry and exit positions respectively. ANOVA results revealed that feed rate had an overwhelming effect on entry $F_d$ both for first and last hole drilled with a high PCR of 64 and 78% respectively, see Table 4.11 and Table 4.12. This further confirmed the strong correlation between delamination and thrust force, which has been reported by several researchers [68, 71, 73]. None of the other factors or interactions evaluated were found to be statistically significant at the 5% level in terms of entry $F_d$.

With regard to exit $F_d$ analysis, feed rate was the sole significant factor for first hole drilled with a PCR of 25%, while feed rate, prepreg type and prepreg form had significant influence in relation to last hole drilled with PCRs of 39, 31 and 5% respectively, see Table 4.13 and Table 4.14.

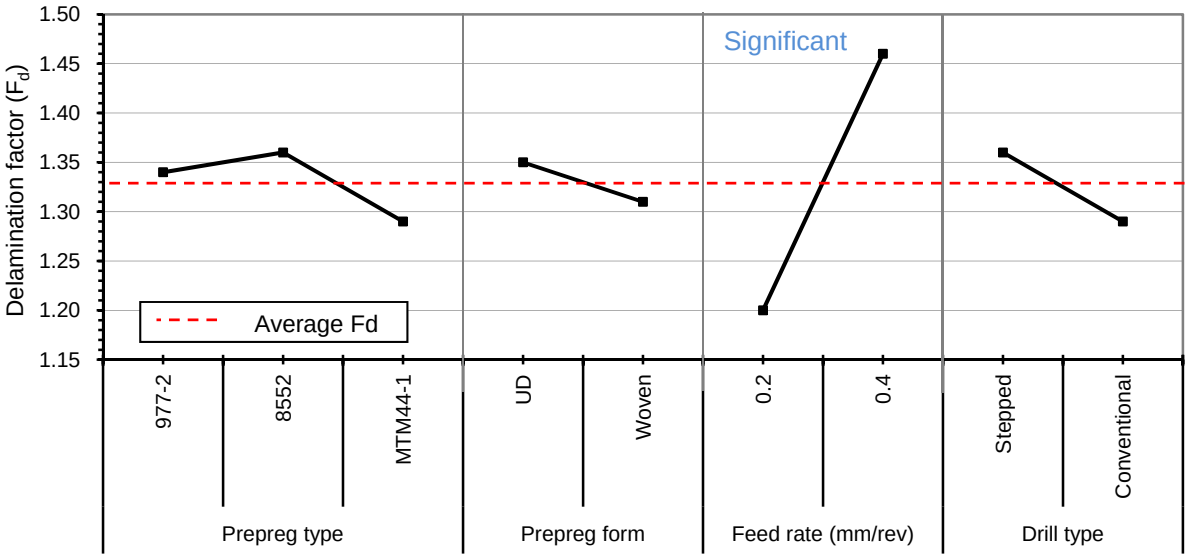


Figure 4.54: Main effects plot, means for entry $F_d$ for the first hole (Phase 2A)

| Factor | DF | SS | Exp SS | F | P | PCR |
|---|---|---|---|---|---|---|
| **A (prepreg type)** | 2 | 0.01901 | -0.031 | 0.38 | 0.689 | 0.00 |
| **B (prepreg form)** | 1 | 0.00734 | -0.01766 | 0.29 | 0.595 | 0.00 |
| **C (feed rate mm/rev)** | 1 | 1.01024 | 0.985236 | 40.4 | 0.000* | 63.98 |
| **D (drill type)** | 1 | 0.05324 | 0.028236 | 2.13 | 0.162 | 1.83 |
| **Error** | 18 | 0.45007 | | | | 34.19 |
| **Total** | 23 | 1.5399 | | | | |

Table 4.11: ANOVA results for entry $F_d$ (first hole)

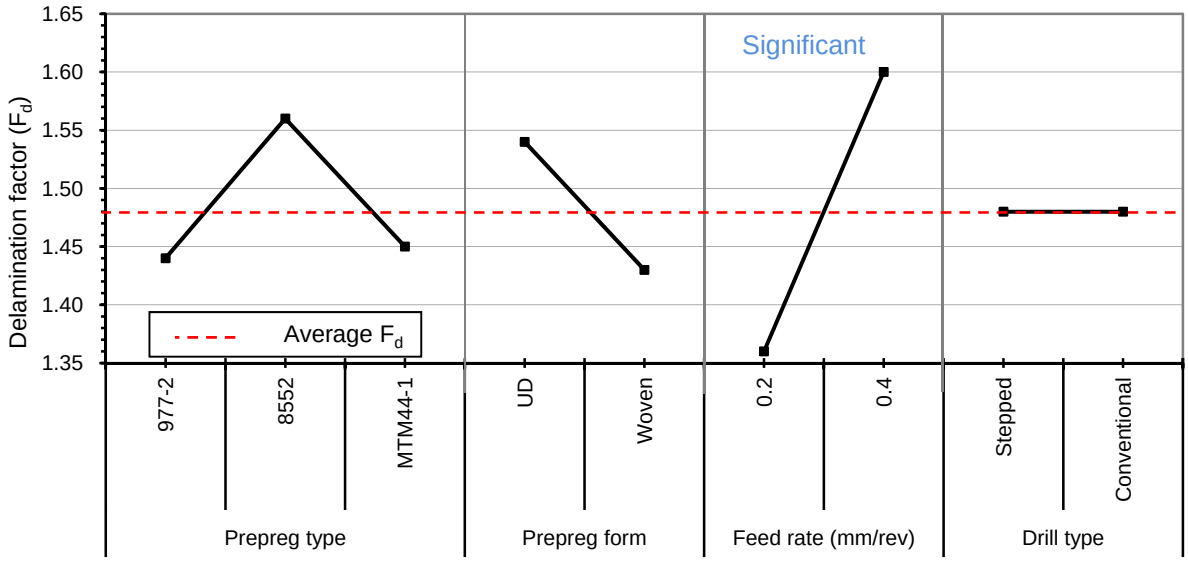


Figure 4.55: Main effects plot, means for entry $F_d$ for the last hole (Phase 2A)

| Factor | DF | SS | Exp SS | F | P | PCR |
|---|---|---|---|---|---|---|
| **A (prepreg type)** | 2 | 0.27103 | 0.130477 | 1.93 | 0.174 | 8.47 |
| **B (prepreg form)** | 1 | 0.11402 | 0.043743 | 1.62 | 0.219 | 2.84 |
| **C (feed rate mm/rev)** | 1 | 1.27724 | 1.206963 | 18.17 | 0.000* | 78.38 |
| **D (drill type)** | 1 | 0.01874 | -0.05154 | 0.27 | 0.612 | 0.00 |
| **Error** | 18 | 1.26498 | | | | 10.31 |
| **Total** | 23 | 2.94601 | | | | |

Table 4.12: ANOVA results for entry $F_d$ (last hole)

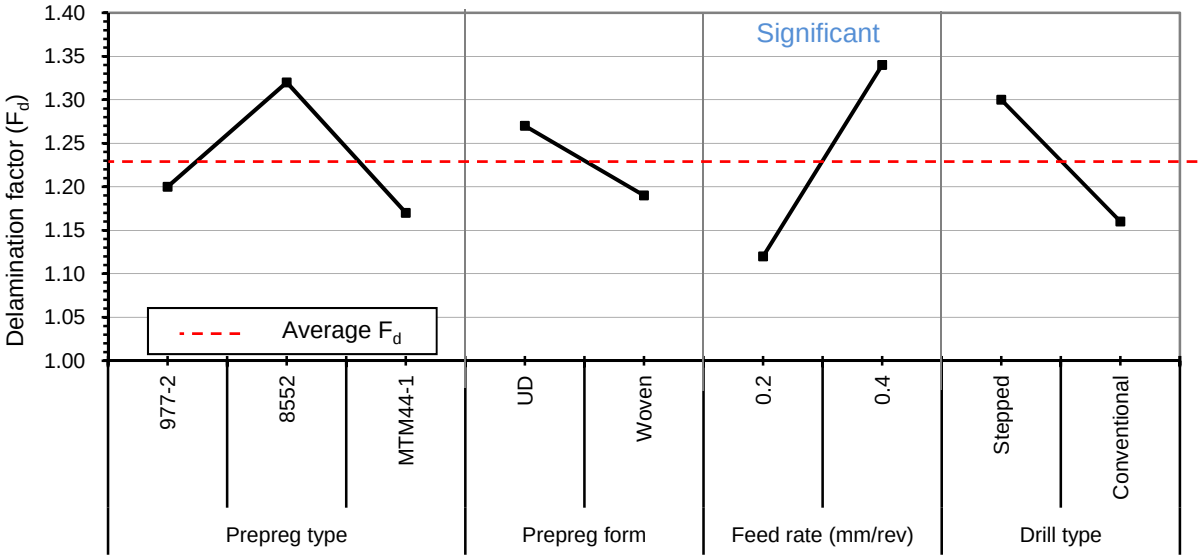


Figure 4.56: Main effects plot, means for exit $F_d$ for the first hole (Phase 2A)

| Factor | DF | SS | Exp SS | F | P | PCR |
|---|---|---|---|---|---|---|
| **A (prepreg type)** | 2 | 0.30992 | 0.141626 | 1.84 | 0.187 | 4.40 |
| **B (prepreg form)** | 1 | 0.14644 | 0.062293 | 1.74 | 0.204 | 1.94 |
| **C (feed rate mm/rev)** | 1 | 0.89174 | 0.807593 | 10.6 | 0.004* | 25.09 |
| **D (drill type)** | 1 | 0.35561 | 0.271463 | 4.23 | 0.055 | 8.43 |
| **Error** | 18 | 1.51465 | | | | 60.14 |
| **Total** | 23 | 3.21836 | | | | |

Table 4.13: ANOVA results for exit $F_d$ (first hole)

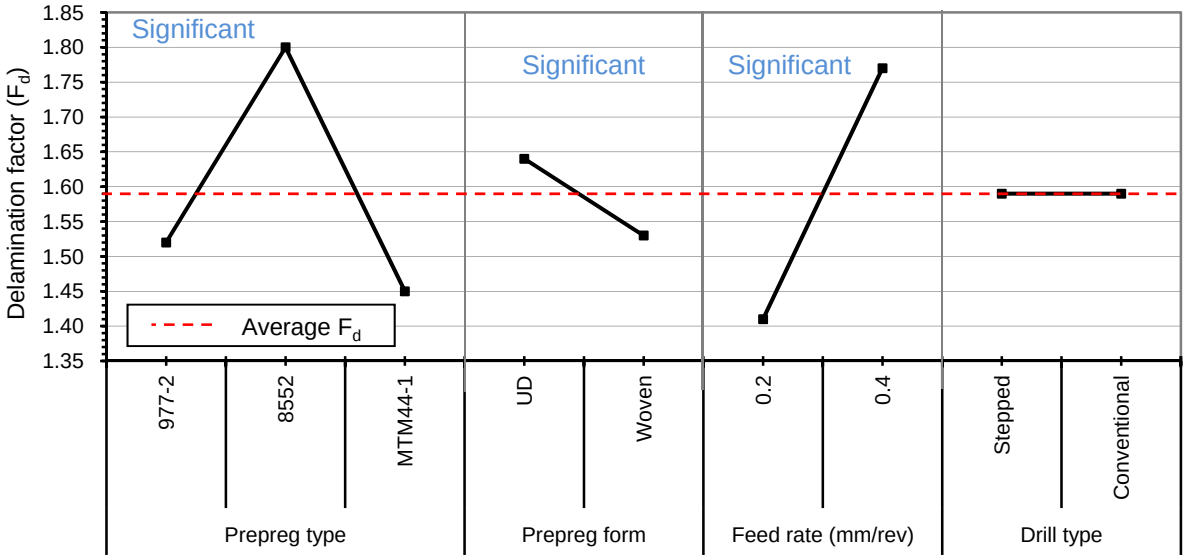


Figure 4.57: Main effects plot, means for exit $F_d$ for the last hole (Phase 2A)

| Factor | DF | SS | Exp SS | F | P | PCR |
|---|---|---|---|---|---|---|
| **A (prepreg type)** | 2 | 2.6397 | 2.4654 | 15.15 | 0* | 31.46 |
| **B (prepreg form)** | 1 | 0.4972 | 0.41005 | 5.71 | 0.028* | 5.23 |
| **C (feed rate mm/rev)** | 1 | 3.1187 | 3.03155 | 35.79 | 0* | 38.68 |
| **D (drill type)** | 1 | 0.0127 | -0.07445 | 0.15 | 0.707 | 0.00 |
| **Error** | 18 | 1.5687 | | | | 24.63 |
| **Total** | 23 | 7.8371 | | | | |

Table 4.14: ANOVA results for exit $F_d$ (last hole)

The nature and extent of delamination around drilled holes in composites can vary significantly and can be generally difficult to quantify/characterise by the traditional delamination factor ($F_d$) parameter alone, where only a diameter ratio is considered. A more representative assessment can be provided in some cases by the adjusted delamination factor ($F_{da}$) which was detailed in Chapter 2. Figure 4.58 shows selected cases where the adjusted delamination factor gave better discrimination of hole damage compared to the conventional $F_d$, which was identical for these examples. A closer visual inspection of the damage patterns at the exit of the last hole drilled in Test 1 and 10 (both having the same $F_d$ value) further emphasises the greater discriminating ability of the $F_{da}$ parameter, see Figure 4.58 (a) & (b). Although not detailed, the main effects plots and analysis of variance on $F_{da}$ for both hole entry and exit were equivalent to results based on $F_d$. In addition, feed rate was found to give the highest contribution in all cases evaluated, with a PCR of up to 78%, while residuals for $F_{da}$ were equivalent to those for $F_d$.

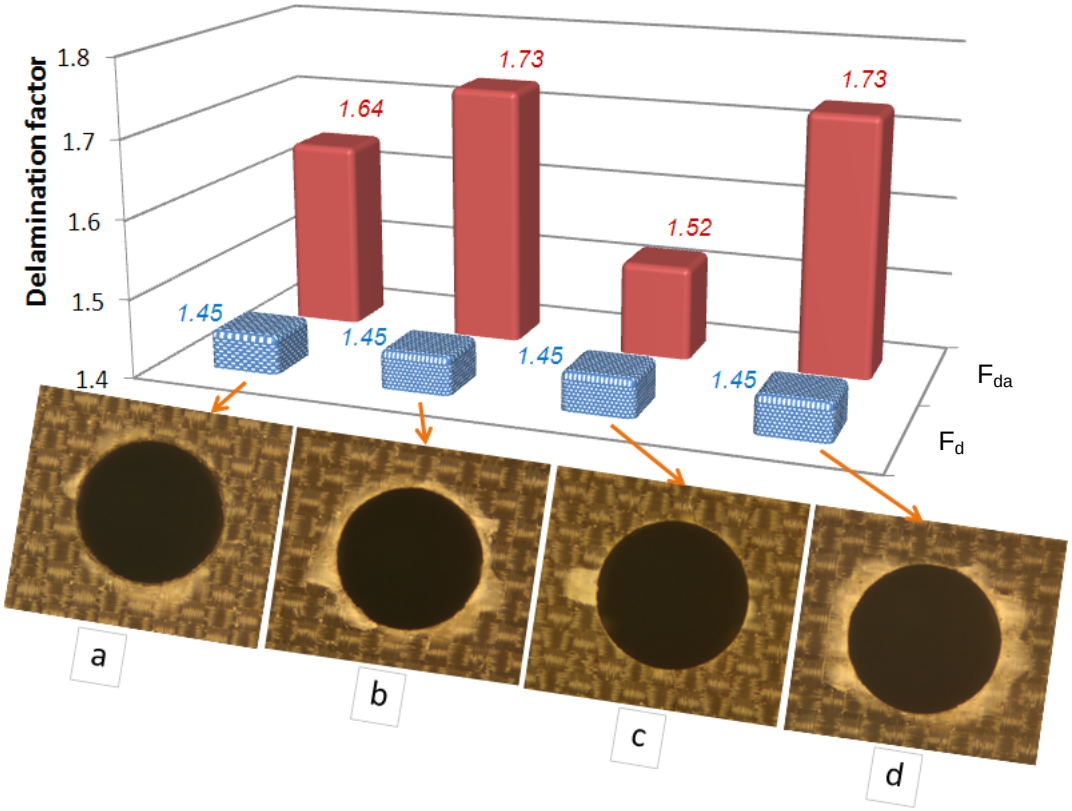


Figure 4.58: Examples for conventional and adjusted $F_d$: a) Last hole exit – Test 1, b) Last hole exit – Test 10, c) First hole exit – Test 5 and d) First hole entry –Test 10

### 4.3.4 Hole size measurement

Holes with a small taper were observed where the larger diameter occurred at hole entry. The maximum diametrical difference measured between hole entry and exit was 17 μm over a 2 mm height. Only the middle point reading (1.5 mm distance from hole entry or exit) was considered in further analysis. Here, the diameter of the drilled holes was found to be undersize for all conditions tested by up to 73 μm (~5%) and 39 μm (2.6%) at the end of tool life using stepped and conventional drills respectively as shown in Figure 4.59. This is not uncommon in the drilling process due to tool wear, which reduces tool diameter (and hence hole diameter) as the operation proceeds.

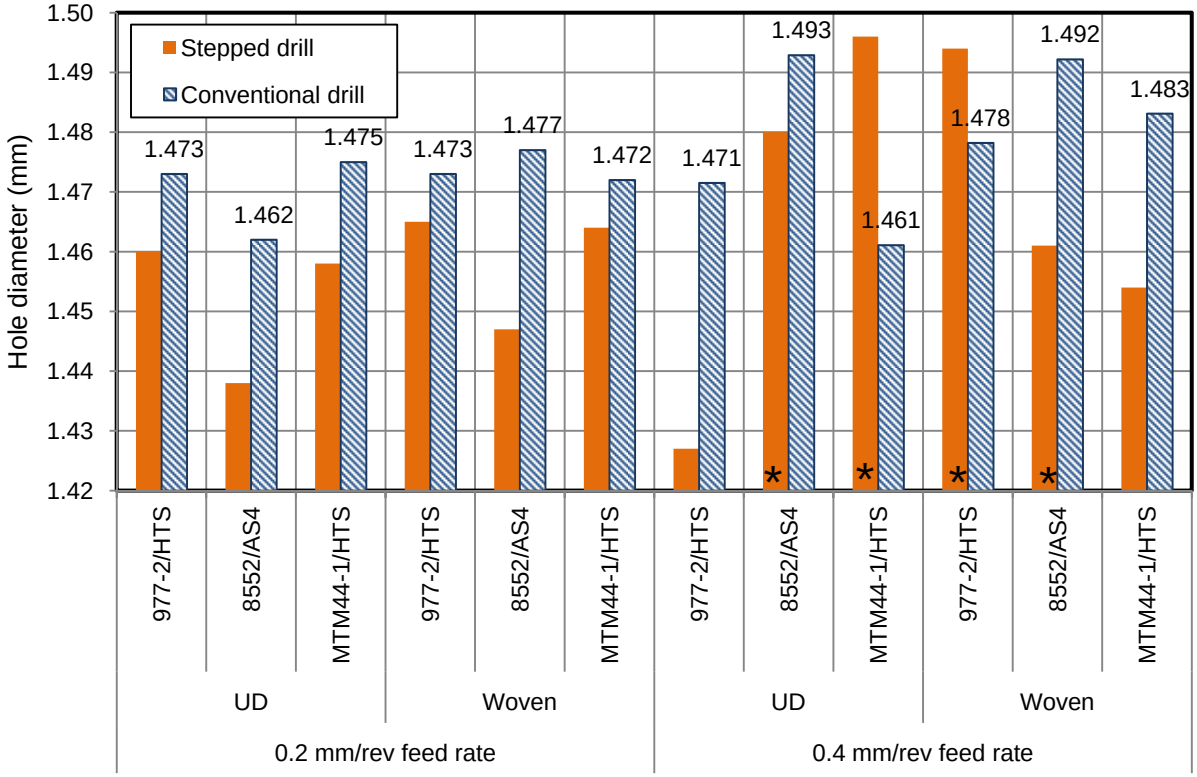


Figure 4.59: Hole diameter measurement results (Phase 2A)

The main effects plot and associated ANOVA however revealed that none of the evaluated variables were statistically significant. This was most likely due to the catastrophic fractures which occurred with several of the stepped drills. The average hole diameter over all trials was 1.469 mm (undersized holes by 31 μm), see Figure 4.60. The plot also shows that superior hole tolerance was obtained at the higher feed rate. This however was somewhat misleading as all cases of premature tool fracture took place at 0.4 mm/rev before the tool wear criterion was achieved (lower number of holes drilled) and consequently the holes had less variation from the nominal size.

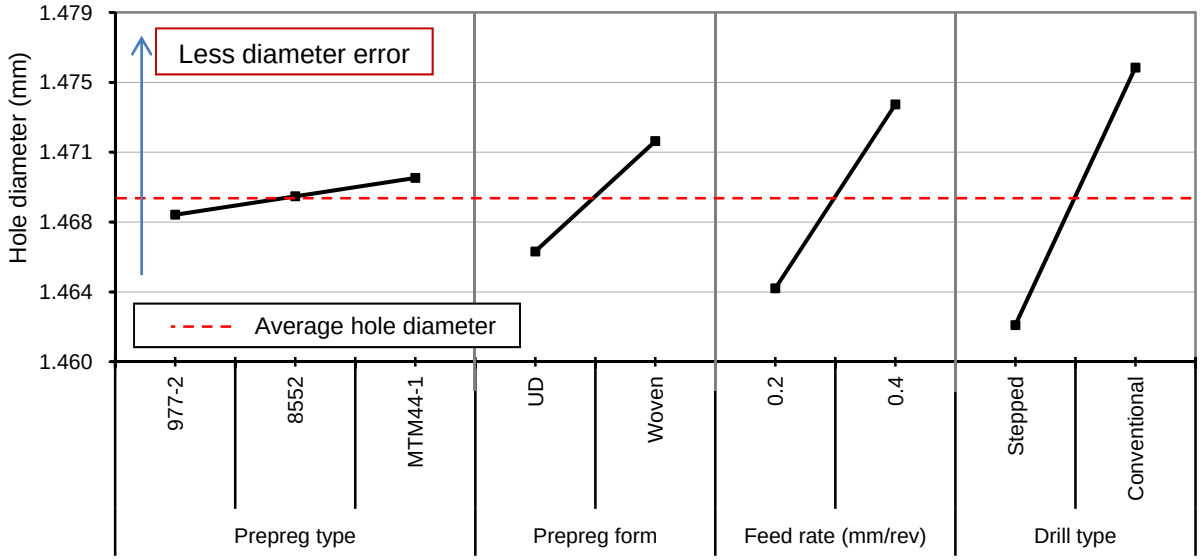


Figure 4.60: Main effects plot, means for hole diameter (Phase 2A)

### 4.3.5 Chip analysis

Limited chip analysis was carried out using optical microscopy. Two different shapes of swarf were obtained; continuous/spiral chips produced from cutting the peel ply (Figure 4.61) and discontinuous swarf from the panel core (CFRP) in the shape of fragmented and powdery chips. This was due to brittle fracture of both the fibres as well as the cured matrix [12]. Neither type of chip caused flute packing and cleared easily from the cutting zone, which was subject to a particle extraction system able to remove dust down to ~ 0.3 μm. Figure 4.62 shows micrographs for different shapes of chip when drilling CFRP. Additionally, SEM analysis confirmed that chips were predominantly in the form of discontinuous clumps (fibres gathered by the matrix material) as shown in Figure 4.63, which was similar to results from Hocheng and Puw [52].

Figure 4.61: Continuous/spiral nylon peel ply chip

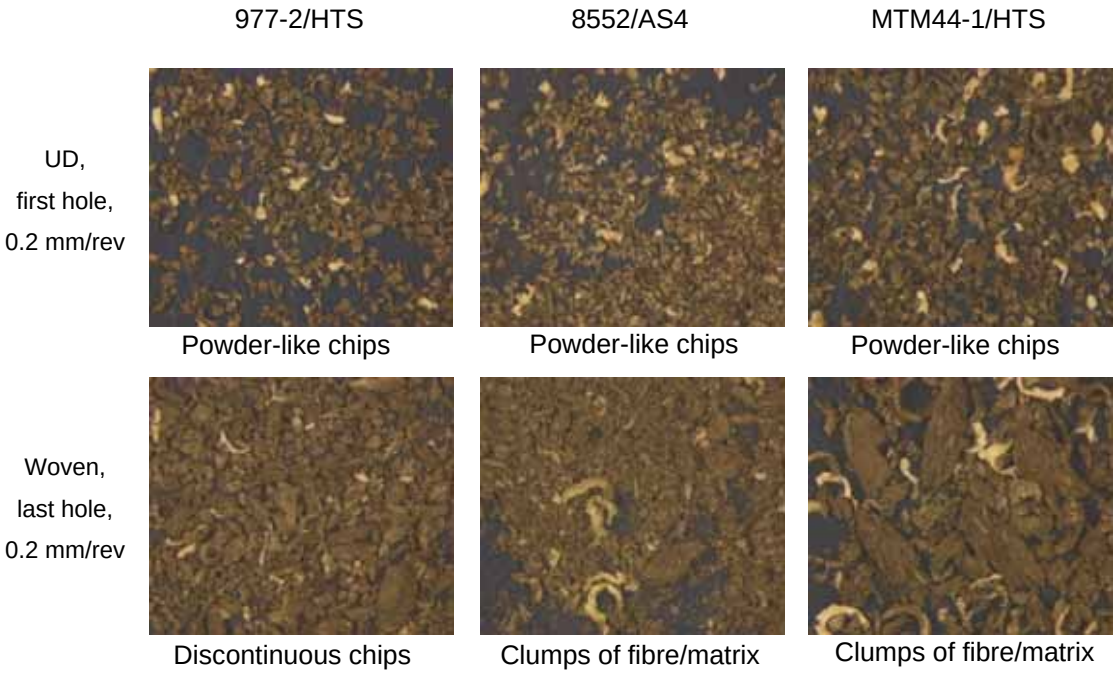


Figure 4.62: Various chip shapes when drilling CFRP

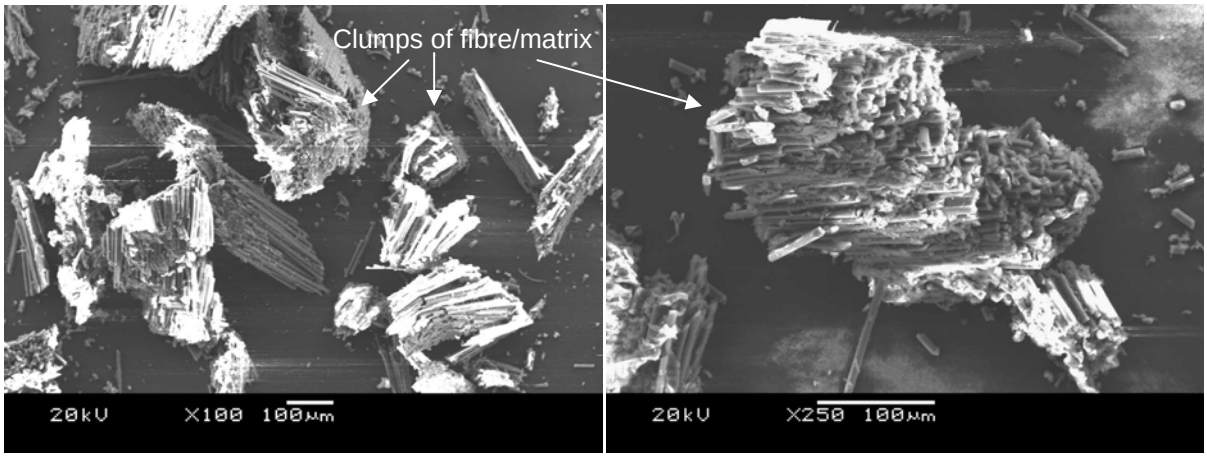


Figure 4.63: SEM images of chips produced from tests in Phase 2A

## 4.4 Phase 2B: Evaluation of diamond based coatings

### 4.4.1 Tool wear and tool life

Figure 4.64 shows flank wear progress when drilling the UD MTM44-1/HTS composite at 0.2 mm/rev feed rate. Similar trends were also obtained when cutting the woven 977-2/HTS laminate at the same feed rate but with comparatively lower tool lives. Figure 4.65 shows corresponding tool life end point comparisons for tests conducted at the low and high feed

rate levels. DLC coated drills had the longest tool lives, particularly when machining UD MTM44-1/HTS CFRP at 0.2 mm/rev feed rate, where up to 1800 holes was obtained prior to reaching the tool wear criterion. Conversely, all three CVD diamond coated tools experienced catastrophic failure at an early stage with the exception of the Rhobest diamond coated drill at 0.2 mm/rev. Figure 4.66 shows micrographs of all the drills used at 0.2 mm/rev feed rate in the new and worn (end of life) conditions. The majority of the CVD coated drills fractured after < 50 holes. SEM analysis of new uncoated and DLC coated tools revealed sharp/consistent cutting and chisel edges while poor edge definition/rounded edges together with bubbles/clumps and rough surfaces were seen on the corresponding CVD diamond coated drills, see Figure 4.67 (a). A possible factor causing the premature tool fracture experienced by the CVD diamond coated drills was the likely cobalt depletion from the carbide substrate during the coating process and consequent reduction of tool strength. It was also observed that the diamond coating layers generally 'peeled away' prior to chipping/fracture of the tools, see Figure 4.67 (b).

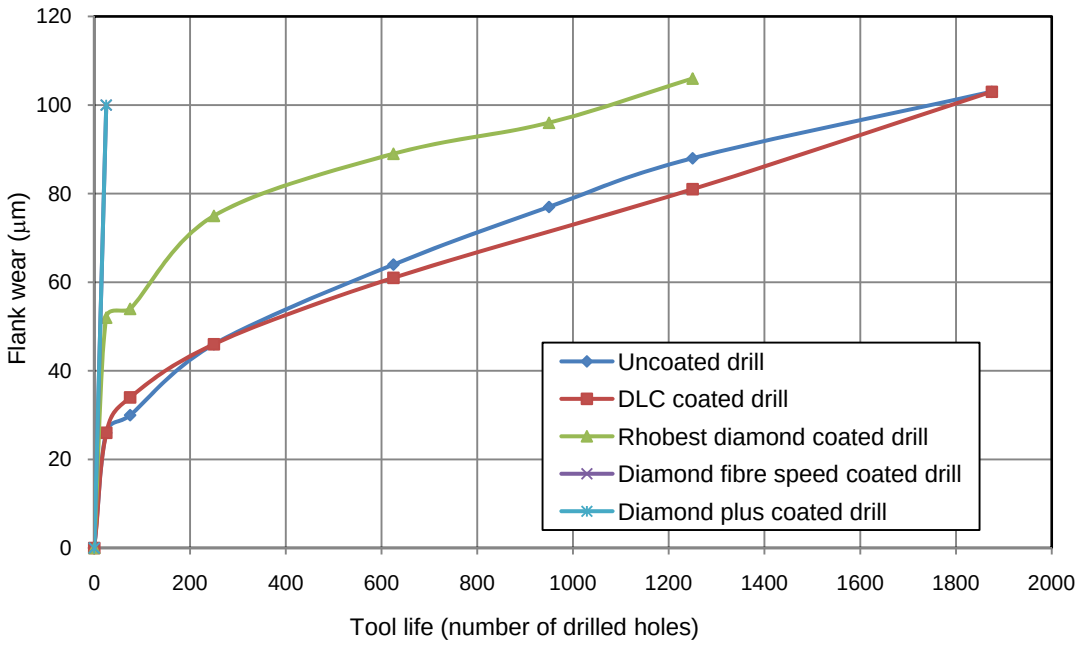


Figure 4.64: Flank wear results for different coatings when drilling UD MTM 44-1/HTS

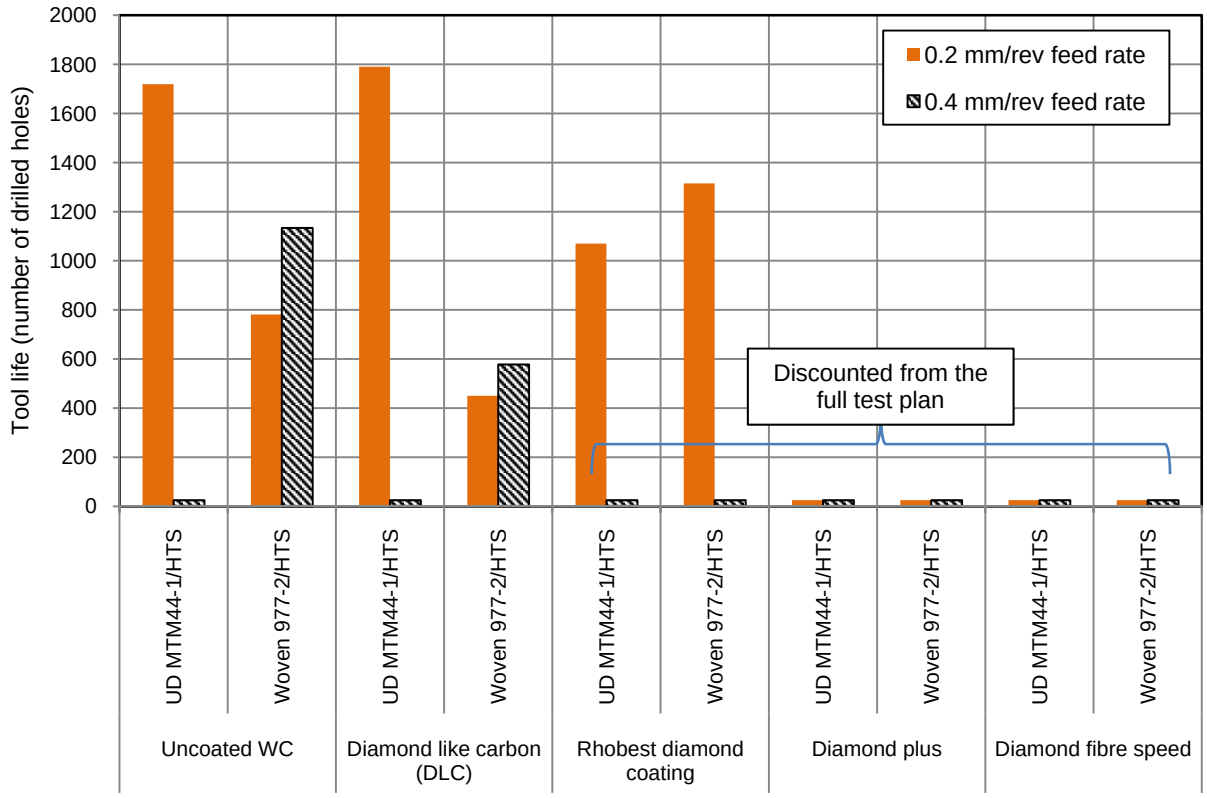


Figure 4.65: Tool life in terms of number of drilled holes

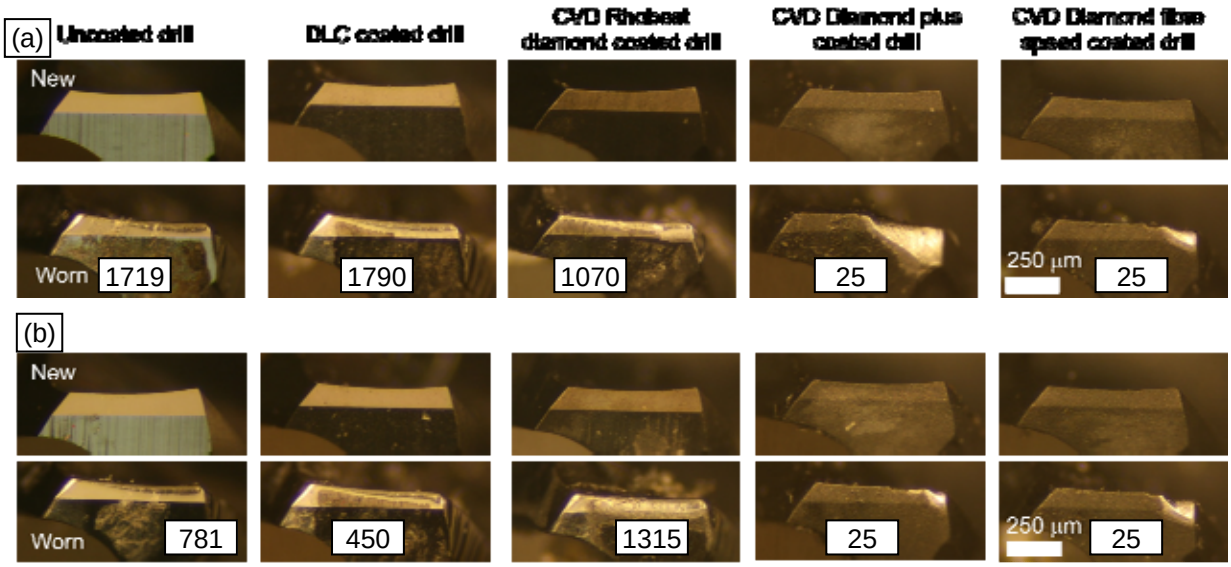


Figure 4.66: Micrographs of tools used at 0.2 mm/rev feed rate: (a) UD MTM44-1/HTS and (b) woven 977-2 laminates, number of drilled holes is shown for the worn tools

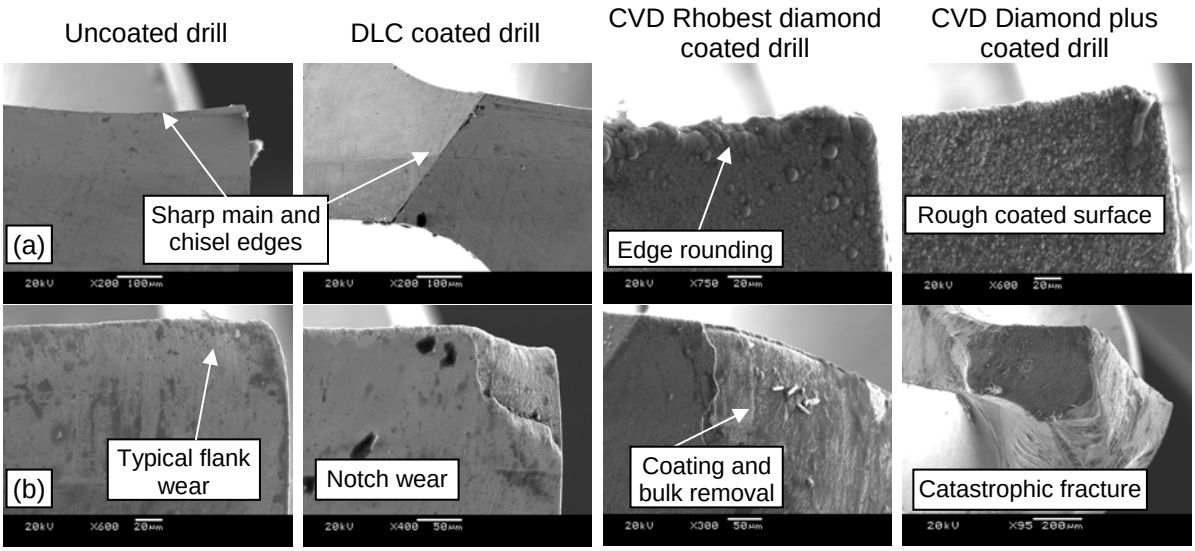


Figure 4.67: SEM images for the drills used at 0.4 mm/rev feed rate: (a) new and (b) worn

Figure 4.68 details tool life for tests conducted using uncoated and DLC coated drills at the various feed rates. The use of DLC coated drills to machine UD MTM44-1/HTS gave the highest tool life (~ 2500 holes) with a maximum allowable operating feed rate of 0.3 mm/rev. The majority of tools experienced typical flank wear growth except when cutting the UD MTM44-1/HTS at 0.4 mm/rev, at which premature edge fracture occurred. This was attributed to the excessive loads on the tool cutting edges as well as the highly abrasive nature of the fibres. The associated main effects plot is shown in Figure 4.69. Average tool life results for the uncoated drills marginally exceeded that for DLC drills although they both exhibited similar performance when cutting UD MTM44-1/HTS. This was in agreement with findings by Murphy et al. [93] who concluded that DLC coatings gave limited beneficial effect when drilling CFRP. Associated ANOVA results however revealed that feed rate and prepreg type together with interactions in coating material /prepreg type and feed rate/prepreg type were statistically significant at the 5% level. The highest PCR (39.46%) was understandably associated with the interaction between feed rate and prepreg type, where both variables were individually significant in influencing tool life. While the UD MTM44-1/HTS material caused catastrophic tool failure at the high feed rate (0.4 mm/rev), the woven 977-2/HTS laminates produced longer tool lives. This indicates a strong correlation / interaction between composite properties and the allowable operating feed rate. Additionally, a very low error level (2.46%) was obtained with the ANOVA results, affirming that all important variables were considered in the trials.

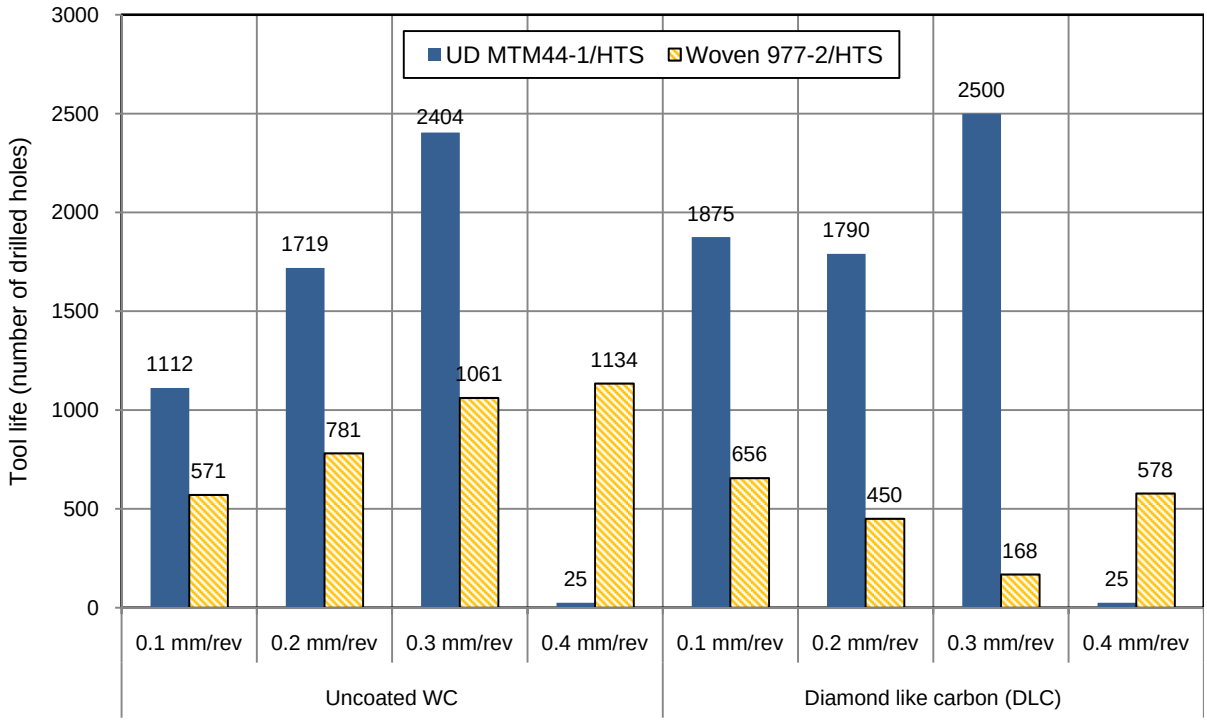


Figure 4.68: Tool life for uncoated and DLC coated drills

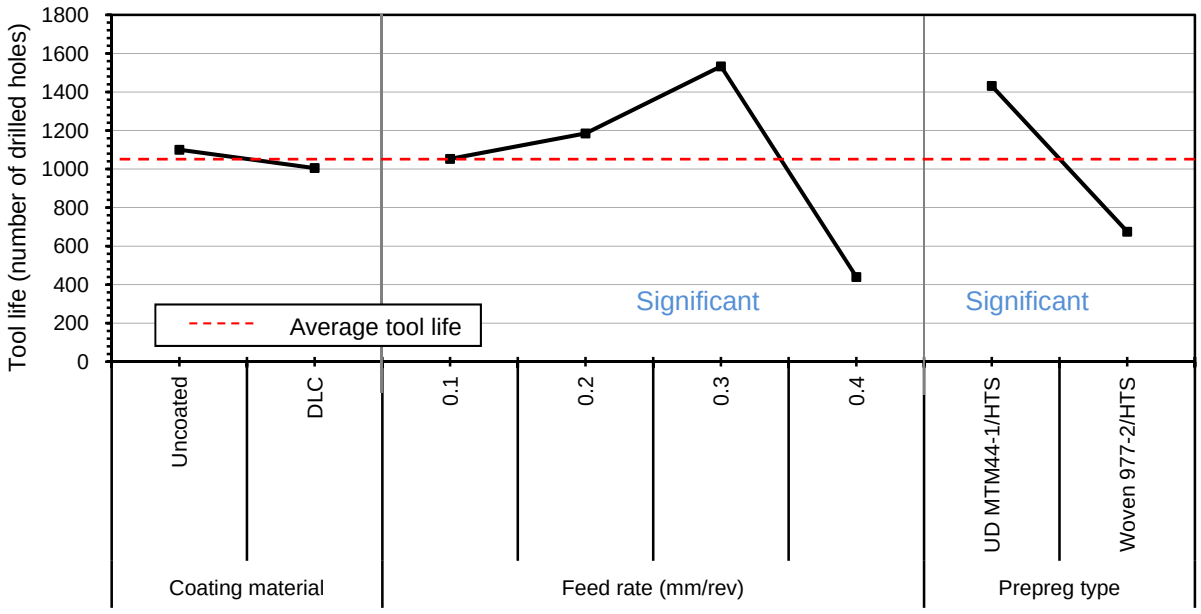


Figure 4.69: Main effects plot, means for tool life (Phase 2B)

| Factor | DF | SS | Exp SS | F | P | PCR |
|---|---|---|---|---|---|---|
| **A (Coating material)** | 1 | 36577 | 21086.33 | 2.36 | 0.222 | 0.22 |
| **B (Feed rate) (mm/rev)** | 3 | 2432095 | 2385623 | 52.33 | 0.004* | 25.27 |
| **C (Prepreg type)** | 1 | 2326388 | 2310897 | 150.18 | 0.001* | 24.48 |
| **AB** | 3 | 396186 | 349714 | 8.53 | 0.056 | 3.70 |
| **AC** | 1 | 430664 | 415173.3 | 27.8 | 0.013* | 4.40 |
| **BC** | 3 | 3771376 | 3724904 | 81.15 | 0.002* | 39.46 |
| **Error** | 3 | 46472 | | | | 2.46 |
| **Total** | 15 | 9439756 | | | | |

Table 4.15: ANOVA results for tool life (Phase 2B)

### 4.4.2 Thrust force and torque

In general, thrust force during the first hole ranged between 24 and 125 N depending on the operating feed rate, when uncoated and DLC coated drills were used as detailed in Figure 4.70. Similar trends were observed for the last hole drilled where thrust force gradually increased with feed rate as expected up to 160 N at 0.4 mm/rev, see Figure 4.71. Initial trials also highlighted a significant increase in thrust force to ~ 380 N with CVD diamond coated drills, which may account for their premature fracture, further details are provided in Appendix D.

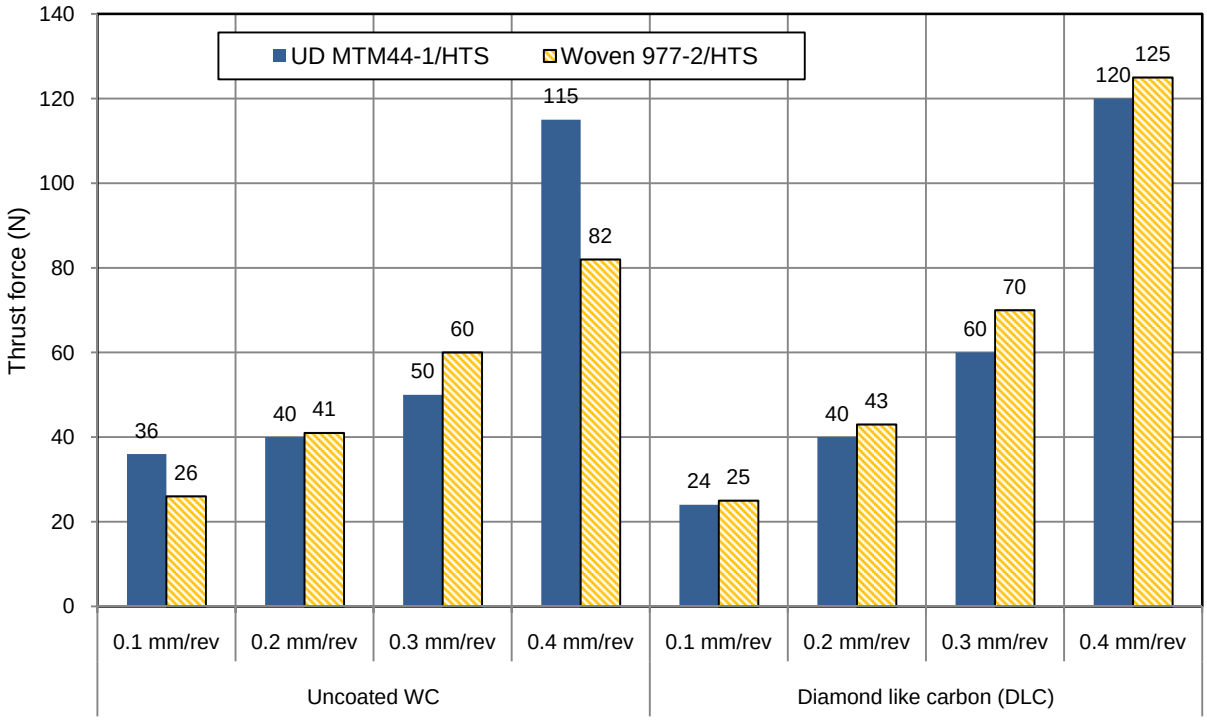


Figure 4.70: Thrust force results for the first hole drilled (Phase 2B)

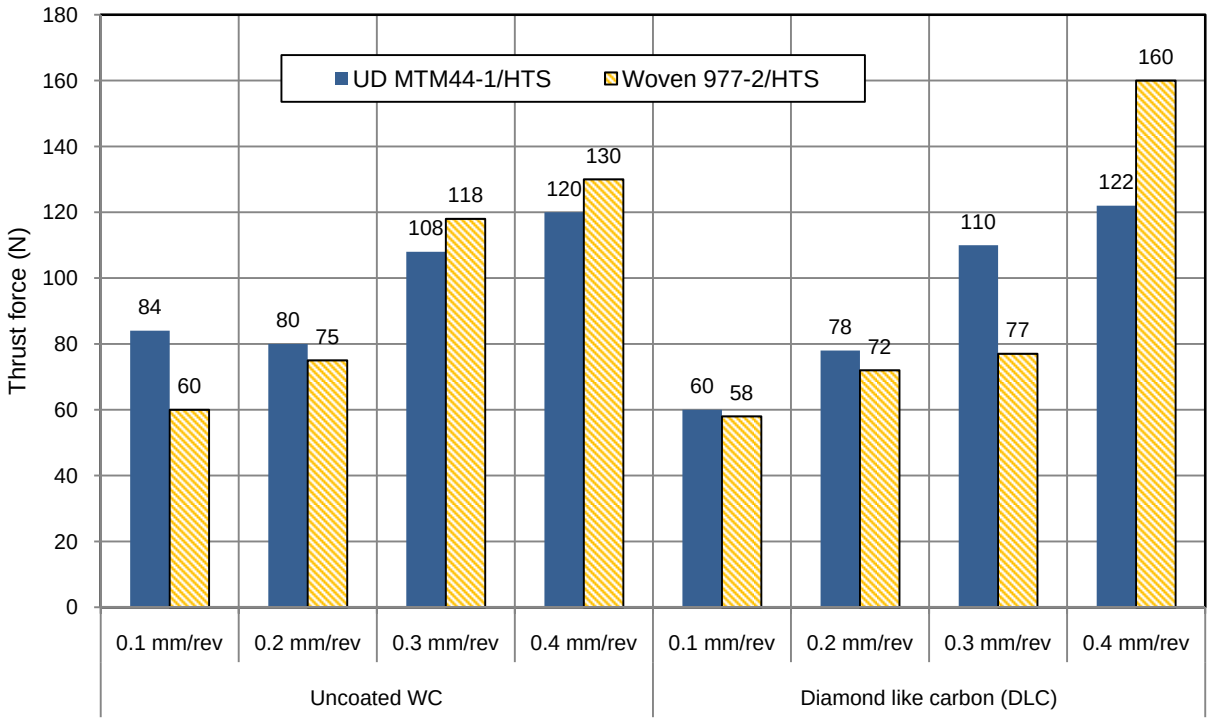


Figure 4.71: Thrust force for the last hole drilled (Phase 2B)

Main effects plot and ANOVA results in relation to thrust force for both first and last holes were similar. The average thrust force increased from 60 to 95 N from the first to the last hole drilled as a result of tool wear, see Figure 4.72 and Figure 4.73. Feed rate had an overriding effect on thrust force in both cases with extremely high PCR's of between 76% - 90%, as detailed in Table 4.16 - Table 4.17. The non-linear progression of feed rate in the main effects plot would appear to suggest that a critical/limiting feed rate level exists. Based on the data in Figure 4.72 together with previous results relating to tool life, the critical feed rate was estimated to be 0.3 mm/rev. The best factor/level combination for achieving minimum thrust force (during the last hole) corresponded to that found for maximum tool life i.e. DLC coating and UD MTM44-1/HTS. In contrast to tool life results, no interactions between any of the specified operating parameters were found.

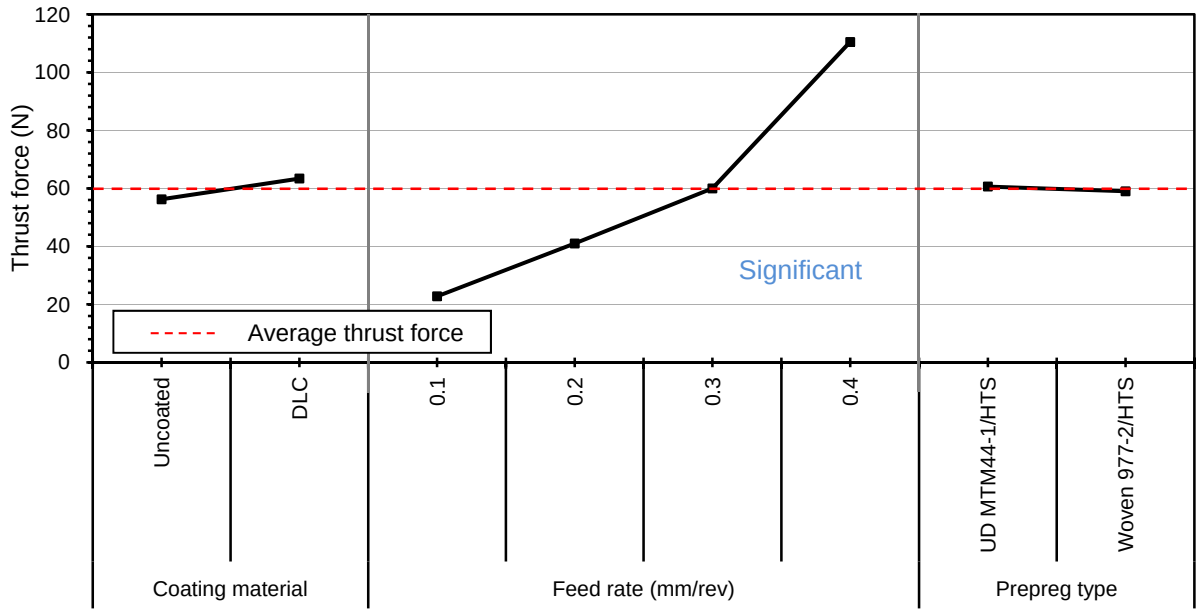


Figure 4.72: Main effects plot, means of thrust force (first hole)

| Factor | DF | SS | Exp SS | F | P | PCR |
|---|---|---|---|---|---|---|
| **A (Coating material)** | 1 | 203.1 | 81.29 | 1.67 | 0.226 | 0.47 |
| **B (Feed rate) (mm/rev)** | 3 | 15804.7 | 15439.27 | 43.25 | 0* | 89.57 |
| **C (Prepreg type)** | 1 | 10.6 | -111.21 | 0.09 | 0.774 | 0.00 |
| **Error** | 10 | 1218.1 | | | | 9.95 |
| **Total** | 15 | 17236.4 | | | | |

Table 4.16: ANOVA results for thrust force (first hole)

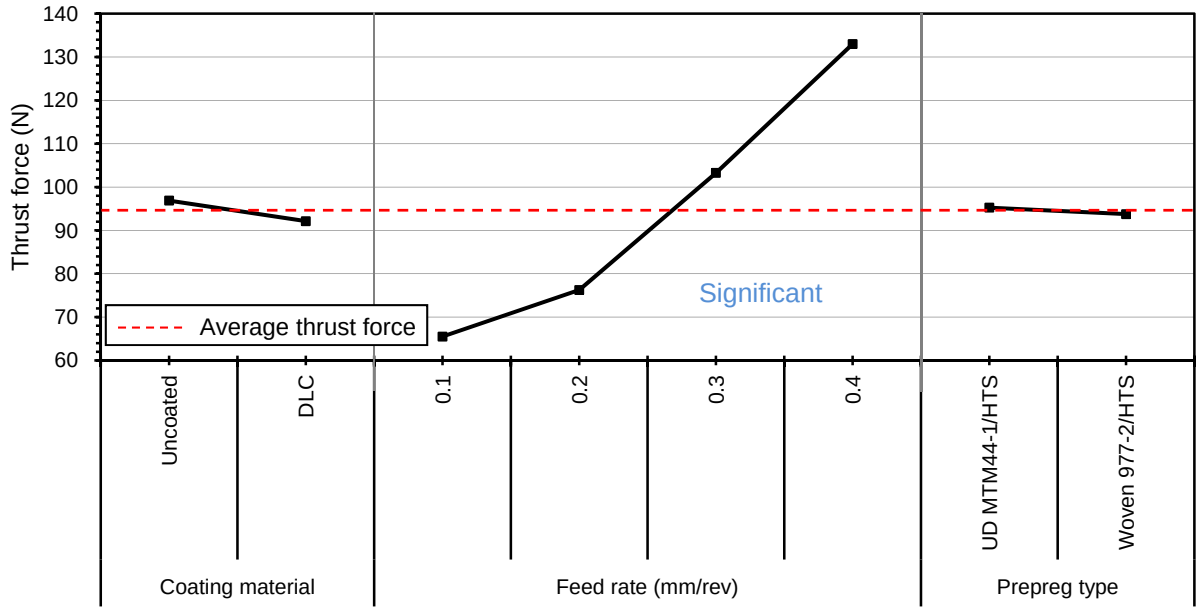


Figure 4.73: Main effects plot, means of thrust force (last hole)

| Factor | DF | SS | Exp SS | F | P | PCR |
|---|---|---|---|---|---|---|
| **A (Coating material)** | 1 | 90.3 | -149.62 | 0.38 | 0.553 | 0.00 |
| **B (Feed rate) (mm/rev)** | 3 | 10931.5 | 10211.74 | 15.19 | 0* | 76.04 |
| **C (Prepreg type)** | 1 | 9 | -230.92 | 0.04 | 0.85 | 0.00 |
| **Error** | 10 | 2399.2 | | | | 23.96 |
| **Total** | 15 | 13430 | | | | |

Table 4.17: ANOVA results for thrust force (last hole)

In general, low torque values were measured with the maximum associated with 0.3 mm/rev feed rate of up to 78 N.mm, see Figure 4.74. Main effects plot and ANOVA results for torque at last hole drilled are shown in Figure 4.75 and Table 4.18 respectively. In general, average torque was 54 N.mm, which increased gradually with feed rate up to 0.3 mm/rev, followed by a sudden drop at 0.4 mm/rev. This was in all likelihood due to the premature tool fracture which prevented the progress of wear at drill lands. Similarly, the use of DLC coatings when drilling UD MTM44-1/HTS prepreg material was expected to produce minimum torque.

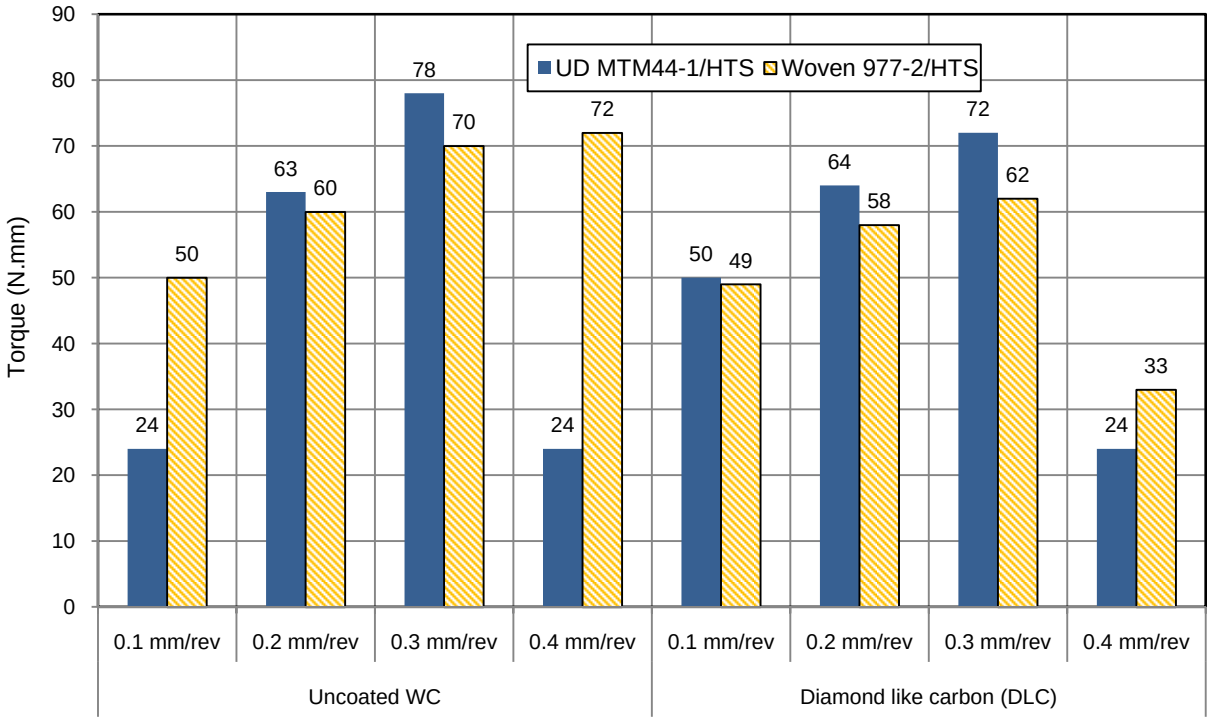


Figure 4.74: Torque results for the last hole drilled (Phase 2B)

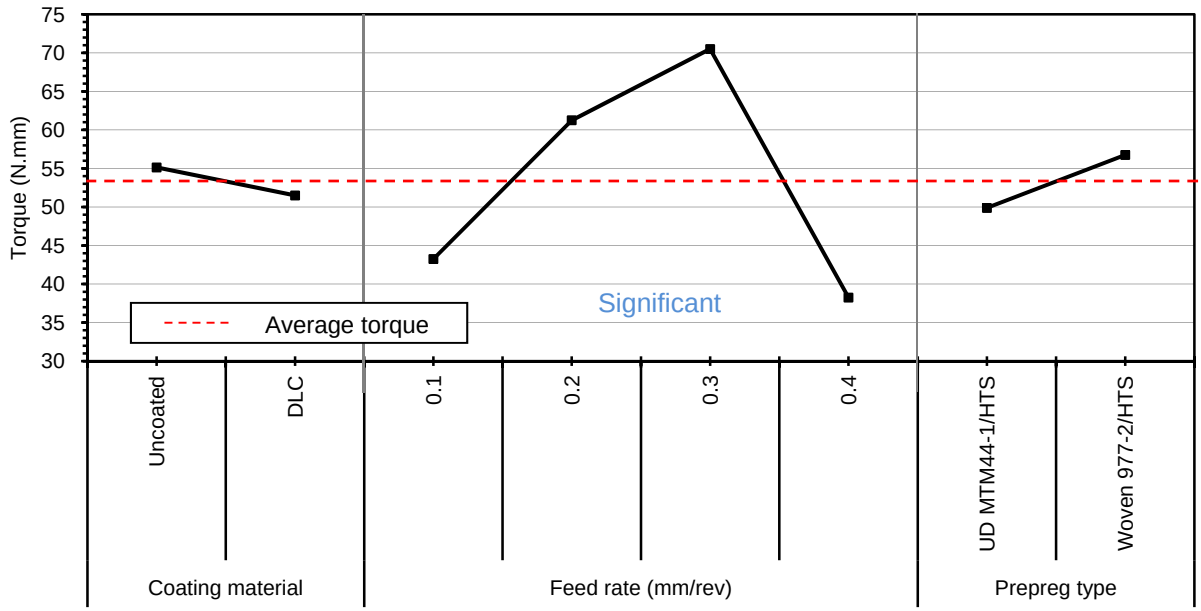


Figure 4.75: Main effects plot, means of torque (last hole)

| Factor | DF | SS | Exp SS | F | P | PCR |
|---|---|---|---|---|---|---|
| **A (Coating material)** | 1 | 52.6 | -145.36 | 0.27 | 0.618 | 0.00 |
| **B (Feed rate) (mm/rev)** | 3 | 2746.2 | 2152.32 | 4.62 | 0.028* | 43.33 |
| **C (Prepreg type)** | 1 | 189.1 | -8.86 | 0.96 | 0.351 | 0.00 |
| **Error** | 10 | 1979.6 | | | | 56.67 |
| **Total** | 15 | 4967.4 | | | | |

Table 4.18: ANOVA results for torque (last hole)

### 4.4.3 Drilled hole quality and damage

Exit hole damage was generally greater than entry with higher amounts of damage generated when machining UD MTM 44-1/HTS laminates compared to woven 977-2/HTS materials. This was attributed to the lower tendency for bending of the weave configuration which helped to impede the progress of delamination during drill push-out. Significant deterioration of hole edge quality with tool wear was observed especially when cutting UD MTM44-1/HTS laminate. Additionally, no significant variation in hole damage was seen between uncoated and DLC coated drills, while the use of CVD diamond coated drills during initial trials resulted in significantly larger damage owing to the extremely high induced thrust forces, see Figure 4.76. Figure 4.77 shows the typical delamination patterns associated with exit holes produced with uncoated and DLC coated tools at different feed rates.

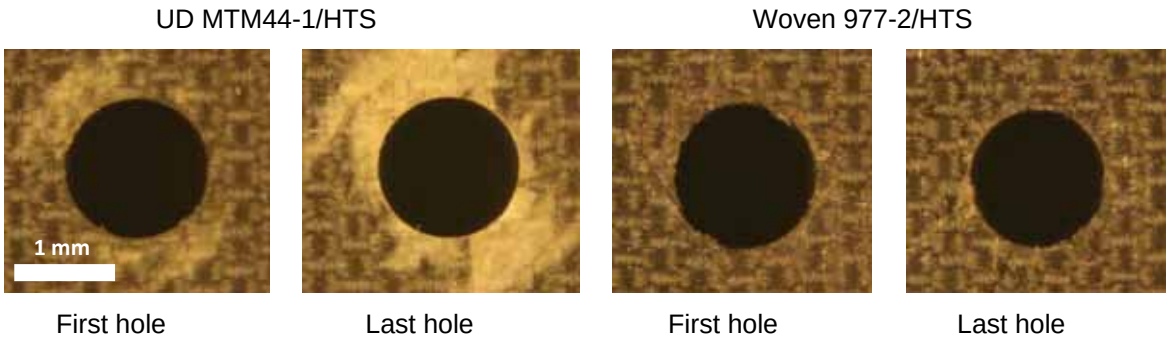


Figure 4.76: Sample drilled holes showing exit delamination when drilling UD MTM44-1 and woven 977-2 laminates using Rhobest diamond coated drill at 0.4 mm/rev feed rate

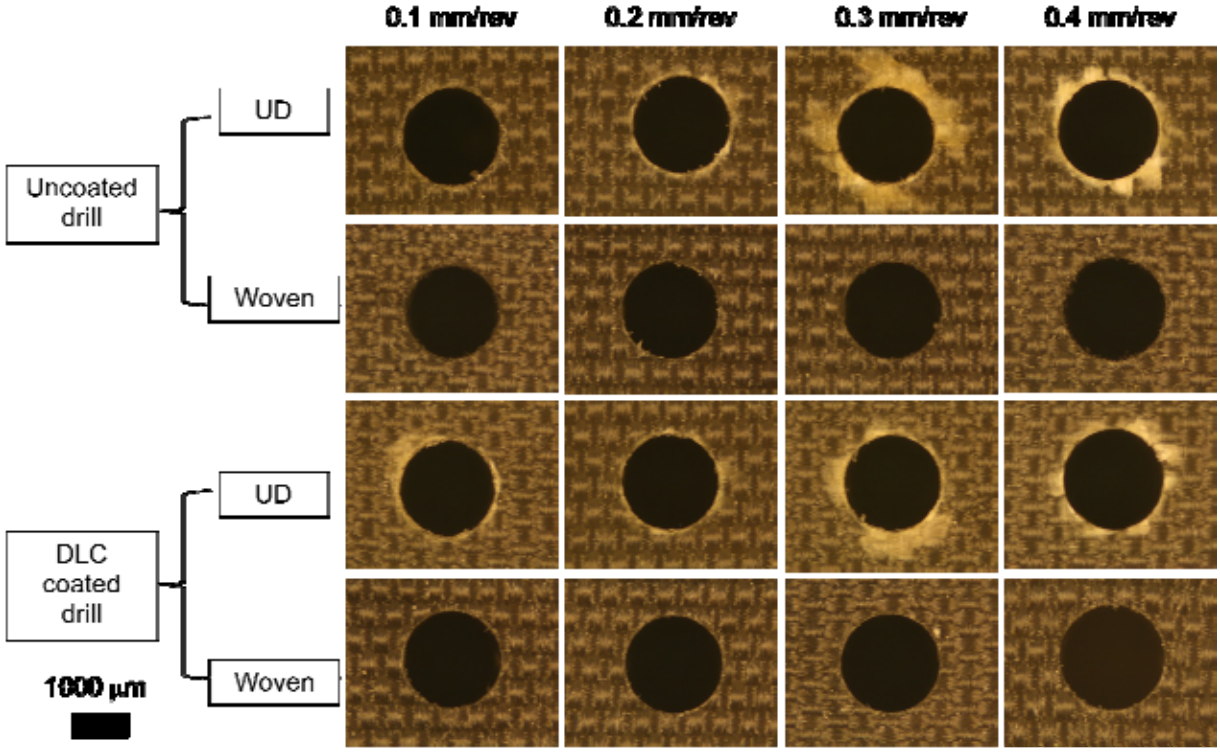


Figure 4.77: Exit delamination images for the last hole

Figure 4.78 shows exit delamination results when employing various coated drills at 0.4 mm/rev feed rate. Here, the exit delamination factor ($F_d$) ranged between 1 and 1.9 for the first hole drilled, with the damage seen to be significantly worse when employing CVD diamond coated tools irrespective of the CFRP laminate structure. Not surprisingly, the $F_d$ increased dramatically for the last hole cut, with levels of up to 2.2 recorded for the Diamond plus coating when machining UD MTM44-1/HTS. Where only uncoated and DLC coated tools were utilised, $F_d$ was up to 1.84 and 1.15 for UD MTM44-1/HTS and woven 977-2/HTS laminates respectively as shown in Figure 4.79.

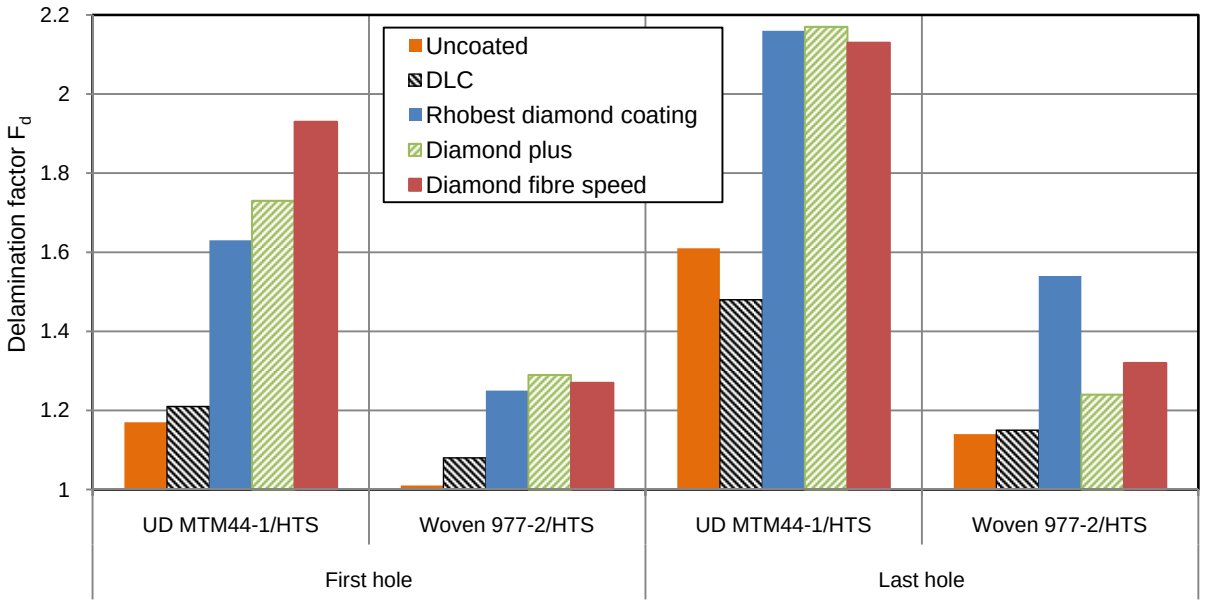


Figure 4.78: Exit delamination factor results for all drills used at 0.4 mm/rev feed rate

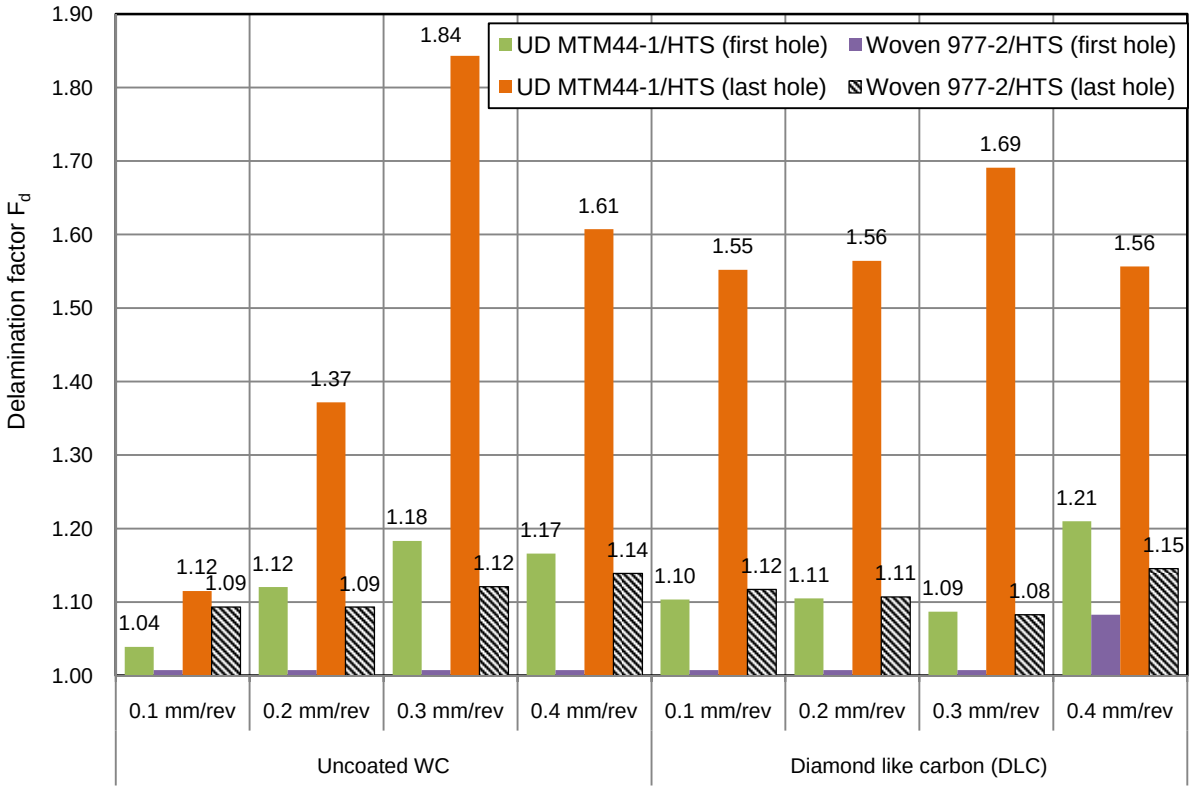


Figure 4.79: Exit delamination factor results (Phase 2B)

Figure 4.80 and Figure 4.81 show the corresponding main effects plots for mean exit $F_d$ of the first and last hole with average values of 1.07 and 1.32 respectively. In terms of laminate configuration, the woven 977-2/HTS material consistently showed lower exit delamination, with the uncoated drill producing marginally better results. First hole $F_d$ increased gradually with variation in feed rate up to 0.3 mm/rev, while a steep rise was observed between 0.3 to 0.4 mm/rev indicating that this feed rate can be considered as the critical/limiting operating level. A similar trend was reported for last hole $F_d$ except that a drop was seen when feed rate varied from 0.3 to 0.4 mm/rev, which was primarily due to the premature end of several tests conducted at 0.4 mm/rev. Table 4.19 and Table 4.20 detail the corresponding ANOVA results for exit $F_d$ measured for the first and last hole respectively. In both cases, prepreg type was the key variable affecting exit $F_d$ with PCR's of 62 and 66% respectively. The analysis of variance also revealed slightly higher than acceptable error levels for both the first and last hole $F_d$, indicating a possible contribution from interactions between control factors as well as difficulties in measurement.

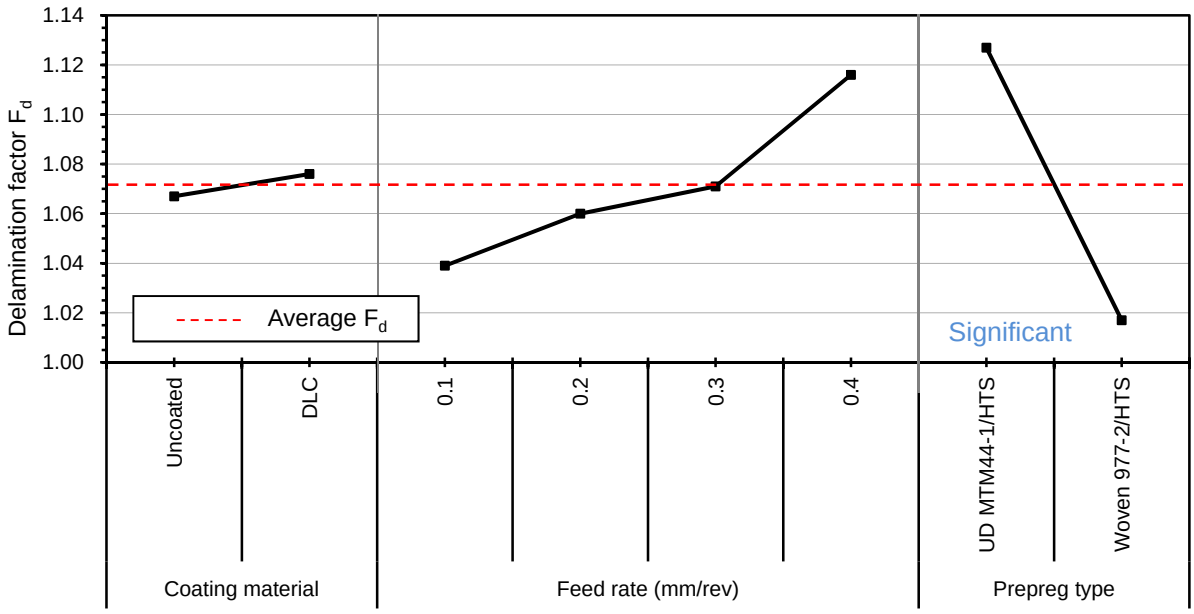


Figure 4.80: Main effects plot, means for exit $F_d$ for the first hole (Phase 2B)

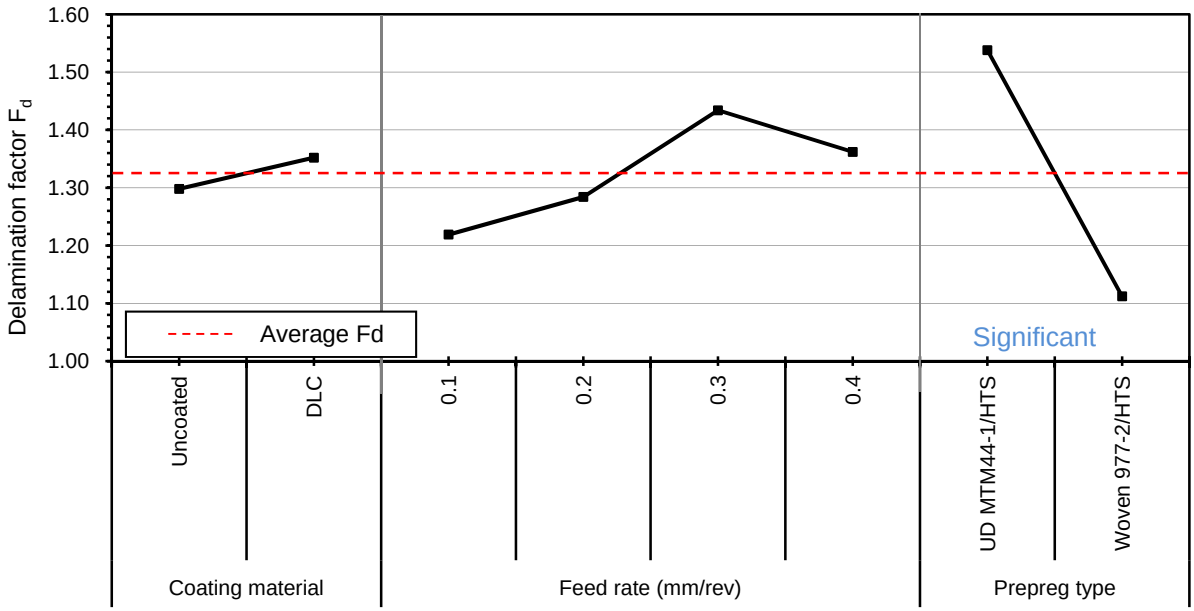


Figure 4.81: Main effects plot, means for exit $F_d$ for the last hole (Phase 2B)

| Factor | DF | SS | Exp SS | F | P | PCR |
|---|---|---|---|---|---|---|
| **A (Coating material)** | 1 | 0.000314 | -0.00106 | 0.23 | 0.643 | 0.00 |
| **B (Feed rate) (mm/rev)** | 3 | 0.012666 | 0.008532 | 3.06 | 0.078 | 11.39 |
| **C (Prepreg type)** | 1 | 0.048135 | 0.046757 | 34.93 | 0* | 62.43 |
| **Error** | 10 | 0.01378 | | | | 26.18 |
| **Total** | 15 | 0.074895 | | | | |

Table 4.19: ANOVA results for exit delamination factor (first hole)

| Factor | DF | SS | Exp SS | F | P | PCR |
|---|---|---|---|---|---|---|
| **A (Coating material)** | 1 | 0.0117 | -0.00991 | 0.54 | 0.479 | 0.00 |
| **B (Feed rate) (mm/rev)** | 3 | 0.10466 | 0.03983 | 1.61 | 0.247 | 3.77 |
| **C (Prepreg type)** | 1 | 0.72331 | 0.7017 | 33.47 | 0* | 66.46 |
| **Error** | 10 | 0.2161 | | | | 29.77 |
| **Total** | 15 | 1.05579 | | | | |

Table 4.20: ANOVA results for exit delamination factor (last hole)

## 4.5 Phase 3A: Preliminary drilling trials in separate CFRP and Ti workpieces and multilayer stacks

### 4.5.1 Tool wear and tool life

Figure 4.82 details tool wear results for wet drilling trials in individual CFRP and Ti-6Al-4V plates together with a stack of CFRP/Ti. The bespoke straight fluted domed PCD drill (developed/manufactured by E6) significantly outperformed the Sandvik tool when employed for CFRP where 1213 holes were produced, corresponding to a flank wear of 157 µm (estimated 2400 holes at 300 µm flank wear level, ~10 fold increase in tool life). Conversely, the drill experienced catastrophic failure during the first hole when used to cut Ti-6Al-4V, which was most likely due to poor chip evacuation with the straight flute geometry leading to separation of the PCD tip from the carbide base. Coated drills on the other hand were more reliable as wear developed 'normally' towards the flank wear criterion with both CFRP and Ti as well as the stack material. The trial involving the stack (Test 5) however had to be halted after 105 holes due to the limited availability of workpiece material. Severe edge rounding was the dominant form of wear when drilling CFRP as shown in Figure 4.83 while typical adhesion and peeling of the coating layer was encountered when drilling Ti-6Al-4V see Figure 4.84. Similar wear has been reported by other researchers [134, 143, 148].

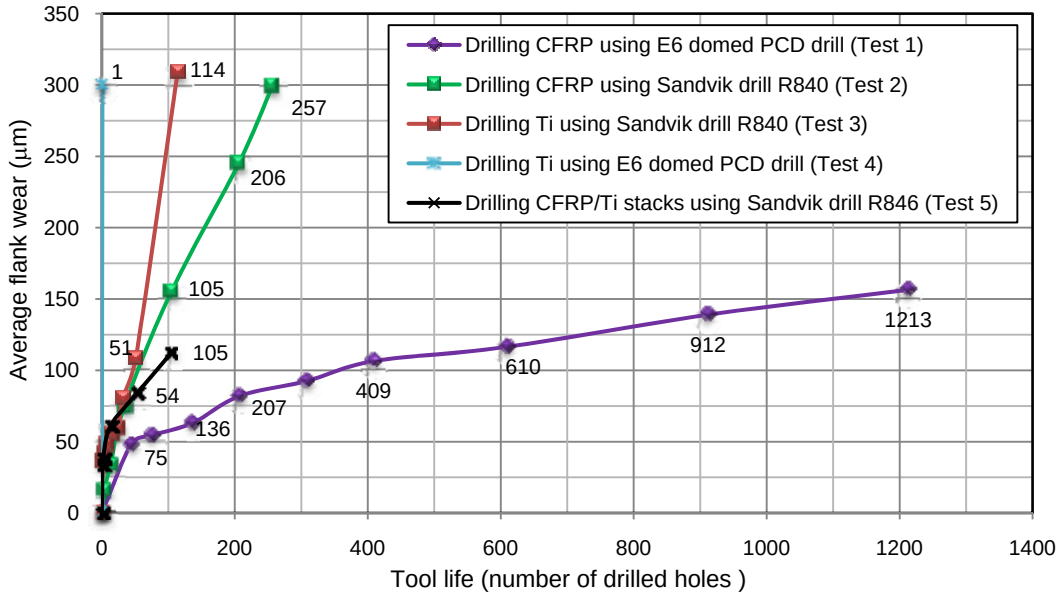


Figure 4.82: Tool wear results for tests performed using through coolant adaptor

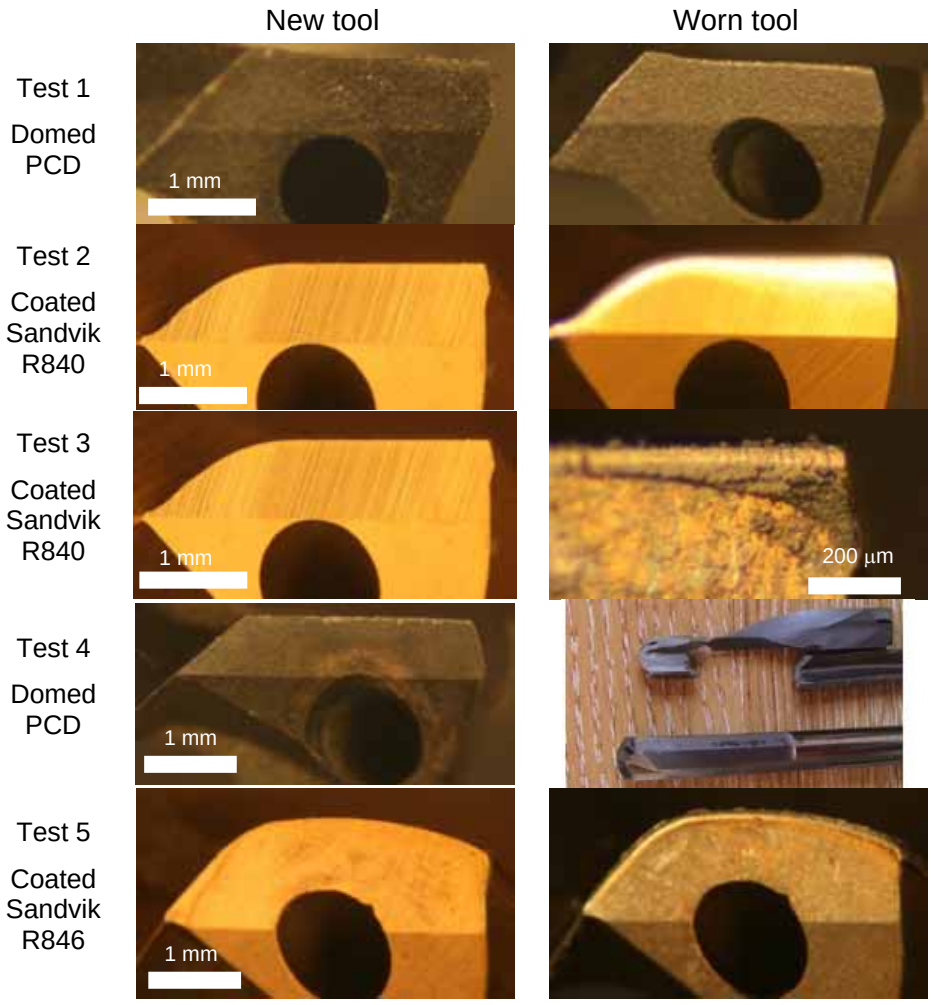


Figure 4.83: Micrographs for new and worn cutting edges used in Phase 3A

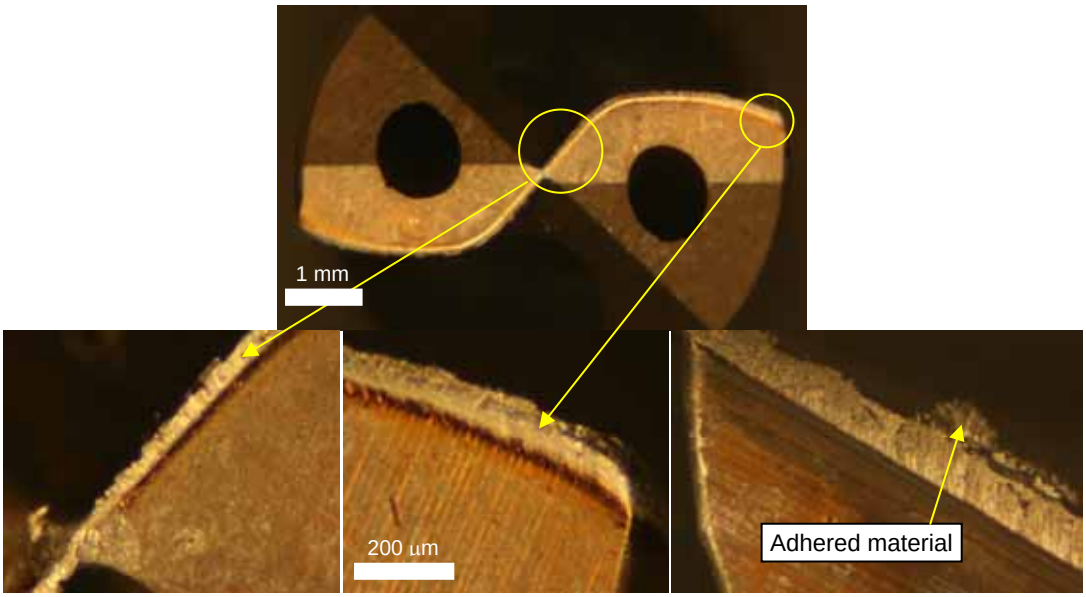


Figure 4.84: Micrographs for a worn coated Sandvik R846 drill (Test 5) showing titanium adhered to cutting edges

### 4.5.2 Thrust force and torque

Figure 4.85 displays the typical thrust force and torque profile obtained when drilling a single hole through a CFRP/Ti stack. The momentary drop in thrust force relates to a programmed retraction (1 mm) of the drill as it initially penetrates the CFRP layer in order to accommodate the transition of tool rotational speed. While thrust force increased rapidly to its maximum level, the torque associated with the titanium layer was found to rise gradually (over ~3 s period) to its steady state. This was most likely due to the adhesion of titanium on the cutting edges and subsequent rubbing with the hole surface. Not surprisingly, measured force and torque when cutting titanium was up to 3 times higher than when drilling CFRP. The maximum thrust force (at end of life) when drilling CFRP was 866 N when using the coated Sandvik R840 tool. In contrast, thrust force peaked at 1641 N when drilling the Ti section within the stack material, see Figure 4.86. Additionally, torque levels reached 66 and 629 N.cm when drilling CFRP and Ti respectively, see Figure 4.87. In terms of tooling, PCD tools produced considerably lower thrust force and torque when used to cut CFRP compared with the coated carbide tools as a consequence of their higher hardness, which resulted in a significantly lower wear rate (greater resistance to abrasion by carbon fibres).

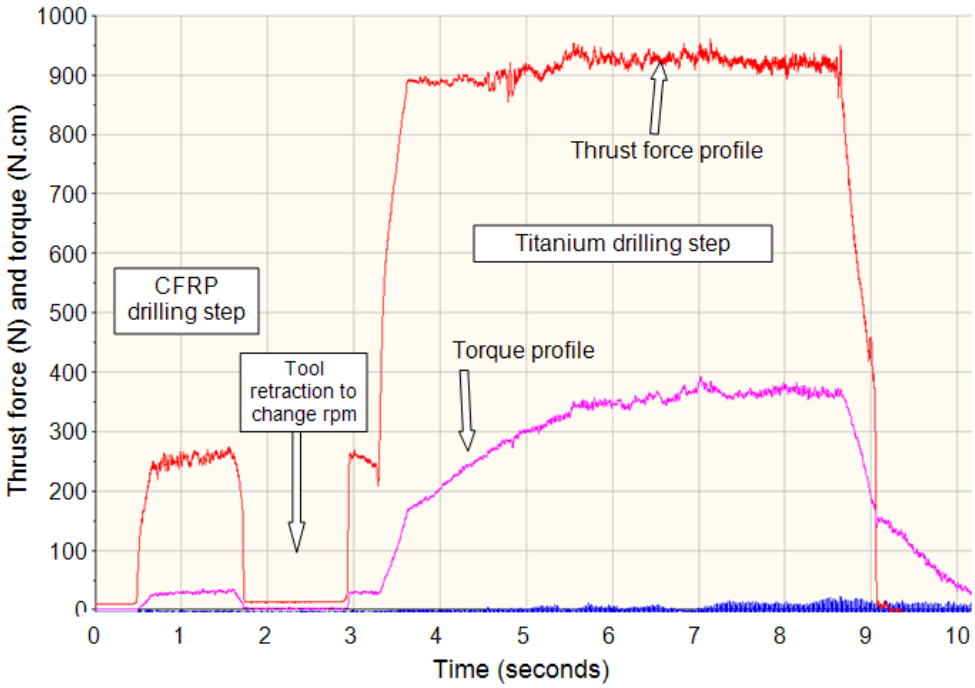


Figure 4.85: Force and torque signals when drilling 1st hole in CFRP/Ti stack (84/42 m/min and 0.1 mm/rev)

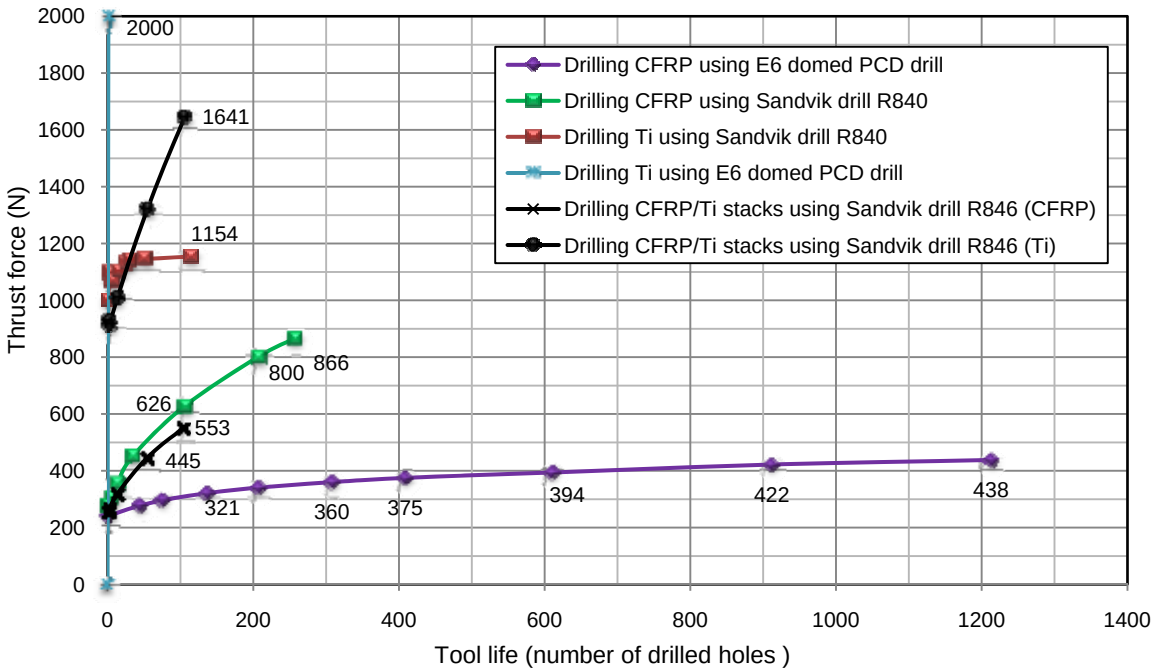


Figure 4.86: Thrust force results for Phase 3A

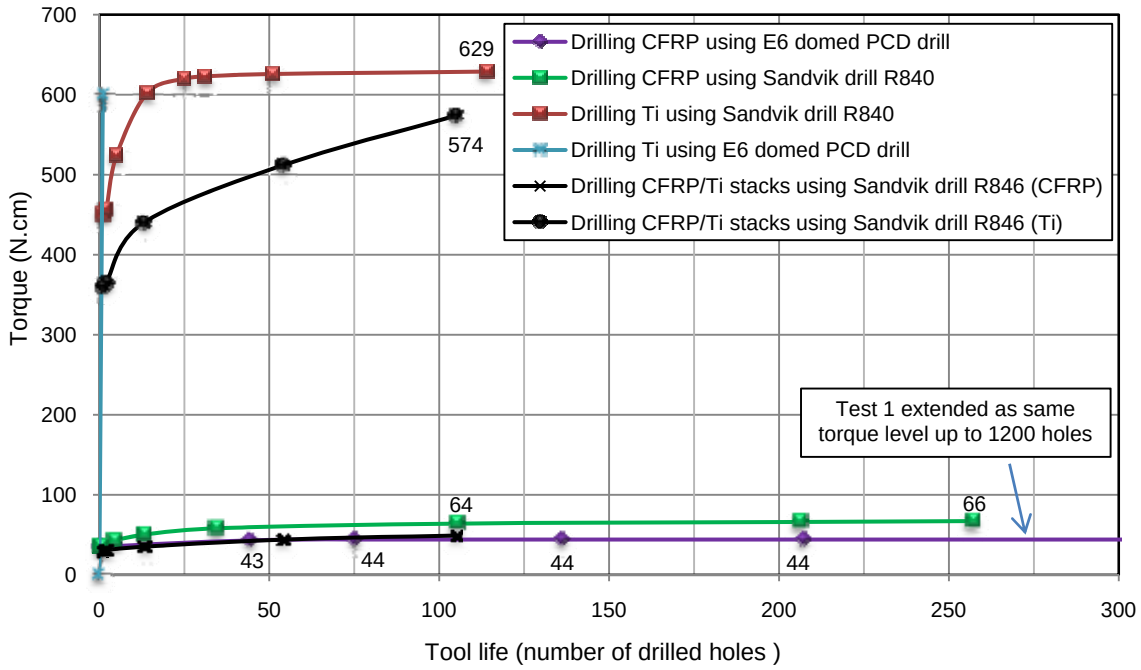


Figure 4.87: Torque results for Phase 3A

### 4.5.3 Hole surface roughness

Figure 4.88 displays surface roughness results measured from the sectioned CFRP and Ti holes. In general, higher Ra values were obtained on CFRP surfaces with a maximum of 5.47 μm at test cessation when employing the coated Sandvik drill. This was attributed to the fibrous nature of CFRP where fibre pull-out as well as matrix decomposition/degradation during the cutting created craters/voids on the machined surfaces, which is not uncommon when drilling such materials [43]. Additionally, sharp titanium swarf may scratch CFRP hole surfaces, also contributing to greater surface roughness levels. Conversely, measured Ra at Ti hole surfaces gave a maximum of 0.6 μm at the end of the experiment.

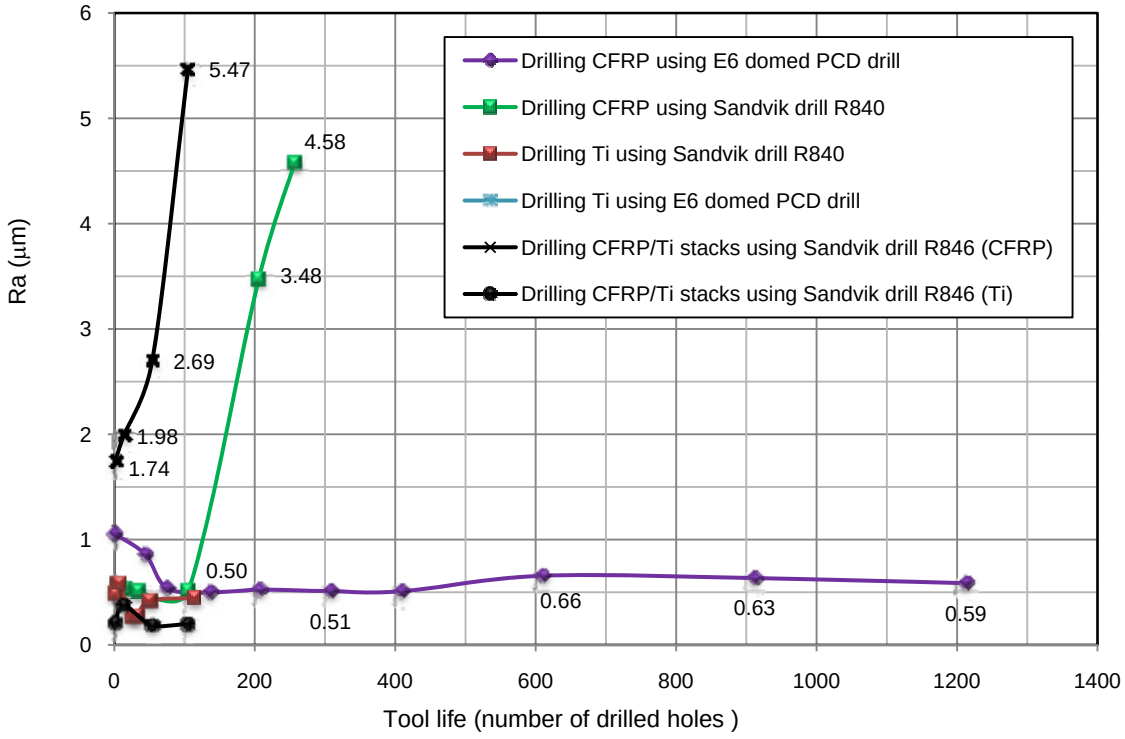


Figure 4.88: Surface roughness results for CFRP and Ti hole surfaces

### 4.5.4 Burr height on Ti sections

A maximum burr height of 150 μm was recorded at hole exit when drilling using the coated R846 Sandvik drill as shown in Figure 4.89. Typically, exit burrs are generally larger than those at hole entry however in the current work, entry burrs on the Ti plates drilled using the Sandvik R840 tool were found to be uncharacteristically larger than corresponding exit burrs by approximately 36% (131 μm versus 96 μm). Conversely, measured burr height at

hole exit when drilling CFRP/Ti stacks was up to 150 µm compared to 129 µm recorded for hole entry. This was attributed to the supportive action of the CFRP material on the hole entry at the Ti section.

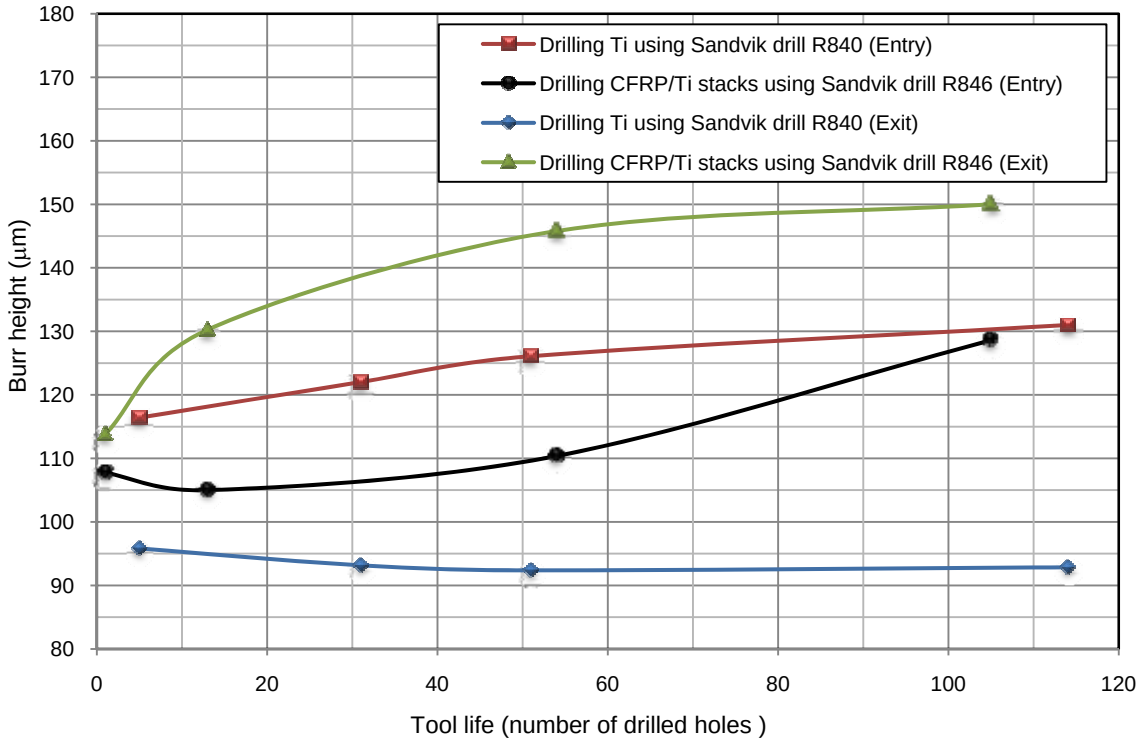


Figure 4.89: Burr height results for entry and exit holes on Ti workpiece

### 4.5.5 Entry/exit hole damage

Typical damage forms when drilling un-backed composites were observed at hole exit [43, 95]. These include spalling, fuzzing, delamination and edge chipping as shown in Figure 4.90 (Test 1 and 2). Significantly improved edge quality was obtained when machining CFRP in the stack arrangement as the Ti layer served to arrest the progress of composite delamination/damage (Test 5). Limited defects were observed at hole entry in all cases, even for last holes drilled. Conversely, hole edge quality on Ti sections was principally affected by the formation of burrs at the both entry and exit. Plastic deformation extended around the periphery of the drilled hole resulting mainly in uniform burrs, see Figure 4.91. Additionally, some limited adhered material can be seen at different locations around the hole edge, indicating that a further finishing process may be necessary. Ti burr caps and swarf were also occasionally found to remain in the drilled holes resulting in various forms of damage particularly in the CFRP section as highlighted in Figure 4.92.

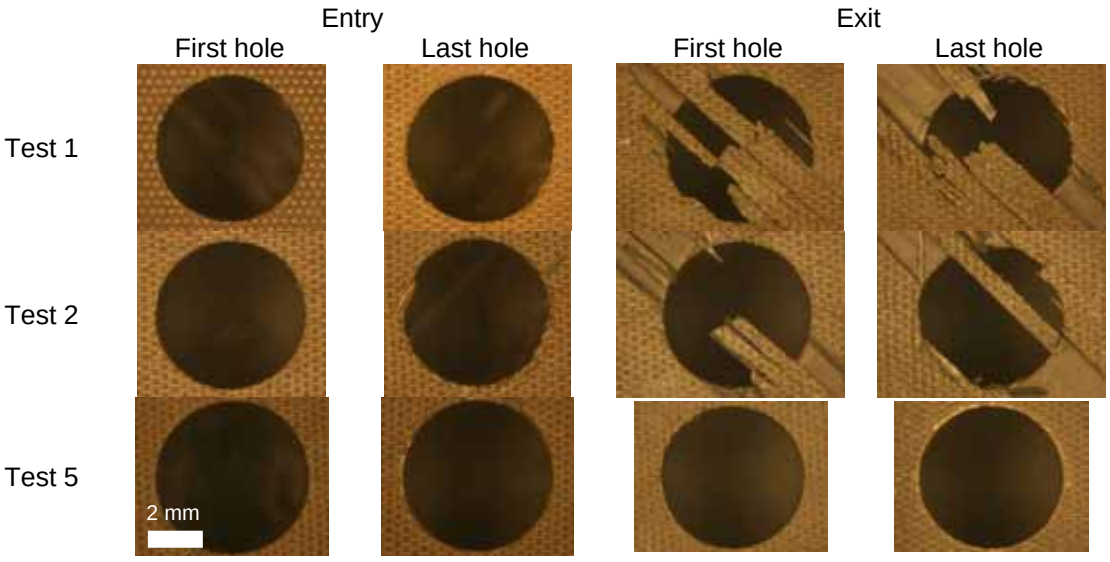


Figure 4.90: Entry and exit hole damage for CFRP sections

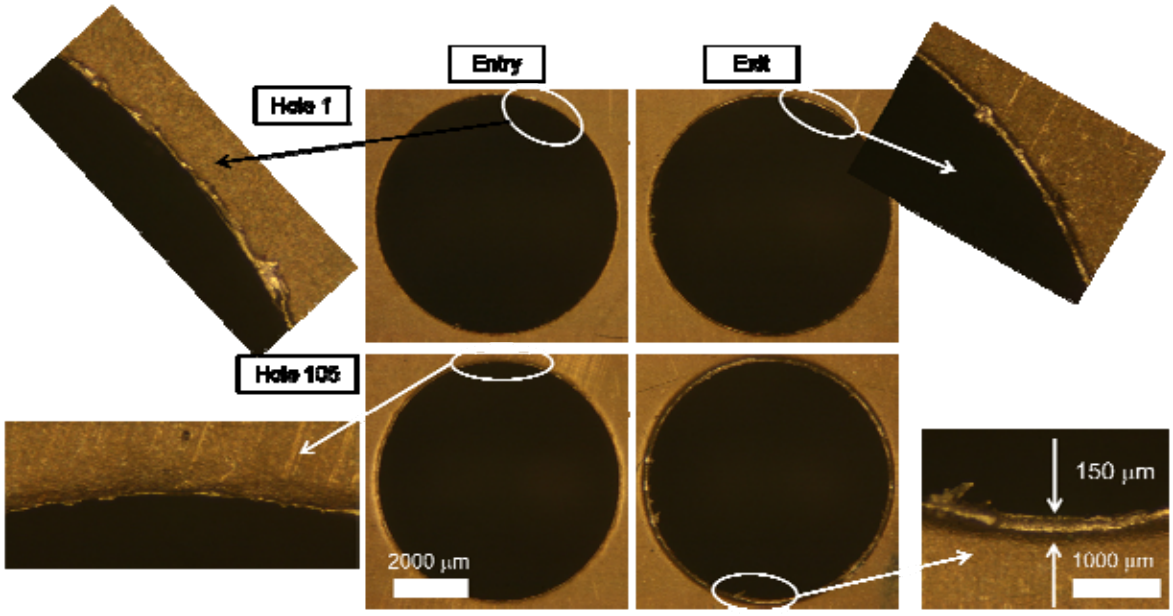


Figure 4.91: Hole edge quality at hole entry and exit (Ti - Test 5)

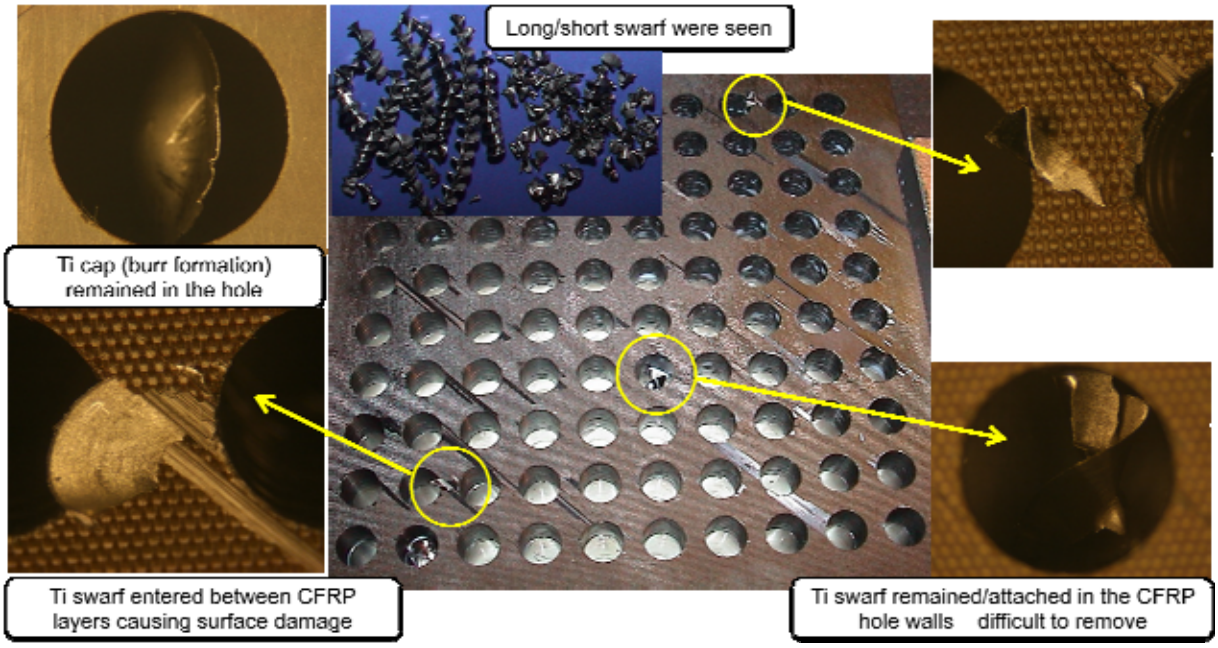


Figure 4.92: Chip disposal difficulties encountered when drilling CFRP/Ti stacks

## 4.6 Phase 3B: Impact of stack arrangement and performance of PCD tools

### 4.6.1 Tool wear and tool life

Table 4.21 details tool life results for tests performed using two different stack arrangements (Al/CFRP/Ti and Ti/CFRP/Al). The corresponding tool wear curves are shown in Figure 4.93. The majority of tests performed with the Al/CFRP/Ti stack order experienced premature catastrophic tool fracture or in the case of the brazed PCD drills, chisel edge failure, see Figure 4.94. For drills which reached the end of life criteria, severe peeling of the coating layer along the cutting edge and chisel edge was prevalent. Additionally, all coated drills experienced severe corner rounding after only a few holes. This tended to cause rubbing between the drill and workpiece material when retracting the tool from the holes. While contrary to initial expectations, the poor performance of the brazed PCD drills can be attributed to the relatively thin chisel edge section (due to the absence of carbide backing), which was unable to withstand the loads during drilling, see Figure 3.8 (b). All drills used at the high feed rate (0.2 mm/rev) experienced fracture at early stages of the test (<5 holes). Another contributing factor was the poor titanium chip evacuation from the bottom of the stack.

| Test no. | Drill used | Cutting speed (m/min) | Feed rate (mm/rev) | Tool life (no of drilled holes) and tool failure mode |
|---|---|---|---|---|
| **Tests performed with Al/CFRP/Ti material order** | | | | |
| 1 | C7 coated WC | 60/20 | 0.05 | 150 holes (207 mm flank wear) |
| 2 | C7 coated WC | 80/30 | 0.1 | 21 holes (tool broke) |
| 3 | C7 coated WC | 100/40 | 0.15 | 150 holes (300 mm flank wear) |
| 4 | C7 coated WC | 120/50 | 0.2 | 1 hole (tool fractured) |
| 5 | CVD diamond coated | 80/30 | 0.2 | 1 hole (tool fractured) |
| 6 | CVD diamond coated | 100/40 | 0.05 | 4 holes (cutting edge fractured) |
| 7 | CVD diamond coated | 120/50 | 0.1 | 1 hole (cutting edge fractured) |
| 8 | Brazed PCD | 80/30 | 0.05 | 24 holes (chisel edge fractured) |
| **Tests performed with Ti/CFRP/Al material order** | | | | |
| 9 | CVD diamond coated | 30/80 | 0.1 | 108 holes (136 mm flank wear) |
| 10 | Brazed PCD | 20/60 | 0.1 | 1 hole (chisel edge fractured) |
| 11 | Domed PCD (E6) | 40/100 | 0.05 | 1 hole (tool broke) |

Table 4.21: Tool life results for Phase 3B

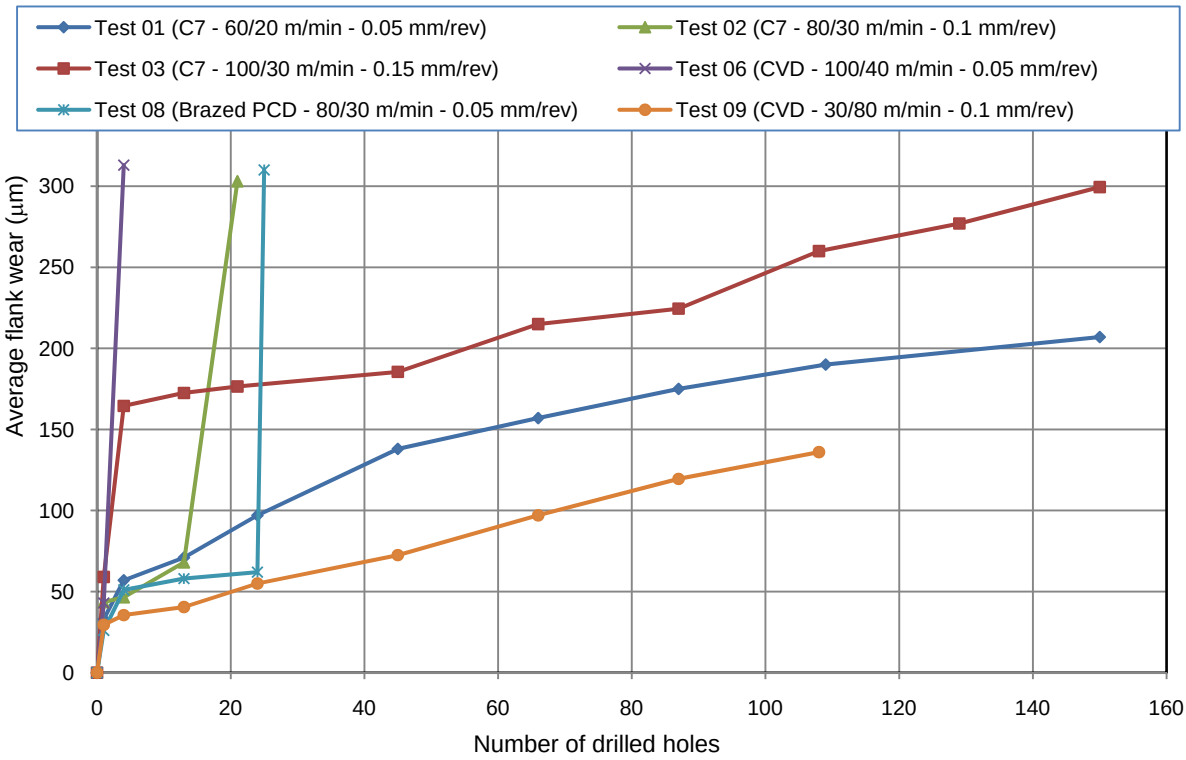


Figure 4.93: Tool wear curves for tests performed in Phase 3B

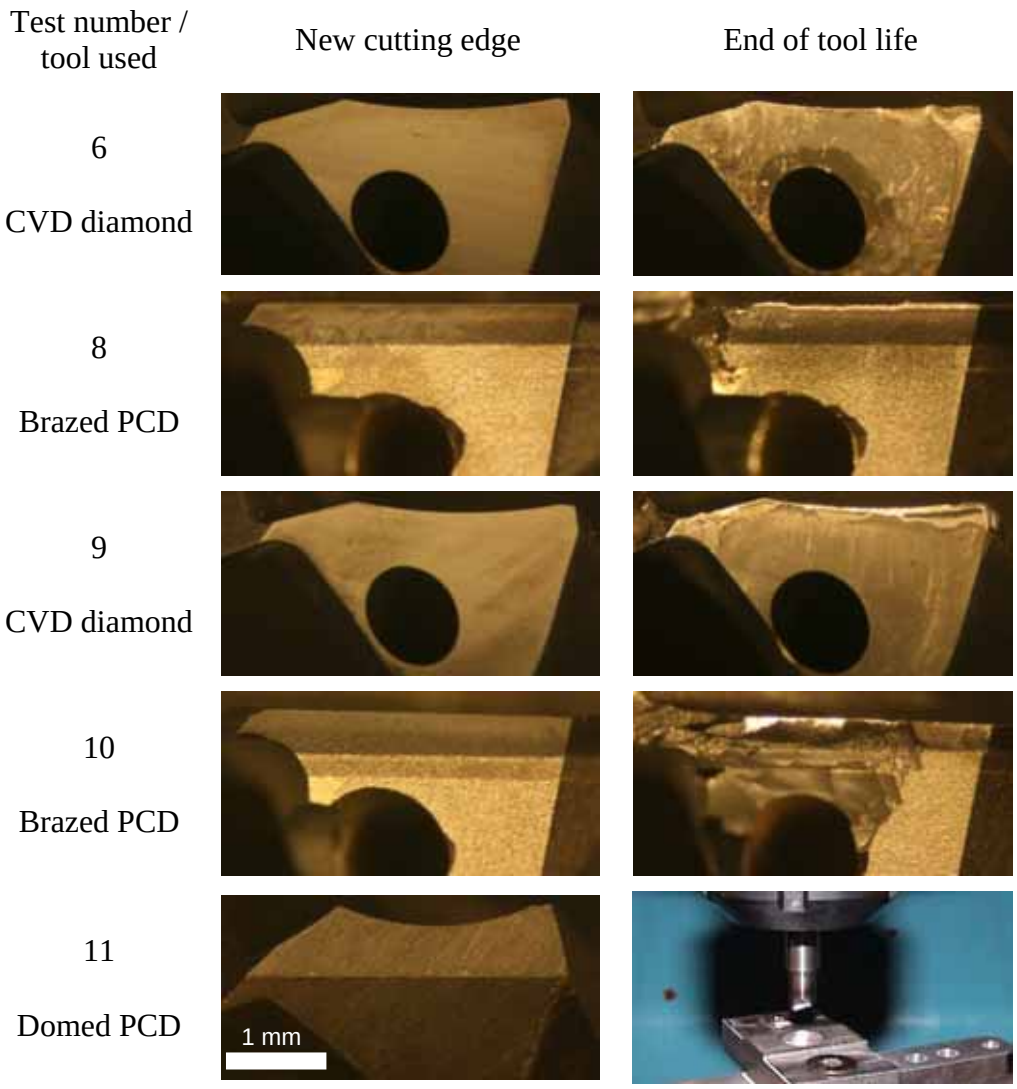


Figure 4.94: Micrographs for new and worn cutting edges (Phase 3B)

When cutting commenced from the Ti layer (over a similar range of drilling conditions), the diamond coated drills showed the best results where cutting progressed smoothly without tool clogging. Here, the tool life of the CVD diamond coated drills improved significantly to 108 holes (at 136 μm flank wear) compared with <5 holes when drilling commenced from aluminium layer. Unfortunately, no significant benefit was obtained from varying the material sequence of the stack in relation to the brazed and domed PCD drills. The former again suffered failure at the chisel edge while the modified domed PCD design experienced catastrophic fracture on the tool body. A possible reason for the extremely poor performance of the PCD drills was the relatively low fracture toughness of the material (~6.89 $MPam^{1/2}$,

compared to 14 MPam$^{1/2}$ for K10 carbide). The cutting edge failure of the PCD tools when machining titanium alloys was not unexpected, which was also reported by Narutaki et al. [133] when using PCD tools for turning Ti-6Al-4V. However, results with the domed PCD drill suggests that flute clogging by titanium/aluminium swarf leading to high stresses was the primary failure mode rather than cutting edge wear. There is therefore scope for further development of the current domed PCD drill geometry in order to accommodate the drilling of metallic/composite stacks. Another observation when drilling the Al/CFRP/Ti configuration was the severe noise (squealing) encountered while the tool was in contact with the titanium layer, which significantly reduced when the stack was turned over. All coated tools also showed evidence of adhered workpiece material on both cutting and chisel edges, see Figure 4.95. This built up layer was seen from the first hole and was formed principally due to the high pressures developed during machining and the high chemical affinity between the workpiece (Ti) and tool material. This was in line with published data by Rahman et al., Centero et al. and Zeilmann et al. [134, 143, 148].

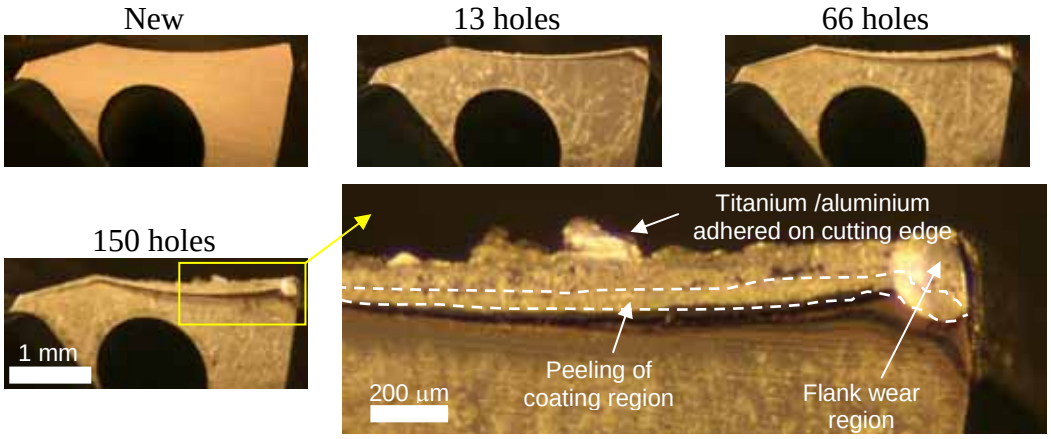


Figure 4.95: Tool wear evolution for Test 3 (C7 – 83/30 m/min – 0.15 mm/rev – wet cutting)

### 4.6.2 Thrust force and torque

Figure 4.96 shows thrust force against the number of drilled holes from the three materials when the sequence of drilling was Al/CFRP/Ti as tool flank wear experienced gradual growth (Test 1). In general, the force levels for Ti were 3 times higher than for CFRP and Al sections. Cutting of stacks in the reverse order (Ti/CFRP/Al) significantly reduced force and torque signal fluctuations, which were most probably due to improved evacuation of

titanium swarf from the hole, see Figure 4.97. The thrust force reduced by ~ 30% and torque by ~ 60% (1100 N to 650 N and 600 N.cm to 200 N.cm). With the domed PCD drill however, a steep spike in thrust force was recorded while cutting through aluminium, which was probably due to the chip clogging, see Figure 4.98 (a). The force profile recorded when using the brazed PCD drill suggests that the chisel edge fracture (shown in Figure 4.94) occurred as tool penetrated the Ti layer and consequently resulted in severe signal fluctuations, see Figure 4.98 (b).

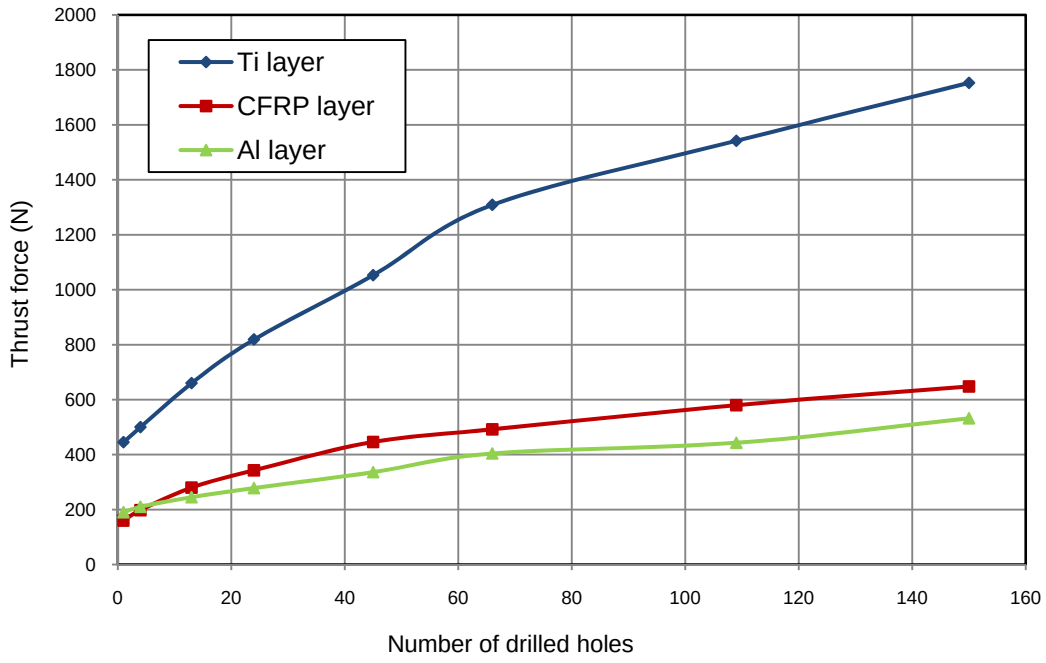


Figure 4.96: Evolution of thrust force versus number of drilled holes in Test 1 (C7 coated drill – 60/20 m/min – 0.05 mm/rev – wet cutting in Al/CFRP/Ti stack)

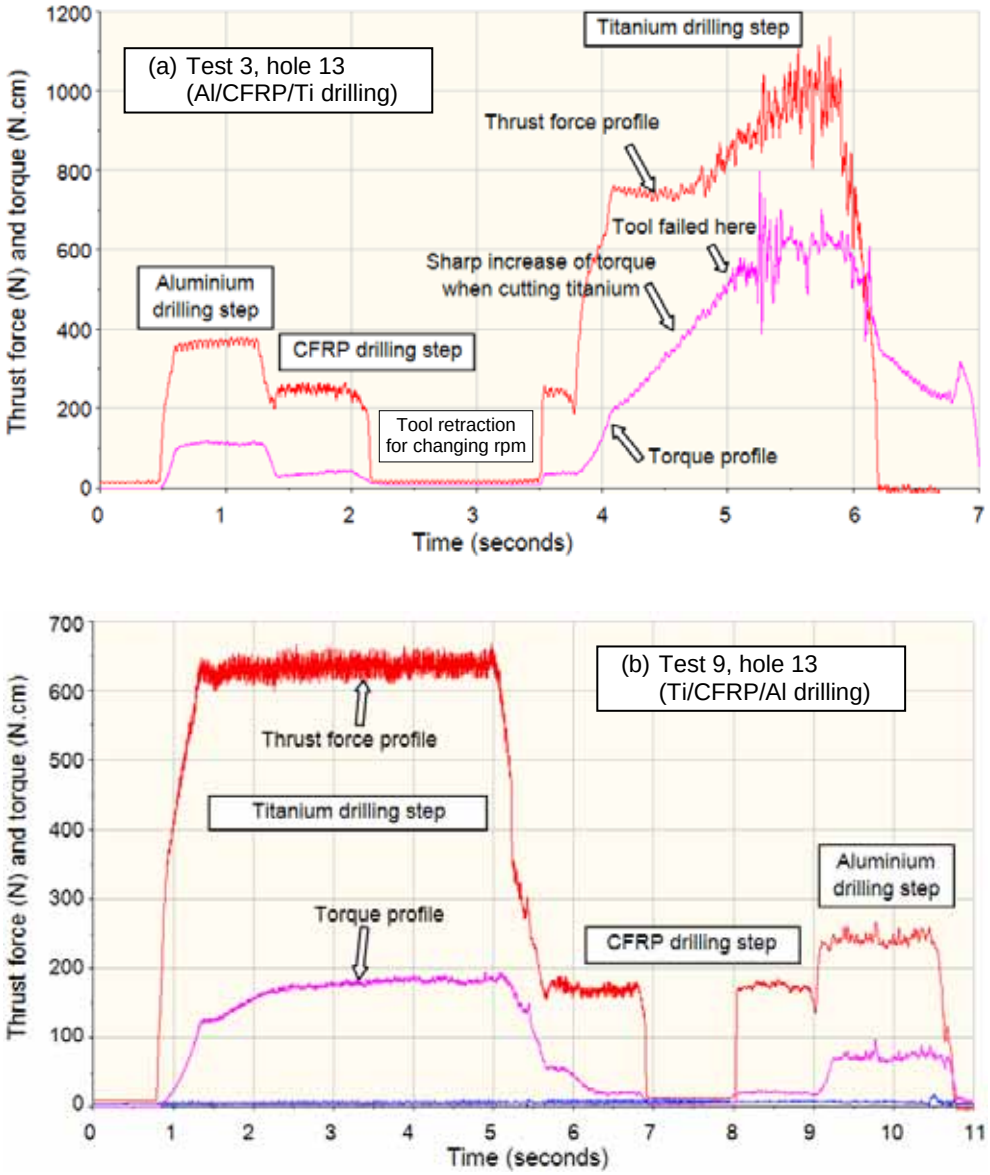


Figure 4.97: Force and torque profiles when drilling various stack orders

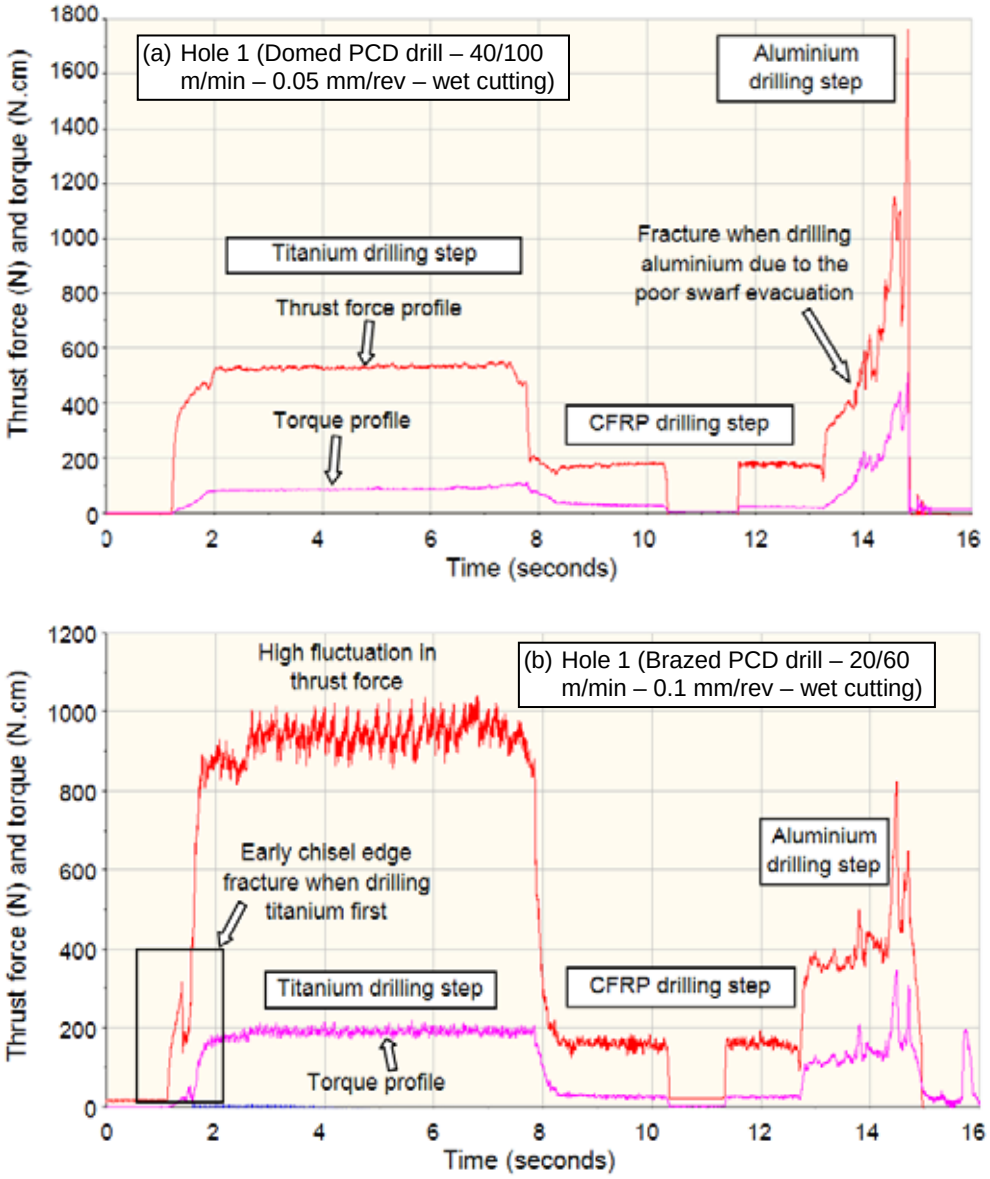


Figure 4.98: Samples for typical thrust force and torque signatures

## 4.7 Phase 3C: Effect of tool coatings and operating parameters

### 4.7.1 Tool wear and tool life

Figure 4.99 and Figure 4.100 show tool flank wear progression versus number of drilled holes under wet/flood coolant and spray mist conditions respectively. The best performance (310 holes) was obtained when cutting wet using an uncoated drill at 20/40 m/min with a corresponding feed rate of 0.05 mm/rev. All trials performed at the lowest cutting speed under spray mist application experienced elevated noise levels due to rubbing between the tool and titanium layer, regardless of drill coating. Tool life was poor in comparison and the number of drilled holes did not exceed 100, with test cessation brought about by catastrophic tool failure (discussed later). Further tests at intermediate and high cutting speed using the uncoated drill exacerbated the squealing and tool life was even shorter, furthermore sparking was also observed. Based on this, trials involving CVD diamond and C7 coated drills at intermediate and high speeds were also expected to give a similarly undesirable performance and were therefore withdrawn from the test programme.

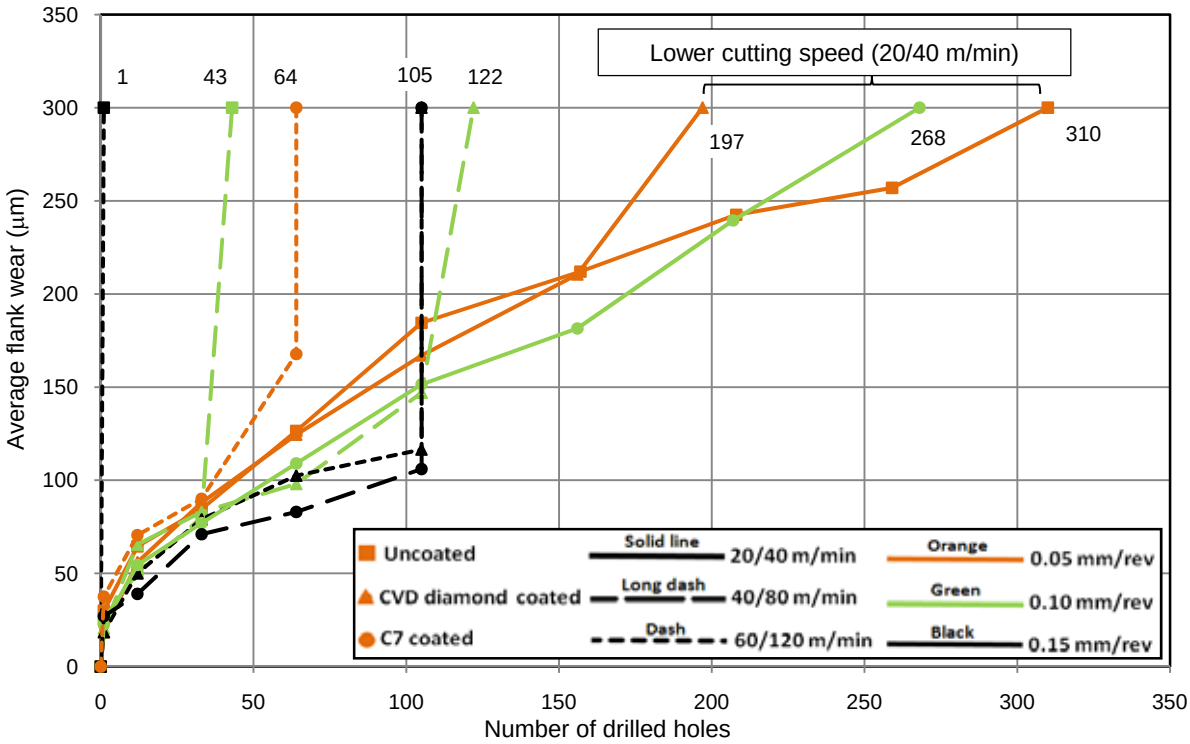


Figure 4.99: Tool wear curves for tests performed using flood coolant

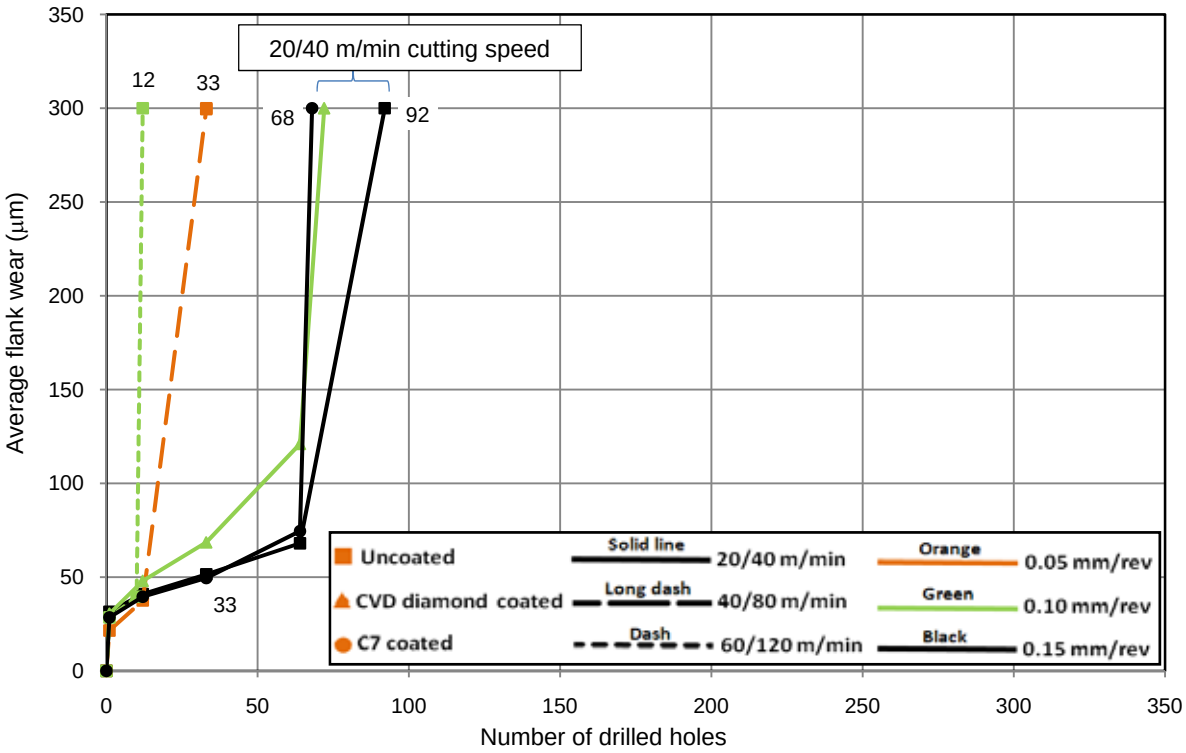


Figure 4.100: Tool wear curves for tests performed using spray mist

Figure 4.101 details tool life results as a function of operating parameters and drill coating for experiments carried out with flood coolant application. Cutting speed had an overriding influence on tool life with a steep decline in the number of drilled holes as speed was trebled from 20/40 m/min to 60/120 m/min, irrespective of the magnitude of feed rate or tool coating. This trend was particularly evident when uncoated drills were used where the tool failed after only one hole when machining at the highest speed level. Figure 4.102 shows sample micrographs of worn drills for the different coating types at varying test parameters. Peeling of the CVD diamond coating was apparent in all tests involving this tool and typically occurred within the first few holes drilled, however this did not appear to be a limiting factor in terms of tool life, especially at the lowest cutting speed.

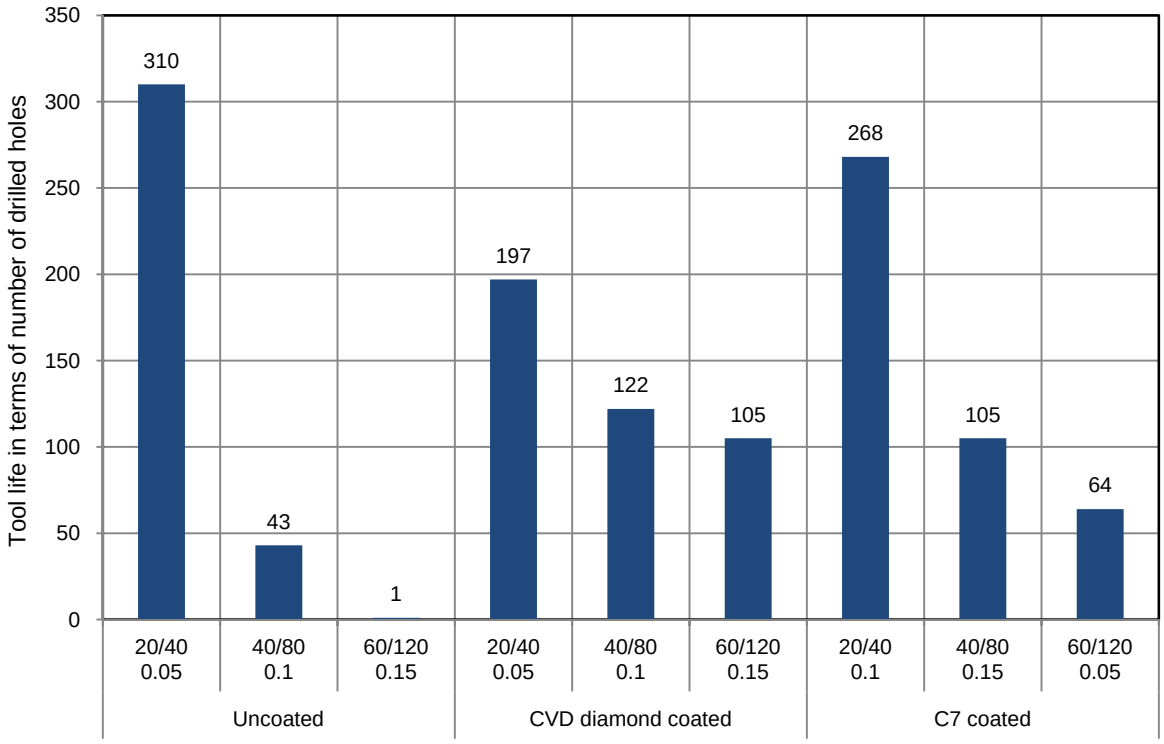


Figure 4.101: Tool life results using wet cutting

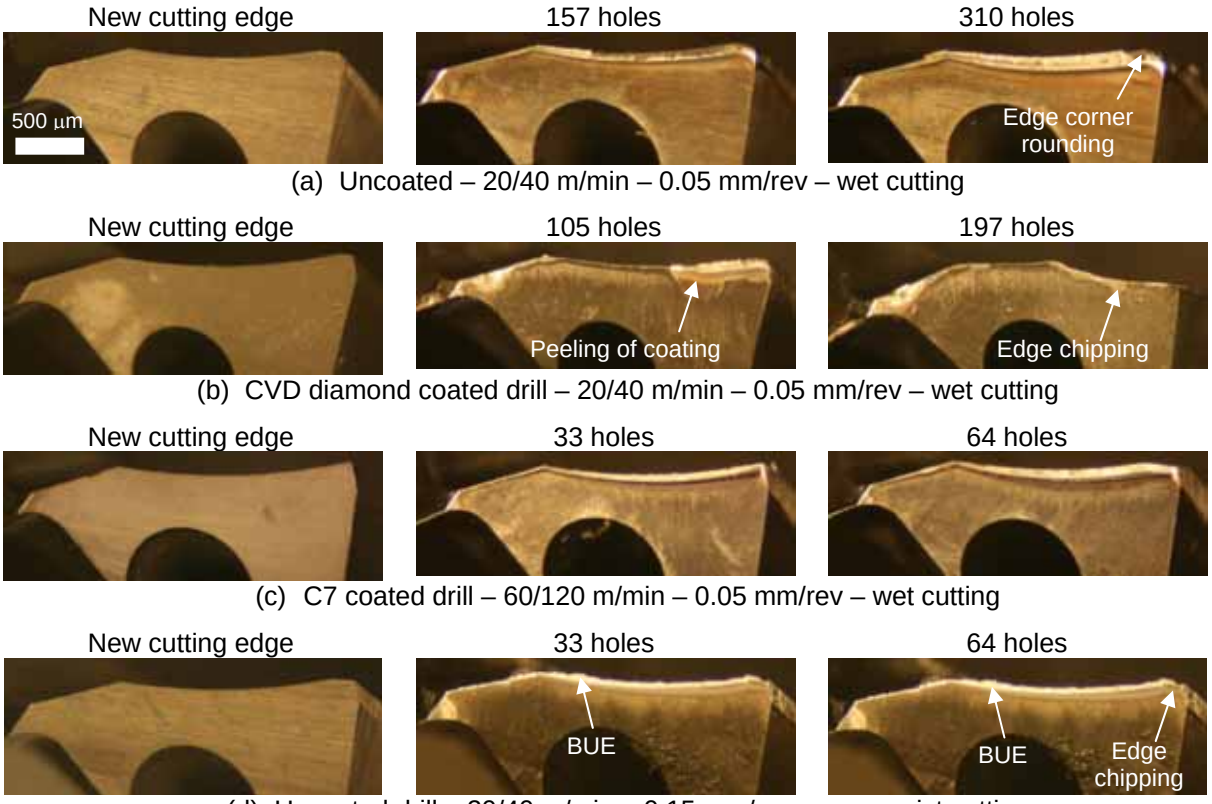


Figure 4.102: Sample flank wear micrographs

The 3 drills employed at 20/40 m/min under wet conditions generally exhibited steady flank wear evolution up to the end of life criterion, although edge chipping was seen with the CVD diamond coated tool after 197 holes. All other drills however experienced sudden tool failure through various mechanisms. These included tool breakage at the cutting portion, which was thought to be associated with high torque values caused by adhesion of titanium to the tool in addition to clogging of drill flutes by chips (Tests 2, 3, 10, 13 and 16), fracture of cutting lips as a result of built up edge (BUE) formation/smearing (Tests 4, 5, 6 and 9) and severe cutting edge corner rounding due to the abrasion by CFRP (Test 8). BUE was prevalent in trials involving spray mist application and was found to form mainly on the primary cutting lips as well as drill margins. A likely reason for this was the poor access/transport of the spray mist lubricant to the cutting zone, especially as the drill moved deeper into the stack.

The main effects plot and corresponding ANOVA table for tool life are shown in Figure 4.103 and Table 4.22 respectively. The former suggests that the maximum number of holes would be obtained by operating at the lowest cutting speed and feed rate under wet conditions, irrespective of drill coating. However, the ANOVA highlighted that cutting speed and environment were the only statistically significant factors at the 5% level with percentage contribution ratios of 41.9% and 31.6% respectively. A relatively high residual error value (26.3%) was also observed, most probably due to the premature failure of drills encountered in several of the tests together with possible interaction between factors. The considerable influence of cutting speed on tool life can be attributed to the probable increase in temperature at higher drilling speeds coupled with the poor thermal conductivity of both titanium (~ 7 W/mK) and CFRP (~ 1 W/mK perpendicular to the fibre direction), which restricted the dissipation of heat from the cutting zone. Similarly, the greater cooling capacity of the high pressure (70 bar) through coolant spindle system was thought to partially account for the higher average tool life achieved, despite the superior lubricity of the spray mist configuration.

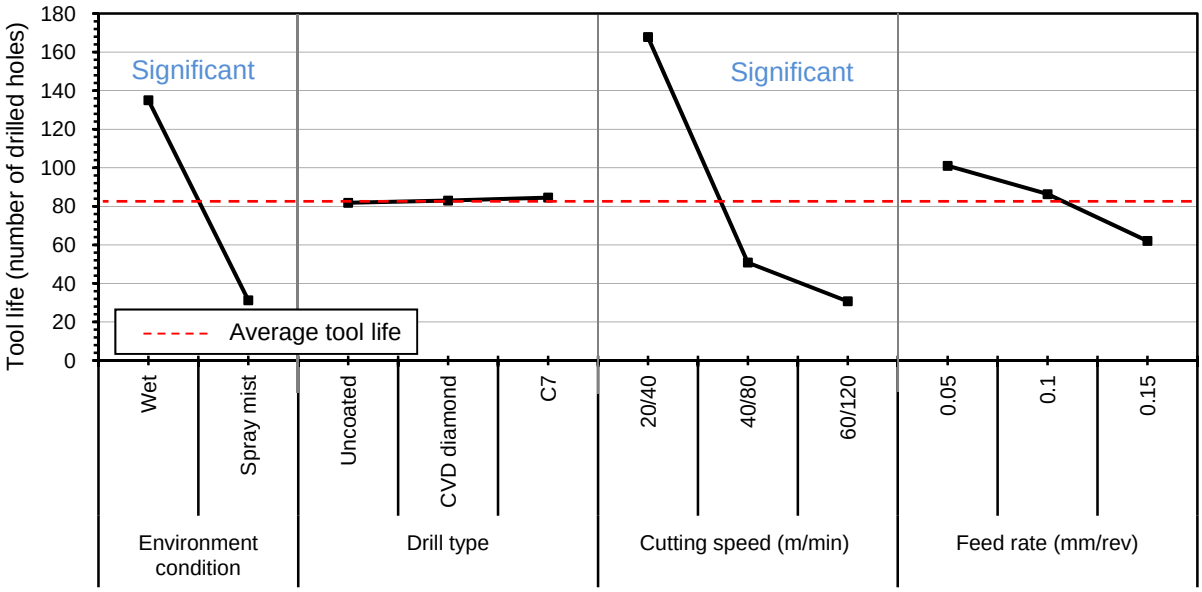


Figure 4.103: Main effects plot, means for tool life (Phase 3C)

| Factor | DF | SS | Exp SS | F | P | PCR |
|---|---|---|---|---|---|---|
| **Environment condition** | 1 | 48568 | 45986 | 18.81 | 0.001* | 31.66 |
| **Drill type** | 2 | 30 | -5134 | 0.01 | 0.994 | 0.00 |
| **Cutting speed (m/min)** | 2 | 66136 | 60972 | 12.81 | 0.002* | 41.98 |
| **Feed rate (mm/rev)** | 2 | 4686 | -478 | 0.91 | 0.434 | 0.00 |
| **Error** | 10 | 25820 | | | | 26.36 |
| **Total** | 17 | 145241 | | | | |

Table 4.22: ANOVA results for tool life in terms number of drilled holes (Phase 3C)

### 4.7.2 Thrust force and torque

Figure 4.104 displays typical thrust force and torque signals obtained when drilling a single hole through the Ti/CFRP/Al stack using different conditions. Oscillation of the force signal was clearly seen when uncoated drills were employed, see Figure 4.104 (a), owing to the tendency for titanium to adhere to the drill, which agreed with previous investigations by Rahman et al. [134]. Coated tools did not experience a similar response, see Figure 4.104 (b) which was most probably due to the lower friction at the tool/chip interface. When spray mist was employed, severe noise in the force profile was observed when drilling the aluminium layer as a consequence of the possible lack of fluid supply and poor chip evacuation, see Figure 4.104 (c).

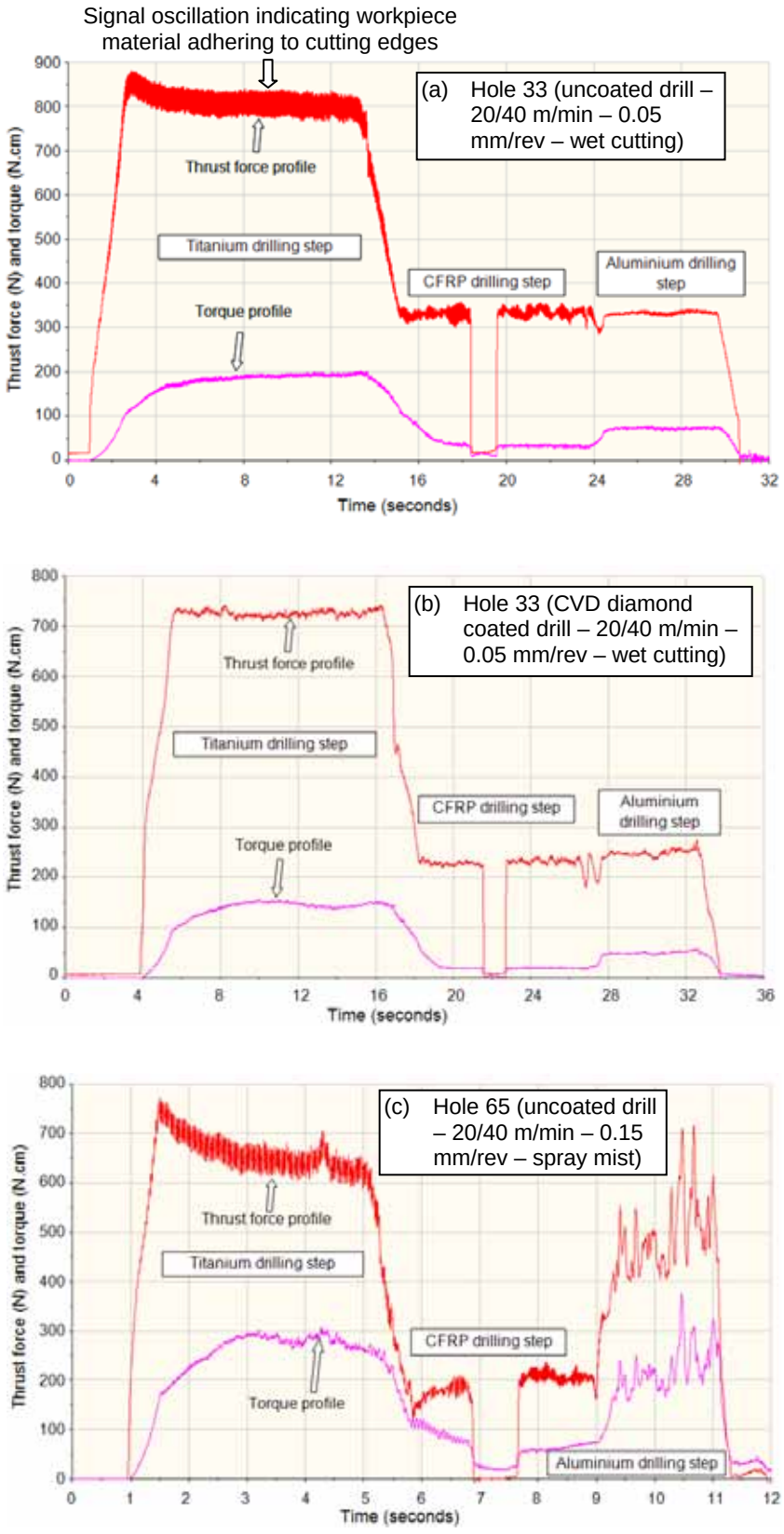


Figure 4.104: Samples for typical thrust force and torque signatures

The progression of average thrust forces and torque with respect to number of drilled holes for the individual material layers (Ti, CFRP & Al) in Test 1 are detailed in Figure 4.105. In general, the force levels recorded when drilling Ti were ~ 3 times greater compared to those when cutting CFRP and Al, which were approximately equal over the duration of the test, except when tools were in the new condition. Similar results were obtained in the majority of trials prior to the onset of catastrophic tool failure. Torque was found to be lowest when drilling the CFRP followed by Al and Ti, which can be explained by the tendency for both titanium and aluminium swarf to adhere onto drill edges and lips. The greater sensitivity of thrust force to changes in tool wear compared to torque was in accordance with results from previous work by [186]. In any event, the maximum thrust force attained with worn tools was approximately 2400 N while torque did not exceed 600 N.cm over the test conditions employed.

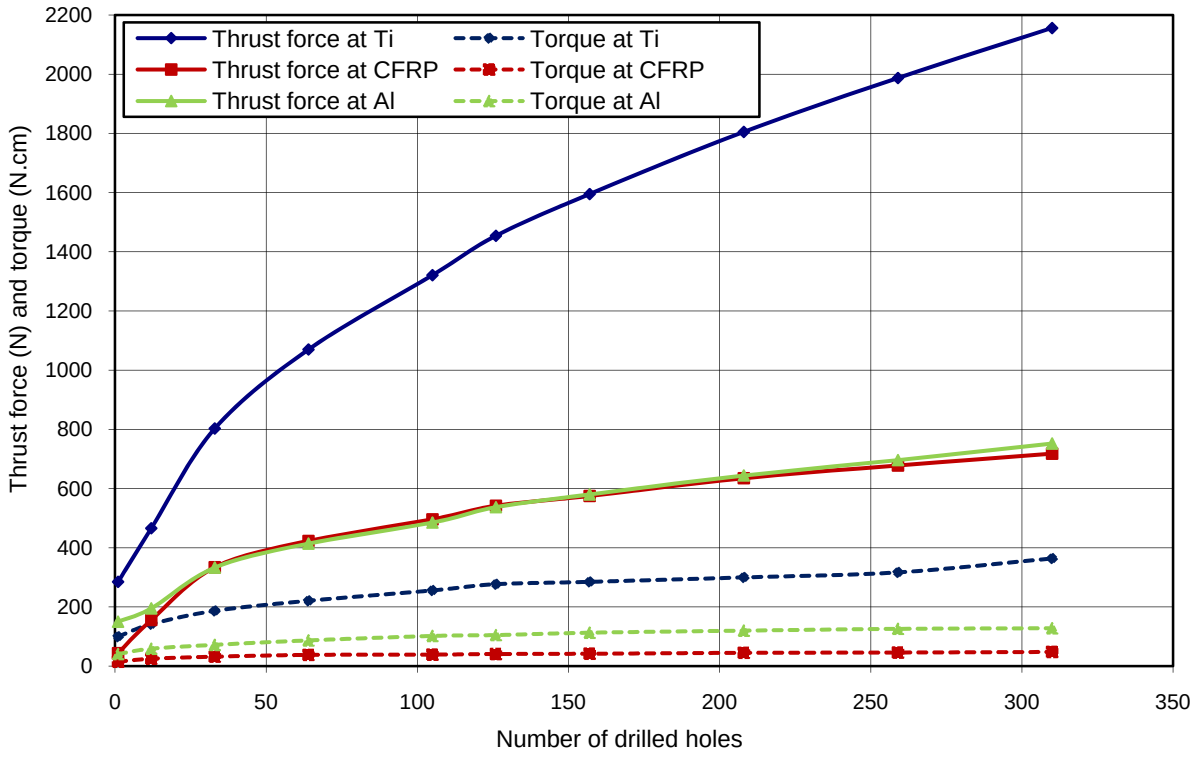


Figure 4.105: Evolution of thrust force and torque versus number of drilled holes in Test 1 (uncoated drill – 20/40 m/min – 0.05 mm/rev – wet cutting)

Figure 4.106 details the thrust forces recorded in the 3 different material layers for the first hole drilled (new tool) for each test. As outlined previously, the forces associated with Ti (ranging from 285 – 600 N depending on operating parameters) were considerably higher compared to both Al (135 – 342 N) and CFRP (44 – 190 N) when cutting with flood coolant. This however was not the case with the spray mist environment, where thrust forces in the Al layer (234 – 540 N) were comparable, and in some cases exceeded the values produced in the Ti alloy (239 – 426 N). The results would appear to support the earlier assertion that reduced levels of spray mist lubricant penetrated to the Al layer. In terms of thrust force for the last hole drilled (worn tool), the maximum corresponded to the use of a C7 coated drill at 20/40 m/min and 0.1 mm/rev where this was 2343, 814 and 817 N in the Ti, CFRP and Al layers respectively (thrust force results for the worn tool can be seen in Appendix D).

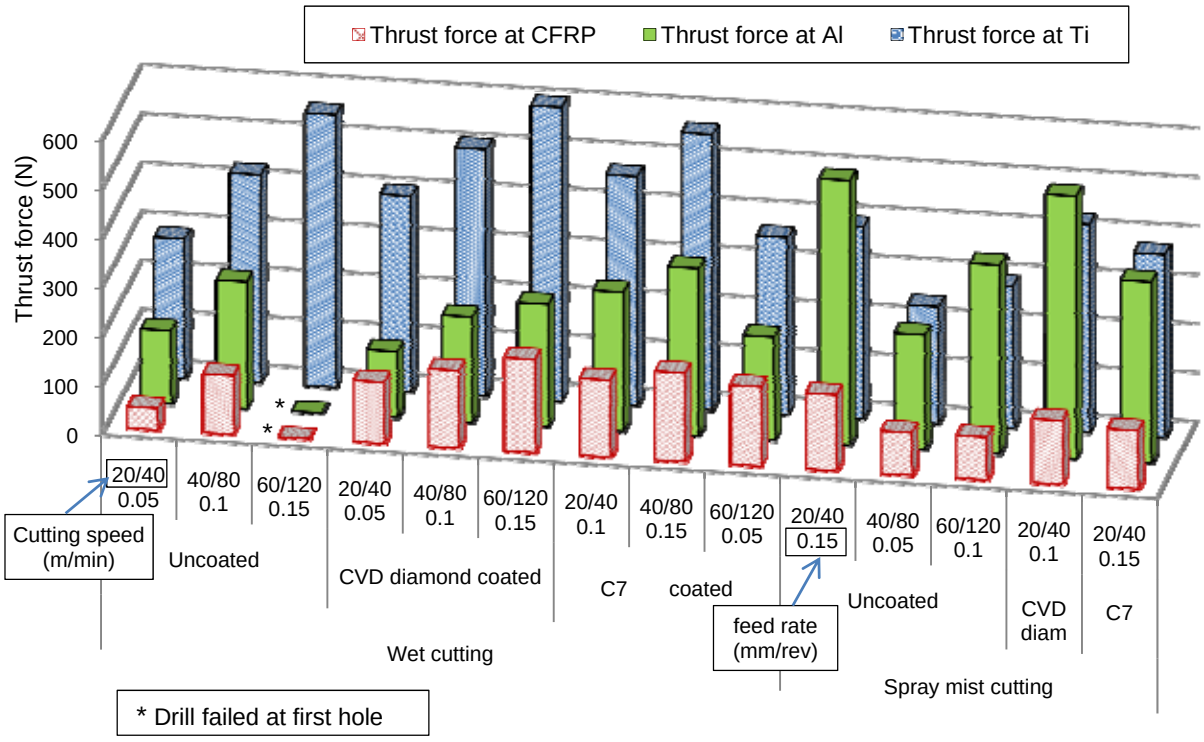


Figure 4.106: Thrust force results for new tool (first hole)

Figure 4.107 shows torque results for worn tools (at test cessation). The data however relates to the last measurement recorded and may not necessarily correspond to the actual value at the last hole drilled, particularly if the tool experienced an unexpected fracture prior to a periodic collection of force and torque results. This was one of the reasons why the average torque relating to the spray mist test appeared to be lower than that for wet cutting. In general, torque values associated with Ti (156 – 566 N.cm) were considerably higher compared to both Al (95 – 313 N.cm) and CFRP (30 – 84 N.cm) when cutting with flood coolant. This however was not the case with spray mist application, where torque in the Al layer was up to 313 N.cm, which exceeded the values produced in the Ti layer (up to 302 N.cm). Therefore, excessive torque level can be considered as a limiting factor affecting the machinability of composite/metallic stacks and can be taken as a good indicator for monitoring drilling process performance and predicting tool life.

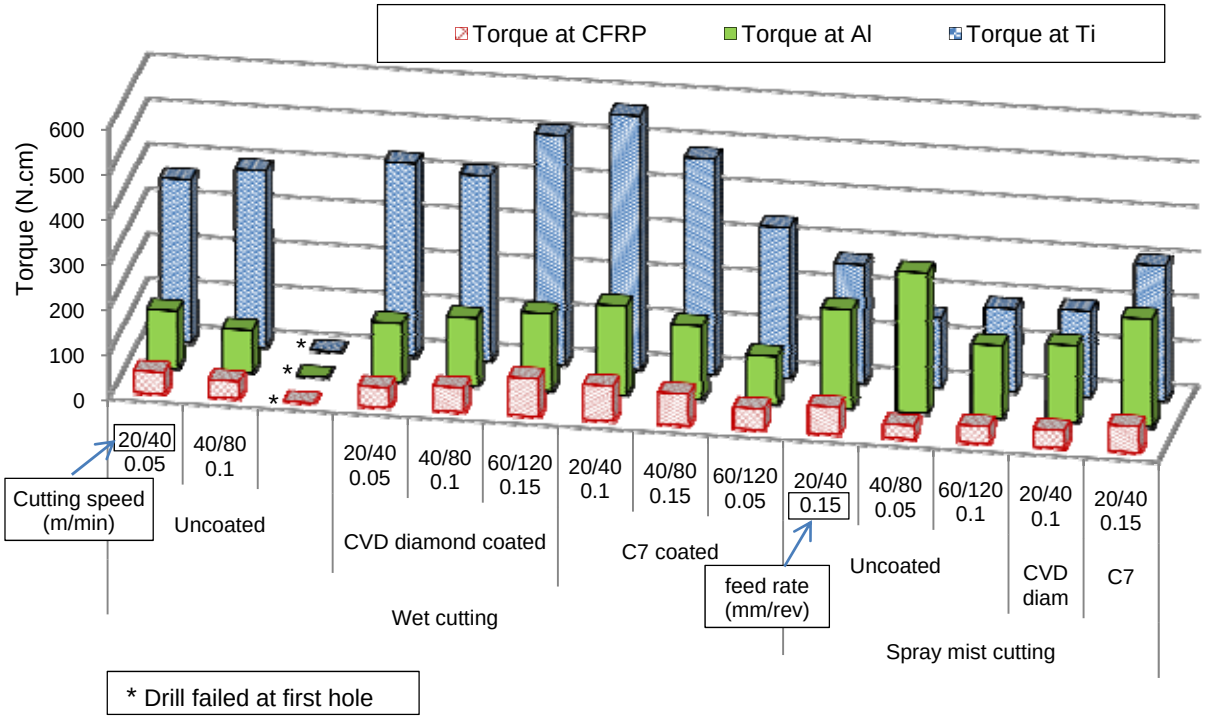


Figure 4.107: Torque results for the last hole (worn tool)

The main effects plot for thrust force when cutting through Ti/CFRP/Al stacks during the first hole is shown in Figure 4.108. All three materials exhibited near identical trends with respect to changes in control variable levels. The sole exception was the response of aluminium where thrust force was higher with spray mist as opposed to wet conditions, in contradiction to results seen for titanium and carbon fibre composite. Related ANOVA data, shown in Table 4.23, Table 4.24 and Table 4.25 highlighted the fact that feed rate had a significant impact on thrust force in all 3 layers with PCR's of 40%, 31% and 20% for Ti, CFRP and Al respectively. The environment condition was also a major contributing factor when drilling the Ti and Al with PCR's of 22% and 32%, while drill coating was only prominent in respect of the Ti layer (PCR of 23%). In terms of thrust force results using worn tools (last hole), environment condition consistently had an overriding influence on the three materials with corresponding PCR's of 62, 68 and 33 for Ti, CFRP and Al layers respectively. Surprisingly, feed rate was not statistically significant at the 5% level owing to the large contribution of the environment condition variable.

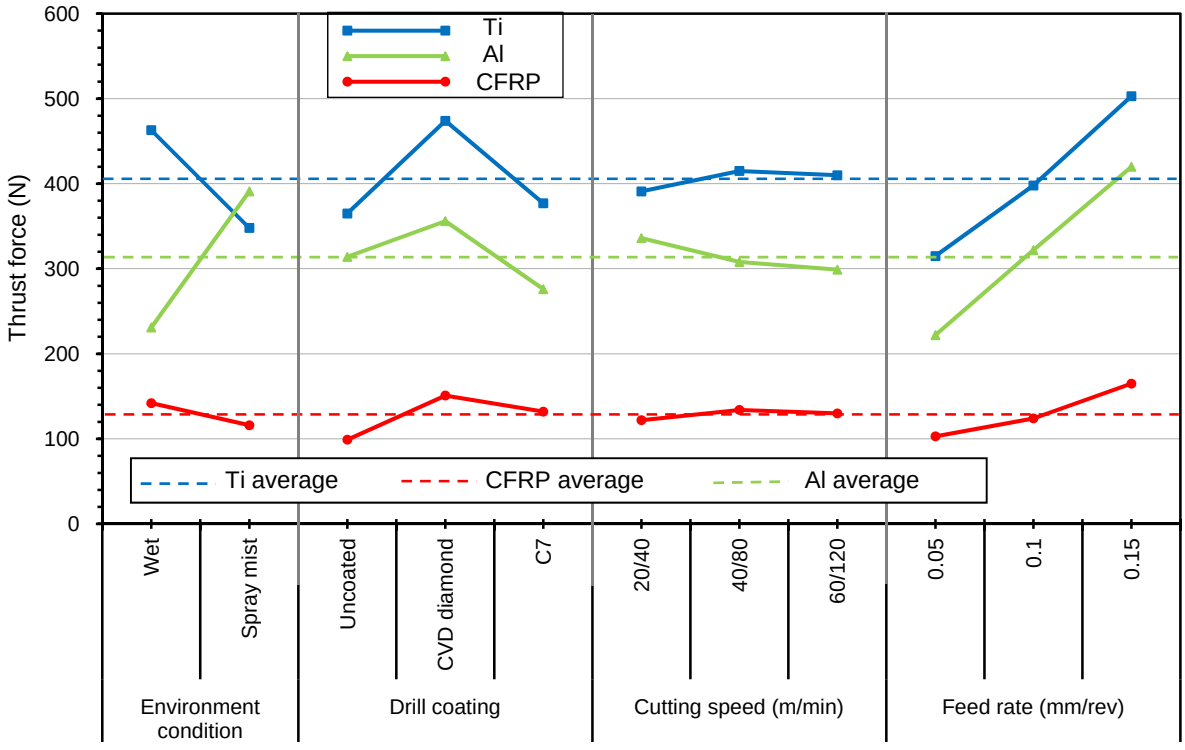


Figure 4.108: Main effects plot, means for thrust force following the first hole (new tool)

| Factor | DF | SS | Exp SS | F | P | PCR |
|---|---|---|---|---|---|---|
| **Environment condition** | 1 | 45321 | 43832 | 32.52 | 0* | 21.83 |
| **Drill type** | 2 | 55855 | 52877 | 14.87 | 0.001* | 26.33 |
| **Cutting speed (m/min)** | 2 | 3785 | 807 | 0.58 | 0.581 | 0.40 |
| **Feed rate (mm/rev)** | 2 | 82457 | 79479 | 27.7 | 0* | 39.58 |
| **Error** | 10 | 13397 | | | | 11.86 |
| **Total** | 17 | 200815 | | | | |

Table 4.23: ANOVA results for thrust force corresponded to Ti layer (new tool)

| Factor | DF | SS | Exp SS | F | P | PCR |
|---|---|---|---|---|---|---|
| **Environment condition** | 1 | 2793 | 1976.6 | 3.9 | 0.08 | 7.22 |
| **Drill type** | 2 | 6729.8 | 5097 | 2.73 | 0.118 | 18.63 |
| **Cutting speed (m/min)** | 2 | 487.7 | -1145.1 | 0.4 | 0.682 | 0.00 |
| **Feed rate (mm/rev)** | 2 | 10008.1 | 8375.3 | 6.13 | 0.021* | 30.60 |
| **Error** | 10 | 7347.6 | | | | 43.55 |
| **Total** | 17 | 27366.2 | | | | |

Table 4.24: ANOVA results for thrust force corresponded to CFRP layer (new tool)

| Factor | DF | SS | Exp SS | F | P | PCR |
|---|---|---|---|---|---|---|
| **Environment condition** | 1 | 108311 | 98796 | 9.8 | 0.012* | 31.92 |
| **Drill type** | 2 | 20309 | 1279 | 1.01 | 0.403 | 0.41 |
| **Cutting speed (m/min)** | 2 | 8462 | -10568 | 0.19 | 0.827 | 0.00 |
| **Feed rate (mm/rev)** | 2 | 86768 | 67738 | 4.56 | 0.043* | 21.89 |
| **Error** | 10 | 85634 | | | | 45.78 |
| **Total** | 17 | 309482 | | | | |

Table 4.25: ANOVA results for thrust force corresponded to Al layer (new tool)

Figure 4.109 depicts the main effects plot for torque when cutting through Ti/CFRP/Al stacks during the first hole. As expected, torque values for each material increased with increasing feed rate although this parameter was only significant for Ti and Al, the former with a PCR of 72% and 24% for the Al. Conversely, cutting environment had the greatest influence in the Al section where it had a moderate effect on CFRP drilling and Ti, see Table 4.26, Table 4.27 and Table 4.28. As anticipated, cutting speed showed a significant effect on torque with the CFRP. In terms of the last hole drilled, environment condition had the greatest effect on torque at last hole drilled at Ti with a PCR of 71% while only feed rate was statistically significant in the CFRP section (41%). Although none of the control variables had significant influence on torque results following last hole drilled in Al layer at the 5% level, environment condition had the greatest PCR of 40%. This may be due to the high level of signal noise encountered with Al torque and force profiles in addition to the premature tool

failure experienced in several tests.

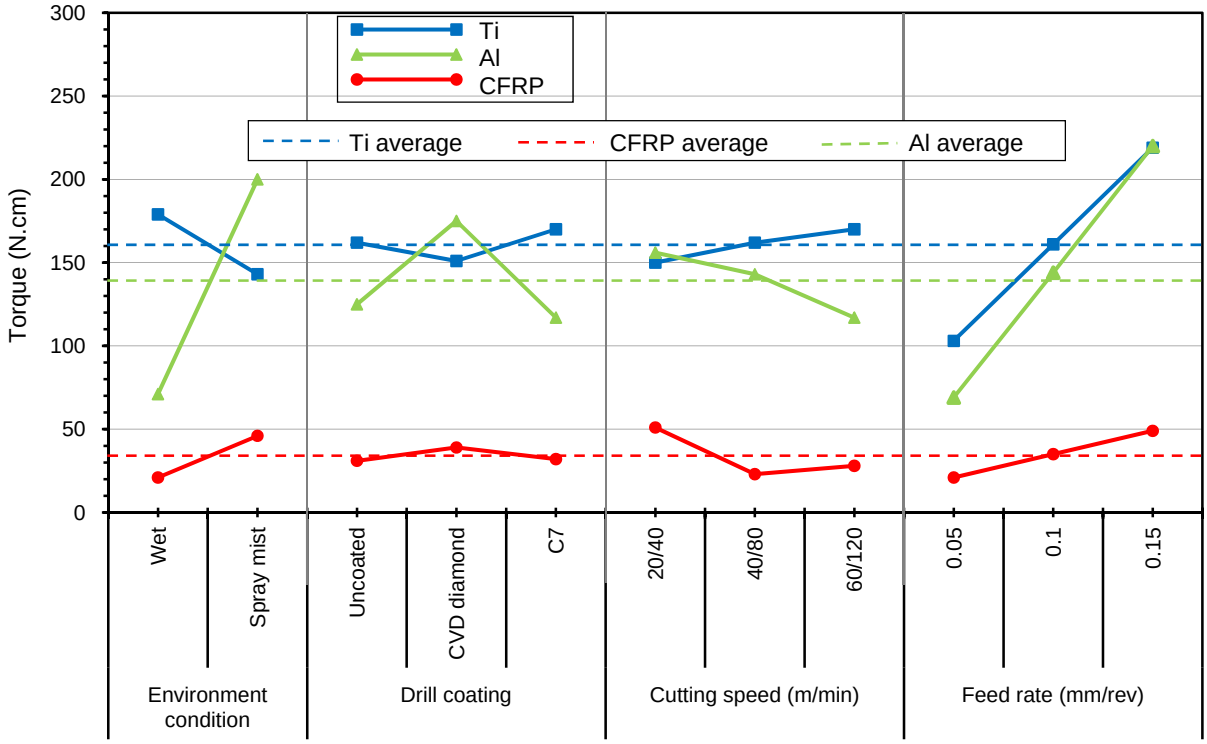


Figure 4.109: Main effects plot, means for torque following the first hole

| Factor | DF | SS | Exp SS | F | P | PCR |
|---|---|---|---|---|---|---|
| **Environment condition** | 1 | 1925 | 1535.6 | 7.16 | 0.025* | 4.17 |
| **Drill type** | 2 | 3042.8 | 2264 | 2.19 | 0.168 | 6.15 |
| **Cutting speed (m/min)** | 2 | 1004 | 225.2 | 0.53 | 0.606 | 0.61 |
| **Feed rate (mm/rev)** | 2 | 27354 | 26575.2 | 35.13 | 0* | 72.16 |
| **Error** | 10 | 3504 | | | | 16.92 |
| **Total** | 17 | 36830 | | | | |

Table 4.26: ANOVA results for torque corresponded to Ti layer (new tool)

| Factor | DF | SS | Exp SS | F | P | PCR |
|---|---|---|---|---|---|---|
| **Environment condition** | 1 | 2623.6 | 2361.5 | 9.69 | 0.012* | 24.44 |
| **Drill type** | 2 | 328.3 | -195.9 | 0.53 | 0.604 | 0.00 |
| **Cutting speed (m/min)** | 2 | 2931 | 2406.8 | 5.19 | 0.032* | 24.91 |
| **Feed rate (mm/rev)** | 2 | 1418.4 | 894.2 | 2.71 | 0.12 | 9.26 |
| **Error** | 10 | 2359.2 | | | | 41.39 |
| **Total** | 17 | 9660.5 | | | | |

Table 4.27: ANOVA results for torque corresponded to CFRP layer (new tool)

| Factor | DF | SS | Exp SS | F | P | PCR |
|---|---|---|---|---|---|---|
| **Environment condition** | 1 | 70434 | 67523 | 22.44 | 0.001* | 40.71 |
| **Drill type** | 2 | 14053 | 8231 | 2.11 | 0.178 | 4.96 |
| **Cutting speed (m/min)** | 2 | 9665 | 3843 | 0.83 | 0.465 | 2.32 |
| **Feed rate (mm/rev)** | 2 | 45524 | 39702 | 7.82 | 0.011* | 23.93 |
| **Error** | 10 | 26199 | | | | 28.08 |
| **Total** | 17 | 165876 | | | | |

Table 4.28: ANOVA results for torque corresponded to Al layer (new tool)

As mentioned previously in Chapter 3, geometrical characteristics, burr height and surface roughness were only assessed for tests which produced more than 150 drilled holes in addition to the longest tool life obtained with spray mist operation. These include test number 1, 4, 7 and 10. Microhardness measurements for the Al and Ti holes were only performed for two tests which demonstrated the longest tool life (Test 1 and 7).

### 4.7.3 Hole size and geometrical accuracy

Hole diameter results measured in the Ti section are presented in Figure 4.110. All tests performed using flood coolant produced undersized holes at test cessation, with the largest deviation of 14 μm corresponding to Test 7. Conversely, the test conducted under the spray mist environment resulted in oversized holes by up to 6 μm at the end the trial. The variation in hole diameter produced between drills in the new and worn conditions was up to 20 μm. Surprisingly, a smaller discrepancy was reported for the test producing the longest tool life (Test 1), at which hole tolerance ranged between -10 μm and +7 μm. This was possibly due to the lower torque values recorded when cutting Ti.

In terms of hole size in the CFRP layer, the majority of holes produced under wet cutting conditions were undersized, with a maximum error of -20 μm (Test 1) as shown in Figure 4.111. Contrastingly, the spray mist trials gave rise to significantly oversized holes in the CFRP of up to 120 μm for worn drills. This was most likely due to thermal expansion of the matrix from the increased cutting temperature caused by the lack of lubricant/coolant access and poor chip evacuation. Variation of diameter within each hole over the three material sections was evident, which was likely due to the different mechanical properties of the stack and in particular elastic modulus [163]. With regard to hole size in the Al layer, the limits ranged between -15 μm (Test 1) and + 12 μm (Test 7) for tests involving flood coolant.

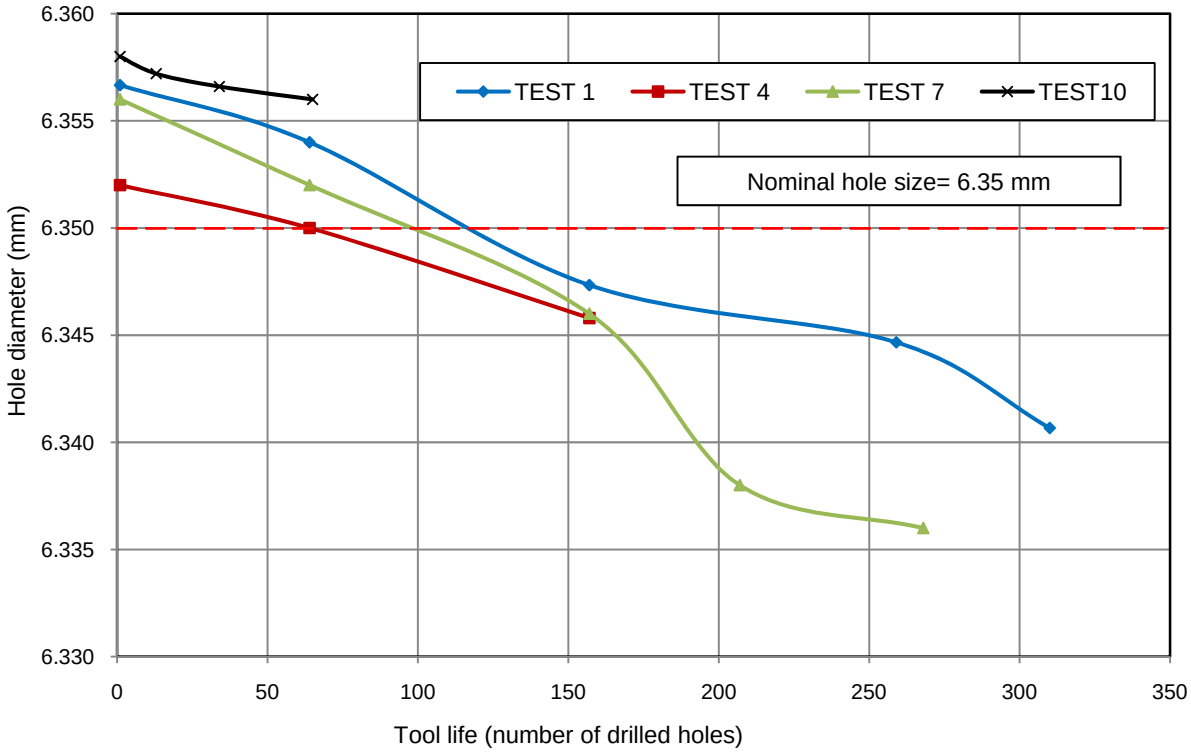


Figure 4.110: Hole diameter results at Ti layer

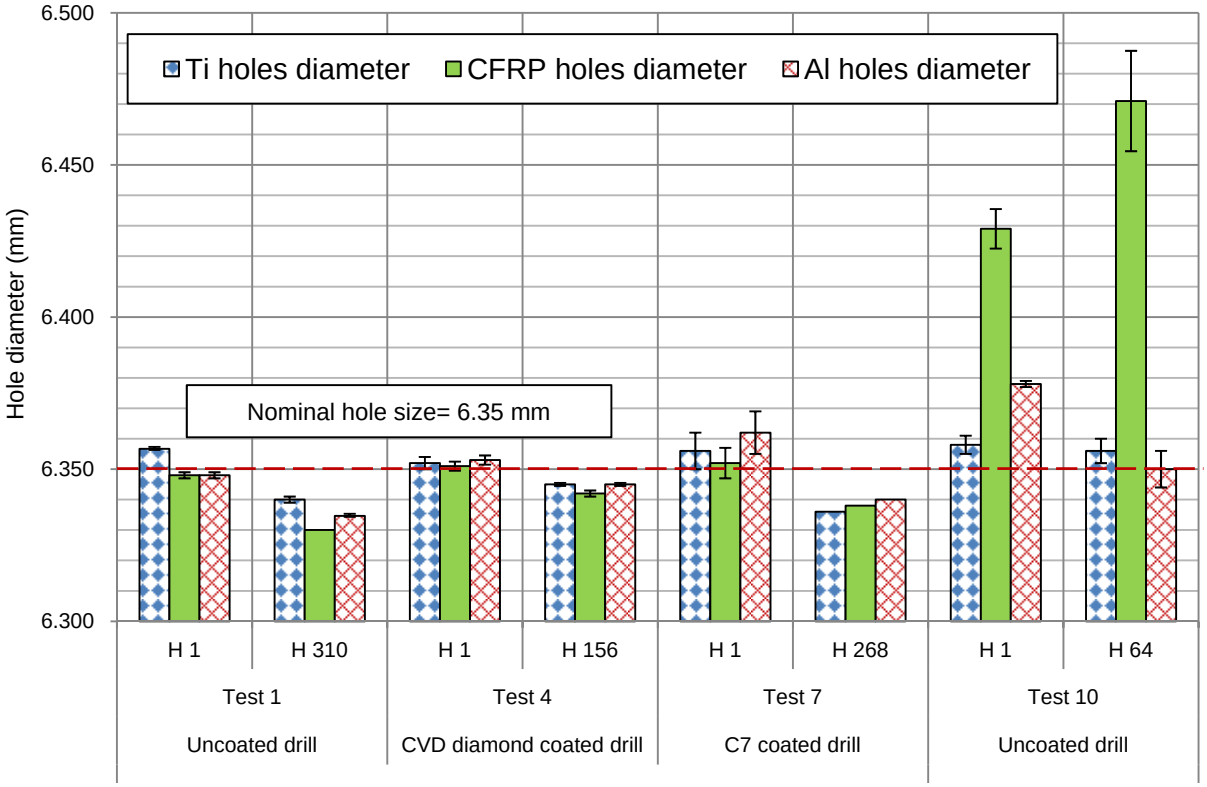


Figure 4.111: Hole diameter results for the first and last holes drilled at all material sections

An example of geometrical error measures in terms of cylindricity and roundness are presented in Figure 4.112. Roundness shows how the individual circular cross section of a hole approximates a true circle while cylindricity refers to how much the entire cylinder deviates. In terms of the hole shape, typical three looped holes were produced in the majority of sections. Surprisingly, roundness and cylindricity both improved as the tests proceeded except for the one performed with spray mist application as shown in Figure 4.113 and Figure 4.114. In general, variations in hole roundness was up to 78, 39 and 53 μm for the Ti, CFRP and Al layers respectively while cylindricity error over the entire stack varied between 23 and 120 μm when cutting wet. This increased up to an average of 170 μm in the spray mist environment. The geometrical discrepancies observed however were not considered high and could be minimised/eliminated with a post process operation following drilling.

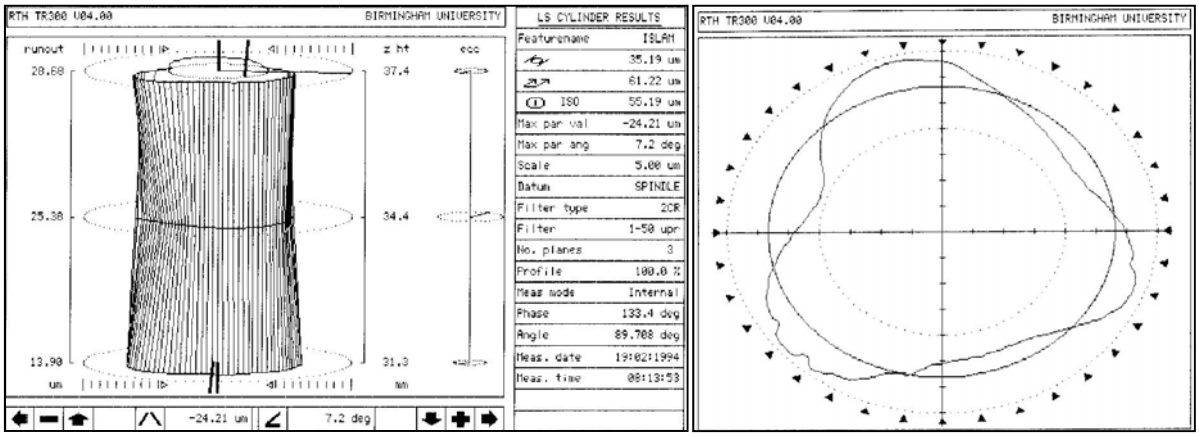


Figure 4.112: Captured images for sample measurements of (a) cylindricity and (b) roundness

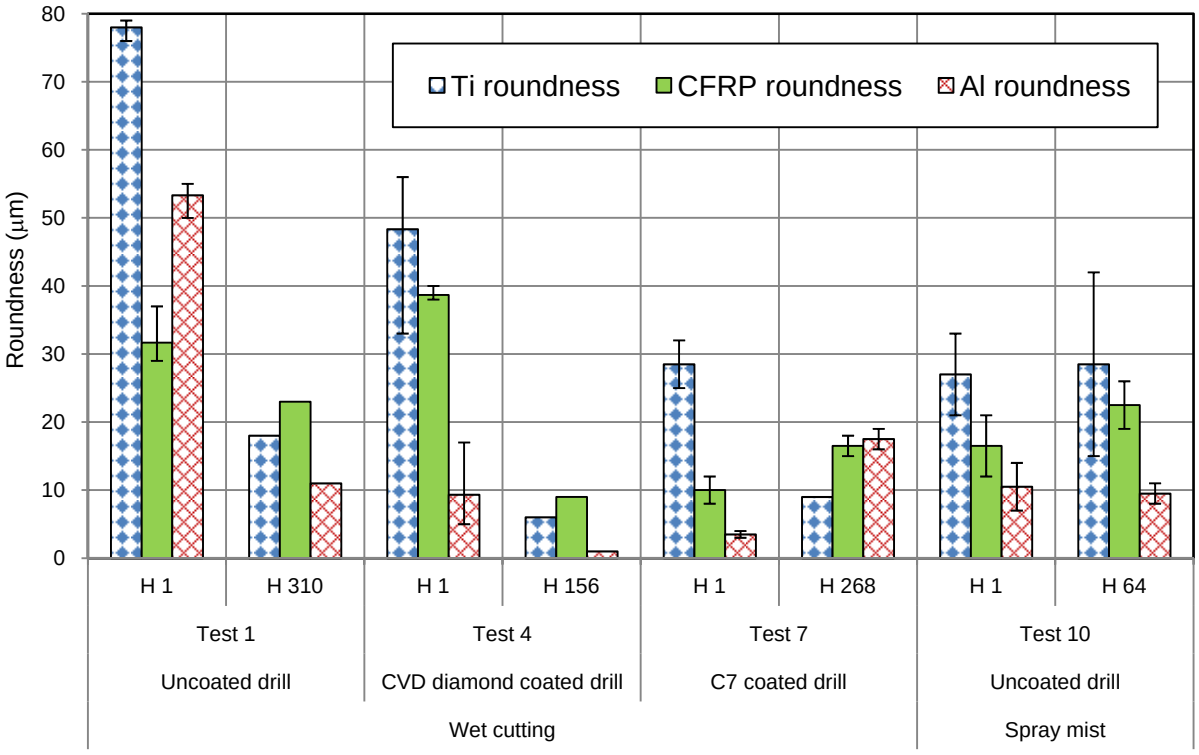


Figure 4.113: Roundness measurement results

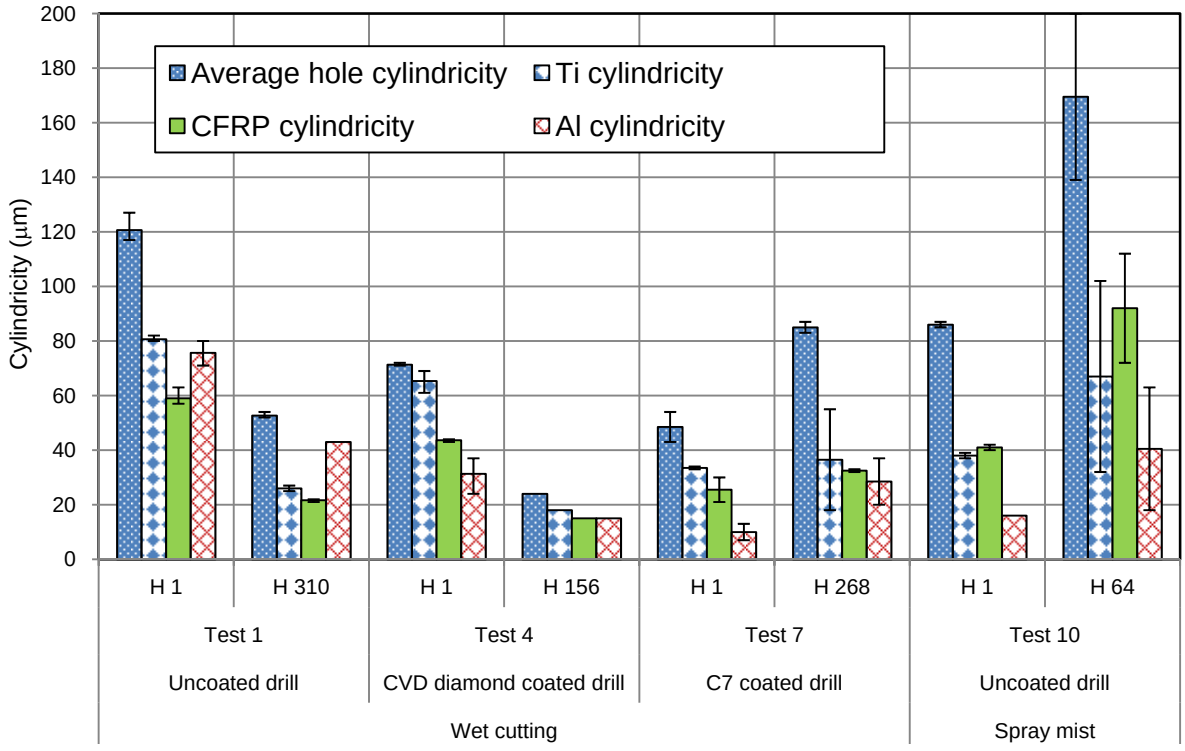


Figure 4.114: Cylindricity measurement results

### 4.7.4 Hole surface roughness

Figure 4.115 details the progression of average surface roughness for the three materials in Test 1 (wet cutting – uncoated drill – 20/40 m/min – 0.05 mm/rev). The Ra on the CFRP surfaces reached ~5 μm after 310 holes while corresponding values on the Ti and Al were only 0.9 μm and 0.2 μm respectively. In terms of the influence of operating conditions, Figure 4.116 shows Ra values for the Ti layer for Tests 1, 4, 7 and 10. Surface roughness did not exceed 1 μm Ra regardless of the drill type, cutting parameters or environment conditions. As drilling commenced from the Ti layer, sufficient coolant and lubrication reached the cutting zone, even when spray mist was used. Conversely, CFRP surfaces showed elevated roughness values of up to 9 μm Ra together with a large scattering of data (particularly with Test 7), see Figure 4.117. The lowest Ra was obtained when cutting with the CVD diamond coated drill (Test 4, up to 2.7 μm Ra) while the trial carried out at the lowest cutting parameters (Test 1) experienced moderately high Ra of up to ~ 5 μm. The increased Ra levels on CFRP surfaces were in part because of the inhomogeneous nature of the laminates [85, 86].

Hole surfaces in the Al plates were consistently smooth, and stabilised at ~ 0.2 μm Ra for all 3 tests carried out using flood coolant. The surface quality however deteriorated rapidly under spray mist conditions, see Figure 4.118. No evidence of damage due to Al swarf or marks from tool feed/retraction were seen on CFRP hole surfaces however small parallel grooves were observed on 3D topographic maps made at test cessation, as shown in Figure 4.119 (a) and (b). These could indicate possible interlaminar separation between fibre layers and may explain the elevated surface roughness values associated with the CFRP holes.

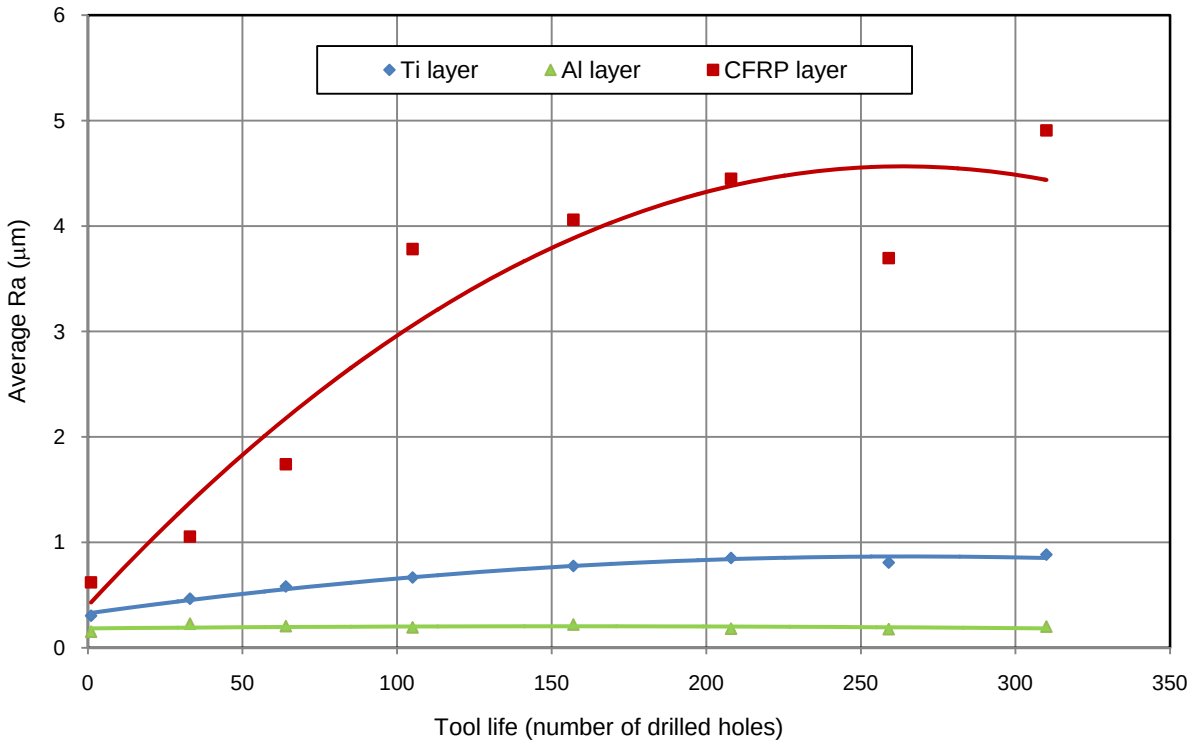


Figure 4.115: Average surface roughness (Ra) results for the three materials in Test 1

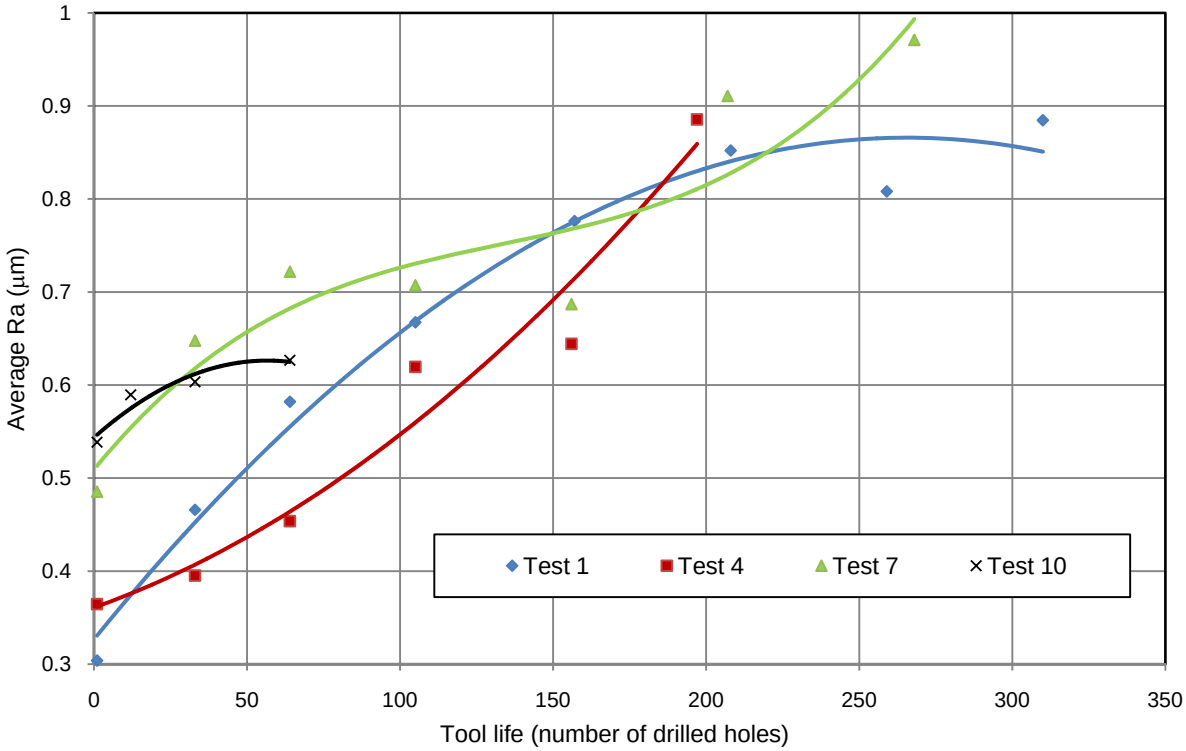


Figure 4.116: Average surface roughness (Ra) results for the Ti section

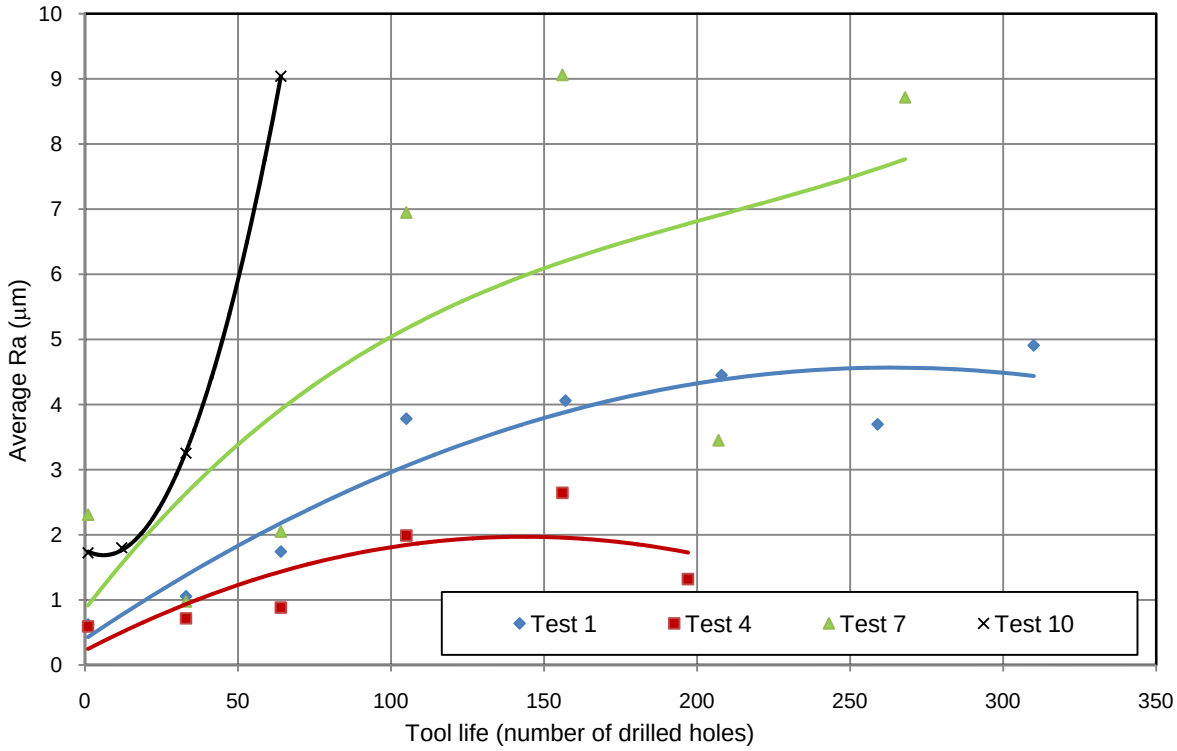


Figure 4.117: Average surface roughness (Ra) results for the CFRP section

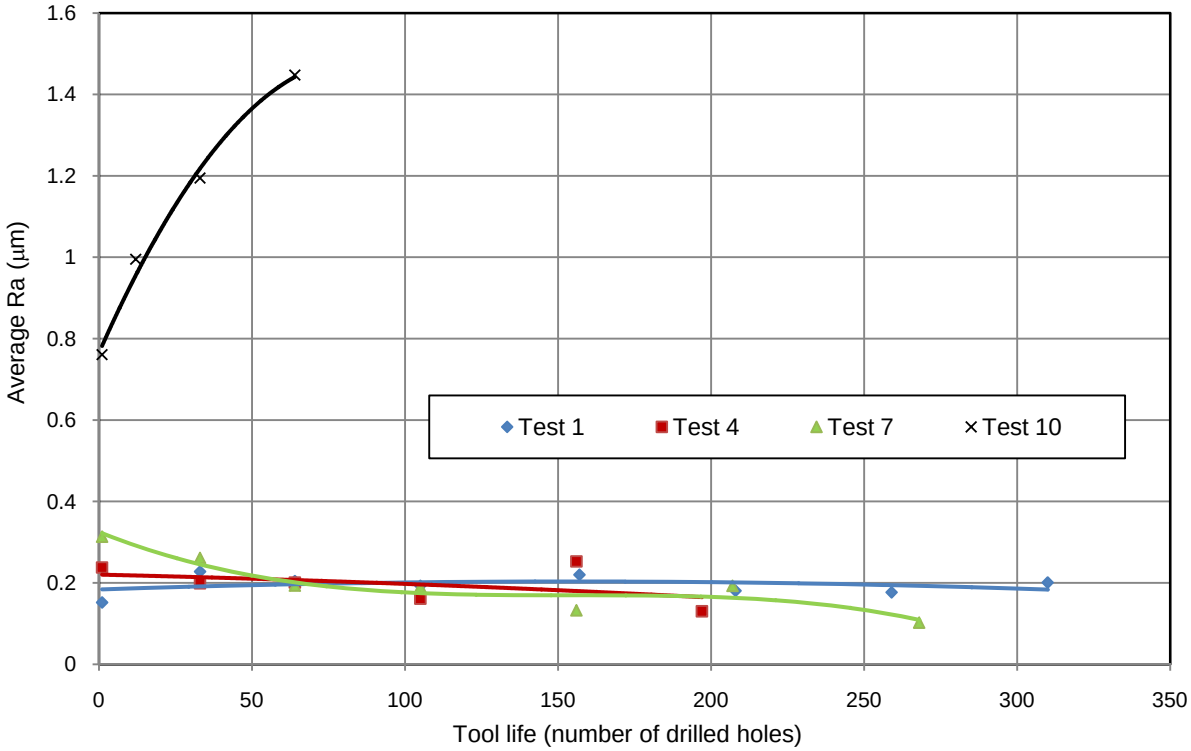


Figure 4.118: Average surface roughness (Ra) results for the Al section

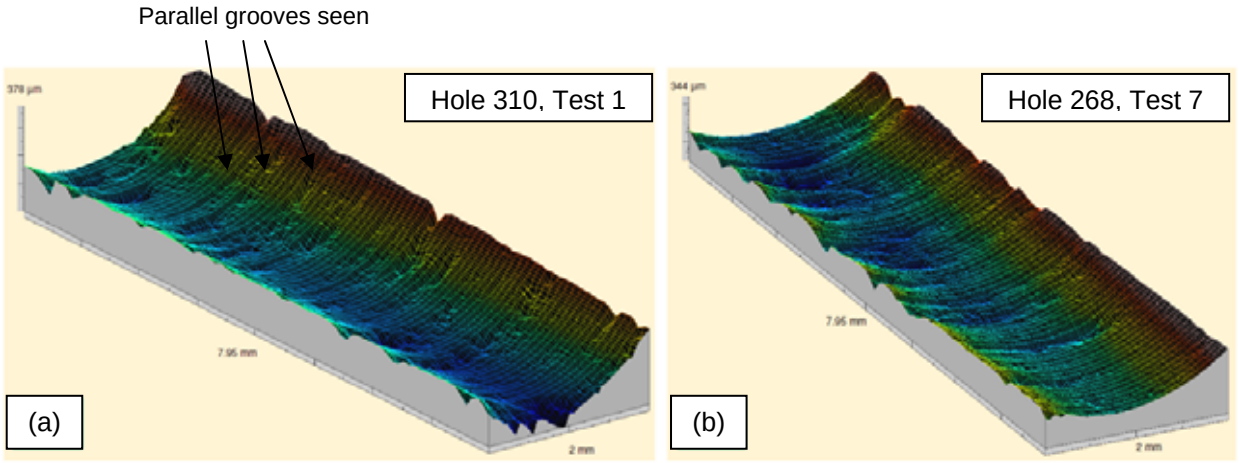


Figure 4.119: 3D topographic maps for the last hole drilled in CFRP: (a) Test 1 and (b) Test 7

SEM analysis showed that the majority of holes in titanium had chips redeposited onto the machined surfaces as detailed in Figure 4.120. This was probably the result of trapped/adhered material between drill flutes which was subsequently transferred and pressure welded to the hole surfaces as the tool passed through the stack. The findings are in agreement with results by Sharman et al. [187] who reported similar adhering chips when drilling Inconel 718. In contrast, surfaces on the aluminium layer showed very limited chip adhesion/workpiece smearing, which was attributed to the lower tendency of Al-7050 to adhere compared to Ti-6Al-4V. This could partly account for the higher surface roughness found with the titanium section as opposed to aluminium.

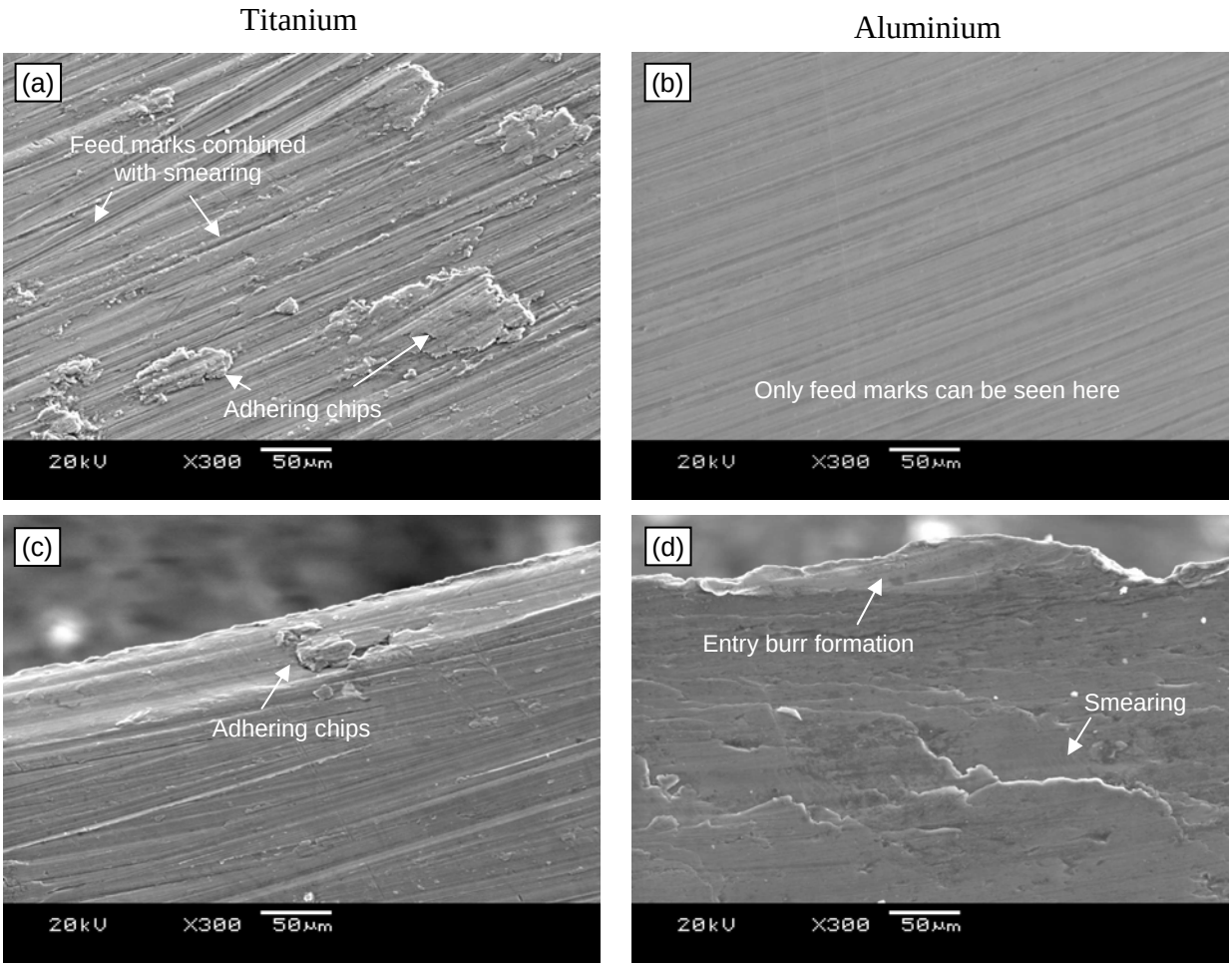


Figure 4.120: SEM images for the machined surface quality (Test 1): (a), (b) middle of hole 1, (c) entry of hole 1 and (d) entry of hole 310

### 4.7.5 Burr height for Ti and Al sections

Figure 4.121 shows sample burrs from the last hole drilled in the Ti and Al layers (Test 1 and 7). In general, uniform burrs with and without caps were obtained throughout the test programme at hole exit while rolled-back burrs were prevalent at hole entry. Rolled-back burrs are not uncommon at hole entry as previously reported by Dornfeld et al. [144] when dry and wet cutting of Ti alloys. Figure 4.122 shows sample SEM images for burr formation at the hole exit of titanium and aluminium workpieces. Greater deformation was seen with the latter due to its un-backed condition, and the higher ductility of Al-7050 (E = 72 GPa) compared to Ti-6Al-4V (E = 114 GPa) [30, 34].

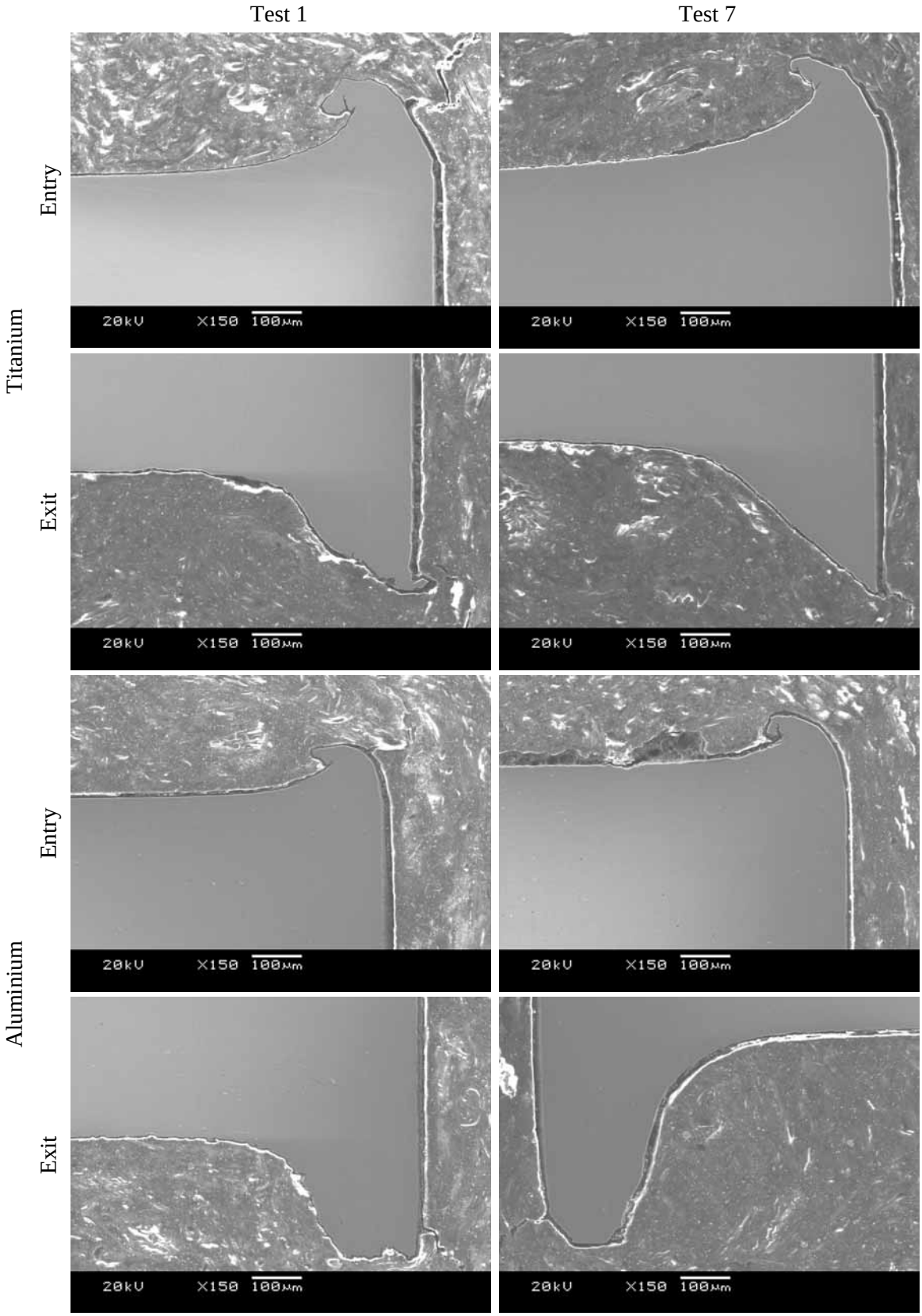


Figure 4.121: Uniform burr formation at entry and exit last hole drilled in Ti and Al

Crown burrs were only obtained when spray mist was employed, especially under high cutting speeds, see Figure 4.123. As expected, burr size increased as tool wear progressed, see Figure 4.124. For last holes drilled in titanium (worn tool), burr height was generally up to 300 μm while this reached 450 μm for the Al section, except in Test 4 when the cutting edge partially fractured (CVD diamond coated drill at hole 197) causing the exit burrs to reach ~1 mm. Additionally, exit burrs were typically larger than corresponding entry burrs, see Figure 4.125.

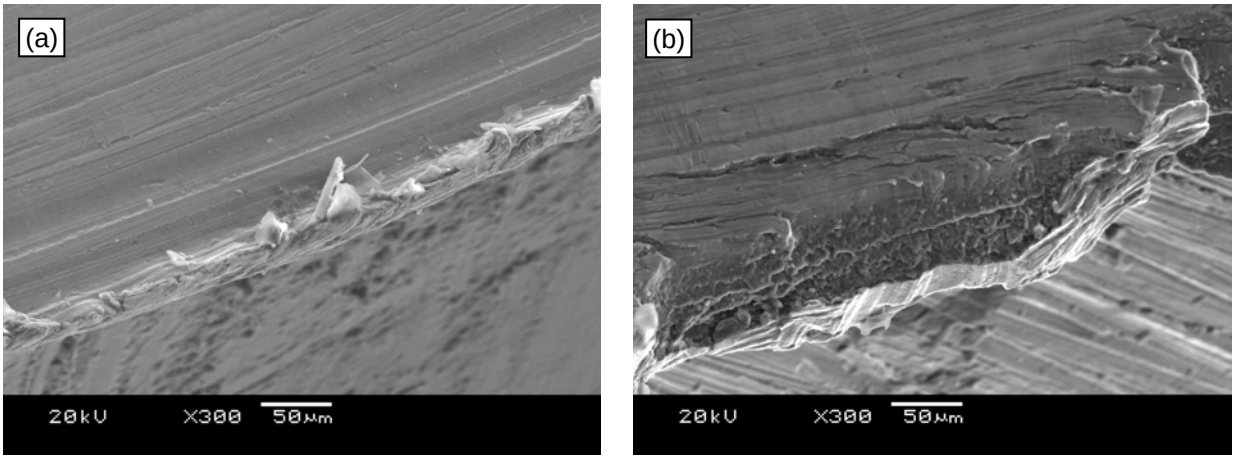


Figure 4.122: SEM images for exit burr formation at Test 1: (a) titanium and (b) aluminium

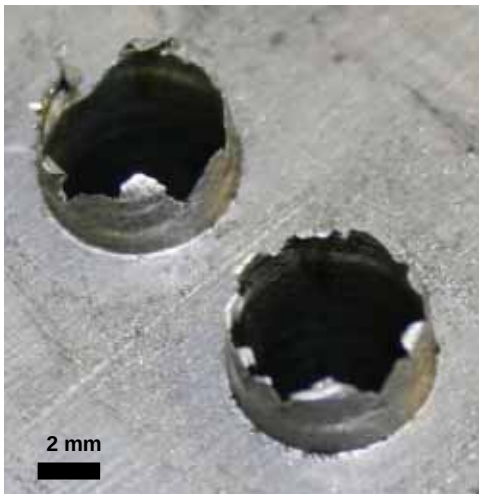


Figure 4.123: Crown burr formation when spray mist was used (Al exit, Test 12)

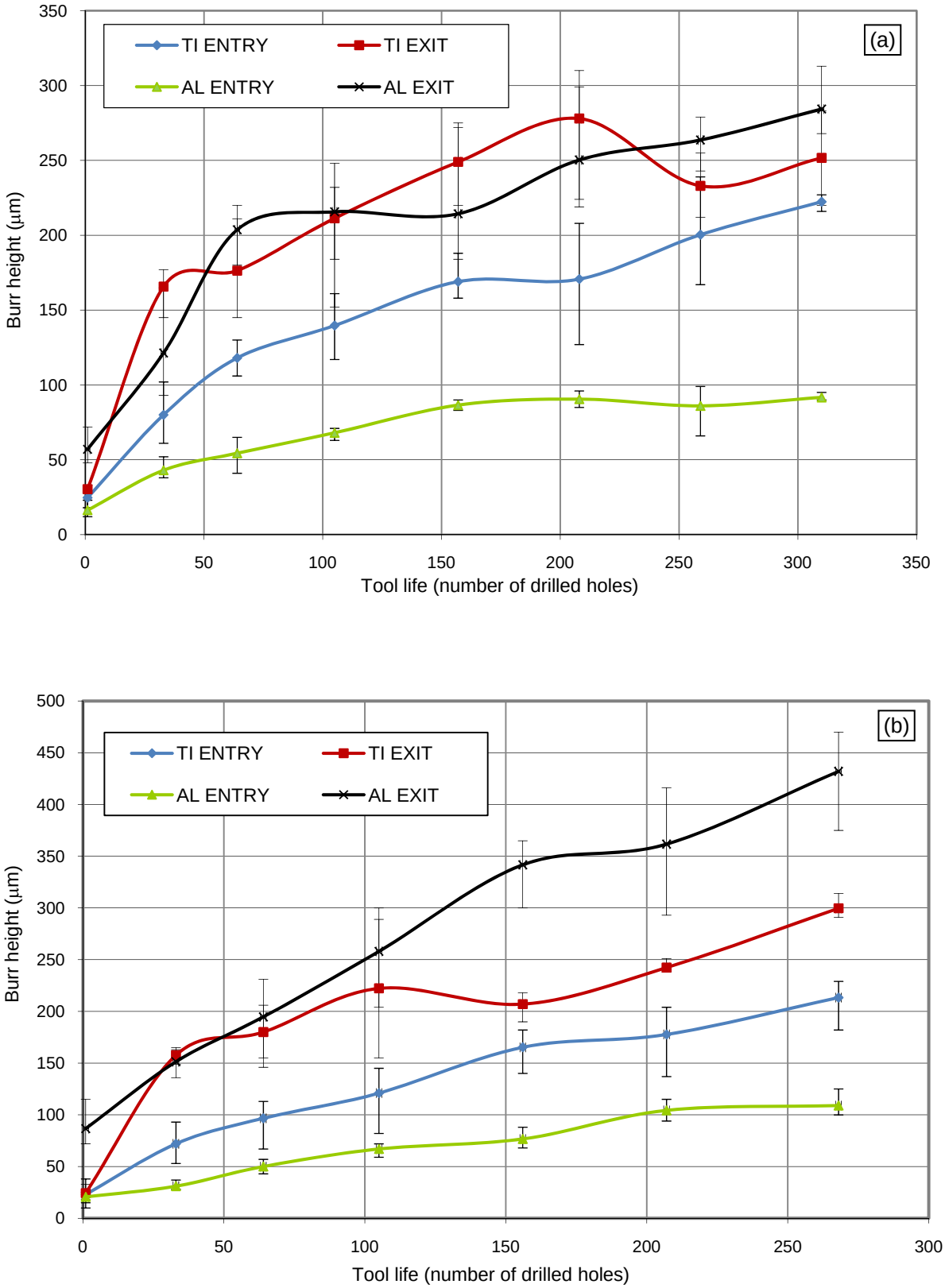


Figure 4.124: Burr height results for tests performed using: (a) uncoated (Test 1) and (b) C7 coated (Test 7) drills using flood coolant

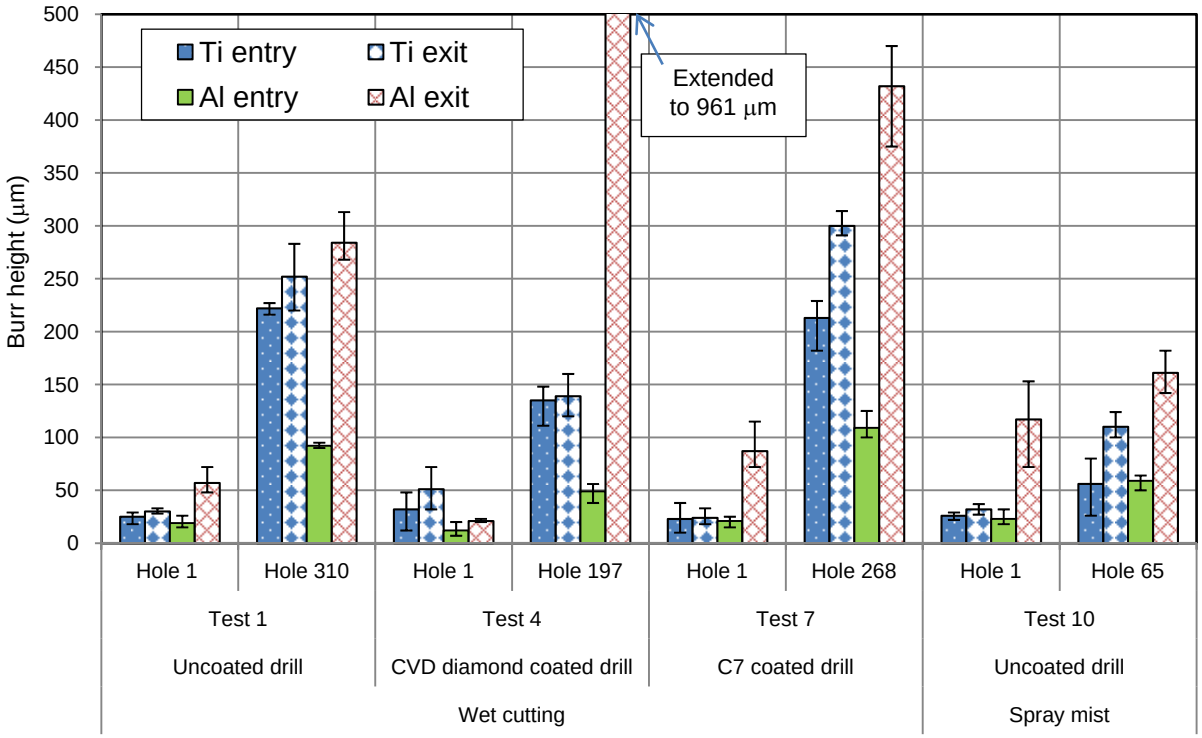


Figure 4.125: Burr height results for holes entry and exit (Ti and Al sections)

### 4.7.6 Hole edge quality

Limited damage was seen as a result of burr formation particularly at Ti hole exit. This extended to only several tens of micrometres and no evidence was seen for other damage, see Figure 4.126. In terms of CFRP hole edge quality, a significant reduction in both entry and exit damage was achieved when drilling them in a stack arrangement, see Figure 4.127. Typical defects including delamination and fibre pull out were not encountered regardless of the cutting conditions used due to the supportive backing provided by the Ti and Al layers.

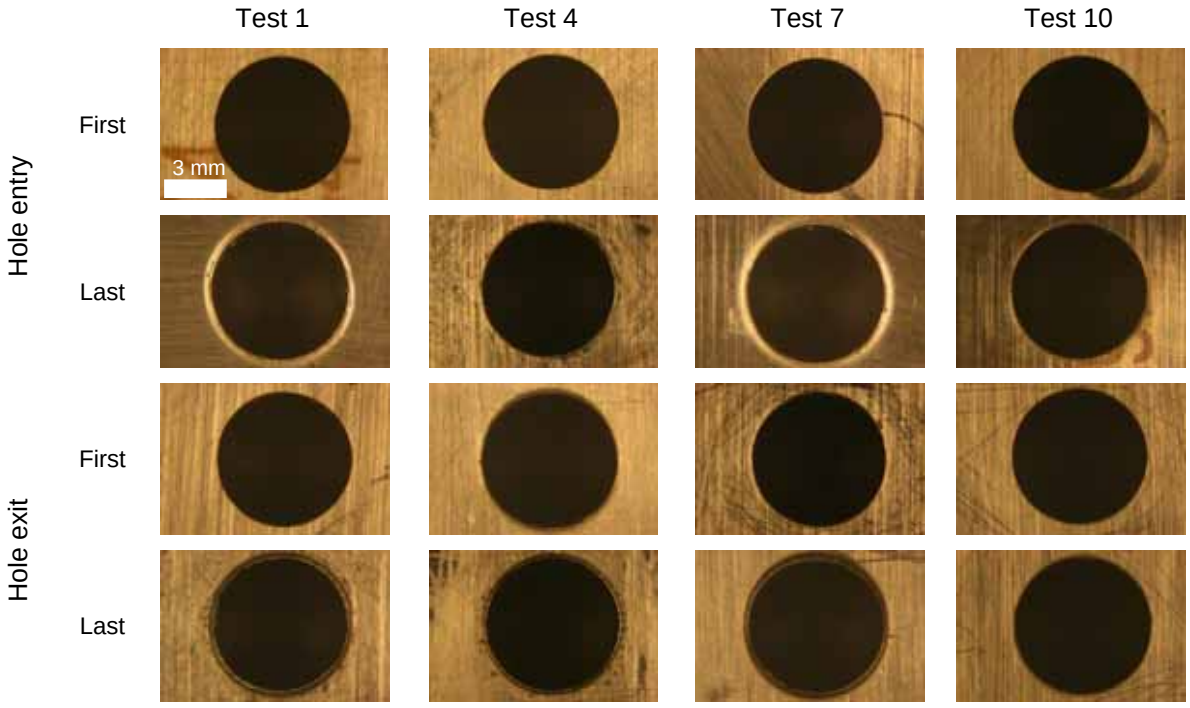


Figure 4.126: Hole edge quality for Ti layer

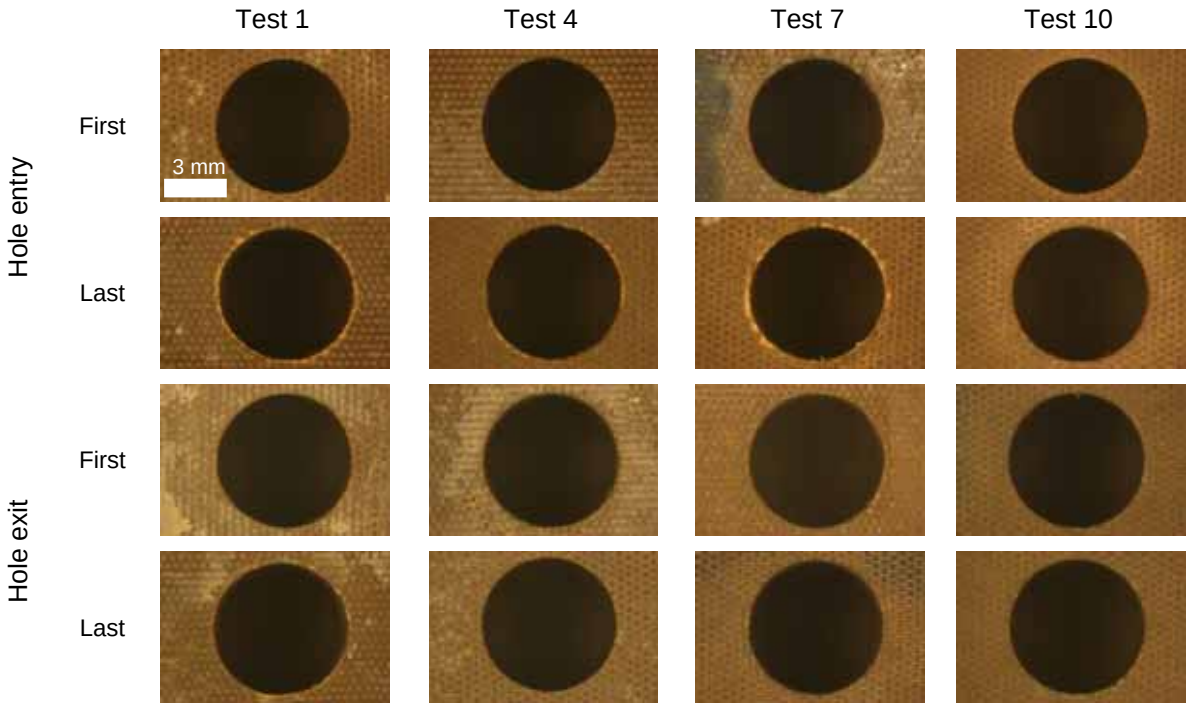


Figure 4.127: Hole edge quality for CFRP layer

### 4.7.7 Microhardness of metallic sections

Figure 4.128 and Figure 4.129 show microhardness depth profile results following the last hole drilled in the Al and Ti sections respectively (only for Test 1 and 7). Limited strain hardening on both materials was measured which extended up to ~500 μm beneath the machined surface in Al and ~800 μm for the Ti. The hardness increase in the Al was between 20 and 30 HK while for the Ti, it was 42 to 50 HK. Such responses are common when cutting Ti and Al and have been reported even for alternative machining processes [141].

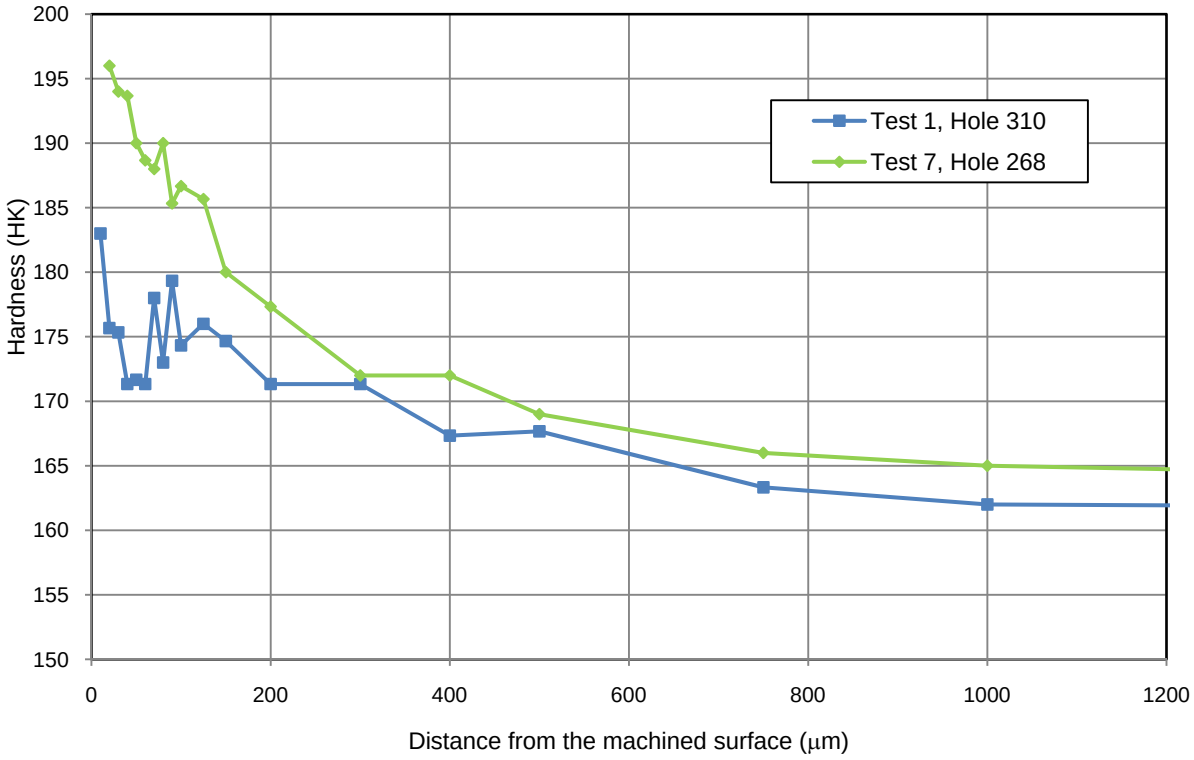


Figure 4.128: Microhardness results for Al sectioned holes

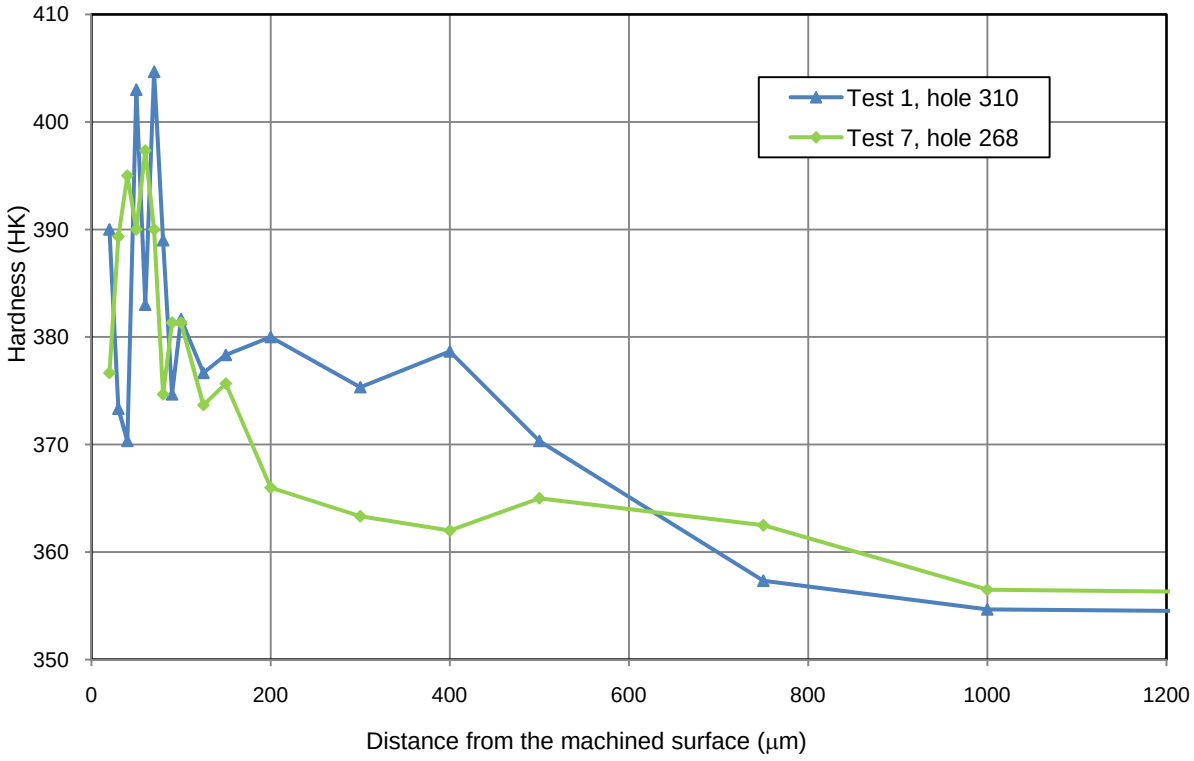


Figure 4.129: Microhardness results for Ti sectioned holes

### 4.7.8 Chip analysis

Figure 4.130 shows the different types of chips obtained in the test programme. In general, long and short spiral titanium swarf were seen when cutting stacks, especially when drilling using new cutting edges under both wet cutting and spray mist, regardless of the operating conditions and tool coating type. Similarly, long and short aluminium chips were produced when wet cutting, while curled/deformed swarf was obtained when spray mist was employed, see Figure 4.131. Chips frequently remained/clogged in drill flute which resulted in premature tool failure. SEM analysis of the titanium swarf showed typical sharp and serrated edges which accounts for the high dynamic/cyclic cutting forces [140] similar to those detailed in Section 2.6.5, see Figure 4.132. CFRP particles/debris were seen to regularly attach onto aluminium swarf or take the contour shape of the drill flute when spray mist was employed as shown in Figure 4.133. Dust-like CFRP particles was predominant when wet cutting was used. The combination of aluminium and CFRP chips resulted in clogging of the drill flutes and was a reason for increased cutting temperature and variability in tool life, see Figure 4.134.

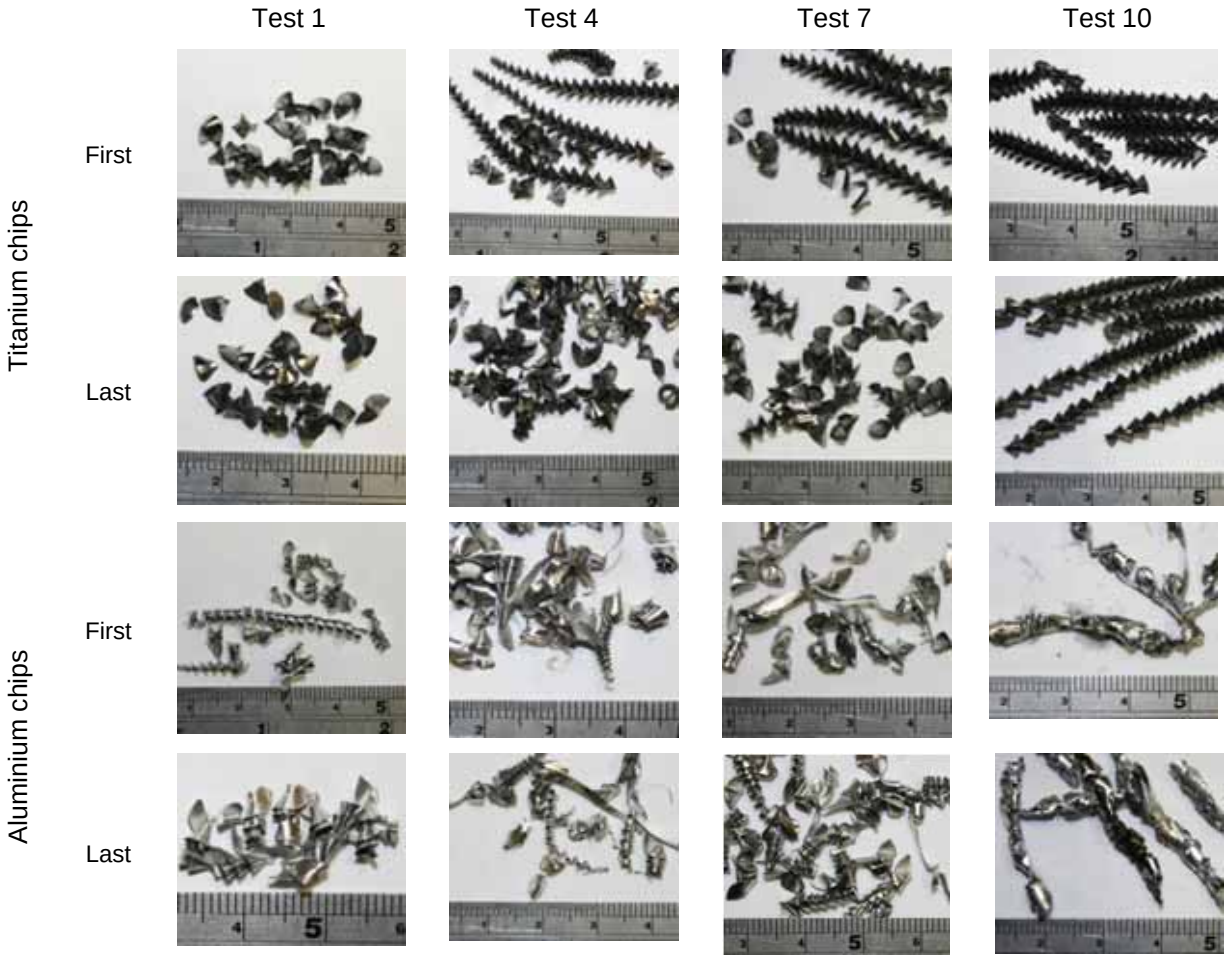


Figure 4.130: Various chips produced from Ti and Al holes

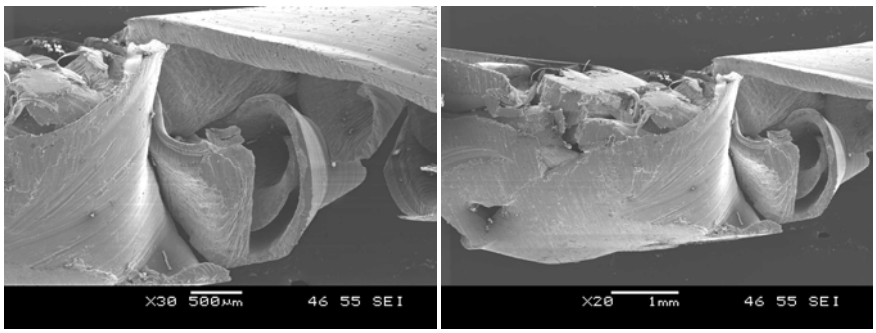


Figure 4.131: Curled/deformed aluminium swarf (formed in the spray mist environment)

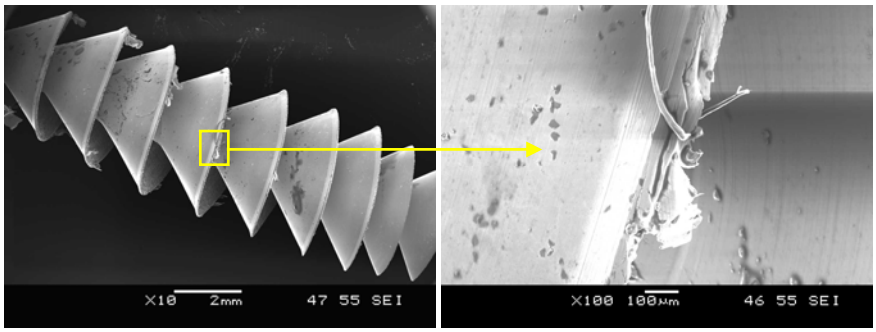


Figure 4.132: Spiral titanium swarf


Figure 4.133: (a) CFRP particles fused with aluminium swarf and (b) CFRP chips formed according to contour of drill flutes

Figure 4.134: CFRP particles attached to Al swarf causing clogging of drill flutes under spray mist conditions

# 5. CONCLUSIONS

## 5.1 Literature review

- Research into the drilling of CFRP composites is extensive however the vast majority of published work has involved drills in the region of 5 – 6 mm diameter. The preferred cutting speed and feed rate when using HSS tools is ~ 60 m/min and ~ 185 mm/min respectively. The maximum feed rate recommended when drilling CFRP using carbide twist drills (while maintaining acceptable workpiece quality) is 0.145 mm/rev, however this is generally considered low for practical applications, particularly in relation to aerospace and automotive components.
- Special drill types/geometries such as core, candlestick, core-saw, straight flute and saw drills have typically been shown to produce lower workpiece damage and correspondingly higher tool life when compared to standard twist drills. Delamination is commonly seen as the primary damage form when drilling CFRP. The magnitude and onset of composite delamination can usually be correlated to thrust force (critical force) which is dependent on feed rate, drill bit geometry and tool wear.
- Limited investigations employing advanced hardmetal and diamond coatings have shown considerable potential for improving performance and productivity when cutting CFRP.
- Laser drilling demonstrated significantly greater cutting rates compared to conventional twist drilling (approximately 10 – 20 times), however the resulting heat affected zone and fumes were cited as major drawbacks. Conversely, low cutting speeds, high operational costs and noise were given as the principal limitations of waterjet drilling. While ultrasonic drilling generally produces superior workpiece surface finish as compared to other processes, its relatively high investment cost, low productivity and high tool wear rates have curtailed industrial adoption.
- Extremely limited research has been reported on the drilling of multilayer stacks, particularly those involving Ti, Al and CFRP.

## 5.2 Experimental work – small hole (1.5 mm) drilling of CFRP (Phase 1 and 2)

### 5.2.1 Influence of peel ply layers

- The presence of the nylon peel ply layer significantly improved hole quality, particularly in respect of entry and exit delamination with considerable reduction in defects such as fibre breakage, fuzzing and edge chipping. The peel ply was thought to provide a 'barrier' against peel-up and push-out delamination at hole entry and exit respectively.
- Both tool wear and thrust force were found to be marginally lower with samples where the peel ply was removed however there was no substantial difference in terms of internal hole surface roughness and dimensional accuracy. Additionally, dimensional error/hole undersize did not exceed 30μm on diameter, even after 1875 holes.

### 5.2.2 Effect of tool geometry and operating parameters

- Drill type/geometry and feed rate were the main contributing factors affecting tool life and thrust force, while cutting speed and feed rate had the most significant effect on torque.
- In terms of tool life, uncoated stepped drills with $140^{o}$ point and $30^{o}$ helix angles, at 15 m/min cutting speed and 0.2 mm/rev feed rate produced the maximum number of drilled holes (2900). Low thrust force values of up 100 N were recorded even at test cessation while drilling torque levels reached 85 N.mm.
- The reduction in thrust force when employing the stepped geometry was due to the lower chisel edge/workpiece material interaction, while the increase in feed rate minimised contact time between the cutting tool and workpiece material, thus reducing the abrasive action and anticipated rise in cutting temperature.
- Entry and exit delamination factor ($F_d$) did not exceed 2 even at the end of tool life, while the type of damage present was very similar on both the entry and exit surfaces.

### 5.2.3 Effect of composite material, fibre orientation and machining parameters

- The longest tool life was achieved when drilling woven MTM44-1/HTS at a feed rate of 0.4 mm/rev (3750 holes) using a stepped drill configuration. The corresponding ANOVA revealed that the most significant factor was prepreg type with a PCR of ~25%. However, the majority of stepped drills tested at the higher feed rate level (0.4mm/rev) experienced catastrophic failure, which was attributed to the reduction in strength of the tool due to the smaller diameter of the pilot segment.
- A maximum allowable operating feed rate of 0.2 mm/rev is recommended for stepped drills irrespective of composite orientation while conventional drill geometry can be used at higher feed rates.
- Measured thrust forces ranged from 40 to 90 N for the first hole drilled which increased to between 58 and 142 N for the last hole, with feed rate having a statistically significant effect. Torque values were generally below 100 N.mm.
- Entry delamination factor ($F_d$) was below ~1.9 while the maximum corresponding exit $F_d$ was up to 2.1, with damage tending to be somewhat more severe for last holes. The associated ANOVA results showed that feed rate had an overriding effect on delamination factor with an overwhelming PCR of up to 73%. In terms of material influence, the UD and woven 8552/AS4 AC resin system (fibre tensile strength and modulus are 4480 MPa and 231 GPa respectively) typically experienced greater damage, especially when drilling at high feed rate (0.4 mm/rev).
- The diameter of drilled holes was generally undersize by 36 μm (~2.5%) and 73 μm (~5%) at the end of tool life for conventional and stepped drills respectively.
- The results from statistical analysis of the adjusted delamination factor ($F_{da}$) were generally in agreement with results based on $F_d$, although the $F_{da}$ measure provided better discrimination of damage in certain cases.

### 5.2.4 Evaluation of diamond based coatings

- When machining UD MTM44-1/HTS laminates, uncoated or diamond like carbon (DLC) coated drills were found to be the best/preferred choice in order to maximise tool life. The results suggest adopting a maximum allowable operating feed rate of 0.3 mm/rev with either uncoated and DLC coated conventional twist drills.

- Severe tool wear and catastrophic tool fracture was prevalent when using CVD diamond coated drills. Tool life was less than 100 holes for the vast majority of tests.
- Thrust force ranged from 60 to 160 N when using uncoated or DLC coated drills while relatively high thrust forces were obtained (~380 N) when CVD diamond coated drills were employed. This was attributed in part to the inferior cutting edge condition/sharpness and rougher surface of the CVD diamond coating. Additionally, relatively low values of torque were generated (from 25 to 80 N.mm) over the range of variables evaluated.
- DLC coated and uncoated drills typically produced lower values of exit delamination factor compared to the 3 different CVD diamond coated tools, with the Rhobest product causing the greatest degree of workpiece damage ($F_d$ of ~2.9).
- The unexpectedly poor performance of the CVD diamond coated drills could be ascribed in part to the likely reduction of cobalt binder content in the carbide substrate leading to a weakening of the tool.
- The relatively high feed rate (0.4 mm/rev) utilised in the present investigation was unsuitable when employing CVD diamond coated drills and resulted in premature tool failure and unacceptable hole quality.

## 5.3 Experimental work – drilling of multilayer stacks (Phase 3)

### 5.3.1 Preliminary drilling trials in separate CFRP and Ti plates and multilayer stacks

- Higher tool life was achieved when drilling 10 mm thick CFRP laminates using the novel E6 domed PCD drills (1213 holes for only 157 μm flank wear), while alternative WC coated drills produced only 257 holes for 300 μm flank wear.
- The straight fluted E6 domed PCD drill however broke during the first hole when drilling Ti-6Al-4V with corresponding high thrust force values of ~1100 N.
- Burr height in titanium holes was generally less than 200 μm for both hole entry and exit while severe exit damage was observed when drilling CFRP irrespective of tool material. This significantly decreased when CFRP was drilled in a stack arrangement with titanium.

- When drilling stacks of CFRP/Ti, the spiral titanium swarf regularly caused damage to the CFRP hole surface. Surface roughness ranged from 0.2 to 0.5 μm Ra for Ti holes while it exceeded 5 μm in the CFRP.

### 5.3.2 Impact of stack arrangement and performance of PCD tools

- When drilling stacks of Al/CFRP/Ti, higher tool life was achieved using C7 coated drills (150 holes at 300 μm flank wear) while CVD diamond coated drills produced < 5 holes regardless of the operating conditions.
- The performance of CVD diamond coated drills improved significantly when drilling the stack in the sequence: Ti/CFRP/Al (tool life increased to 108 holes at 136 μm flank wear level compared to <5 holes when machining commenced from the Al layer).
- Brazed PCD drills generally experienced fracture on the chisel edge while the helical fluted, domed PCD drills typically broke at the carbide sections of the tool due to poor chip evacuation/high chip packing. The former are expected to perform better if the chisel edge is strengthened with either carbide support or by increasing the diamond thickness. The domed PCD drills however require further design modifications in order to accommodate the drilling of metallic/composite stacks (such as different helix angles etc.).
- Unusually high thrust force and torque levels were measured when employing domed PCD and brazed PCD drills; 1400 and 800 N respectively with torque up to 400 N.cm.
- Drilling stacks comprising Ti/CFRP/Al sections is preferred over Al/CFRP/Ti due to improved titanium swarf evacuation as well as better coolant transport to the titanium section.
- When drilling in the Al/CFRP/Ti configuration, severe noise was encountered as the tool engaged the titanium layer.

### 5.3.3 Effect of tool coatings and operating parameters

- Tool life in terms of number of drilled holes was primarily dependent on cutting speed and cutting environment. Here, up to 310 holes in Ti/CFRP/Al stacks was achieved when employing an uncoated drill at low cutting speed (20/40 m/min) and feed rate of (0.05 mm/rev) under flood coolant conditions. The corresponding ANOVA showed that

cutting speed and environment condition were statistically significant with PCRs of 42% and 32% respectively. No major benefits in terms of tool life, thrust force or torque were apparent when using the CVD diamond or C7 hardmetal coating over uncoated WC drills.

- Higher feed rate (0.15 mm/rev) levels with spray mist caused catastrophic fracture while coated drills experienced partial cutting edge fracture in a wet cutting environment.
- When cutting wet with new drills, thrust force was highest in the titanium layer (up to 600 N) while lowest levels were recorded with the CFRP material (190 N). Tests involving spray mist application however generally highlighted greater thrust forces in the aluminium alloy. The corresponding ANOVA showed that feed rate and environment condition were statistically significant at the 5% level in relation to thrust force for both Ti and Al. Both factors were also found to influence torque generation within the Ti and Al layers of the stack. While feed rate had an overriding 72% effect on Ti, environment condition was the primary variable affecting torque with Al.
- In general, the use of high pressure through spindle coolant (~ 70 bar) is recommended over external spray mist application due to the superior cooling properties and improved access to the cutting zone provided by the former.
- When cutting using flood coolant, undersized holes were produced at test cessation, with the largest deviation of 14 μm on diameter at the Ti section corresponding to Test 7 (C7 coated drill at 20/40 m/min and 0.05 mm/rev), while this was 20 and 15 μm at the CFRP and Al layers respectively for Test 1 (uncoated drill at 20/40 m/min and 0.05 mm/rev). Conversely, the spray mist trials gave rise to oversized holes in the CFRP of up to 120 μm for worn drills.
- Surface roughness was considerably lower when using through spindle coolant in comparison to spray mist application, especially at the Al section. High surface roughness of up to 9 μm Ra was obtained on CFRP hole surfaces while values of up to 1 and 0.3 μm Ra were measured on corresponding Ti and Al surfaces respectively. The surface roughness at the Al section however deteriorated to 1.5 μm Ra at test cessation when spray mist environment was employed (after only 64 drilled holes). Adhering chips were seen on Ti machined surfaces as was workpiece smearing, indicating the potential need of a finishing process when drilling Ti/CFRP/Al stacks.

- Burr height was generally below 500 μm except when spray mist was used, which increased burr levels significantly up to ~ 1 mm, particularly in the Al section.
- Delamination of the CFRP laminates was significantly reduced due to support from the Al and Ti layers. Only minor damage around hole edges of the CFRP was observed, which was caused by sharp Ti exit burrs.
- Microhardness results showed marginal hardening up to 800 μm from the machined Ti surface (maximum of 50 $HK_{0.025}$ above the bulk value) while strain hardening extended to a depth of 500 μm in the Al material.

## 5.4 Overall conclusions and recommended operating conditions

### 5.4.1 Small hole drilling in CFRP

- Despite slightly higher forces, retention of the nylon peel ply layer during drilling is imperative to significantly improve hole quality as well as reduce delamination and fibre breakage.
- Rounding of the cutting and chisel edges due to abrasion was the principal wear mode.
- Cutting speed (over the range investigated) had no significant effect on all responses investigated. A maximum operating feed rate of 0.2 mm/rev is recommended for stepped drill geometry while for conventional drills this was 0.3 mm/rev. This provided a cutting time of between 0.4 – 0.7 seconds per hole (including drill positioning and retraction).
- In general, woven laminates produced lower delamination than UD laminates.
- CVD diamond coated tools showed no appreciable benefits over uncoated or PVD diamond coated drills. Therefore, uncoated WC (K10) drills are recommended for small hole drilling of CFRP.
- In general, the longest tool life (3000 – 3500 holes depending on feed rate and drill type used) was achieved when drilling MTM44-1/HTS prepreg laminates.
- Table 5.1 lists recommended/preferred operating conditions when small hole drilling in CFRP.

| Parameter | Value |
|---|---|
| Cutting speed | 40 - 50 m/min |
| Feed rate | 0.2 – 0.3 mm/rev |
| Tool material / coating | Uncoated WC |
| Tool geometry | Conventional twist drill with $118^o$ and $24^o$ point and helix angle |
| Composite resin system | MTM 44-1/HTS |
| Prepreg form | UD or woven |
| **Expected tool life** | **3000 holes in 3 mm thick CFRP laminate** |

Table 5.1: List of preferred operating parameters and workpiece material for small hole drilling of CFRP

### 5.4.2 Drilling of multilayer stacks (Ti/CFRP/Al)

- Stacks comprising Ti/CFRP/Al layers can be successfully drilled in a one shot operation using WC tools (K10). In terms of preferred cutting conditions, low to moderate feed rate (0.05 – 0.1 mm/rev) together with low cutting speed (20/40 m/min) provided the best tool life (~ 300 holes).
- BUE on the primary cutting lips as well as drill margins was prevalent in trials involving spray mist application, while rounding on the main cutting and chisel edge as well as adhered workpiece material (Ti and/or Al) were found in tests performed using flood coolant.
- Uncoated and C7 coated WC drills outperformed PCD and CVD diamond coated tools in terms of tool life and with no appreciable improvement in hole quality characteristics.
- Thrust force and torque were found to be 3 - 5 times greater when cutting the Ti compared to the Al and CFRP even when flood coolant was used.
- The use of high pressure through spindle coolant (70 bar) is essential when drilling multilayer metallic/composite stacks to ensure sufficient transport of lubrication/coolant to the bottom of the stack in addition to aiding chip evacuation.
- Table 5.2 details the recommended/preferred operating conditions for one shot drilling of Ti/CFRP/Al stacks.

| Parameter | Value |
|---|---|
| Cutting speed | 20 m/min for Ti<br>40 m/min for CFRP and Al |
| Feed rate | 0.05 – 0.1 mm/rev |
| Tool coating | Uncoated or C7 coated WC |
| Cutting environment | High pressure through spindle flood coolant (70 bar) |
| Stack sequence | Ti/CFRP/Al |
| **Expected tool life** | **300 holes in 30 mm thick stacks** |

Table 5.2: List of preferred operating parameters for drilling multilayer stacks

# 6. RECOMMENDATIONS FOR FUTURE WORK

A list of publications stemming from the project is shown in Appendix F, however a number of areas were highlighted during the research which warrants further investigation. These include:

- Investigation of the use of small diameter PCD drills to improve productivity and performance when machining CFRP.
- Measurement of induced cutting temperature when cutting dissimilar multilayer stacks (implanted thermocouple).
- Further design development of PCD drills to accommodate the successful drilling of Ti/CFRP/Al stacks.
- Investigation of scale effects through correlation of output measures at the macro-meso-micro levels when drilling FRPs.
- Further analysis relating to the fundamentals of step drill engagement when drilling small diameter holes in CFRP.
- Evaluation of vibration assisted drilling of Ti/CFRP/Al stacks in order to improve chip evacuation / formation and consequently enhance productivity and surface finish/integrity.
- Use of finite element modelling (FEM) to simulate the drilling of CFRP and multilayer stack workpiece materials.
- Analysis of different cost elements involved when drilling CFRP and multilayer stacks.

# REFERENCES


1. Herakovich, C., Mechanics of fibrous composites. 1998, New York: John Wiley & Sons, Inc., ISBN: 0471106364
2. Teti, R., Machining of composite materials. Annals of the CIRP, 2002. 51(2): p. 611-634, ISSN: 0007-8506.
3. Peters, S. T., Introduction, composite basic and road map, in Handbook of Composites, S. T. Peters, Editor. 1998, Chapman & Hall: London. p. 1-20, ISBN: 0412540207.
4. William D. Callister, J., Fundamentals of materials science and engineering. 5th Edition ed. 2000: Wiley, ISBN: 047139551X.
5. Anon, An introduction to advanced composites and prepreg technology. 2009, The centre of composite technology, Advanced composites group Ltd. p. 1-26.
6. Burton, R., Of developing importance, in Aerospace manufacturing. 2008, MIT publishing limited: Kent, UK. p. 21-22.
7. Calder, N., Advances Composites Applications, in Aerospace Manufacturing. 2008, MIT Publishing Limited: Kent, UK. p. 19-20.
8. Herbeck, L., Wilmes, H., Kolesnikov, B. and Kleineberg, M., Technology and design development for a CFRP fuselage. SAMPLE Europe 2003, 2003,
9. Kaddick, C., Stur, S. and Hipp, E., Mechanical simulation of composite hip stems. Medical Engineering & Physics, 1997. 19(5): p. 431-439, ISSN: 1350-4533.
10. Soutis, C., Carbon fiber reinforced plastics in aircraft construction. Materials Science and Engineering A, 2005. 412(1-2): p. 171-176, ISSN: 0921-5093.
11. Aspinwall, D. K. and Soo, S. L., Keeping pace with composites. Metal Working Production, 2007. 151(2): p. 42-43, ISSN: 0026-1033.
12. Sheikh-Ahmed, J. Y., Machining of polymer composites. 2009, New York: Springer, ISBN: 9780387355399.
13. Anon, Sky high success for CVD diamond coated tools. Industrial Diamond Review, 2007(3): p. 69-70, ISSN: 0019-8145.
14. Garrick, R., Drilling advanced aircraft structures with PCD (Poly-crystalline diamond) drills. SAE International, 2007. ATC-18,
15. Samant, A. N. and Dahotre, N. B., Laser machining of structural ceramics--A review. Journal of the European Ceramic Society, 2009. 29(6): p. 969-993, ISSN: 0955-2219.
16. Reinhart, T. J., Overview of composite materials, in Handbook of Composites, S. T. Peters, Editor. 1998, Chapman & Hall: London. p. 21-26, ISBN: 0412540207.
17. Clements, L., Organic fibers, in Handbook of Composites, S. T. Peters, Editor. 1998, Chapman & Hall: London. p. 201-209, ISBN: 0412540207.
18. Chung, D. D. L., Carbon Fiber Composites. 1994, Newton: Butterworth-Heinemann. 215, ISBN: 0750691697
19. Lafdi, K. and Wright, M., Carbon fibres, in Handbook of Composites, S. T. Peters, Editor. 1998, Chapman & Hall: London. p. 169-186, ISBN: 0412540207.
20. Capello, E., Langella, A., Nele, L., Paoletti, A., Santo, L. and Tagliaferri, V., Drilling polymeric matrix composites, in Machining: Fundamentals and recent advances, J. P. Davim, Editor. 2008, Springer: London. p. 167-194, ISBN: 9781848002128.
21. Daniel, I. M. and Ishai, O., Engineering mechanics of composite materials. 2nd ed. 2006, New York: Oxford University Press, ISBN: 019515097X

22. Shim, H., Seo, M. and Park, S., Thermal conductivity and mechanical properties of various cross-section types carbon fiber-reinforced composites. Journal of materials science, 2002. 37(9): p. 1881-1885, ISSN: 0022-2461.
23. Osha, Polymer matrix materials: Advanced composites, in OSHA technical manual. 2010, Occupational safety and health administration (OSHA).
24. Anon, Safety data sheet for SL-2 ComfortWalk Prepreg. 2006, Otto Bock Health Care: Minneapolis.
25. Klocke, F., Koenig, W., Wuertz, C. and Dietz, C., Environmental effects and safety in machining fibrous composites, in Machining of Ceramics and Composites, S. Jahanmir, M. Ramulu and P. Koshy, Editors. 1999, CRC Press. p. 411-425, ISBN: 082470178X.
26. Fletcher, D., Analysis of carbon fibres chips produced from drilling process. 2007, Health and Safety Laboratory: Derbyshire.
27. Ezugwu, E. O. and Wang, Z. M., Titanium alloys and their machinability--a review. Journal of Materials Processing Technology, 1997. 68(3): p. 262-274, ISSN: 0924-0136.
28. Lütjering, G. and Williams, J., Titanium. 2nd ed, ed. B. Derby. 2007, New York: Springer, ISBN: 9783540713975.
29. Trent, E. and Wright, P., Metal cutting. 4th ed. 2001, Boston: Butterworth-Heinemann. 464, ISBN: 075067069X.
30. Polmear, I., Light alloys: Metallurgy of the light metals. 3rd ed. 1995, London: Arnold,Hodder Headline PLC, ISBN: 0340700777
31. Ezugwu, E. O., Bonney, J. and Yamane, Y., An overview of the machinability of aeroengine alloys. Journal of Materials Processing Technology, 2003. 134(2): p. 233-253, ISSN: 0924-0136.
32. Anon, ASM Materials properties handbook - Titanium alloys. 4th ed, ed. R. Boyer, G. Welsch and E. Collings. 2007: USA: ASM International, ISBN: 0871704811.
33. Boyer, R. R., An overview on the use of titanium in the aerospace industry. Materials Science and Engineering: A, 1996. 213 (1-2): p. 103-114, ISSN: 0921-5093.
34. Anon, metals reference book. 3rd ed. ASM International, ed. M. Bauccio. 1993, USA, ISBN: 0871704781.
35. Yamada, M., An overview on the development of titanium alloys for non-aerospace application in Japan. Materials Science and Engineering: A, 1996. 213(1-2): p. 8-15, ISSN: 0921-5093.
36. Niinomi, M., Recent research and development in titanium alloys for biomedical applications and healthcare goods. Science and Technology of Advanced Materials, 2003. 4(5): p. 445-454, ISSN: 1468-6996.
37. Williams, J. C. and Starke, E. A., Progress in structural materials for aerospace systems. Acta Materialia, 2003. 51(19): p. 5775-5799, ISSN: 1359-6454.
38. Konig, W., Wulf, C., Grass, P. and Willerscheid, H., Machining of fibre reinforced plastics. Annals of the CIRP, 1985. 34(2): p. 537-548, ISSN: 0007-8506.
39. Bhatnagar, N., Ramakrishnan, N., Naik, N. K. and Komanduri, R., On the machining of fiber reinforced plastic (FRP) composite laminates. International Journal of Machine Tools and Manufacture, 1995. 35(5): p. 701-716, ISSN: 0890-6955.
40. Mkaddem, A., Demirci, I. and Mansori, M. E., A micro-macro combined approach using FEM for modelling of machining of FRP composites: Cutting forces analysis. Composites Science and Technology, 2008. 68(15-16): p. 3123-3127, ISSN: 0266-3538.
41. Ferreira, J. R., Coppini, N. L. and Miranda, G. W. A., Machining optimisation in carbon fibre reinforced composite materials. Journal of Materials Processing Technology, 1999. 92-93: p. 135-140, ISSN: 0924-0136.

42. Rao, G. V. G., Mahajan, P. and Bhatnagar, N., Micro-mechanical modeling of machining of FRP composites - Cutting force analysis. Composites Science and Technology, 2007. 67(3-4): p. 579-593, ISSN: 0266-3538.
43. Konig, W. and Grass, P., quality definition and assessment in drilling of fibre reinforced thermosets. Annals of the CIRP, 1989. 38(1): p. 119-124, ISSN: 0007-8506.
44. Singh, I., Bhatnagar, N. and Viswanath, P., Drilling of uni-directional glass fiber reinforced plastics: Experimental and finite element study. Materials & Design, 2008. 29(2): p. 546-553, ISSN: 0261-3069.
45. Davim, J. P. and Reis, P., Damage and dimensional precision on milling carbon fiber-reinforced plastics using design experiments. Journal of Materials Processing Technology, 2005. 160(2): p. 160-167, ISSN: 0924-0136.
46. Rahman, M., Ramakrishna, S., Prakash, J. R. S. and Tan, D. C. G., Machinability study of carbon fiber reinforced composite. Journal of Materials Processing Technology, 1999. 89-90: p. 292-297, ISSN: 0924-0136.
47. Velayudham, A. and Krishnamurthy, R., Effect of point geometry and their influence on thrust and delamination in drilling of polymeric composites. Journal of Materials Processing Technology, 2007. 185(1-3): p. 204-209, ISSN: 0924-0136.
48. Wang, D. H., Ramulu, M. and Arola, D., Orthogonal cutting mechanisms of graphite/epoxy composite. Part I: unidirectional laminate. International Journal of Machine Tools and Manufacture, 1995. 35(12): p. 1623-1638, ISSN: 0890-6955.
49. Wang, X. M. and Zhang, L. C., An experimental investigation into the orthogonal cutting of unidirectional fibre reinforced plastics. International Journal of Machine Tools and Manufacture, 2003. 43(10): p. 1015-1022, ISSN: 0890-6955.
50. Arola, D., Ramulu, M. and Wang, D. H., Chip formation in orthogonal trimming of graphite/epoxy composite. Composites Part A: Applied Science and Manufacturing, 1996. 27(2): p. 121-133, ISSN: 1359-835X.
51. Nayak, D., A Bhatnagar, N. and A Mahajan, P., Machining studies of uni-directional glass fiber reinforced plastic (UD-GFRP) composites Part 1: Effect of geometrical and process parameters. Machining Science and Technology, 2005. 9: p. 481-501, ISSN: 1532-2483.
52. Hocheng, H. and Puw, H. Y., On drilling characteristics of fiber-reinforced thermoset and thermoplastics. International Journal of Machine Tools and Manufacture, 1992. 32(4): p. 583-592, ISSN: 0890-6955.
53. Kalpakjian, S. and Schmid, S., Manufacturing Engineering and Technology. 5th Edition ed. 2006: Prentice Hall, ISBN: 0201361310
54. Youssef, H. and El-Hofy, H., Machining technology: Machine tools and operations 1st ed. 2008, New York: CRC Press. 672, ISBN: 9781420043396.
55. Bradley, S., Personal communication. GKN Aerospace, 2010,
56. Zhang, L. B., Wang, L. J. and Liu, X. Y., A mechanical model for predicting critical thrust forces in drilling composite laminates. Proceedings of the Institution of Mechanical Engineers, Part B: Journal of Engineering Manufacture, 2001. 215(2): p. 135-146, ISSN: 0954-4054.
57. Abrate, S. and Walton, D. A., Machining of composite materials. Part I: Traditional methods. Composites Manufacturing, 1992. 3(2): p. 75-83, ISSN: 0956-7143.
58. Abrao, A. M., Faria, P. E., Rubio, J. C. C., Reis, P. and Davim, J. P., Drilling of fiber reinforced plastics: A review. Journal of Materials Processing Technology, 2007. 186(1-3): p. 1-7, ISSN: 0924-0136.
59. Malhotra, S. K., Some studies on drilling of fibrous composites. Journal of Materials Processing Technology, 1990. 24: p. 291-300, ISSN: 0924-0136.

60. Zhang, H., Chen, W., Chen, D. and Zhang, L., Assessment of the exit defects in carbon fibre-reinforced plastic plates caused by drilling. Key Engineering Materials, 2001. 196: p. 43-52, ISSN: 1662-9795.
61. Chen, W. C., Some experimental investigations in the drilling of carbon fiber-reinforced plastic (CFRP) composite laminates. International Journal of Machine Tools and Manufacture, 1997. 37(8): p. 1097-1108, ISSN: 0890-6955.
62. Davim, J. P. and Reis, P., Drilling carbon fiber reinforced plastics manufactured by autoclave-experimental and statistical study. Materials and Design, 2003. 24(5): p. 315-324, ISSN: 0261-3069.
63. Davim, J. P. and Reis, P., Study of delamination in drilling carbon fiber reinforced plastics (CFRP) using design experiments. Composite Structures, 2003. 59(4): p. 481-487, ISSN: 0263-8223.
64. Davim, J. P., Rubio, J. C. and Abrao, A. M., A novel approach based on digital image analysis to evaluate the delamination factor after drilling composite laminates. Composites Science and Technology, 2007. 67(9): p. 1939-1945, ISSN: 0266-3538.
65. Enemuoh, E. U., El-Gizawy, A. S. and Chukwujekwu Okafor, A., An approach for development of damage-free drilling of carbon fiber reinforced thermosets. International Journal of Machine Tools and Manufacture, 2001. 41(12): p. 1795-1814, ISSN: 0890-6955.
66. Gaitonde, V. N., Karnik, S. R., Rubio, J. C., Correia, A. E., Abrão, A. M. and Davim, J. P., Analysis of parametric influence on delamination in high-speed drilling of carbon fiber reinforced plastic composites. Journal of Materials Processing Technology, 2008. 203(1-3): p. 431-438, ISSN: 0924-0136.
67. Gilchrist, M. D. and Svensson, N., A fractographic analysis of delamination within multidirectional carbon/epoxy laminates. Composites Science and Technology, 1995. 55(2): p. 195-207, ISSN: 0266-3538.
68. Ho-Cheng, H. and Dharan, C. K. H., Delamination during drilling in composite laminates. Journal of engineering for industry, 1990. 112(3): p. 236-239, ISSN: 0022-1817.
69. Hocheng, H. and Tsao, C. C., Effects of special drill bits on drilling-induced delamination of composite materials. International Journal of Machine Tools and Manufacture, 2006. 46(12-13): p. 1403-1416, ISSN: 0890-6955.
70. Lin, S. C. and Chen, I. K., Drilling carbon fiber-reinforced composite material at high speed. Wear, 1996. 194(1-2): p. 156-162, ISSN: 0043-1648.
71. Stone, R. and Krishnamurthy, K., A neural network thrust force controller to minimize delamination during drilling of graphite-epoxy laminates. International Journal of Machine Tools and Manufacture, 1996. 36(9): p. 985-1003, ISSN: 0890-6955.
72. Tsao, C. C., Effect of deviation on delamination by saw drill. International Journal of Machine Tools and Manufacture, 2007. 47(7-8): p. 1132-1138, ISSN: 0890-6955.
73. Tsao, C. C. and Hocheng, H., Taguchi analysis of delamination associated with various drill bits in drilling of composite material. International Journal of Machine Tools and Manufacture, 2004. 44(10): p. 1085-1090, ISSN: 0890-6955.
74. Tsao, C. C. and Hocheng, H., Computerized tomography and C-Scan for measuring delamination in the drilling of composite materials using various. International Journal of Machine Tools and Manufacture, 2005. 45(11): p. 1282-1287, ISSN: 0890-6955.
75. Karnik, S. R., Gaitonde, V. N., Rubio, J. C., Correia, A. E., Abrão, A. M. and Davim, J. P., Delamination analysis in high speed drilling of carbon fiber reinforced plastics (CFRP) using artificial neural network model. Materials & Design, 2008. 29(9): p. 1768-1776, ISSN: 0261-3069.

76. Marques, A. T., Durão, L. M., Magalhães, A. G., Silva, J. F. and Tavares, J. M. R. S., Delamination analysis of carbon fibre reinforced laminates: Evaluation of a special step drill. Composites Science and Technology, 2009. 69(14): p. 2376-2382, ISSN: 0266-3538.
77. Park, K., Choi, J. and Lee, D., Delamination-Free and High Efficiency Drilling of Carbon Fiber Reinforced Plastics. Journal of Composite Materials, 1995. 29: p. 1988 - 2002, ISSN: 1530-793X.
78. Rubio, J., Abrao, A., Faria, P., Correia, A. and Davim, J., Delamination in High Speed Drilling of Carbon Fiber Reinforced Plastic (CFRP). Journal of Composite Materials, 2008. 42: p. 1523-1532, ISSN: 1530-793X.
79. Tsao, C. C. and Hocheng, H., Effect of tool wear on delamination in drilling composite materials. International Journal of Mechanical Sciences, 2007. 49(8): p. 983-988, ISSN: 0020-7403.
80. Rawat, S. and Attia, H., Characterization of the dry high speed drilling process of woven composites using Machinability Maps approach. CIRP Annals - Manufacturing Technology, 2009. 58(1): p. 105-108, ISSN: 0007-8506.
81. Persson, E., Eriksson, I. and Zackrisson, L., Effects of hole machining defects on strength and fatigue life of composite laminates. Composites Part A: Applied Science and Manufacturing, 1997. 28(2): p. 141-151, ISSN: 1359-835X.
82. Tsao, C. C., Investigation into the effects of drilling parameters on delamination by various step-core drills. Journal of Materials Processing Technology, 2008. 206(1-3): p. 405-411, ISSN: 0924-0136.
83. Tsao, C. C., Experimental study of drilling composite materials with step-core drill. Materials & Design, 2008. 29(9): p. 1740-1744, ISSN: 0261-3069.
84. Tsao, C. C. and Hocheng, H., Evaluation of thrust force and surface roughness in drilling composite material using Taguchi analysis and neural network. Journal of Materials Processing Technology, 2008. 203(1-3): p. 342-348, ISSN: 0924-0136.
85. Durão, L. M. P., Gonçalves, D. J. S., Tavares, J. M. R. S., De Albuquerque, V. H. C., Aguiar Vieira, A. and Torres Marques, A., Drilling tool geometry evaluation for reinforced composite laminates. Composite Structures. 92(7): p. 1545-1550, ISSN: 0263-8223.
86. Wern, C. W., Ramulu, M. and Colligan, K., A study of the surface texture of composite drilled holes. Journal of Materials Processing Technology, 1993. 37(1-4): p. 373-389, ISSN: 0924-0136.
87. Won, M. S. and Dharan, C. K. H., Drilling of aramid and carbon fiber polymer composites. Journal of Manufacturing Science and Engineering, Transactions of the ASME, 2002. 124(4): p. 778-783, ISSN: 10871357.
88. Jain, S. and Yang, D. C. H., Delamination-free drilling of composite laminates. Journal of Engineering for industry, Transactions of the ASME, 1994. 116: p. 475-481, ISSN: 0022-0817.
89. Fernandes, M. and Cook, C., Drilling of carbon composites using a one shot drill bit. Part I: Five stage representation of drilling and factors. International Journal of Machine Tools and Manufacture, 2006. 46(1): p. 70-75, ISSN: 0890-6955.
90. Jain, S. and Yang, D. C. H., Effects of Feedrate and Chisel Edge on Delamination in Composites Drilling. Journal of Engineering for industry, Transactions of the ASME, 1993. 115: p. 398-405, ISSN: 0022-0817.
91. Tsao, C. C. and Hocheng, H., Parametric study on thrust force of core drill. Journal of Materials Processing Technology, 2007. 192-193: p. 37-40, ISSN: 0924-0136.
92. Wang, X., Wang, L. J. and Tao, J. P., Investigation on thrust in vibration drilling of fiber-reinforced plastics. Journal of Materials Processing Technology, 2004. 148(2): p. 239-244, ISSN: 0924-0136.

93. Murphy, C., Byrne, G. and Gilchrist, M. D., The performance of coated tungsten carbide drills when machining carbon fibre-reinforced epoxy composite materials. Proceedings of the Institution of Mechanical Engineers, Part B: Journal of Engineering Manufacture, 2002. 216(2): p. 143-152, ISSN: 0954-4054.
94. Won, M. S. and Dharan, C. K. H., Chisel edge and pilot hole effects in drilling composite laminates. Journal of Manufacturing Science and Engineering, Transactions of the ASME, 2002. 124(2): p. 242-247, ISSN: 10871357.
95. Tsao, C. C. and Hocheng, H., Effects of exit back-up on delamination in drilling composite materials using a saw drill and a core drill. International Journal of Machine Tools and Manufacture, 2005. 45(11): p. 1261-1270, ISSN: 0890-6955.
96. Arul, S., Vijayaraghavan, L., Malhotra, S. K. and Krishnamurthy, R., The effect of vibratory drilling on hole quality in polymeric composites. International Journal of Machine Tools and Manufacture, 2006. 46(3-4): p. 252-259, ISSN: 0890-6955.
97. Piquet, R., Ferret, B., Lachaud, F. and Swider, P., Experimental analysis of drilling damage in thin carbon/epoxy plate using special drills. Composites Part A: Applied Science and Manufacturing, 2000. 31(10): p. 1107-1115, ISSN: 1359-835X.
98. Shaw, M., Metal cutting principles. 1st ed. 1997, New York: Oxford University Press Inc. 594, ISBN: 0198590202.
99. Faraz, A., Biermann, D. and Weinert, K., Cutting edge rounding: An innovative tool wear criterion in drilling CFRP composite laminates. International Journal of Machine Tools and Manufacture, 2009. 49(15): p. 1185-1196, ISSN: 0890-6955.
100. Hocheng, H. and Tsao, C. C., The path towards delamination-free drilling of composite materials. Journal of Materials Processing Technology, 2005. 167(2-3): p. 251-264, ISSN: 0924-0136.
101. Hong, S. Y. and Ding, Y., Cooling approaches and cutting temperatures in cryogenic machining of Ti-6Al-4V. International Journal of Machine Tools and Manufacture, 2001. 41(10): p. 1417-1437, ISSN: 0890-6955.
102. Kitagawa, T., Kubo, A. and Maekawa, K., Temperature and wear of cutting tools in high-speed machining of Inconel 718 and Ti-6Al-6V-2Sn. Wear, 1997. 202(2): p. 142-148, ISSN: 0043-1648.
103. Masuda, M., Kuroshima, Y. and Chujo, Y., Failure of tungsten carbide-cobalt alloy tools in machining of carbon materials. Wear, 1993. 169(2): p. 135-140, ISSN: 0043-1648.
104. Aoyama, E., Inoue, H., Hirogaki, T., Nobe, H., Kitahara, Y. and Katayama, T., Study on small diameter drilling in GFRP. Composite Structures, 1995. 32(1-4): p. 567-573, ISSN: 0263-8223.
105. Ogawa, K., Aoyama, E., Inoue, H., Hirogaki, T., Nobe, H., Kitahara, Y., Katayama, T. and Gunjima, M., Investigation on cutting mechanism in small diameter drilling for GFRP (thrust force and surface roughness at drilled hole wall). Composite Structures, 1997. 38(1-4): p. 343-350, ISSN: 0263-8223.
106. Inoue, H., Aoyama, E., Hirogaki, T., Ogawa, K., Matushita, H., Kitahara, Y. and Katayama, T., Influence of tool wear on internal damage in small diameter drilling in GFRP. Composite Structures, 1997. 39(1-2): p. 55-62, ISSN: 0263-8223.
107. Aoyama, E., Nobe, H. and Hirogaki, T., Drilled hole damage of small diameter drilling in printed wiring board. Journal of Materials Processing Technology, 2001. 118(1-3): p. 436-441, ISSN: 0924-0136.
108. Shanmugam, D. K., Chen, F. L., Siores, E. and Brandt, M., Comparative study of jetting machining technologies over laser machining technology for cutting composite materials. Composite Structures, 2002. 57(1-4): p. 289-296, ISSN: 0263-8223.

109. Wang, J., A machinability study of polymer matrix composites using abrasive waterjet cutting technology. Journal of Materials Processing Technology, 1999. 94(1): p. 30-35, ISSN: 0924-0136.
110. Lemma, E., Chen, L., Siores, E. and Wang, J., Study of cutting fiber-reinforced composites by using abrasive water-jet with cutting head oscillation. Composite Structures, 2002. 57(1-4): p. 297-303, ISSN: 0263-8223.
111. Miller, D. S., Micromachining with abrasive waterjets. Journal of Materials Processing Technology, 2004. 149(1-3): p. 37-42, ISSN: 0924-0136.
112. Linbo, Z., Lijiang, W. and Xin, W., Study on vibration drilling of fiber reinforced plastics with hybrid variation parameters method. Composites Part A: Applied Science and Manufacturing, 2003. 34(3): p. 237-244, ISSN: 1359-835X.
113. Young, T. and O'driscoll, D., Impact of Nd-YAG laser drilled holes on the strength and stiffness of laminar flow carbon fibre reinforced composite panels. Composites Part A: Applied Science and Manufacturing, 2002. 33(1): p. 1-9, ISSN: 1359-835X.
114. Tagliaferri, V., Di Ilio, A. and Visconti, C., Laser cutting of fibre-reinforced polyesters. Composites, 1985. 16(4): p. 317-325, ISSN: 1359-835X.
115. Cenna, A. A. and Mathew, P., Analysis and prediction of laser cutting parameters of fibre reinforced plastics (FRP) composite materials. International Journal of Machine Tools and Manufacture, 2002. 42(1): p. 105, ISSN: 0890-6955.
116. Pan, C. T. and Hocheng, H., Evaluation of anisotropic thermal conductivity for unidirectional FRP in laser machining. Composites Part A: Applied Science and Manufacturing, 2001. 32(11): p. 1657-1667, ISSN: 1359-835X.
117. Lau, W. S., Yue, T. M., Lee, T. C. and Lee, W. B., Un-conventional machining of composite materials. Journal of Materials Processing Technology, 1995. 48(1-4): p. 199-205, ISSN: 0924-0136.
118. Pan, C. T. and Hocheng, H., The anisotropic heat-affected zone in the laser grooving of fiber-reinforced composite material. Journal of Materials Processing Technology, 1996. 62(1-3): p. 54-60, ISSN: 0924-0136.
119. Cheng, C. F., Tsui, Y. C. and Clyne, T. W., Application of a three-dimensional heat flow model to treat laser drilling of carbon fibre composites. Acta Materialia, 1998. 46(12): p. 4273-4285, ISSN: 1359-6454.
120. Cenna, A. A. and Mathew, P., Evaluation of cut quality of fibre-reinforced plastics - A review. International Journal of Machine Tools and Manufacture, 1997. 37(6): p. 723-736, ISSN: 0890-6955.
121. Rodden, W. S. O., Kudesia, S. S., Hand, D. P. and Jones, J. D. C., A comprehensive study of the long pulse Nd:YAG laser drilling of multi-layer carbon fibre composites. Optics Communications, 2002. 210(3-6): p. 319-328, ISSN: 0030-4018.
122. Hirogaki, T., Aoyama, E., Inoue, H., Ogawa, K., Maeda, S. and Katayama, T., Laser drilling of blind via holes in aramid and glass/epoxy composites for multi-layer printed wiring boards. Composites Part A: Applied Science and Manufacturing, 2001. 32(7): p. 963-968, ISSN: 1359-835X.
123. Hocheng, H. and Hsu, C. C., Preliminary study of ultrasonic drilling of fiber-reinforced plastics. Journal of Materials Processing Technology, 1995. 48(1-4): p. 255-266, ISSN: 0924-0136.
124. Masuzawa, T., State of the art of micromachining Annals of the CIRP, 2000. 49(2): p. 473-488, ISSN: 0007-8506.
125. Hocheng, H., Tai, N. H. and Liu, C. S., Assessment of ultrasonic drilling of C/SiC composite material. Composites Part A: Applied Science and Manufacturing, 2000. 31(2): p. 133-142, ISSN: 1359-835X.

126. Tsao, C. C. and Chen, W. C., Prediction of the location of delamination in the drilling of composite laminates. Journal of Materials Processing Technology, 1997. 70(1-3): p. 185-189, ISSN: 0924-0136.
127. Hocheng, H. and Tsao, C. C., Comprehensive analysis of delamination in drilling of composite materials with various drill bits. Journal of Materials Processing Technology, 2003. 140(1-3 SPEC.): p. 335-339, ISSN: 0924-0136.
128. Hocheng, H. and Tsao, C. C. Analysis of delamination in drilling composite materials using core-saw drill. in 7th International Conference on Progress of Machining Technology. 2004. p. 38-43.
129. Tsao, C. C. and Hocheng, H., The effect of chisel length and associated pilot hole on delamination when drilling composite materials. International Journal of Machine Tools and Manufacture, 2003. 43(11): p. 1087-1092, ISSN: 0890-6955.
130. Tsao, C. C. and Hocheng, H., Effect of eccentricity of twist drill and candle stick drill on delamination in drilling composite materials. International Journal of Machine Tools and Manufacture, 2005. 45(2): p. 125-130, ISSN: 0890-6955.
131. Fernandes, M. and Cook, C., Drilling of carbon composites using a one shot drill bit. Part II: empirical modeling of maximum thrust force. International Journal of Machine Tools and Manufacture, 2006. 46(1): p. 76-79, ISSN: 0890-6955.
132. Zitoune, R. and Collombet, F., Numerical prediction of the thrust force responsible of delamination during the drilling of the long-fibre composite structures. Composites Part A: Applied Science and Manufacturing, 2007. 38(3): p. 858-866, ISSN: 1359-835X.
133. Narutaki, N., Murakoshi, A., Motonishi, S. and Takeyama, H., Study on Machining of Titanium Alloys. CIRP Annals - Manufacturing Technology, 1983. 32(1): p. 65-69, ISSN: 0007-8506.
134. Rahman, M., Wong, Y. and Zareena, A., Machinability of Titanium Alloys. JSME International Journal Series C, 2003. 46 (Special Issue on Advanced Production Scheduling ): p. 107-115, ISSN: 1344-7653.
135. Freeman, R., The machining of titanium and some of its alloys, in Department of Industrial Metallurgy. 1974, University of Birmingham: Birmingham.
136. Nabhani, F., Machining of aerospace titanium alloys. Robotics and Computer-Integrated Manufacturing, 2001. 17(1-2): p. 99-106, ISSN: 0736-5845.
137. Sreejith, P. S. and Ngoi, B. K. A., Dry machining: Machining of the future. Journal of Materials Processing Technology, 2000. 101(1-3): p. 287-291, ISSN: 0924-0136.
138. Kamata, Y. and Obikawa, T., High speed MQL finish-turning of Inconel 718 with different coated tools. Journal of Materials Processing Technology, 2007. 192-193: p. 281-286, ISSN: 0924-0136.
139. Hua, J. and Shivpuri, R., Prediction of chip morphology and segmentation during the machining of titanium alloys. Journal of Materials Processing Technology, 2004. 150(1-2): p. 124-133, ISSN: 0924-0136.
140. Sun, S., Brandt, M. and Dargusch, M. S., Characteristics of cutting forces and chip formation in machining of titanium alloys. International Journal of Machine Tools and Manufacture, 2009. 49(7-8): p. 561-568, ISSN: 0890-6955.
141. Che-Haron, C. H. and Jawaid, A., The effect of machining on surface integrity of titanium alloy Ti-6% Al-4% V. Journal of Materials Processing Technology, 2005. 166(2): p. 188-192, ISSN: 0924-0136.
142. Ribeiro, M. V., Moreira, M. R. V. and Ferreira, J. R., Optimization of titanium alloy (6Al-4V) machining. Journal of Materials Processing Technology, 2003. 143-144: p. 458-463, ISSN: 0924-0136.

143. Cantero, J. L., Tardío, M. M., Canteli, J. A., Marcos, M. and Miguélez, M. H., Dry drilling of alloy Ti-6Al-4V. International Journal of Machine Tools and Manufacture, 2005. 45(11): p. 1246-1255, ISSN: 0890-6955.
144. Dornfeld, D. A., Kim, J. S., Dechow, H., Hewson, J. and Chen, L. J., Drilling Burr Formation in Titanium Alloy, Ti-6AI-4V. CIRP Annals - Manufacturing Technology, 1999. 48(1): p. 73-76, ISSN: 0007-8506.
145. Li, R., Hegde, P. and Shih, A. J., High-throughput drilling of titanium alloys. International Journal of Machine Tools and Manufacture, 2007. 47(1): p. 63-74, ISSN: 0890-6955.
146. Li, R. and Shih, A. J., Spiral point drill temperature and stress in high-throughput drilling of titanium. International Journal of Machine Tools and Manufacture, 2007. 47(12-13): p. 2005-2017, ISSN: 0890-6955.
147. Sharif, S. and Rahim, E. A., Performance of coated- and uncoated-carbide tools when drilling titanium alloy--Ti-6Al4V. Journal of Materials Processing Technology, 2007. 185(1-3): p. 72-76, ISSN: 0924-0136.
148. Zeilmann, R. P. and Weingaertner, W. L., Analysis of temperature during drilling of Ti6Al4V with minimal quantity of lubricant. Journal of Materials Processing Technology, 2006. 179(1-3): p. 124-127, ISSN: 0924-0136.
149. Rivero, A., Aramendi, G., Herranz, S. and López De Lacalle, L. N., An experimental investigation of the effect of coatings and cutting parameters on the dry drilling performance of aluminium alloys. The International Journal of Advanced Manufacturing Technology, 2006. 28(1-2): p. 1-11, ISSN: 0268-3768.
150. Kelly, J. F. and Cotterell, M. G., Minimal lubrication machining of aluminium alloys. Journal of Materials Processing Technology, 2002. 120(1-3): p. 327-334, ISSN: 0924-0136.
151. List, G., Nouari, M., Géhin, D., Gomez, S., Manaud, J. P., Le Petitcorps, Y. and Girot, F., Wear behaviour of cemented carbide tools in dry machining of aluminium alloy. Wear, 2005. 259(7-12): p. 1177-1189, ISSN: 0043-1648.
152. Nouari, M., List, G., Girot, F. and Géhin, D., Effect of machining parameters and coating on wear mechanisms in dry drilling of aluminium alloys. International Journal of Machine Tools and Manufacture, 2005. 45(12-13): p. 1436-1442, ISSN: 0890-6955.
153. Bhowmick, S. and Alpas, A. T., The performance of hydrogenated and non-hydrogenated diamond-like carbon tool coatings during the dry drilling of 319 Al. International Journal of Machine Tools and Manufacture, 2008. 48(7-8): p. 802-814, ISSN: 0890-6955.
154. Bhowmick, S. and Alpas, A. T., Minimum quantity lubrication drilling of aluminium-silicon alloys in water using diamond-like carbon coated drills. International Journal of Machine Tools and Manufacture, 2008. 48(12-13): p. 1429-1443, ISSN: 0890-6955.
155. Hanyu, H., Kamiya, S., Murakami, Y. and Kondoh, Y., The improvement of cutting performance in semi-dry condition by the combination of DLC coating and CVD smooth surface diamond coating. Surface and Coatings Technology, 2005. 200(1-4): p. 1137-1141, ISSN: 0257-8972.
156. Batzer, S. A., Haan, D. M., Rao, P. D., Olson, W. W. and Sutherland, J. W., Chip morphology and hole surface texture in the drilling of cast Aluminum alloys. Journal of Materials Processing Technology, 1998. 79(1-3): p. 72-78, ISSN: 0924-0136.
157. Tang, Z. T., Liu, Z. Q., Pan, Y. Z., Wan, Y. and Ai, X., The influence of tool flank wear on residual stresses induced by milling aluminum alloy. Journal of Materials Processing Technology, 2009. 209(9): p. 4502-4508, ISSN: 0924-0136.
158. Kim, D. and Ramulu, M., Drilling process optimization for graphite/bismaleimide-titanium alloy stacks. Composite Structures, 2004. 63(1): p. 101-114, ISSN: 0263-8223.
159. Ramulu, M., Branson, T. and Kim, D., A study on the drilling of composite and titanium stacks. Composite Structures, 2001. 54(1): p. 67-77, ISSN: 0263-8223.

160. Kim, D. and Ramulu, M., Study on the Drilling of Titanium/Graphite Hybrid Composites. Journal of Engineering Materials and Technology, 2007. 129(3): p. 390-396, ISSN: 1528-8889.
161. Zitoune, R., Krishnaraj, V. and Collombet, F., Study of drilling of composite material and aluminium stack. Composite Structures, 2010. 92(5): p. 1246-1255, ISSN: 0263-8223.
162. Dawson, S., Personal communication. 2010, Unimerco Ltd.
163. Brinksmeier, E. and Janssen, R., Drilling of Multi-Layer Composite Materials consisting of Carbon Fiber Reinforced Plastics (CFRP), Titanium and Aluminum Alloys. CIRP Annals - Manufacturing Technology, 2002. 51(1): p. 87-90, ISSN: 0007-8506.
164. Park, I. W. and Dornfeld, D. A., A Study of Burr Formation Processes Using the Finite Element Method: Part II-The Influences of Exit Angle, Rake Angle, and Backup Material on Burr Formation Processes. Journal of Engineering Materials and Technology, 2000. 122(2): p. 229-237, ISSN: 1528-8889.
165. Mills, B., Recent developments in cutting tool materials. Journal of Materials Processing Technology, 1996. 56(1-4): p. 16-23, ISSN: 0924-0136.
166. Heath, P. J., Developments in applications of PCD tooling. Journal of Materials Processing Technology, 2001. 116(1): p. 31-38, ISSN: 0924-0136.
167. Brookes, K., World dictionary and handbook of hardmetals and hard materials. 6th ed. 1996, Hertfordshire: International carbide data. 750, ISBN: 0950899542.
168. May, P. W., CVD diamond: a new technology for the future? Endeavour, 1995. 19(3): p. 101-106, ISSN: 0160-9327.
169. Davim, J. P. and Mata, F., Chemical vapour deposition (CVD) diamond coated tools performance in machining of PEEK composites. Materials & Design, 2008. 29(8): p. 1568-1574, ISSN: 0261-3069.
170. Köpf, A., Feistritzer, S. and Udier, K., Diamond coated cutting tools for machining of non-ferrous metals and fibre reinforced polymers. International Journal of Refractory Metals and Hard Materials, 2006. 24(5): p. 354-359, ISSN: 0263-4368.
171. Gäbler, J., Schäfer, L. and Westermann, H., Chemical vapour deposition diamond coated microtools for grinding, milling and drilling. Diamond and Related Materials. 9(3-6): p. 921-924, ISSN: 0925-9635.
172. Miyake, S., Tribological properties of hard carbon films: extremely low friction mechanism of amorphous hydrogenated carbon films and amorphous hydrogenated SiC films in vacuum. Surface and Coatings Technology, 1992. 54-55(Part 2): p. 563-569, ISSN: 0257-8972.
173. Vandevelde, T. C. S., Vandierendonck, K., Van Stappen, M., Du Mong, W. and Perremans, P., Cutting applications of DLC, hard carbon and diamond films. Surface and Coatings Technology, 1999. 113(1-2): p. 80-85, ISSN: 0257-8972.
174. Jiang, J. and Arnell, R. D., The effect of substrate surface roughness on the wear of DLC coatings. Wear, 2000. 239(1): p. 1-9, ISSN: 0043-1648.
175. Monaghan, D. P., Teer, D. G., Logan, P. A., Efeoglu, I. and Arnell, R. D., Deposition of wear resistant coatings based on diamond like carbon by unbalanced magnetron sputtering. Surface and Coatings Technology, 1993. 60(1-3): p. 525-530, ISSN: 0257-8972.
176. Kinoshita, H., Ippei, I., Sakai, H. and Ohmae, N., Synthesis and mechanical properties of carbon nanotube/diamond-like carbon composite films. Diamond and Related Materials, 2007. 16(11): p. 1940-1944, ISSN: 0925-9635.
177. Smith, G., Cutting Tool Technology 2008, London: Springer. 25, ISBN: 9781848002043.
178. Coelho, R. T., Yamada, S., Aspinwall, D. K. and Wise, M. L. H., The application of polycrystalline diamond (PCD) tool materials when drilling and reaming aluminium based

alloys including MMC. International Journal of Machine Tools and Manufacture, 1995. 35(5): p. 761-774, 0890-6955.
179. Schouwenaars, R., Jacobo, V. H. and Ortiz, A., Transition from normal to severe wear in PCD during high-speed cutting of a ductile material. International Journal of Refractory Metals and Hard Materials, 2009. 27(2): p. 403-408, ISSN: 0263-4368.
180. Ramulu, M., Faridinia, M., Garbini, J. and Jorgensen, J., Machining of Graphite/Epoxy Composite Materials with Polycrystalline Diamond (PCD) Tools. Journal of engineering materials and technology, Transactions of the ASME, 1991. 113: p. 430-436, ISSN: 10871357.
181. Ding, X., Liew, W. Y. H. and Liu, X. D., Evaluation of machining performance of MMC with PCBN and PCD tools. Wear, 2005. 259(7-12): p. 1225-1234, ISSN: 0043-1648.
182. Montgomery, D. C., Design and Analysis of Experiments. 6th ed. 2005, New York: Wiley, ISBN: 047148735X
183. Ross, P. J., Taguchi Techniques for quality Engineering. 2nd edition ed. 1996, New York: McGraw-Hill, ISBN: 0070539588.
184. Pignatiello, J. and Ramberg, J., Top ten triumphs and tragedies of Genichi Taguchi. Quality engineering, 1991-92. 4(2): p. 211-225, ISSN: 1532-4222.
185. Taguchi, G., Taguchi Quality Engineering 2005, New Jersey: Wiley, ISBN: 0471413348.
186. Lin, S. C. and Ting, C. J., Tool wear monitoring in drilling using force signals. Wear, 1995. 180(1-2): p. 53-60, ISSN: 0043-1648.
187. Sharman, A. R. C., Amarasinghe, A. and Ridgway, K., Tool life and surface integrity aspects when drilling and hole making in Inconel 718. Journal of Materials Processing Technology, 2008. 200 (1-3): p. 424-432, ISSN: 0924-0136.

# APPENDIX A

## Industrial collaborator's contact details

# APPENDIX B

## Manufacturing procedure for CFRP composite part

The fabrication of a CFRP composite part begins by grouping individual fibre filaments to form a tow. A group of tows are then collected to form a roving (optional for filament winding to produce weave fabric). Tows are then combined with the resin (retaining all fibres in the same direction) to form a unidirectional prepreg tape (prepregging). Prepreg tapes are typically stored in the freezers for a finite shelf life. UD prepreg tapes are then trimmed and stacked to form the final composite laminate [12]. With reference to CFRP composites in particular, the fabrication process typically comprises formulation, prepregging, laying up or filament winding, vacuum bagging, autoclave or oven curing and post cure (optional).

1. **Formulation:** is the operation of mixing the resin, curing agent and other elements together. Most thermosets are delivered in liquid form where cross-linking and solidification take place after the addition solidification/cross-linking agents. This step typically takes between few hours to several days depending on the type of the thermoset and corresponding agents. If the thermosets are delivered partially solid, they are normally stored for a limited shelf life at -20$^{o}$C.
2. **Prepregging:** is the process of impregnating a blend of resin and curing agent (hardener) into the reinforcing fibres which form the prepregs. Thus, prepreg is an abbreviation for pre-impregnated layer of a blend of resin mix (resin and hardener) and fibres. The suppliers for these materials are commercially known as prepreggers (e.g. Toray, Hexcel, Cytec, Advanced composite group, etc.). Each of them formulates their own resin blend which discriminates the available commercial resin systems. The prepregs can be fabricated in the form of unidirectional tape, weave pattern fabrics, or roving as shown in Figure B-1. The prepregs are usually cured in order to be partially consolidated for handling and storage in a freezer. Typically, unidirectional tapes and woven fabric are used for the manual or automatic lay-up process while the roving fabrics are used for the filament winding to produce cylinders and tubes.

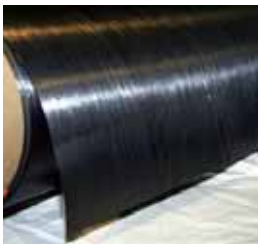
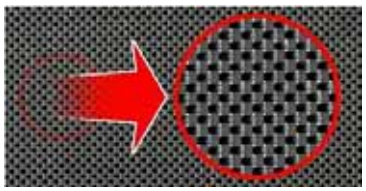


Unidirectional tape Weave fabric Roving

Figure B-1: Different forms of fibre prepregs

3. **Lay-up process:** is the process where the prepregs are stacked to form a composite laminate. Manual or automatic laying-up can be employed, however only manual lay-up will be discussed in the thesis because of its relevance to the workpiece tested.

   Steps for the lay-up process:

a) Prepreg rolls should be removed from the freezer and allowed to thaw with the polyethylene bag. This typically takes a few hours for the 20 linear metre roll extracted from -18 $^{o}$C freezer.

b) The prepregs are trimmed into the required shape in addition to other various material layers which are used in the vacuum bagging process. Glass scrim (optional layer for aerospace applications), is used to prevent galvanic corrosion (if aluminium fittings are used) as well as a method of minimising the effect of drill breakout. The nylon peel ply layer can be left on the composite laminate to reduce the risk of breakout during machining processes and also helps to keep the surface clean if secondary bonding is to take place. Perforated film is to regulate the flow of the excess resin from the part into the bleeder layer. The bleeder material absorbs and retains excess resin drawn from composite part while the release film prevents resin from crossing into the breather material. Breather layer (same material as bleeder) is used to enable the vacuum to uniformly pass and distribute through the fabric and ensure consistent and even pressure over the entire laminate. Finally, cutting the vacuum bag material oversize in order to cover the entire mould and also protects the component at the curing process in the autoclave.

c) The laying up process begins with putting a release film on a wood or carbon mould followed by prepregs, glass scrim, peel ply, perforated film, bleeder, release film, breather, and finally the vacuum bag. Prepregs are laid up on the mould in accordance with design instructions. Every 3 - 4 plies, the prepregs should be debulked by applying a vacuum in order to pull out bubbles and air gaps between the prepregs and to ensure that the laminate matches the mould shape.

d) The mould edges are also covered with pressure sensitive tape and sealing tape in order to seal the vacuum bag with the mould surface. The layup product is subsequently placed under vacuum (750 - 980 mbar) for 5 – 10 minutes in order to release air and compress the lay-up laminate. Vacuum should be checked using gauges positioned on different locations on the vacuum bag to ensure even distribution.

4. **Curing process:** is used to release the moisture, excess air, volatiles from the composite laminate and facilitate composite laminate consolidation, this is typically carried out in either an oven or autoclave. Two elements are essential for the curing cycle; heating and pressure. Heating is used to cure the resin material and reduce its viscosity while pressure is employed to consolidate and compress the composite laminate, see Figure B-2 for typical curing cycle for a monolithic composite component. The oven is used with the vacuum bag moulding for complex and relatively large components curing. Even pressure is applied up to 1bar. Vacuum bag and oven can produce reasonable quality components despite their relatively low cost compared to the autoclave process. Autoclave is a large heated pressure vessel which is similar to the vacuum bag and oven cured processing except the required additional pressure (up to 7 bar). The autoclave is employed when high quality composite components are required, e.g. for aircraft structural components such as wing spars and skins, fins and fuselage. Curing can be in two stages (initial and post curing) or only one stage (full curing). Post curing is essential for products initially cured below 150$^{o}$C where full properties of the composite part such as maximum $T_g$ can be achieved.

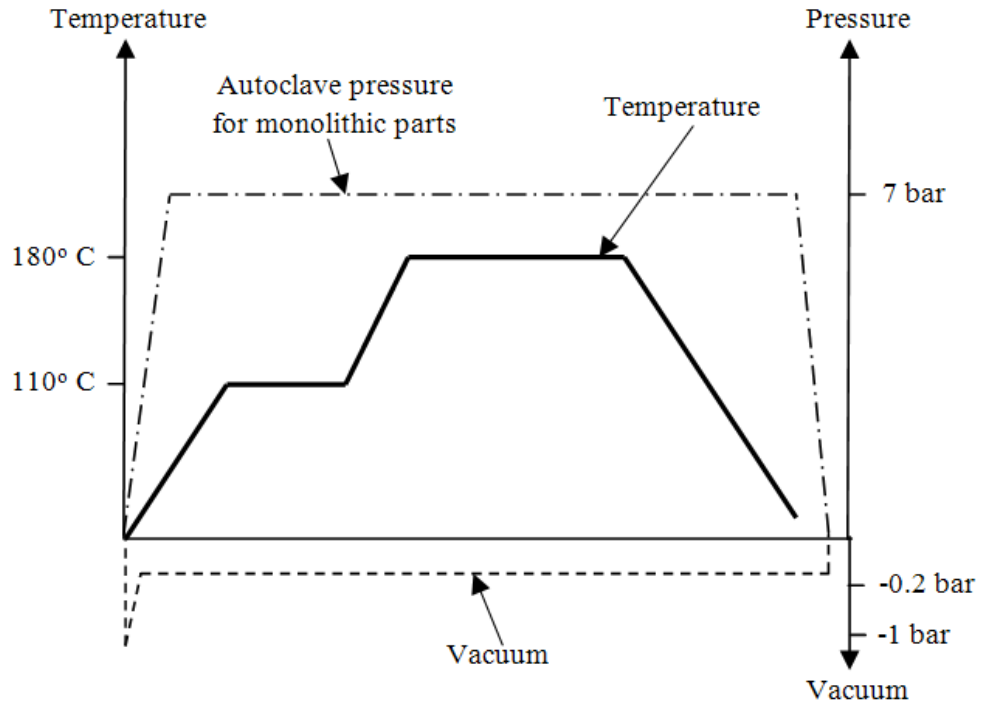


Figure B-2: Typical curing cycle for monolithic components [Adopted from Hexcel Corporation]

An example for the curing cycle is detailed below (courtesy of ACG for MTM44-1 prepregs).

**Curing**: Oven cured with a heat up rate of 1°C/min with a step dwell of 80°C for 30 minutes followed by a heat up rate of 1°C to 135°C for 4 hrs all held at a minimum vacuum of 27"Hg (914 mbar). **Post curing**: heat up rate of 2.5°C/min to 135°C followed by a heat up rate of 0.2°C/min to a temperature of 180 - 200°C for 4 hrs. Free standing with no vacuum applied. Subsequently, cool at rate of 2°C/min to 70°C.

# APPENDIX C

## Material safety data sheet (MSDS) for CFRP

**1. Introduction**

Carbon fibre reinforced plastic CFRP composites are used in a wide range of industries such as aerospace, automotive, aircraft and sports. Processing of CFRP needs special precautions/considerations due to hazards of dusts and fumes which are produced during decomposition or cutting. The body of evidence suggests that in all likelihood carbon fibres are not carcinogenic but they may cause irritation, coughing and pulmonary oedema. Hence the purpose of the following information is to identify potential hazards and ways of avoiding such problems.

**2. Product identification**

**Product:** MTM44-1, 977-2 and 8552 Matrix systems (epoxy resin reinforced carbon fibre prepregs) are used in GKN Aerospace in the machining of CFRP sheets products which will be used in the present PhD project.

They are dual cure temperature, high performance epoxy matrix, developed for both infusion and prepreg processing. Prepreg material can be in the following forms: fabric, roving, 0-90 degree woven cloth and unidirectional tape.

**3. Physical and chemical characteristics**

| |
|---|
| Constituents: 55-59% carbon fibres and 34% epoxy resin |
| Physical state: solid |
| Appearance: black |
| Odour: nearly odourless |
| Cured resin density: 1.18 gm/cm$^3$ [1]<br>Boiling point: NA |
| Melting point: > 2760 $^oC$ [2] |
| Vapour pressure: NA |
| Evaporation rate: NA |
| Solubility in water: NA |

4. **Hazard ingredients/identification**

| Composite component | Organ system target | Possible health effect [3] |
|---|---|---|
| Epoxy resins | Skin, lungs and eyes | Contact and allergic dermatitis, conjunctivitis |
| Carbon fibres | Skin (lungs) | Skin and respiratory irritation, contact dermatitis (chronic interstitial lung disease) |

**4.1 Primary routes of entry [3]**

- Eye: The abrasive action of dust (which is particulate in nature and usually contains a few fibres – no data of size is available) may damage the outer surface of the eye.
- Skins: The abrasive action of the dust may cause irritation.
- Ingestion: Not a normal route of exposure. Accidental ingestion may cause gastrointestinal disturbances.
- Inhalation: Machining, grinding, or sawing of the material may generate airborne dust. Prolonged or repeated exposure to respirable particles may cause respiratory tract irritation, coughing and pulmonary edema.
- Carcinogen listings: ND

**4.2 Physical/chemical hazard**

Explosive: N/A

**4.3 Adverse human health effects**

Toxicology studies indicate the dust should probably be controlled at levels below the PEL for inert dust, but not approaching the PEL for crystalline quartz.

**4.4 Environmental effects**

Carbon fibre is electrically conductive and it can cause short circuiting of electrical equipment. Airborne carbon fibre can also disturb electrical equipment.

**5. First aid measures [4]**

- General information: Change contaminated clothing.
- Eye: Flush eyes with large amounts of water for 15 minutes. Eyelids should be held away from the eyeballs to ensure through rinsing. Seek medical attention if irritation persists.
- Skin: Wash gently with soap and water to remove dust and fibres.
- Ingestion: Drink extra water to assist natural elimination. Seek medical attention if gastrointestinal irritation persists or other symptoms such as nausea, vomiting, or abdominal pain occur.
- Inhalation: Move to fresh air. Drink water to clear throat and blow nose to remove fibres. Get medical attention if necessary.

**6. Fire fighting measures [5]**

- Flash point: Not known, but very high
  Flammable limits: NA
- Fire extinguishing media: Non-burning.
  Special fire fighting procedures: Treat the surrounding fire
- Unusual fire and explosion hazards: ND
- Hazardous combustion products: ND

**7. Accidental release measures [6]**

- Action to take for spills/leaks: NA
- Personal precautions: wear protective equipment.
  Avoid contact with skin, eyes, and clothing.
  Keep away from unprotected people.
  Provide adequate ventilation.
- Environmental precautions:
  Do not allow to enter ground soil, sewage or drains.
- Methods for cleaning up / spillage removal:
  Remove mechanically, placing in appropriate containers for disposal.

**8. Exposure controls / personal protection**

**8.1 Critical values of exposure [6]**

| ***Chemical name*** | ***type*** | ***Value*** |
|---|---|---|
| Fibre (Carbon Fibre or Glass Fibre) | ACGIH-TWA | 10 mg/m³ |
| | NIOSH-TWA | 3 fibers/cm³ for (Fibres less than or equal to 3.5 μm in diameter and greater than or equal to 10μm in length.) |
| Formulated Epoxy Resin | TWA (Total) | 15 mg/m³ |
| | TWA (Respirable) | 5 mg/m³ |

**8.2 Limitation and monitoring of exposure at workplace [6].**

Provide good ventilation and/or an exhaust system in the work area.

- Respiratory protection: In case of insufficient ventilation or when dust concentration exceeds recommended TLV of 10 mg/m$^3$ (total dust) or 5 mg/m$^3$ (respirable dust) wear an approved particulate respirator. Respiratory protection is also required when product is heated to 48°C or above.
- Hand protection: Rubber or plastic gloves according to EN 374. The glove manufacturer's instructions must be observed concerning the penetrability and the wearing-out time. Apply barrier cream or wear long sleeved shirt to prevent fibrous matter from contacting exposed skin. Wash exposed skin areas before eating and at end of work day.
- Eye protection: Tightly sealed safety glasses with side shields according to EN 166.
- General protection and hygiene measures:
  Wash hands when done working with material; at breaks, lunch, shift changes.
  Avoid contact with skin and eyes.
  When working, do not eat, drink or smoke.
  Eye wash facility must be provided.
  Wash work clothing frequently.

**9. Stability and reactivity**

- Conditions to avoid (hazardous reactions):
  Keep away from heat.
  Carbon Fibre is electrical conductive. It may cause short circuits of electrical apparatus, especially when airborne fibres are drifting in the area.
- Materials to avoid: Avoid contact with strong acids, strong bases and oxidizing agents.
- Hazardous decomposition products: *In case of fire may form carbon monoxide and carbon dioxide and may form toxic materials.*
- Polymerization: will not occur

**10. Handling and storage**

- Handling: store in plastic bags in which the product is shipped, tightly sealed.
- Storage: No special storage considerations are known.

**11. Toxicological information**

- General remarks: Prolonged periods of contamination may lead to mild irritation.
- Sensitization: May cause sensitization by skin contact.

**12. Disposal considerations**

- Do not incinerate. Waste material should be bagged or containerized, sealed and disposed of in an approved landfill in accordance with local regulations. Product as shipped is not considered a hazardous waste under current RCRA regulations.

**13. Special precautions**

- Electrical equipment, enclosures and circuits in or near areas where carbon fibres are used should be protected against infiltration of or contact with airborne particles or filaments.
- Store carbon fibres product in original containers and avoid conditions that may generate carbon dust or lint.
- As with all industrial products, selection of specific personal protective equipment (e.g., gloves, disposable, clothing, respirators) and general control (e.g., local exhaust ventilation) depends upon the type of operation and exposure potential. To avoid ingestion incidental to handling, food and tobacco should not be present in the work area. Wash skin contact areas with soap and water after handling.

**Abbreviations**

| | |
|---|---|
| CFRE | Carbon Fibre Reinforced Epoxy |
| OSHA | Occupational Safety & Health Administration |
| PEL | Personal Exposure Limit |
| N/A | Not Applicable |
| N/D | Not Determined |
| EN | European Standards |
| RCRA | Resource Conservation and Recovery Act (US Environmental protection agency) |
| TLV | Threshold Limit Value |

**References**

[1] Advanced composites group Ltd., MTM 44-1.
[2] Fibre Glast Development Corporation, material safety data sheet for THORNEL pan based standard modulus carbon fibres.
[3] Occupational safety and health administration, http://www.osha.gov.
[4] OSHA's hazard communication standard, MSDS 29 CFR 1910.1200.
[5] MSDS for product no. 91202, 91202-2, 91202-3, 91202-20 carbon fibre, http://www.tedpella.com/msds_html/91202,91202-2,91202-20,91202-3msds.htm
[6] Otto Bock safety data sheet for SL-1 – ADP, SP II, GM, Footplates, http://www.otoobockus.com.

# APPENDIX D

## Additional force and torque curves, charts and ANOVA results

### Thrust force and torque results for phase 2A (all tests)

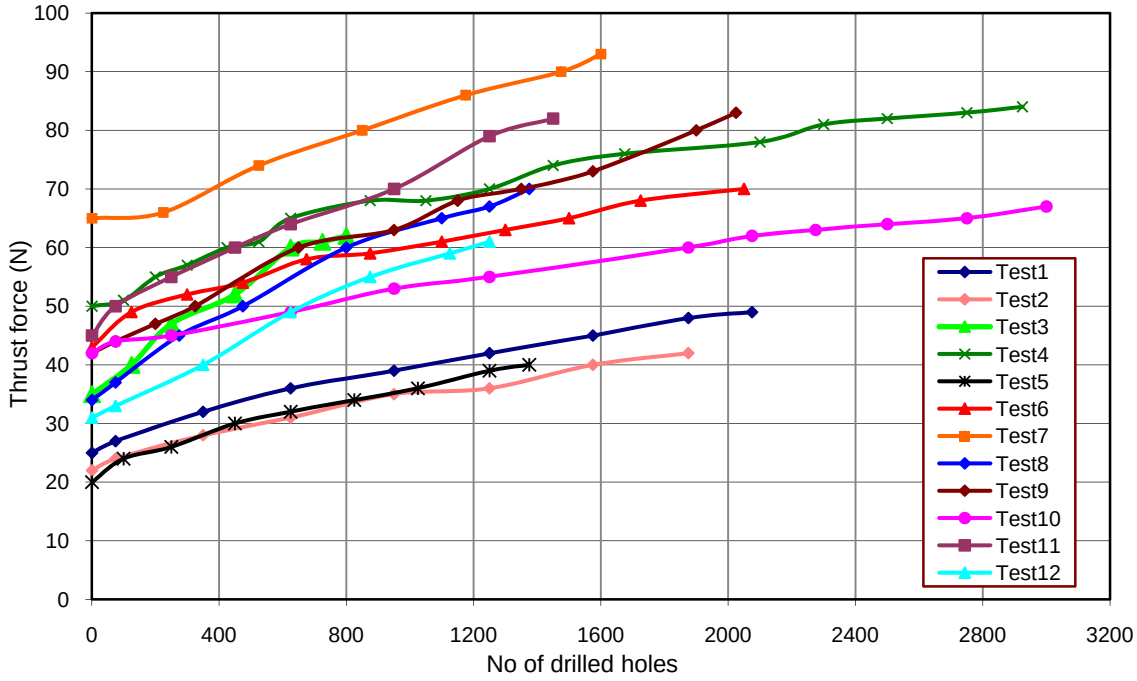


Figure D-1: Thrust force results for Phase 2A

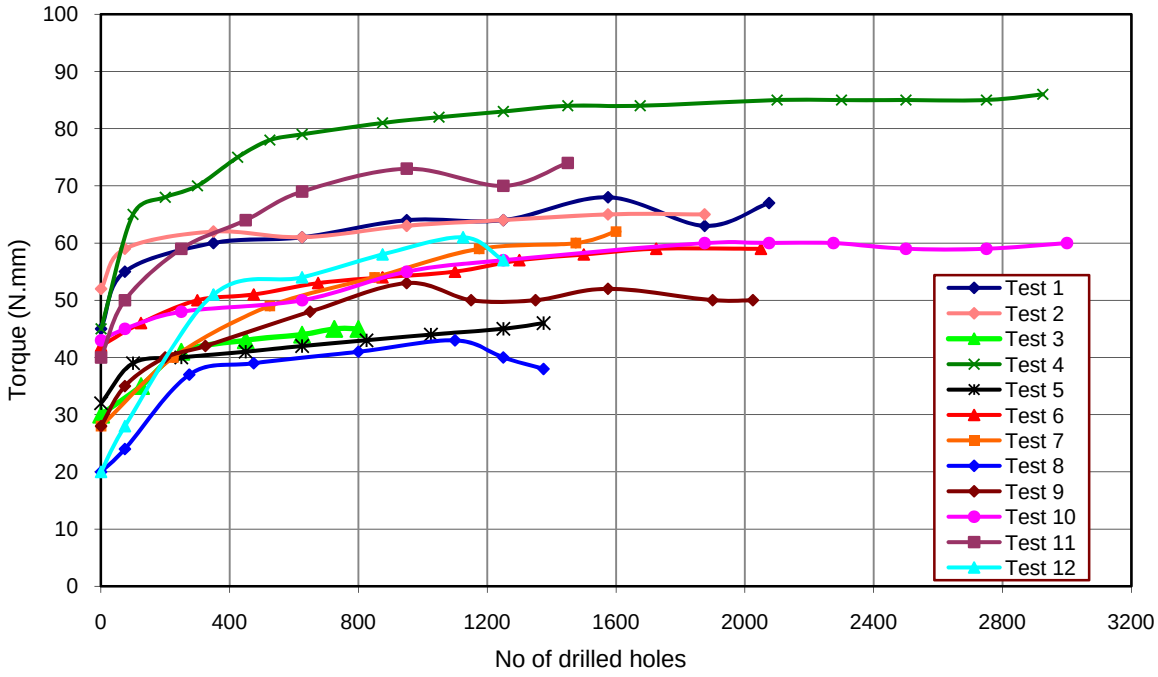


Figure D-2: Torque results for Phase 2A

**Thrust force and torque results for phase 2B**

Figures D-3 and D-4 show thrust force and torque results when using CVD diamond coated drills at 0.4 mm/rev feed rate respectively. Thrust force reached ~ 380 N when using Rhobest diamond coated tools in contrast to up to 170 N for uncoated and DLC coated equivalent.

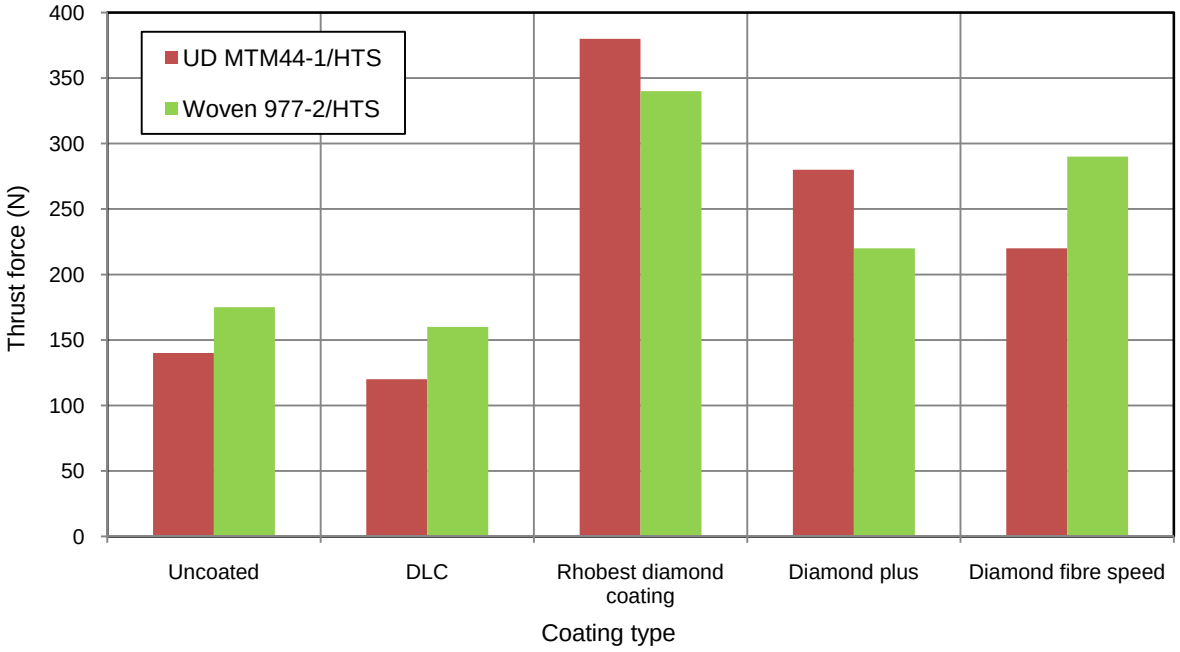


Figure D-3: Thrust force for the last hole drilled at 0.4 mm/rev feed rate

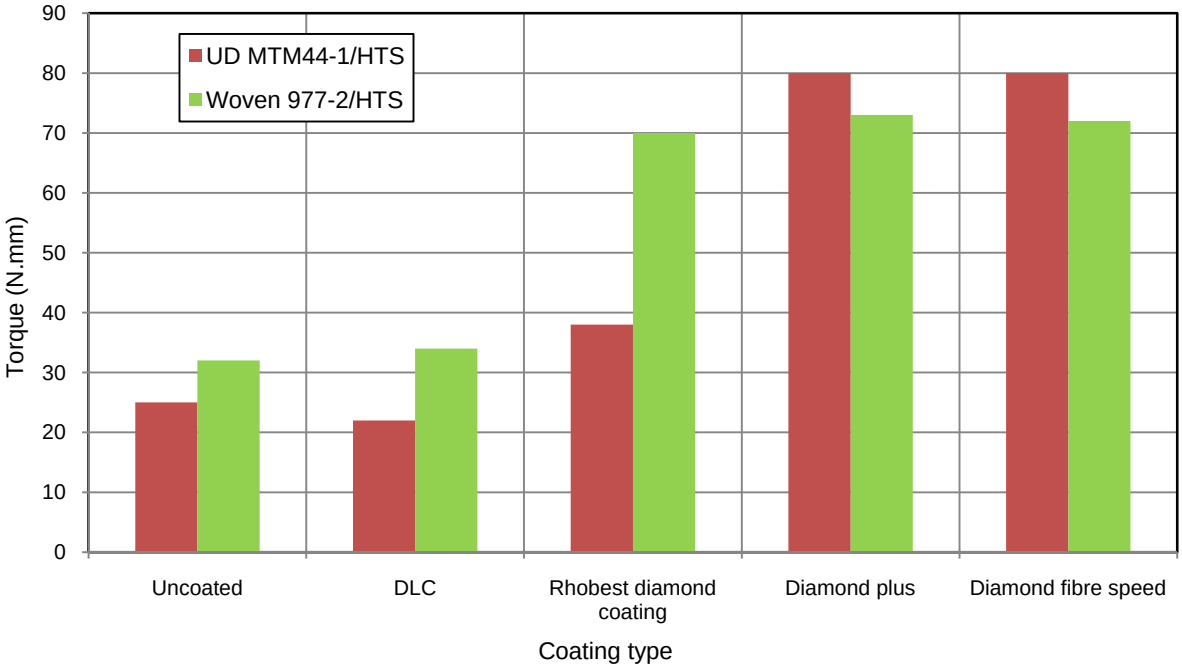


Figure D-4: Torque for the last hole drilled at 0.4 mm/rev feed rate

**Force and torque profiles recorded in Phase 3A**

Figures D-5 and D-6 show thrust force and torque signatures when drilling using pecking and no pecking respectively. Chatter and noise in the signals were reduced in addition to the benefit of saving retraction time.

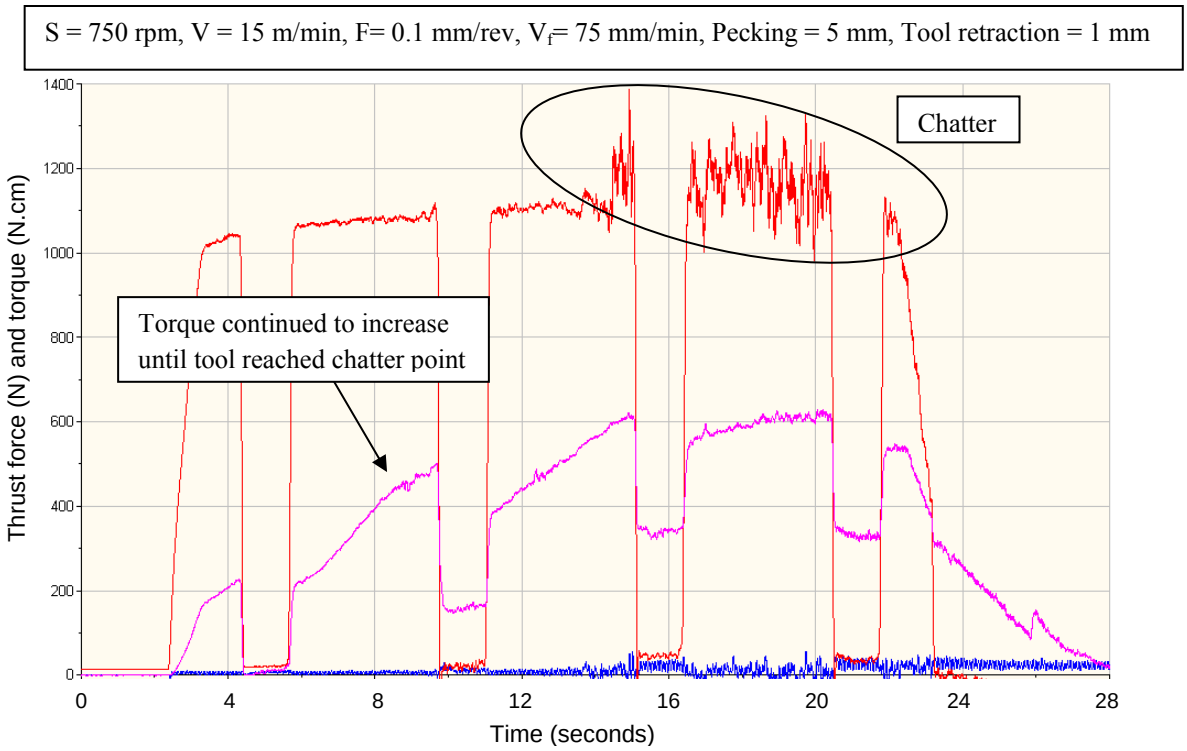


Figure D-5: Thrust force and torque profiles recorded when drilling the first hole

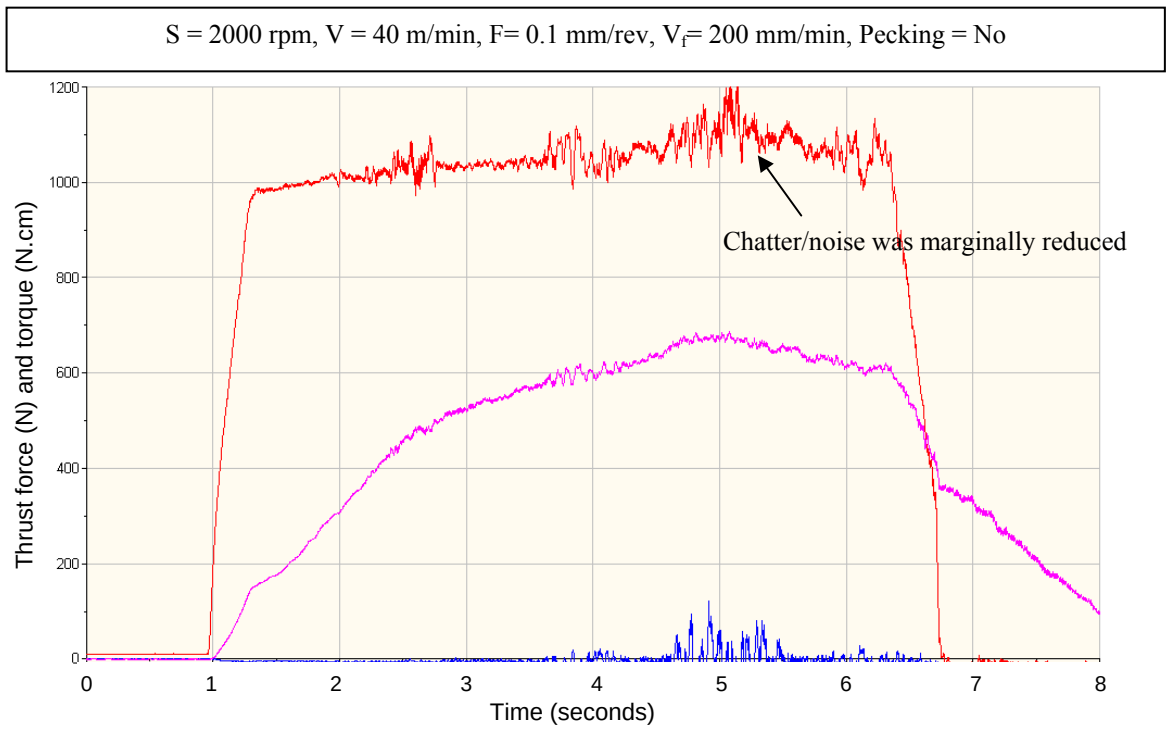


Figure D-6: Thrust force and torque profiles recorded when drilling hole number 115

**Thrust force and torque results for phase 3C**

Figure D-7 depicts thrust force results corresponding to last hole drilled. A maximum force was measured when drilling titanium and was up to ~2500 N at a cutting speed of 20/40 m/min and feed rate of 0.1 mm/rev. Figure D-8 shows torque results corresponding to the first hole. Higher torque levels were measured for tests experiencing premature tool failures in contrast to tests with gradual wear which had comparatively lower torque values.

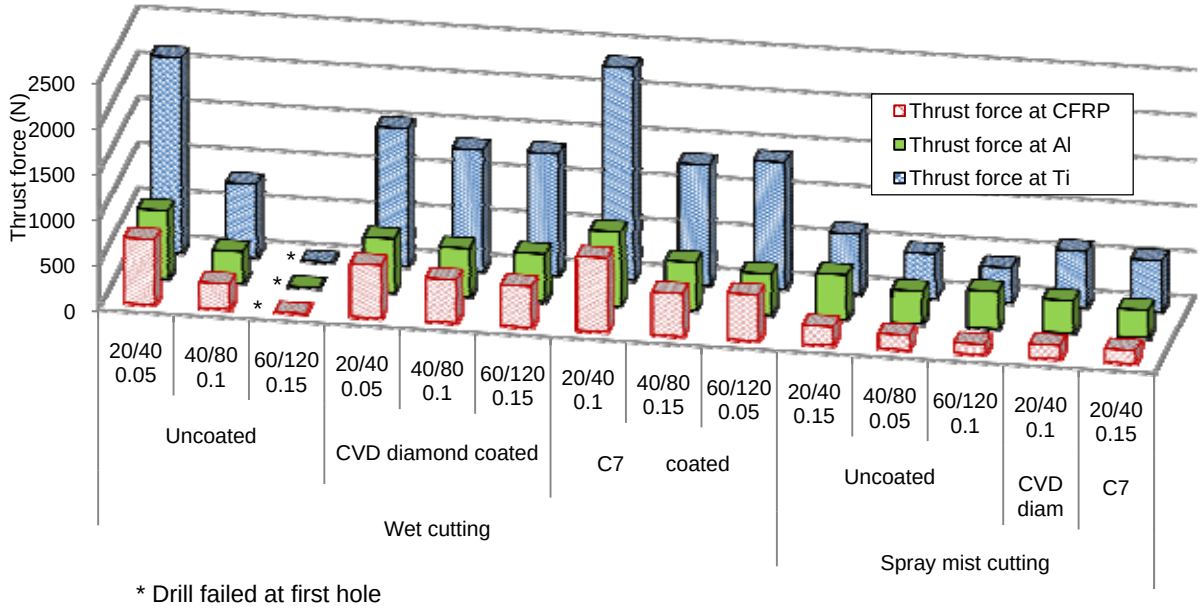


Figure D-7: Thrust force results corresponding to the last hole drilled

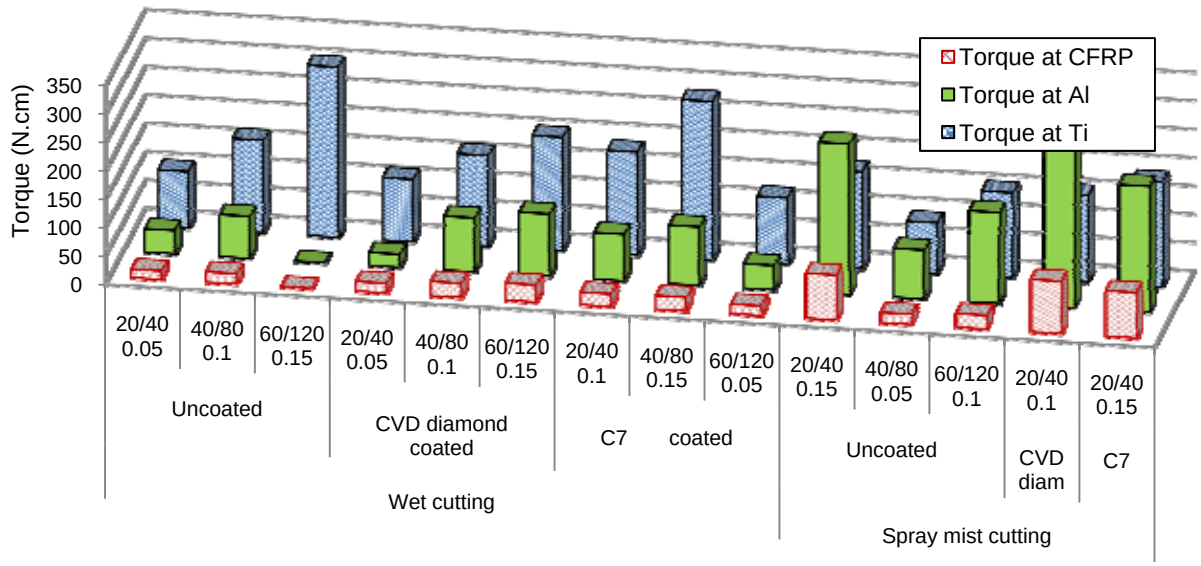


Figure D-8: Torque results corresponding to the first hole drilled

# APPENDIX E

## Cutting temperature measurement results (Phase 2A)

### Introduction

ThermaCAM cameras measure and produce images from all infrared radiation received from an object. Infrared radiation is a function of object surface temperature and this makes it possible for the camera to calculate and display this temperature. Emissivity is the most important object parameter to set correctly for accurate temperature measurement. Values fall in a range from 0.0 to 1.0. Figure E-1 shows the experimental setup employed.

### ThermaCAM S640 specifications

| | |
|---|---|
| Accuracy | +/- 2 $^{o}$C or +/- 2% of the reading |
| Thermal sensitivity | < 0.06 $^{o}$C @ +30 $^{o}$C |
| Resolution | 640x480 pixels |
| Operating temperature range | 0 – 500 $^{o}$C |
| Lens | 40 mm |
| Display type | Large 5.6” Swivel / Color LCD |
| Emissivity adjustment | 0.0 – 1.0 |


Figure E-1: Cutting temperature setup on Matsuura FX-5 using ThermaCAM which was loaned from EPSRC

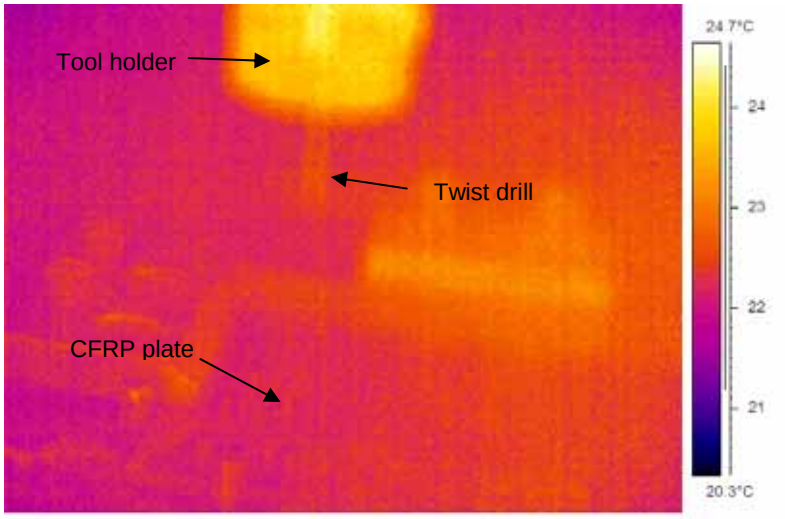


Figure E-2: Drilling UD MTM44-1/HTS OOAC at 0.4 mm/rev feed rate using worn standard twin lipped twist drill (after 3250 holes)

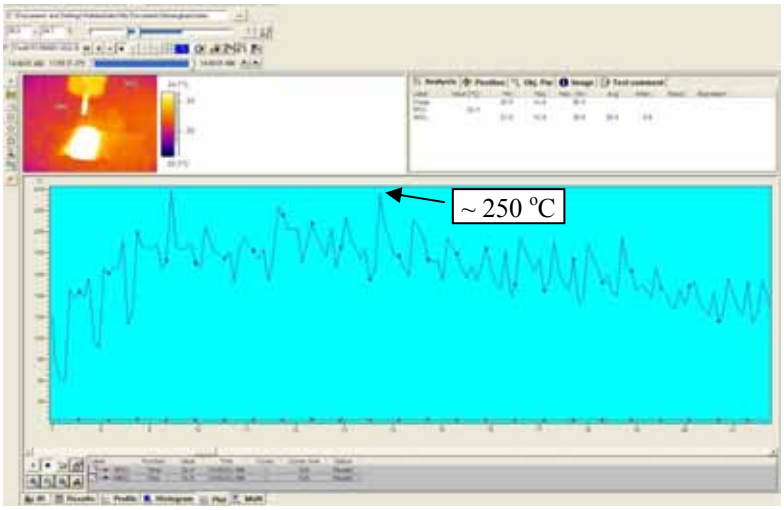


Figure E-3: Temperature curve when drilling UD MTM44-1/HTS OOAC at 0.4 mm/rev feed rate using worn standard twin lipped twist drill (following 3250 holes)

**Findings**

Limited temperature measurements were performed including UD MTM44-1/HTS and woven 977-2/HTS laminates using new and worn cutting tools at the higher feed rate level used in the current work (0.4 mm/rev) respectively. Maximum cutting temperature of ~250 °C after 3350 holes was recorded when cutting UD MTM44-1/HTS (see Figure E-2 and E-3) while this was up to 200 °C when cutting woven 977-2/HTS was measured as shown in Figure E-4.

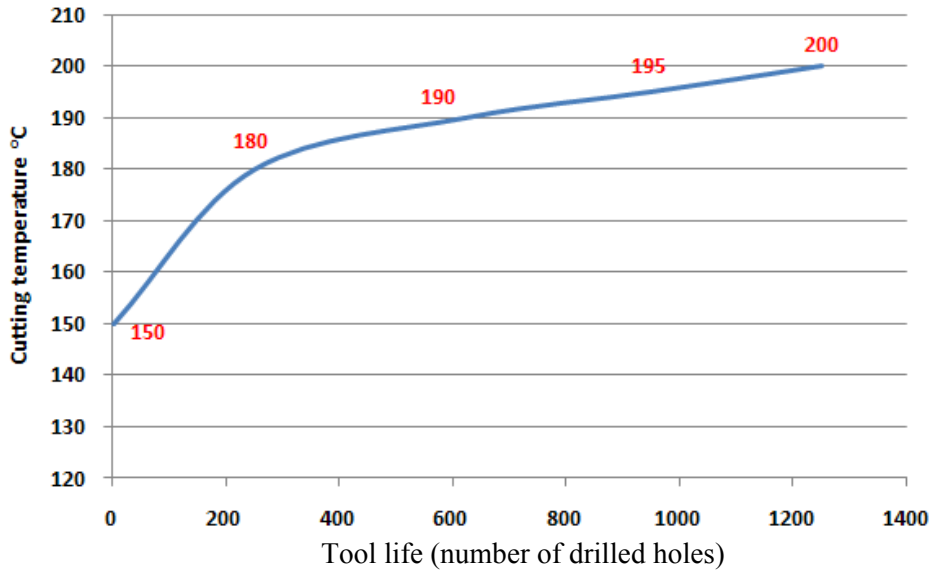


Figure E-4: Maximum drilling temperature development when cutting woven 977-2/HTS AC at 0.4 mm/rev feed rate

# APPENDIX F

## List of publications and awards

### Papers published

Islam Shyha, Sein Leung Soo, David K. Aspinwall, Sam Bradley
**Effect of peel ply when drilling small holes in CFRP**
Proceedings of the Institution of Mechanical Engineers, Part B: Journal of Engineering Manufacture, ***Accepted in press***, 2010
ISSN: 2041-2975

Islam Shyha, Sein Leung Soo, David K. Aspinwall, Sam Bradley, Stuart Dawson, Cornelius J. Pretorius
**Drilling of Titanium/CFRP/Aluminium Stacks**
Key Engineering Materials Vols. 447-448 (2010) pp 624-633 (Selected, peer reviewed paper from the ICoPE2010 & 13th ICPE International Conference on Precision Engineering, Singapore, 28 – 30 July 2010)
ISSN: 1013-9826

Islam Shyha, Sein Leung Soo, David Aspinwall, Sam Bradley
**Effect of laminate configuration and feed rate on cutting performance when drilling holes in carbon fibre reinforced plastic composites**
Journal of Materials Processing Technology, Volume 210, Issue 8, 1 June 2010, Pages 1023-1034
ISSN: 0924-0136

I.S. Shyha, D.K. Aspinwall, S.L. Soo, S. Bradley
**Drill geometry and operating effects when cutting small diameter holes in CFRP**
International Journal of Machine Tools and Manufacture, Volume 49, Issues 12-13, October 2009, Pages 1008-1014
ISSN: 0890-6955

Islam Shyha, Sein Leung Soo, David Aspinwall, Sam Bradley
**Small hole drilling of carbon fibre composites using diamond coated drills**
Energy Efficient & Low Carbon Manufacturing, Proceedings of the 26th International Manufacturing Conference (IMC26), Trinity College Dublin, Ireland, 02-04 September 2009, pp. 87-94
ISBN: 978-0-9562303-8-6

Islam Shyha, Sein Leung Soo, David Aspinwall, Sam Bradley
**Experimental study of small hole drilling in diverse CFRP laminate configurations**
Proceedings of the 9th International Conference on Production Engineering, Design and Control (PEDAC 2009), Alexandria, Egypt, 10-12 February 2009

### Papers under preparation

Islam Shyha, David K. Aspinwall, Sein Leung Soo
Drilling of Carbon Fibre reinforced Plastic Composites: A Review

Islam Shyha, Sein Leung Soo, David K. Aspinwall, Sam Bradley, Stuart Dawson, Cornelius J. Pretorius
Hole quality assessment when drilling metallic/composite stacks using diamond coated drills

### Awards

2009 Best conference student paper award, awarded by the Consortium of Manufacturing engineering Heads (COMEH) at the International Manufacturing Conference (IMC26) for the paper **"Small hole drilling of carbon fibre composites using diamond coated drills"**